Buckling and geometrical

nonlinear beam-type

analyses

of timber structures

by

Trond Even Eggen

Department of Structural Engineering
Norwegian University of Science and Technology
N-7034 Trondheim

April, 2000

Abstract

An existing co-rotated formulation is presented, and a consistent nonlinear 3D beam element, based on 2nd order theory, and with internal geometric stiffness, is developed for implementation in the formulation. The element proves considerably more accurate with respect to predicting buckling loads in linearized buckling analyses, than the beam elements regularly used in co-rotated formulations. This is also true for nonlinear analysis.

The computer program Cfem, which is based on the co-rotated formulation, is used to study several aspects of buckling, mainly lateral torsional buckling, in timber structures. Linearized buckling analyses are used for obtaining simplified or approximate formulas, and nonlinear analyses are used in order to verify these. The problems studied include lateral torsional buckling for beams with eccentricly applied loading and for tapered beams, bracing against lateral torsional buckling, and interaction between flexural and lateral torsional buckling.

Acknowledgements

Contents

Notation

Main symbols

$\mathbf{R}$	-	rotation matrix
$\mathbf{n}$	-	unit vector representing the orientation of the rotation axis
θ	-	rotation angle
$\boldsymbol{\theta}$	-	rotation pseudo-vector
C	-	configuration
$\mathbf{T}$	-	transformation matrix
$\mathbf{r}$	-	position vector with respect to global origin
$\mathbf{x}$	-	position vector with respect to local origin
$\mathbf{e}$	-	eccentricity vector
$\mathbf{u}$	-	displacement vector
$\mathbf{v}$	-	nodal displacement vector
δ	-	variation operator
∂	-	partial differentiation operator
$\boldsymbol{\omega}$	-	instantaneous rotation axis (chapter 3)
$\mathbf{P}$	-	projector matrix or part of projector matrix
δ_{ab}	-	Kronecker delta
$\mathbf{I}$	-	identity matrix
$\mathbf{0}$	-	matrix containing only zeros
$\mathbf{G}$	-	matrix relating the variation of rigid body rotation with the variation of the degrees of freedom
$\mathbf{H}$	-	deformational rotation pseudo-vector Jacobian
$\mathbf{E}$	-	eccentricity matrix
P	-	point load
q	-	distributed load
N	-	axial force
M	-	bending moment
Π	-	potential energy
U	-	strain energy

H -   load potential
V -   volume of body
$\boldsymbol{\sigma}$ -   stress vector
$\boldsymbol{\epsilon}$ -   strain vector
$\mathbf{B}$ -   strain displacement matrix
$\mathbf{f}$ -   force vector
$\mathbf{k}$ -   stiffness matrix
$\mathbf{K}$ -   stiffness matrix
E -   Young's modulus
I -   2nd moment of area
$\mathbf{p}$ -   external force vector
$\mathbf{r}$ -   residual vector
λ -   load level parameter
$\mathbf{N}$ -   shape function vectors/matrices
$\boldsymbol{\omega}$ -   vector of rotation (chapter 4)
$\boldsymbol{\kappa}$ -   vector of curvature
A -   area of cross section
L -   length of element
u -   displacement in the x-direction
v -   displacement in the y-direction
w -   displacement in the z-direction
α -   dimensionless shear constant
h -   depth of beam
b -   width of beam

Subscripts

n	-	time step identifier
a	-	point identifier
r	-	rigid body
d	-	deformational
c	-	center or centerline
T	-	tangent
e	-	internal
G	-	geometric
M	-	material
yy	-	for bending about the y-axis
zz	-	for bending about the z-axis
ϵ	-	axial strain
σ	-	axial stress
γ	-	shear strain
τ	-	shear stress
lin	-	for linearized buckling
s	-	shear
y	-	along the y-axis
z	-	along the z-axis
u	-	for displacement along the x-axis
v	-	for displacement along the y-axis
w	-	for displacement along the z-axis
ω	-	for rotation
κ	-	for curvature

Superscripts

n	-	time step identifier
T	-	transposed

Accents

$\tilde{\ }$	-	measured with respect to local coordinate system
$'$	-	eccentricity point
$\bar{\ }$	-	measured in the cross section coordinate system
$()_R$	-	measured in co-rotated frame

Chapter 1

Introduction

1.1 Motivation

The history of structural accidents and catastrophies shows that buckling or instability have played an important role in a large number of these accidents. The reason for this, often dramatical behaviour of structures has been a topic of much speculation through centuries [1][1].

In structural engineering, two types of structural instability usually have to be considered. For slender, axially compressed members, *flexural buckling* may be an issue, and for transversly loaded slender beams with high depth to width ratios, *lateral torsional buckling* may cause problems. In timber design codes, like the Norwegian NS3470[2] and the emerging European code, Eurocode 5[3] or EC5 for short, especially lateral torsional buckling is handled in a rather vague manner, emphasizing the difficulty this topic is associated with. Comparing NS3470 and EC5, several questions and inconsistencies are encountered, one of which is the handling of interaction between lateral torsional buckling and flexural buckling. EC5 seems to imply that the lateral torsional buckling capacity of beams are not influenced by axial loading, whereas NS3470 recognizes such an interaction. Which assumption is correct? With respect to bracing against lateral torsional buckling, both EC5 and NS3470 seem to imply that only bracing placed on the compression side of the influenced beam is effective. In all fairness, neither design code explicitly states that bracing located other than on the compression side should be disregarded, but no help is offered for determination of the effect of such bracing. In the section dealing with tapered beams,

---

[1]Author's translation

NS3470 states that *"lateral torsional buckling shall be considered"*[2]. However, no rules or guidelines are stated as to how the engineer can take due care of this problem.

The design codes provide simplified methods for handling structural instability, usually methods based on solutions of differential equations with respect to stability for simplified systems. The structure has to be simplified into a series of simple systems that can be solved by the differential equation approach, and since these cases are relatively few, the approach result in approximate, normally conservative, results. However, similar solutions for whole systems or parts of structures can be found numerically by applying a *linearized buckling analysis* on a computer. Thus, a computer based finite element method can be used to aid in assessing structural instability in a simplified design procedure. Through a curve fitting procedure, tabulated values for simplified systems not readily solvable by the differential equation approach can be obtained.

But why stop at this? An approach based on a linearized buckling type analysis or a solution of differential equations is a mathematical approach that focuses only on the critical load (causing indeterminate displacement). The design strength of the material(s) as well as the imperfections of the system being considered are accounted for by additional considerations, leading to a coefficient based simplified design. A structural member is, however, never mathematically straight (certainly not timber members), and stability problems are therefore in reality *displacement problems* governed by *geometric imperfections*, and subsequently stress or strength problems. By including geometric imperfections, an incremental nonlinear analysis, combined with material failure tests at each increment, will yield a design load for the structure that also accounts for any stability problems.

When this work was initiated, the main objective was to use standard, state-of-the-art nonlinear finite element method programs to investigate structural stability, and particularly lateral torsional buckling in typical timber structures. This objective has been maintained, but as the work evolved, other interesting issues arose. It became apparent that there was room for some improvement in beam element behaviour with respect to stability calculations. This led to a fairly extensive investigation into pure finite element technology.

For this reason the work splits in two distinct parts. In the first part, the theoretical foundation for a fully consistent nonlinear co-rotated element formulation for implementation in a computer code is described, and a 3D finite beam element based on second order theory is developed for use in the co-rotated formulation. In the second part, a computer program based on the finite element formulation presented in the first part is used to obtain results for a series

---

[2]Author's translation

of stability problems. In the latter part topics concerned with both linearized buckling analyses and full nonlinear analyses are adressed.

The computer program used is based on a program made by Haugen [4], and goes by the name of *Cfem*. A good many changes have been made in order to facilitate solution of the problems at hand. Among other things, a linearized buckling analysis capability had to be implemented.

With this approach to the problem, the work is presented for two audiences: Those mainly concerned with FEM technology and those mainly concerned with timber design. An attempt has been made to keep the two main parts separated so that no deeper insight in one part is necessary to understand the other. Thus, if the element formulation is taken at face value, it should not be necessary for those mainly concerned with timber design to thoroughly read (and understand) the first part in order to appreciate the second part.

1.2   Background

Co-rotated formulation as a concept was introduced by Wempner[5] in 1969 for use in static nonlinear analysis of shell structures. The idea of a shadow configuration was first proposed by Fraeijs de Veubeke[6], but then for the complete structure. Bergan and Horrigmoe[7, 8] used the concept of rotating Cartesian frames attached to elements, whereas Bergan and Nygård[9, 10] used shadow configurations on the element level. A significant contribution towards the consistent treatment of co-rotated coordinates and large rotations was made by Argyris et al.[11, 12], while Crisfield[13], through his work concerning a three dimensional nonlinear beam element, introduced the concept of a *consistent co-rotational formulation* in 1990. Rankin and Brogan[14] introduced the idea of an *element independent co-rotated formulation* in 1986. This was later refined by Nour-Omid and Rankin[15]. In his co-rotational formulation for 3D beams from 1994, Teigen[16] accounted for the effects of eccentricity, but did this inconsistently. In 1994 Haugen[4] presented a co-rotated element formulation influenced mainly by Bergan and colleagues[7, 8, 9, 10] and their idea of element shadow configurations, and by Rankin and colleauges[14, 15] and their emphasis on element independency and consistency demands. Haugen and Felippa[17, 18] have later extended the formulation in order to consistently handle rigid eccentricities.

Much work has been done developing beam elements, see for instance [19, 20, 21], but usually the emphasis has been on developing standalone beam elements for nonlinear analysis that account for large displacements as part of the formulation.

One of the main advantages of the co-rotated element formulation is the idea of reuse of existing, and possibly linear elements, as these can be put in co-rotated frames handling the possibly large rigid body displacement. Thus, the beam elements usually implemented in corotated formulations, see [4, 13, 16], are linear elements based on Euler-Bernoulli or Mindlin-Reissner theory [22]. But any displacement-based beam element may in principle be implemented.

For solution of the nonlinear problem an incremental solution algorithm is usually applied. In a purely incremental algorithm, a systematic drift-off error accumulates, causing the computed results to deviate from the equilibrium path (see for instance [23]). In large displacement analyses, this is usually remedied by introducing Newton-Raphson equilibrium iterative methods (see [24]). These methods do, however, require that the tangent stiffness is *consistent* with respect to the force vector, in order to consistently yield a good rate of convergence towards the equilibrium path. This means that for the elements used in such analyses, the tangent stiffness should reflect the variation of the force vector.

Elements based on second order theory for displacements can be made to account for stability problems by including internal geometric stiffness accounting for the loss/gain of stiffness in the element due to existing stress. This has for instance been shown for two-dimensional elements by Bergan and Syvertsen[1]. However, usually only geometric stiffness due to axial loading is included, and even Vašek[25], who puts a large effort into including geometric stiffness due to shear, does not seem to include the geometric stiffness effect of bending. Thus, geometric stiffness that accounts for lateral torsional buckling is omitted in these element formulations.

Beam elements based on second order theory can be used in the co-rotated formulation. However, as purely incremental methods are usually used as solution procedures in second order finite element formulation codes, it does not appear that much emphasis has been put into finding consistent beam elements based on this theory. Thus, existing beam elements based on second order theory would have to undergo rather extensive modification in order to be candidates for use in fully nonlinear analyses.

Whereas Euler presented the first solution of the differential equation for a column with respect to stability in 1744 [26], it was not until 1899 that the first case of lateral torsional buckling was solved by Prandtl[27] and Michell[28], according to Timoshenko and Gere [29]. A number of other cases of beams and columns solved with respect to stability, by use of differential equations, are given and summarized in Timoshenko and Gere[29, 30]. More work has been done by, for instance, Flint[31, 32], which was used by Hooley and Madsen[33] for comparison when doing experiments on timber beams with respect to lateral torsional buckling.

Van der Put[34] used differential equations to study (timber) beams subjected to bending about two axes and axial compression, with respect to stability, in an effort to obtain a more general and consistent stability design for Eurocode 5. Burgess[35, 36, 37] and Brüninghoff[38] study the effect of bracing on columns and deep beams, with the ultimate goal of obtaining design code rules for use in Eurocode 5. A number of other papers concerning flexural and lateral torsional buckling of timber structures have been presented at various CIB-conferences, see for instance Burgess[39, 40], Blaß[41], Johansson[42] and Larsen[43, 44].

1.3   Current timber design codes

Of the many different timber design codes, only two are considered in this work: the existing Norwegian code, NS3470 [2][3], and Eurocode 5 or EC5[3]. The basics of these two design codes are the same. They are both based on the concept of partial coefficients, and the different code checks are performed in the stress space. However, Eurocode 5 offers less in terms of guidelines and help practical design work.

With respect to stability, the main difference between the two design codes, is the handling of flexural buckling. Eurocode 5 bases the code check on buckling curves obtained from statistical simulations. By measuring geometric imperfections and material properties of a large number of beams, the statistical distributions of these properties for the beams were established. In turn, these were used in Monte Carlo type analyses of buckling of simple columns to obtain buckling factors for the columns. In these analyses, a nonlinear stress-strain curve for the material was chosen. For more information, see [45]. In NS3470, a more theoretical approach was applied. According to this design code, the maximum allowed geometrical imperfection for a member is a given fraction of the length of the member. Imposing a sinusoidal imperfection, with amplitude equal to the maximum allowed geometric imperfection, on a simply supported column subjected to axial loading and applying a simple strength criterion, an expression for the buckling load is obtained, which in turn can be used to find the buckling factor for a column with a given buckling length. A linear stress-strain relationship was used in the derivation of the buckling factor. This topic is described in [46].

One other major difference between EC5 and NS3470, of interest for this work, is the handling of combined bending and axial loading. This issue is adressed more extensively in chapter 8.

---

[3]The latest revision, NS3470-1 of 1999, has not been considered in this work.

1.4   The organization of this thesis

This work is conveniently divided into two main parts.

In the first part, consisting of chapters 3, 4 and 5, a general co-rotated formulation is described (chapter 3) and a new consistent 3D beam element with internal geometric stiffness is presented(chapter 4). The element formulation is assessed through analyses presented in chapter 5.

The second part consists of chapters 6, 7, and 8, and presents results and discussion of results from linearized buckling analyses and nonlinear analysis of timber structures.

Chapter 2

Basic concepts and assumptions

2.1 Types of analysis

The various types of finite element analyses for static problems referred in this work are briefly summarized below.

2.1.1 Linear analysis

Linear analysis is based on the assumption that the material is linearly elastic and that all displacements are small such that both equilibrium and kinematic relations refer to the undeformed geometry.

Superposition applies and the solution of a linear problem is unique.

2.1.2 Linearized buckling analysis

When establishing differential equations for solution of structural stability problems, equilibrium of the structure is studied in a deformed state, where the displacements are assumed to be small (infinitesimal), see for instance [30]. After the differential equation is established, the critical load is found by solving the equation with respect to the lowest value of the load that leaves the magnitude

of the displacement indetermined. The problem with this method lies not necessarily in establishing the differential equations, but rather in the solution of the equations.

The finite element equivalent to the differential equation approach is the linearized buckling analysis. This type of analysis is based on the displacement being small, and it leads to the eigenvalue problem

$$\left(\mathbf{k}_1 - \lambda \mathbf{k}_G\right) \mathbf{v} = \mathbf{0} \tag{2.1}$$

This equation is solved with respect to the load factor λ (eigenvalue), and the displacement vector $\mathbf{v}$ (eigenvector) whose amplitude is indeterminate. Traditionally, $\mathbf{k}_1$ is the so-called *material stiffness* which is the stiffness independent on the stress state of the structure, whereas $\mathbf{k}_G$ is dependent on the stress in the structure and is called *geometric stiffness*. Note, however, that a linearized buckling analysis can be applied about any given configuration, even a prestressed one.

A variation of the linearized buckling analysis is the *secant linearized buckling analysis*, where instead of a linearization about a given configuration, linearization is applied *between* two configurations, and beyond.

Both the linearized buckling analysis and the secant linearized buckling analysis are useful for obtaining estimates of the buckling load for a structure. However, since the basic assumption is small displacements, the accuracy of these estimates is dependent on the flexibility of the structure in the interval between the configuration at which the linearization is applied and the configuration for which the structure actually buckles.

In addition to the estimate of the buckling load, the linearized buckling analysis also gives an estimate of the buckling shape of the structure. A scaled version of this shape has in many cases proved to be a good choice for the geometric imperfection in nonlinear analyses.

As will be seen in section 2.1.4, the secant linearized buckling analysis has another important application.

2.1.3   2nd order analysis

This type of analysis is often (erroneously) referred to as nonlinear analysis. Allthough it allows for nonlinear effects in both geometry and material properties, this method of analysis is based on the assumption of small displacements, but equilibrium is required with respect to deformed geometry. Usually iterative methods have to be applied in order to obtain results from a 2nd order analysis,

as the stress distribution in the structure for this kind of analysis is dependent on the displacements.

2nd order analysis can be used to obtain estimates of the buckling loads, since the displacement increases rapidly and approaches infinity when the load level approaches the buckling load. However, since the displacements are assumed small, the accuracy of the buckling load estimation is highly dependent on the flexibility of the structure.

2.1.4 Nonlinear analysis

As the name indicates, a nonlinear analysis is capable of accounting for nonlinear effects. Both geometric and material nonlinearities can be handled. The basic assumptions are that the deformation is finite, but not necessarily small, and equilibrium is required with respect to the deformed geometry. Thus, the nonlinear analysis is applicable to both rigid and flexible systems.

Nonlinear analyses of static problems are usually performed by some incremental approach. This may introduce an (increasing) error in the solution as the analysis proceeds, and equilibrium corrections are therefore usually applied. The actual process depends on the type of solution procedure being used, and on the relative size of the increments.

Buckling is detected in a nonlinear analysis by an indefinite system of equations governing the analysis. In a second order analysis, the buckling load is associated with indeterminate displacements. In a complete nonlinear analysis, however, buckling is really a point; a socalled *bifurcation point*, at which two equilibrium paths crosses. In order to detect the bifurcation point and traversing it correctly, a secant linearized buckling analysis between one configuration before and one after instability is applied.

Through a so-called nonlinear *bifurcation analysis*, it is thus possible to follow the equilibrium path of the structure through buckling and beyond.

2.2 Computational models

2.2.1 Two-dimensional (2D) models

The most common computational model used by the structural engineer, is the two-dimensional model. In such a model, all points have only three possible

displacement components, two translations and one rotation. Most structures can be simplified into a set of substructures, each of which can be presented in a two-dimensional plane. One of the main advantages of this kind of model is the relative ease with which a graphical computer user interface can be made in which it is easy to model the structure and represent computed data.

The obvious disadvantage of this approach is its inability to capture out-of-the-plane action. This makes it impossible (or at least very difficult) to correctly account for interaction between the different substructures.

2.2.2   Three-dimensional (3D) models

All structures are three-dimensional, and a complete solution can only be obtained by a 3D-model. The step up from 2D is, however, a major one. Not only is the formulation more complex, mainly due to the difficulties associated with rotations in three dimensions, and the computational costs much higher, the modelling as well as the representation and interpretation of the results are also much more challenging in 3D than in 2D.

2.2.3   2 1/2D models

A fairly new concept, the 2 1/2D model seeks to combine the relatively easy modelling procedure of the 2D model with the computational versatility of the 3D model(see for instance [47]). In this approach the model and the loading is 2D, but it has 3D degrees of freedom, and it is therefore analyzed as a 3D structure. All out-of-the-plane non-fixed boundary conditions are accounted for by use of springs.

The major disadvantage of this approach is that the adjoining members has to be replaced by fictitious springs. For complex systems it may be difficult to assign properties to these springs. However, in connection with buckling, the bracing effect of adjoining structural members seems to be quite insensitive to the bracing stiffness of the members, providing they have sufficient stiffness. Thus, for some kinds of problems the 2 1/2D models may represent a useful extension to the 2D model.

2.3 Material

The material considered is timber. Being a natural material, timber has a wide variation in its material properties. Even two specimens out of the same tree may be considerably different. In this work, the usual assumption of linear elastic behaviour is made throughout.

However, for generality, the element formulation established in chapter 3 and 4 is developed for *hyperelastic material*; this is a material that follow the same, not necessarily linear, stress-strain curve in unloading as in loading.

The material properties used in the numerical part of the work are taken from NS3470[2].

NS3470 provides two sets of elastic stiffness parameters. The 5-percentile values are to be used for stability calculations, whereas the mean values should be used in deformational calculations. However, NS3470 does not provide any guidelines as to which set is to be used in computer analyses. At first glance, this may not seem to represent any problems. For linearized buckling analyses, which undoubtedly are stability type analyses, the 5-percentile values should be used. Likewise, in analyses, be they linear or nonlinear, aiming to find displacements, at least for the servicibility limit state, the mean values should be used. However, a problem arises when considering nonlinear analysis of members prone to buckling. In a nonlinear analysis, buckling is an integral part of the analysis, and not a special phenomenon. So, which set of material properties should be used in such analyses? This is actually a problem concerning all nonlinear analyses, as the stiffness will, to a certain degree, affect the results obtained from these analyses.

Eurocode 5 provides some guidelines for the use of 2nd order theory analysis. It states that the stiffness moduli to be used are the 5-percentile values, reduced by the k_{mod} factor (accounting for moisture and load-duration effects), as well as by the material factor.

In appendix D, results from some analyses of simple beams are presented. There is one case of flexural buckling, and two cases of lateral torsional buckling. For each of these cases, and for each design code, four analyses are performed, each with its own set of material properties. In addition, the design load as found from using the simplified methods in the design code is included.

The results consistently show that nonlinear analysis using the mean values of the stiffness parameters resulted in a much too high design load compared to the simplified methods. As for the results for the other sets of material properties, that all include some form of the 5-percentile values of the stiffness moduli, no

conclusion can be drawn with respect to what set of material properties should be used.

In the nonlinear analyses presented in this thesis, the unreduced 5-percentile values of the stiffness moduli are used, unless otherwise stated.

As indicated earlier, the unreduced 5-percentile values of the stiffness moduli are also used in the linearized buckling analyses.

2.4   Cross section

Allthough various cross sections are used in timber structures, by far the most common is the rectangular section. Therefore, only rectangular cross sections are considered in this study.

For rectangular cross-sections, the warping stiffness is negligible compared to the St.Venant torsional stiffnes, and it is therefore omitted from all calculations in this work.

It should be noted, however, that the element formulation presented in chapters 3 and 4 is applicable to all kinds of cross sections, as long as the warping stiffness is negigible compared to the St.Venant torsional stiffness.

Part I

Theoretical background

Chapter 3

Co-rotated formulation

Three different schools of finite element formulation exist for solving static problems involving large displacements.

The *total-lagrangian school* seeks to formulate elements based on expressions for total displacements, which include both rigid-body displacements and deformational displacements, resulting in rather complex element formulations. However, if performed successfully, the resulting elements are able to represent large displacement *and* large deformations. In this formulation, strain and stress is usually measured with respect to the base configuration.

If the *updated lagrangian school* is followed, the elements are still based on large displacements, that still may include both rigid-body displacements and deformational displacements. But as a target configuration is reached, it becomes the new reference configuration. *Strains and stresses are redefined as soon as the reference configuration is updated* [23]. According to Felippa[23], the updated lagrange formulation is of diminishing interest, as it is gradually being replaced by the co-rotated formulation.

In a *co-rotated formulation*, the rigid body displacements and the deformational displacements are treated seperately. In most problems, deformations are rather small, although the displacements may be large. Herein lies the key to the advantage of the co-rotated element formulation: Since the deformation of each element is small, linear elements may be used to represent the deformation of the element, since the possibly large rigid body displacements are handled seperately.

In this chapter, a co-rotated formulation is presented. The approach is an

adaptation of Haugen's work[4, 17].

3.1   Deformational displacement

The first need is to establish relationships between displacement, deformational displacement, rotation and deformational rotation for an element experiencing large displacement/rotation, but small deformation.

3.1.1   Rotations in three-dimensional space

The main reason why operating in three dimensional space (3D) is considered more complicated than operating in two dimensional space(2D), is the treatment of large rotations. In 2D, only rotation about an axis normal to the plane is possible, and thus rotations may be added as scalars. Hence, rotation can be treated in the same manner as translations.

In 3D space, however, three independent rotation components are possible for any given point. Furthermore, the order in which the rotations about the different axes take place is of significance[1]. Due to this property of rotations in three dimensional space, they may not be added as vectors. It is important, however, to recognize that for small rotations (that is small enough for linearization to be a sufficiently accurate approximation), rotations may be added as vectors.

A number of different ways of treating large rotations in three dimensional space have been examined, including rotation vector parameterization and orthogonal matrix parameterization (see for instance [48]). For the algorithms described in this section, the *Rodriguez representation of the rotation tensor* is used. This is an orthogonal matrix parametrization, in which derivation is based on one rotation about a particular rotation axis. As shown by Argyris [12], Rodriguez formula can be obtained from purely geometric considerations, and it is also consistent with an exponential mapping of rotations [12, 15, 49].

The Rodriguez representation of the rotation tensor for a rotation θ about an axis defined by the unit vector $\mathbf{n}^T = \begin{bmatrix} n_1 & n_2 & n_3 \end{bmatrix}$ is, in [17], given in the form:

$$\mathbf{R}(\mathbf{n}, \theta) = \mathbf{I} + \mathbf{N} \sin\theta + \mathbf{N}^2 \left(1 - \cos\theta\right) \qquad (3.1)$$

---

[1] This is for instance apparent in the Euler angle representation of rotations.

where

$$\mathbf{N} = \mathbf{Spin}\,(\mathbf{n}) = \begin{bmatrix} 0 & -n_3 & n_2 \\ n_3 & 0 & -n_1 \\ -n_2 & n_1 & 0 \end{bmatrix} \tag{3.2}$$

and $\mathbf{I}$ is the 3 by 3 identity matrix. A geometrical interpretation of the Rodriguez representation of the rotation tensor is given in appendix A.

In equation (3.2), the *spin matrix* representation of a vector was introduced. Spin of a 3D vector $\mathbf{a}$ is defined from

$$\mathbf{a} \times \mathbf{b} = \mathbf{Spin}\,(\mathbf{a})\,\mathbf{b} = -\mathbf{Spin}\,(\mathbf{b})\,\mathbf{a} \tag{3.3}$$

where $\mathbf{b}$ is another 3D vector.

Rotation of a vector $\mathbf{r}_0$ into $\mathbf{r}$ by rotating an angle θ about an axis defined by the unit vector $\mathbf{n}$ is now performed by premultiplication by $\mathbf{R}$:

$$\mathbf{r} = \mathbf{R}\mathbf{r}_0 \tag{3.4}$$

Substitution of equation (3.2) into (3.1) yields the explicit form of the rotation matrix, in terms of the rotation axis and angle

$$\mathbf{R}(\mathbf{n}, \theta) = \begin{bmatrix} 1+(1-c)(n_1^2-1) & (1-c)n_1n_2-n_3s & (1-c)n_1n_3+n_2s \\ (1-c)n_2n_1+n_3s & 1+(1-c)(n_2^2-1) & (1-c)n_2n_3-n_1s \\ (1-c)n_3n_1-n_2s & (1-c)n_3n_2+n_1s & 1+(1-c)(n_3^2-1) \end{bmatrix} \tag{3.5}$$

where $c = \cos\theta$ and $s = \sin\theta$. For a given $\mathbf{R}(\mathbf{n}, \theta)$, the rotation axis $\mathbf{n}$ and the rotation angle θ may be found from the following, in which indices (i, j, k) take on the cyclic permutations of (1, 2, 3):

$$d_i = n_i \sin\theta = \frac{1}{2}\left(R_{kj} - R_{jk}\right) \tag{3.6}$$

Exploiting the fact that $\mathbf{n}$ is a unit vector, that is $\left(n_1^2 + n_2^2 + n_3^2\right) = 1$, the rotation angle can be found from $\sin\theta = \sqrt{d_1^2 + d_2^2 + d_3^2}$. Next, the rotation axis is found from $n_i = d_i/\sin\theta$. Thus the rotation *pseudo-vector* associated with the rotation tensor is

$$\boldsymbol{\theta} = \theta\mathbf{n} = \frac{\theta}{\sin\theta}\begin{bmatrix} d_1 \\ d_2 \\ d_3 \end{bmatrix} \tag{3.7}$$

$\boldsymbol{\theta}$ is called a pseudo-vector because, although it "looks" like a vector it does not have vector properties in the algebraic sense.

Examining (3.7) we find that $\boldsymbol{\theta} \to \mathbf{d}$ as $\theta \to 0$. In order to avoid numerical difficulties related to (3.7), the fraction $\theta/\sin\theta$ should, for small angles, be evaluated from a truncated Taylor series about $\theta = 0$.

If Cayley-Hamilton's theorem[2] is applied to $\mathbf{Spin}\,(\boldsymbol{\theta})$, a comparison between a series representation of the exponential function and $\mathbf{R}(\boldsymbol{\theta})$ yields the following equation:

$$\mathbf{R}(\boldsymbol{\theta}) = e^{\mathbf{Spin}(\boldsymbol{\theta})} \tag{3.8}$$

Inversely, the rotation pseudo-vector $\boldsymbol{\theta}$ is given by

$$\boldsymbol{\theta} = \mathbf{Axial}\,(\mathbf{Spin}\,(\boldsymbol{\theta})) = \mathbf{Axial}\,(\ln\,(\mathbf{R})) \tag{3.9}$$

When it comes to differentiation, equation (3.8) has obvious advantages over equation (3.1).

3.1.2   Configurations and coordinate systems
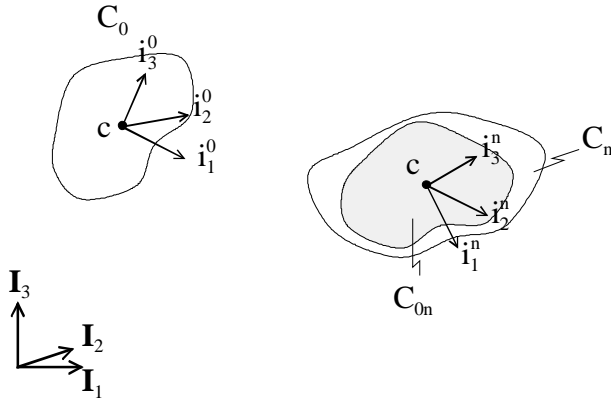
Figure 3.1: *The different configurations and coordinate systems.*

Figure *3.1* shows the different configurations used in this work. The base configuration of a body, is its configuration at the start of the analysis, denoted C_0. Later, the body has been deformed and moved/rotated into another configuration, C_n. Superposed on the body in configuration C_n is the reference configuration C_{0n}. The C_{0n}-configuration is the same as the base configuration C_0, except that it has undergone the same rigid body displacements and rotations as the body when moving from configuration C_0 to C_n. The C_{0n} configuration is frequently also referred to as the *shadow configuration*. In the formulation discussed in this thesis, the shadow configuration is positioned so that it shares area center with configuration C_n.

---

[2]Cayley-Hamilton's theorem: Every square matrix satisfies its own characteristic polynomial[50]. See appendix A.

The deformed configuration C_n and the shadow configuration C_{0n} share a common coordinate system represented by the orthogonal unit vectors $\mathbf{i}_1^n$, $\mathbf{i}_2^n$ and $\mathbf{i}_3^n$. This is the *local coordinate system* of the body, and rotates with the shadow configuration throughout deformation. The fixed global coordinate system is represented by unit vectors $\mathbf{I}_1$, $\mathbf{I}_2$ and $\mathbf{I}_3$.

Subscript n will later be identified with the solution step number in the iterative solution procedure. Vectors given in the local coordinate system are marked with a tilde(˜).

A vector $\mathbf{x}$ in global coordinates is transformed into a vector $\tilde{\mathbf{x}}$ in a local coordinate system by

$$\tilde{\mathbf{x}} = \mathbf{T}\mathbf{x} \tag{3.10}$$

where

$$\mathbf{T} = \begin{bmatrix} \mathbf{i}_1^T \\ \mathbf{i}_2^T \\ \mathbf{i}_3^T \end{bmatrix} \tag{3.11}$$

and $\mathbf{i}_1$, $\mathbf{i}_2$ and $\mathbf{i}_3$ are the three orthonormal vectors defining the local coordinate system. $\mathbf{T}$ is orthonormal, that is $\mathbf{T}^{-1} = \mathbf{T}^T$, and thus the inverse transformation may be written as

$$\mathbf{x} = \mathbf{T}^T\tilde{\mathbf{x}} \tag{3.12}$$

Now, consider two local coordinate systems, the first defined by $\mathbf{i}_1^0$, $\mathbf{i}_2^0$ and $\mathbf{i}_3^0$ and associated with configuration C_0, and the second given by $\mathbf{i}_1^n$, $\mathbf{i}_2^n$ and $\mathbf{i}_3^n$ and associated with configuration C_{0n}. A vector, $\tilde{\mathbf{a}}$, is attached to a local coordinate system as it rigidly moves from configuration C_0 to configuration C_{0n}. In global coordinates, the vector is $\mathbf{a}^0 = \mathbf{T}_0^T\tilde{\mathbf{a}}$ in configuration C_0, and $\mathbf{a}^n = \mathbf{T}_n^T\tilde{\mathbf{a}}$ in configuration C_{0n}. The rotation of $\mathbf{a}^0$ into $\mathbf{a}^n$ is given by

$$\mathbf{a}^n = \mathbf{R}_{0n}\mathbf{a}^0 \tag{3.13}$$

where $\mathbf{R}_{0n}$ is the rigid body rotation tensor from configuration C_0 to configuration C_{0n}.

Writing $\mathbf{a}^n$ and $\mathbf{a}^0$ as transformations of $\tilde{\mathbf{a}}$ into global coordinates, the following expression for the rotation tensor may be obtained

$$\begin{aligned} \mathbf{a}^n &= \mathbf{R}_{0n}\mathbf{a}^0 \\ \mathbf{T}_n^T\tilde{\mathbf{a}} &= \mathbf{R}_{0n}\mathbf{T}_0^T\tilde{\mathbf{a}} \\ \mathbf{T}_n^T\mathbf{T}_0 &= \mathbf{R}_{0n}\mathbf{T}_0^T\mathbf{T}_0 \\ \mathbf{R}_{0n} &= \mathbf{T}_n^T\mathbf{T}_0 \end{aligned} \tag{3.14}$$

Since the transformation matrices are orthogonal, it follows that the rotation matrix is also orthogonal. Thus, the inverse of equation (3.13) is given by

$$\mathbf{a}^0 = \mathbf{R}_{0n}^T \mathbf{a}^n \tag{3.15}$$

3.1.3   Translation of a point from configuration C_0 to configuration C_n.
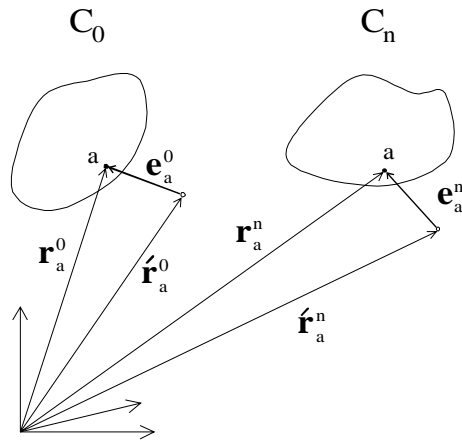
Figure 3.2: *Translation of a point from configuration C_0 to configuration C_n.*

Consider a body as it moves from its initial configuration C_0 to another configuration C_n. During the movement a point identified by subscript a is followed. The point is rigidly attached to another point through the eccentricity vector $\mathbf{e}_a$. The two configurations are shown in figure *3.2*, where the different vectors are denoted by

$\mathbf{r}_a^0, \mathbf{r}_a^n$	-	position vector for point a in configurations C_0 and C_n, respectively
$\acute{\mathbf{r}}_a^0, \acute{\mathbf{r}}_a^n$	-	position vector for eccentricity point in configurations C_0 and C_n, respectively
$\mathbf{e}_a^0, \mathbf{e}_a^n$	-	eccentricity vectors in configurations C_0 and C_n, respectively.

To avoid confusing subscript notation, the a indicating the point is omitted in most of the remaining equations of this chapter.

Handling of rigid eccentricities is included in this formulation because they make a powerful tool for modelling of structures. By using the rigid eccentricities

to model members that are much stiffer than the rest of the members in the structure, these can be handled in a cost-efficient manner without having to worry about the rigid members causing numerical problems. A related area of application is the use of rigid eccentricities for modelling eccentric loading.

Relationships

The relationships between the vectors listed above are as follows:

$$
\begin{aligned}
\mathbf{r}^0 &= \acute{\mathbf{r}}^0 + \mathbf{e}^0 \\
\mathbf{r}^n &= \acute{\mathbf{r}}^n + \mathbf{e}^n \\
&= \acute{\mathbf{r}}^n + \mathbf{R}\mathbf{e}^0
\end{aligned}
\tag{3.16}
$$

$\mathbf{R}$ is the rotation tensor accounting for the rotation of point a between the C_0 configuration and the C_n configuration. This rotation tensor is the subject of the next section.

Displacement vector

The displacement vector is given as the difference between the position vector in configuration C_0 and the position vector in configuration C_n.

$$
\begin{aligned}
\mathbf{u} &= \mathbf{r}^n - \mathbf{r}^0 = \acute{\mathbf{r}}^n + \mathbf{R}\mathbf{e}^0 - \acute{\mathbf{r}}^0 - \mathbf{e}^0 = \acute{\mathbf{u}} + (\mathbf{R} - \mathbf{I})\,\mathbf{e}^0 \\
\acute{\mathbf{u}} &= \acute{\mathbf{r}}^n - \acute{\mathbf{r}}^0
\end{aligned}
\tag{3.17}
$$

Figure *3.3* shows how the displacement vector can be separated into a rigid body displacement vector and a (small) deformational displacement vector. Extracting this field of small deformational displacements is the key to re-using linear finite elements within the co-rotational formulation.

$$
\mathbf{u} = \mathbf{u}_r + \mathbf{u}_d
\tag{3.18}
$$

$\mathbf{u}_r$ - rigid body displacement vector given as the difference between the position vector in initial configuration C_0 and the position vector in shadow configuration C_{0n}.

$\mathbf{u}_d$ - deformational displacement vector given as the difference between the position vector in shadow configuration C_{0n} and the position vector in configuration C_n.
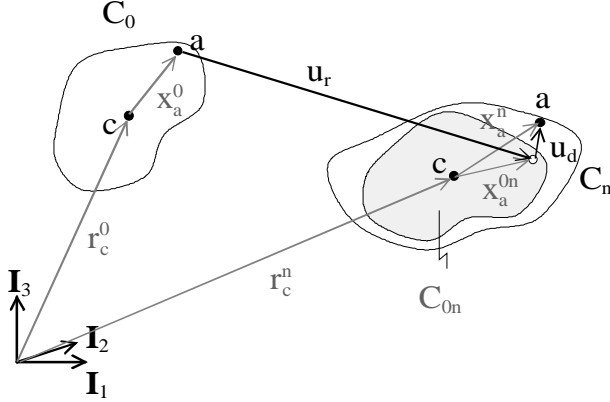
Figure 3.3: *The displacement vector* $\mathbf{u}$ *consists of a rigid body part,* $\mathbf{u}_r$*, and a deformational part,* $\mathbf{u}_d$*.*

Thus, $\mathbf{u}_r$ and $\mathbf{u}_d$ may be expressed as:

$$\mathbf{u}_r = \mathbf{r}^{0n} - \mathbf{r}^0 \qquad (3.19)$$

$$\mathbf{u}_d = \mathbf{r}^n - \mathbf{r}^{0n} \qquad (3.20)$$

Introducing subscript c for the arithmetic mean of the coordinates of all the points in the body[3], the position vectors in initial and shadow element configurations of point a may be written as:

$$\mathbf{r}^0 = \mathbf{r}_c^0 + \mathbf{x}^0 \qquad (3.21)$$

$$\mathbf{r}^{0n} = \mathbf{r}_c^{0n} + \mathbf{x}^{0n}$$

$$= \mathbf{r}_c^0 + \mathbf{u}_c + \mathbf{R}_{0n}\mathbf{x}^0 \qquad (3.22)$$

where $\mathbf{x}^0$ and $\mathbf{x}^{0n}$ are the vectors from the centroid of the body to the point being considered in the C_0 configuration and the C_{0n} configuration respectively.

Substitution of the expressions above into equations (3.18) yields:

$$\mathbf{u}_d = \mathbf{u} - \mathbf{u}_r = \mathbf{u} - (\mathbf{r}^{0n} - \mathbf{r}^0)$$

$$= \mathbf{u} - (\mathbf{r}_c^0 + \mathbf{u}_c + \mathbf{R}_{0n}\mathbf{x}^0 - \mathbf{r}_c^0 - \mathbf{x}^0) \qquad (3.23)$$

$$= \mathbf{u} - \mathbf{u}_c - (\mathbf{R}_{0n} - \mathbf{I})\mathbf{x}^0$$

$\mathbf{u}$ is found from equation (3.17).

---

[3]Thus the centroid in discussion is not necessarily the mass center of the body, although these may (and often do) coincide.

3.1.4 Rotation of a point from configuration C_0 to configuration C_n

The rotation of a point as the body moves from the initial configuration C_0 to the deformed configuration C_n is described by the rotation tensor $\mathbf{R}$. Analogous with the way displacement was treated, the rotation tensor may also be divided into a rigid body rotation tensor $\mathbf{R}_{0n}$ and a deformational rotation tensor $\mathbf{R}_d$. The proper way to "add" rotations, however, is to multiply the rotation tensors. In this multiplication the order is of significance: $\mathbf{R}_d\mathbf{R}_{0n} \neq \mathbf{R}_{0n}\mathbf{R}_d$. Haugen[4] has selected the former multiplication order claiming consistency with *"that employed by Bergan, Rankin and their colleagues."*[10, 14, 9, 51]

$$\mathbf{R} = \mathbf{R}_d\mathbf{R}_{0n} \tag{3.24}$$

Introducing equation (3.14) from page 19 into (3.24), an expression for the deformational rotation tensor is found:

$$\begin{aligned} \mathbf{R} &= \mathbf{R}_d\mathbf{R}_{0n} = \mathbf{R}_d\mathbf{T}_n^T\mathbf{T}_0 \\ \mathbf{R}_d &= \mathbf{R}\mathbf{R}_{0n}^T = \mathbf{R}\mathbf{T}_0^T\mathbf{T}_n \end{aligned} \tag{3.25}$$

The deformational rotation tensor may be transformed into the local coordinate system shared by configurations C_{0n} and C_n through pre-multiplication by $\mathbf{T}_n$ and post-multiplication by $\mathbf{T}_n^T$:

$$\begin{aligned} \tilde{\mathbf{R}}_d &= \mathbf{T}_n\mathbf{R}_d\mathbf{T}_n^T = \mathbf{T}_n\mathbf{R}\mathbf{T}_0^T\mathbf{T}_n\mathbf{T}_n^T \\ &= \mathbf{T}_n\mathbf{R}\mathbf{T}_0^T \end{aligned} \tag{3.26}$$

3.1.5 Element deformational displacement vector

The deformational displacement field $\mathbf{u}_d$ over an element can be obtained from interpolation of displacements at the element nodes.

The position of an element node a with initial coordinates $\mathbf{r}_a^0$, is defined by the translational displacement $\mathbf{u}_a$ and the rotational orientation represented by the pseudo-vector $\boldsymbol{\theta}_a$. Together, the set $(\mathbf{u}_a, \boldsymbol{\theta}_a)$ for $a = 1, ..N$ is the nodal displacement vector $\mathbf{v}$ "visible" to the other elements. It should be stressed that $\mathbf{v}$ is not a true vector, because the components of $\boldsymbol{\theta}_a$ do not transform and add as vectors. "The interpretation of $\mathbf{v}$ as an array of numbers that defines the position of the deformed element is more appropriate."[4]

In order to establish the strain energy, and hence the force vector and tangent stiffness for an element, the deformational displacement vector for the element needs to be established. This vector is denoted $\tilde{\mathbf{v}}_d$ and contains translational and rotational degrees of freedom for each element node ordered as

$$\tilde{\mathbf{v}}_d^T = \left[\tilde{\mathbf{u}}_{d1}^T \tilde{\boldsymbol{\theta}}_{d1}^T \ldots \tilde{\mathbf{u}}_{dN}^T \tilde{\boldsymbol{\theta}}_{dN}^T\right] \tag{3.27}$$

N is the number of element nodes for the element being considered. As the tilde indicates, $\tilde{\mathbf{v}}_d$ is expressed in local coordinates.

Given $\acute{\mathbf{r}}_a^0$, $\mathbf{e}_a^0$, $\acute{\mathbf{u}}_a$ and $\mathbf{R}_a$, $\tilde{\mathbf{v}}_d$ is found by application of the following algorithm:

---

1. Establish the initial local coordinate system $\mathbf{T}_0$ from the initial nodal coordinates, $\mathbf{r}_a^0 = \acute{\mathbf{r}}_a^0 + \mathbf{e}_a^0$, $a = 1 \ldots N$, and form the nodal coordinates in the local coordinate system:

$$\tilde{\mathbf{x}}_a^0 = \mathbf{T}_0 \left(\mathbf{r}_a^0 - \mathbf{r}_c^0\right) \qquad \text{where} \qquad \mathbf{r}_c^0 = \frac{1}{N} \sum_{a=1}^{N} \mathbf{r}_a^0 \tag{3.28}$$

2. Establish the deformed local coordinate system $\mathbf{T}_n$ from the deformed nodal coordinates, $\mathbf{r}_a^n = \acute{\mathbf{r}}_a^0 + \acute{\mathbf{u}}_a + \mathbf{R}_a \mathbf{e}_a^0$, $a = 1 \ldots N$ and form the nodal coordinates in the local system:

$$\tilde{\mathbf{x}}_a^n = \mathbf{T}_n \left(\mathbf{r}_a^n - \mathbf{r}_c^n\right) \qquad \text{where} \qquad \mathbf{r}_c^n = \frac{1}{N} \sum_{a=1}^{N} \mathbf{r}_a^n \tag{3.29}$$

3. Compute deformational translations:

$$\tilde{\mathbf{u}}_{da} = \tilde{\mathbf{x}}_a^n - \tilde{\mathbf{x}}_a^0 \tag{3.30}$$

4. Establish deformational rotation tensor in local coordinates:

$$\tilde{\mathbf{R}}_{da} = \mathbf{T}_n \mathbf{R}_a \mathbf{T}_0^T \tag{3.31}$$

5. Find local deformational rotation pseudo-vector from rotation tensor in local coordinate system:

$$\tilde{\boldsymbol{\theta}}_{da} = \mathbf{Axial}\left(\ln(\tilde{\mathbf{R}}_d)\right) \tag{3.32}$$

6. Collect $\tilde{\mathbf{u}}_{da}$ and $\tilde{\boldsymbol{\theta}}_{da}$ in the element deformational displacement vector:

$$\tilde{\mathbf{v}}_d^T = \left[\tilde{\mathbf{u}}_{d1}^T \tilde{\boldsymbol{\theta}}_{d1}^T \ldots \tilde{\mathbf{u}}_{dN}^T \tilde{\boldsymbol{\theta}}_{dN}^T\right] \tag{3.33}$$

3.2 Variation of the deformational displacement

The force vector and the tangent stiffness matrix of an element will be established from the first and second variation of the strain energy of the element, respectively (see section 3.3).

It is rather straightforward to establish the strain energy using the deformational displacements directly. However, in the derivation of the force vector, the variation of the deformational displacement vector with respect to the element visible degrees of freedom is required. The deformational displacement vector is measured continuously in the local co-rotated frame, whereas the visible degrees of freedom are measured in the global *inertial*[4] frame. Thus, the relevant variation is a variation of a vector measured in a rotating frame with respect to a variation in another vector measured in an inertial frame. Variation of vector $\mathbf{v}_d$ is, by definition

$$(\delta\mathbf{v}_d)_R = \frac{(\partial\mathbf{v}_d)_R}{\partial\mathbf{v}}\delta\mathbf{v} \tag{3.34}$$

The subscript $_R$ is used to indicate that the variation/differential is measured in the co-rotated frame.

In order to obtain the variation of the deformational displacement vector, variation of parts of the deformational displacement are studied one by one, and reassembled after variation.

3.2.1 Degrees of freedom

In the inertial global coordinate system, the degrees of freedom at each node are $\mathbf{v}^T = \begin{bmatrix} \mathbf{u}^T & \boldsymbol{\theta}^T \end{bmatrix}$, where $\boldsymbol{\theta}$ is the pseudo-vector that holds information about the orientation of the node, while $\mathbf{u}$ contains the translations of the node. When taking the variation of $\mathbf{v}$, the *variation* of the orientation is in the infinitesimal linear domain. Hence, the rotations that the variation is performed with respect to, can be represented by an infinitesimal rotation vector, $\delta\boldsymbol{\omega}$. The variatonal degrees of freedom are therefore $\delta\mathbf{v}^T = \begin{bmatrix} \delta\mathbf{u}^T & \delta\boldsymbol{\omega}^T \end{bmatrix}$.

Some of the variations are carried out with respect to the rigid body rotations of the element. These rotations are represented by the orientation of the element shadow configuration, defined by $\mathbf{R}_{0n} = e^{\mathbf{Spin}(\boldsymbol{\theta}_r)}$. The variation of the shadow configuration orientation is taken with respect to $\delta\boldsymbol{\omega}_r$, the instantaneous rotation axis at the coordinate system defined by $\mathbf{R}_{0n}$. The subscript r in $\boldsymbol{\theta}_r$ and

---

[4]An inertial coordinate system is a coordinate system that has constant velocity and no rotation throughout the variation.

$\delta\boldsymbol{\omega}_r$ is used to indicate that these are representations of the orientation of the element shadow configuration.

3.2.2   Variation of the transformation matrix $\mathbf{T}_n$ and the rotation matrix $\mathbf{R}_{0n}$

Since the transformation matrix $\mathbf{T}_n$ transforms a vector from being measured in a global coordinate system to being measured in a local coordinate system, and thus only "changes" the *orientation of the vector*, it is independent of the translation of the element. Hence, $\mathbf{T}_n$ only has a non-zero variation with respect to the rotation of the element. The translation and rotation considered apply to the centre of the element.

$$
\begin{aligned}
\delta\mathbf{T}_n &= \frac{\partial\mathbf{T}_n}{\partial\tilde{\boldsymbol{\omega}}_r}\delta\tilde{\boldsymbol{\omega}}_r \\
&= \begin{bmatrix} \mathbf{0}^T \\ \mathbf{i}_3^{nT} \\ -\mathbf{i}_2^{nT} \end{bmatrix}\delta\tilde{\omega}_{rx} + \begin{bmatrix} -\mathbf{i}_3^{nT} \\ \mathbf{0}^T \\ \mathbf{i}_1^{nT} \end{bmatrix}\delta\tilde{\omega}_{ry} + \begin{bmatrix} \mathbf{i}_2^{nT} \\ -\mathbf{i}_1^{nT} \\ \mathbf{0}^T \end{bmatrix}\delta\tilde{\omega}_{rz} \\
&= \begin{bmatrix} 0 & \delta\tilde{\omega}_{rz} & -\delta\tilde{\omega}_{ry} \\ -\delta\tilde{\omega}_{rz} & 0 & \delta\tilde{\omega}_{rx} \\ \delta\tilde{\omega}_{ry} & -\delta\tilde{\omega}_{rx} & 0 \end{bmatrix}\begin{bmatrix} \mathbf{i}_1^{nT} \\ \mathbf{i}_2^{nT} \\ \mathbf{i}_3^{nT} \end{bmatrix} \\
&= -\mathbf{Spin}\left(\delta\tilde{\boldsymbol{\omega}}_r\right)\mathbf{T}_n
\end{aligned}
\tag{3.35}
$$

Geometrically, this variation is carried out by applying infinitesimally small rotations $\delta\tilde{\boldsymbol{\omega}}_r$ and study the effect this has on the unit vectors defining $\mathbf{T}_n$.

Transformation of $\mathbf{Spin}\left(\delta\tilde{\boldsymbol{\omega}}_r\right)$, expressed in local coordinates, into $\mathbf{Spin}\left(\delta\boldsymbol{\omega}_r\right)$, expressed in global coordinates, is accomplished by pre-multiplication by $\mathbf{T}_n$ and postmultiplication by $\mathbf{T}_n^T$. Utilizing the orthogonality of $\mathbf{T}_n$, variation of the transformation matrix may be written as

$$
\delta\mathbf{T}_n = -\mathbf{Spin}\left(\delta\tilde{\boldsymbol{\omega}}_r\right)\mathbf{T}_n = -\mathbf{T}_n\mathbf{Spin}\left(\delta\boldsymbol{\omega}_r\right)\mathbf{T}_n^T\mathbf{T}_n = -\mathbf{T}_n\mathbf{Spin}\left(\delta\boldsymbol{\omega}_r\right) \tag{3.36}
$$

$\mathbf{Spin}\left(\delta\boldsymbol{\omega}_r\right)$ is anti-symmetric, and the variation of the transposed transformation matrix may therefore be written as

$$
\delta\mathbf{T}_n^T = \mathbf{T}_n^T\mathbf{Spin}\left(\delta\tilde{\boldsymbol{\omega}}_r\right) = \mathbf{Spin}\left(\delta\boldsymbol{\omega}_r\right)\mathbf{T}_n^T \tag{3.37}
$$

The rotation tensor $\mathbf{R}_{0n}$ rotates a vector from the initial configuration to the shadow configuration. Equation (3.14) from page 19 states that this rotation tensor may be written as

$$
\mathbf{R}_{0n} = \mathbf{T}_n^T\mathbf{T}_0 \tag{3.38}
$$

from which the variation of the rotation tensor is found to be

$$
\begin{aligned}
\delta \mathbf{R}_{0n} &= \delta \mathbf{T}_n^T \mathbf{T}_0 + \mathbf{T}_n^T \delta \mathbf{T}_0 = \delta \mathbf{T}_n^T \mathbf{T}_0 = \mathbf{Spin}\left(\delta\boldsymbol{\omega}_r\right) \mathbf{T}_n^T \mathbf{T}_0 \\
&= \mathbf{Spin}\left(\delta\boldsymbol{\omega}_r\right) \mathbf{R}_{0n}
\end{aligned}
\tag{3.39}
$$

3.2.3   Variation of $\mathbf{u}_d$ with respect to v

Haugen[4] expresses the variation of a vector represented in an inertial frame as

$$
\delta\mathbf{x} = (\delta\mathbf{x})_R + \delta\boldsymbol{\omega} \times \mathbf{x} = (\delta\mathbf{x})_R + \mathbf{Spin}\left(\delta\boldsymbol{\omega}\right)\mathbf{x}
\tag{3.40}
$$

where
$(\delta\mathbf{x})_R$ -   variation of the vector measured in the co-rotated frame.
$\delta\boldsymbol{\omega}$ -   variation of the orientation of the frame (measured in the inertial frame).

Equation (3.40) may be used to obtain the variation of co-rotated $\mathbf{u}_d$ with respect to inertial $\mathbf{v}$.

Variation of inertial $\mathbf{u}_d$ with respect to inertial v

Equation (3.23) from page 22 states that the deformational displacement of an element node a is

$$
\mathbf{u}_{da} = \mathbf{u}_a - \mathbf{u}_c - \left(\mathbf{R}_{0n} - \mathbf{I}\right)\mathbf{x}_a^0
\tag{3.41}
$$

where $\mathbf{u}_c$ is the displacement vector of the centroid of the element. As shown previously, it can be replaced by

$$
\mathbf{u}_c = \sum_{b=1}^{N} \frac{1}{N}\mathbf{u}_b
\tag{3.42}
$$

To simplify the resulting equation, we now introduce for $\mathbf{u}_a$

$$
\mathbf{u}_a = \sum_{b=1}^{N} \delta_{ab}\mathbf{u}_b
\tag{3.43}
$$

where δ_{ab} is the Kronecker delta, which has the value 1 for $a = b$ and 0 for $a \neq b$. Substitution of equations (3.42) and (3.43) into (3.41) yields

$$
\begin{aligned}
\mathbf{u}_{da} &= \sum_{b=1}^{N} \left(\delta_{ab} - \tfrac{1}{N}\right)\mathbf{u}_b - \left(\mathbf{R}_{0n} - \mathbf{I}\right)\mathbf{x}_a^0 \\
&= \sum_{b=1}^{N} \mathbf{P}_{ab}\mathbf{u}_b - \left(\mathbf{R}_{0n} - \mathbf{I}\right)\mathbf{x}_a^0 \qquad \text{where} \qquad \mathbf{P}_{ab} = \left(\delta_{ab} - \tfrac{1}{N}\right)\mathbf{I}
\end{aligned}
\tag{3.44}
$$

The variation of inertial $\mathbf{u}_{da}$ with respect to inertial $\mathbf{v}$ may now be found as

$$
\begin{aligned}
\delta\mathbf{u}_{da} &= \sum_{b=1}^{N} \left(\delta\mathbf{P}_{ab}\mathbf{u}_b - \mathbf{P}_{ab}\delta\mathbf{u}_b\right) - \left(\delta\mathbf{R}_{0n} - \delta\mathbf{I}\right)\mathbf{x}_a^0 - \left(\mathbf{R}_{0n} - \mathbf{I}\right)\delta\mathbf{x}_a^0 \\
&= \sum_{b=1}^{N} \mathbf{P}_{ab}\delta\mathbf{u}_b - \delta\mathbf{R}_{0n}\mathbf{x}_a^0
\end{aligned}
\tag{3.45}
$$

since $\delta\mathbf{P}_{ab} = \mathbf{0}$, $\delta\mathbf{I} = \mathbf{0}$ and $\delta\mathbf{x}_a^0 = \mathbf{0}$. Using equation (3.39) as a substitute for $\delta\mathbf{R}_{0n}$, the last term in (3.45) may be written as

$$
\begin{aligned}
\delta\mathbf{R}_{0n}\mathbf{x}_a^0 &= \mathbf{Spin}\left(\delta\boldsymbol{\omega}_r\right)\mathbf{R}_{0n}\mathbf{x}_a^0 = \mathbf{Spin}\left(\delta\boldsymbol{\omega}_r\right)\mathbf{x}_a^{0n} \\
&= -\mathbf{Spin}\left(\mathbf{x}_a^{0n}\right)\delta\boldsymbol{\omega}_r \\
&= -\mathbf{Spin}\left(\mathbf{x}_a^{0n}\right)\mathbf{G}\delta\mathbf{v}
\end{aligned}
\tag{3.46}
$$

The matrix $\mathbf{G}$ connects the variation of the rigid body rotation to the variation of the visible node displacements:

$$
\delta\boldsymbol{\omega}_r = \frac{\partial\boldsymbol{\omega}_r}{\partial v_i}\delta v_i = \mathbf{G}\delta\mathbf{v} = \sum_{b=1}^{N}\mathbf{G}_b\delta\mathbf{v}_b
\tag{3.47}
$$

The matrix $\mathbf{G}_b$ is an element-*type* dependent matrix. That is, it is the same for all three-noded shell elements with six dofs at each node, while it is for instance different for three-noded shell elements and two-noded beam elements, although the dofs at the nodes are the same. As indicated by equation (3.47), $\mathbf{G}$ may be split into its nodal submatrices $\mathbf{G}_a$. In appendix B, $\mathbf{G}$ is derived for a beam element with two nodes and six degrees of freedom at each node.

Substitution of (3.46) into (3.45) yields the expression for the variation of inertial $\mathbf{u}_d$ with respect to inertial $\mathbf{v}$

$$
\delta\mathbf{u}_{da} = \sum_{b=1}^{N}\left(\begin{bmatrix} \mathbf{P}_{ab} & \mathbf{0} \end{bmatrix} + \mathbf{Spin}\left(\mathbf{x}_a^{0n}\right)\mathbf{G}_b\right)\delta\mathbf{v}_b
\tag{3.48}
$$

$\delta\mathbf{v}_b$ is the vector of inertial degrees of freedom vector for node b. That is: $\delta\mathbf{v}_b^T = \begin{bmatrix} \delta\mathbf{u}_b^T & \delta\boldsymbol{\omega}_b^T \end{bmatrix}$.

Variation of co-rotated $\mathbf{u}_d$ with respect to inertial $\mathbf{v}$

The relationship defining the variation of inertial deformational displacement with respect to inertial degrees of freedom is now established. Recalling the

relationship $\mathbf{u}_{da} = \mathbf{x}_a^n - \mathbf{x}_a^{0n}$, we find that the variation of the deformational displacement vector measured in the co-rotated frame, with respect to inertial degrees of freedom is given by

$$(\delta\mathbf{u}_{da})_R = (\delta\mathbf{x}_a^n)_R - (\delta\mathbf{x}_a^{0n})_R = (\delta\mathbf{x}_a^n)_R \tag{3.49}$$

since $(\delta\mathbf{x}_a^{0n})_R = \mathbf{0}$.

Since $\mathbf{x}_a^n = \mathbf{R}_{0n}\mathbf{x}_a^0 + \mathbf{u}_{da}$, the variation of inertial $\mathbf{x}_a^n$ with respect to inertial degrees of freedom is given by

$$
\begin{aligned}
\delta\mathbf{x}_a^n &= \delta\mathbf{R}_{0n}\mathbf{x}_a^0 + \mathbf{R}_{0n}\delta\mathbf{x}_a^0 + \delta\mathbf{u}_{da} \\
&= \delta\mathbf{R}_{0n}\mathbf{x}_a^0 + \delta\mathbf{u}_{da} \\
&= \mathbf{Spin}\left(\delta\boldsymbol{\omega}_r\right)\mathbf{R}_{0n}\mathbf{x}_a^0 + \sum_{b=1}^{N}\mathbf{P}_{ab}\delta\mathbf{u}_b - \mathbf{Spin}\left(\delta\boldsymbol{\omega}_r\right)\mathbf{x}_a^{0n} \\
&= \mathbf{Spin}\left(\delta\boldsymbol{\omega}_r\right)\mathbf{x}_a^{0n} - \mathbf{Spin}\left(\delta\boldsymbol{\omega}_r\right)\mathbf{x}_a^{0n} + \sum_{b=1}^{N}\mathbf{P}_{ab}\delta\mathbf{u}_b \\
&= \sum_{b=1}^{N}\mathbf{P}_{ab}\delta\mathbf{u}_b
\end{aligned}
\tag{3.50}
$$

Substituting $\mathbf{x}_a^n$ for $\mathbf{x}$ in equation (3.40) from page 27 and solving with respect to $(\delta\mathbf{x}_a^n)_R$, the following expression for $(\delta\mathbf{x}_a^n)_R$ is obtained:

$$
\begin{aligned}
(\delta\mathbf{x}_a^n)_R &= \sum_{b=1}^{N}\mathbf{P}_{ab}\delta\mathbf{u}_b - \mathbf{Spin}\left(\delta\boldsymbol{\omega}_r\right)\mathbf{x}_a^n \\
&= \sum_{b=1}^{N}\mathbf{P}_{ab}\delta\mathbf{u}_b + \mathbf{Spin}\left(\mathbf{x}_a^n\right)\delta\boldsymbol{\omega}_r \\
&= \sum_{b=1}^{N}\left(\left[\begin{array}{cc}\mathbf{P}_{ab} & \mathbf{0}\end{array}\right] + \mathbf{Spin}\left(\mathbf{x}_a^n\right)\mathbf{G}_b\right)\delta\mathbf{v}_b
\end{aligned}
\tag{3.51}
$$

Since, according to equation (3.49), $(\delta\mathbf{u}_{da})_R = (\delta\mathbf{x}_a^n)_R$, the variation of the co-rotated deformational displacement vector, with respect to inertial degrees of freedom, may now be expressed as

$$(\delta\mathbf{u}_{da})_R = \sum_{b=1}^{N}\left(\left[\begin{array}{cc}\mathbf{P}_{ab} & \mathbf{0}\end{array}\right] + \mathbf{Spin}\left(\mathbf{x}_a^n\right)\mathbf{G}_b\right)\delta\mathbf{v}_b \tag{3.52}$$

If equations (3.48) and (3.52) are compared, it is seen that they differ in the argument to the $\mathbf{Spin}\left(\right)$-term only. The variation in inertial system has $\mathbf{Spin}\left(\mathbf{x}_a^{0n}\right)$, whereas the variation in the co-rotated system involves $\mathbf{Spin}\left(\mathbf{x}_a^n\right)$.

3.2.4   Variation of co-rotated $\boldsymbol{\theta}_d$ with respect to inertial v

As was the case for co-rotated deformational displacement, the variation of the co-rotated deformational rotations with respect to inertial degrees of freedom can not be found directly. However, the variation of the co-rotated deformational (finite) rotations with respect to the co-rotated (infinitesimal) rotations was investigated by Nour-Omid and Rankin [15] based on a relationship established by Simo [49] and Szwabowicz [52].

$$(\delta\boldsymbol{\theta}_{da})_R = \frac{\partial\boldsymbol{\theta}_{da}}{\partial\boldsymbol{\omega}_{da}}(\delta\boldsymbol{\omega}_{da})_R = \frac{\partial\left(\mathbf{Axial}\left(\ln(\mathbf{R}_{da})\right)\right)}{\partial\boldsymbol{\omega}_{da}}(\delta\boldsymbol{\omega}_{da})_R = \mathbf{H}_a(\delta\boldsymbol{\omega}_{da})_R \quad (3.53)$$

The matrix $\mathbf{H}_a$ is in [15] defined as

$$\mathbf{H}_a = \frac{\partial\boldsymbol{\theta}_a}{\partial\boldsymbol{\omega}} = \mathbf{I} - \frac{1}{2}\mathbf{Spin}\left(\boldsymbol{\theta}_a\right) + \eta\mathbf{Spin}\left(\boldsymbol{\theta}_a\right)^2 \qquad (3.54)$$

where

$$\eta = \frac{\sin(\frac{1}{2}\theta_a) - \frac{1}{2}\theta_a\cos(\frac{1}{2}\theta_a)}{\theta_a^2\sin(\frac{1}{2}\theta_a)} \qquad \text{and} \qquad \theta_a = \sqrt{\boldsymbol{\theta}_a^T\boldsymbol{\theta}_a} = \|\theta_a\| \qquad (3.55)$$

As $\theta_a \to 0$, $\eta \to 0/0$ which may cause numerical problems for small rotation angles. To avoid these problems, η should be computed from a truncated power series for small values of θ_a:

$$\eta \approx \frac{1}{12} + \frac{1}{720}\theta_a^2 + \frac{1}{30240}\theta_a^4 \qquad \text{for} \qquad \theta_a < 0.05\text{radians} \qquad (3.56)$$

The variation of the co-rotated deformational rotation $(\delta\boldsymbol{\omega}_{da})_R$, with respect to inertial degrees of freedom, is the difference between variation of nodal rotation $\delta\boldsymbol{\omega}_a$ and of rigid body rotation $\delta\boldsymbol{\omega}_r$, both varied with respect to inertial degrees of freedom.

$$(\delta\boldsymbol{\omega}_{da})_R = \delta\boldsymbol{\omega}_r - \delta\boldsymbol{\omega}_a = \delta\boldsymbol{\omega}_a - \frac{\partial\boldsymbol{\omega}_r}{\partial v_i}\delta v_i = \delta\boldsymbol{\omega}_a - \mathbf{G}\delta\mathbf{v} \qquad (3.57)$$

$\mathbf{G}$ is defined in equation (3.47). $\delta\boldsymbol{\omega}_{da}$ can now be written as

$$(\delta\boldsymbol{\omega}_{da})_R = \sum_{b=1}^{N}\left(\delta_{ab}\begin{bmatrix}\mathbf{0} & \mathbf{I}\end{bmatrix} - \mathbf{G}_b\right)\delta\mathbf{v}_b \qquad (3.58)$$

since $\delta\mathbf{v}_b^T = \begin{bmatrix}\delta\mathbf{u}_b^T & \delta\boldsymbol{\omega}_b^T\end{bmatrix}$. Introducing (3.58) into equation (3.53) yields the final expression for the variation of co-rotated deformational rotation with respect to inertial degrees of freedom.

$$(\delta\boldsymbol{\theta}_{da})_R = \mathbf{H}_a\sum_{b=1}^{N}\left(\delta_{ab}\begin{bmatrix}\mathbf{0} & \mathbf{I}\end{bmatrix} - \mathbf{G}_b\right)\delta\mathbf{v}_b \qquad (3.59)$$

3.2.5   Variation of inertial v with respect to inertial v́

If degrees of freedom are located at eccentric nodes, the nodal degrees of freedom are defined as

$$
\begin{aligned}
\mathbf{v}_a^T &= \left[\begin{array}{cc} \mathbf{u}_a^T & \boldsymbol{\theta}_a^T \end{array} \right] & \text{Element domain (dummy) dofs} \\
\acute{\mathbf{v}}_a^T &= \left[\begin{array}{cc} \acute{\mathbf{u}}_a^T & \acute{\boldsymbol{\theta}}_a^T \end{array} \right] & \text{Eccentrically located (visible) dofs}
\end{aligned}
\tag{3.60}
$$

which in variational form are reduced to

$$
\begin{aligned}
\delta\mathbf{v}_a^T &= \left[\begin{array}{cc} \delta\mathbf{u}_a^T & \delta\boldsymbol{\omega}_a^T \end{array} \right] \\
\delta\acute{\mathbf{v}}_a^T &= \left[\begin{array}{cc} \delta\acute{\mathbf{u}}_a^T & \delta\acute{\boldsymbol{\omega}}_a^T \end{array} \right]
\end{aligned}
\tag{3.61}
$$

The relationships connecting the two sets of degrees of freedom are

$$
\begin{aligned}
\mathbf{u}_a &= \acute{\mathbf{u}}_a + (\mathbf{R}_a - \mathbf{I})\,\mathbf{e}_a^0 \\
\boldsymbol{\theta}_a &= \acute{\boldsymbol{\theta}}_a
\end{aligned}
\tag{3.62}
$$

The variation of these relationships with respect to inertial degrees of freedom can be expressed as

$$
\begin{aligned}
\delta\mathbf{u}_a &= \delta\acute{\mathbf{u}}_a + \delta\mathbf{R}_a\mathbf{e}_a^0 = \delta\acute{\mathbf{u}}_a + \mathbf{Spin}\,(\delta\boldsymbol{\omega}_a)\,\mathbf{R}_a\mathbf{e}_a^0 \\
&= \delta\acute{\mathbf{u}}_a + \mathbf{Spin}\,(\delta\boldsymbol{\omega}_a)\,\mathbf{e}_a^n = \delta\acute{\mathbf{u}}_a - \mathbf{Spin}\,(\mathbf{e}_a^n)\,\delta\boldsymbol{\omega}_a \\
\delta\boldsymbol{\omega}_a &= \delta\acute{\boldsymbol{\omega}}_a
\end{aligned}
\tag{3.63}
$$

For a more compact form, equation (3.63) may be rewritten as

$$
\delta\mathbf{v}_a = \mathbf{E}_a\delta\acute{\mathbf{v}}_a \qquad \text{where} \qquad \mathbf{E}_a = \left[\begin{array}{cc} \mathbf{I} & -\mathbf{Spin}\,(\mathbf{e}_a^n) \\ \mathbf{0} & \mathbf{I} \end{array} \right]
\tag{3.64}
$$

3.2.6   The variation of co-rotated $\mathbf{v}_d$ with respect to inertial v́ - putting it all together

For an element with N nodes, the nodal degrees of freedom within $\mathbf{v}$ are ordered as follows

$$
\mathbf{v}^T = \left[\begin{array}{ccccc} \mathbf{u}_1^T & \boldsymbol{\theta}_1^T & \cdots & \mathbf{u}_N^T & \boldsymbol{\theta}_N^T \end{array} \right]
\tag{3.65}
$$

If equations (3.52) and (3.59) are ordered accordingly, the result is

$$
\begin{bmatrix}
(\delta\mathbf{u}_{d1})_R \\
(\delta\boldsymbol{\theta}_{d1})_R \\
\vdots \\
(\delta\mathbf{u}_{dN})_R \\
(\delta\boldsymbol{\theta}_{dN})_R
\end{bmatrix}
=
\begin{bmatrix}
\mathbf{I} & \mathbf{0} & \dots & \mathbf{0} & \mathbf{0} \\
\mathbf{0} & \mathbf{H}_1 & \dots & \mathbf{0} & \mathbf{0} \\
\vdots & \vdots & \ddots & \vdots & \vdots \\
\mathbf{0} & \mathbf{0} & \dots & \mathbf{I} & \mathbf{0} \\
\mathbf{0} & \mathbf{0} & \dots & \mathbf{0} & \mathbf{H}_N
\end{bmatrix}
\cdot
\left(
\begin{bmatrix}
\mathbf{P}_{11} & \mathbf{0} & \dots & \mathbf{P}_{1N} & \mathbf{0} \\
\mathbf{0} & \mathbf{I} & \dots & \mathbf{0} & \mathbf{0} \\
\vdots & \vdots & \ddots & \vdots & \vdots \\
\mathbf{P}_{N1} & \mathbf{0} & \dots & \mathbf{P}_{NN} & \mathbf{0} \\
\mathbf{0} & \mathbf{0} & \dots & \mathbf{0} & \mathbf{I}
\end{bmatrix}
\right.
$$

$$
+
\left.
\begin{bmatrix}
\mathbf{Spin}\,(\mathbf{x}_1^n)\,\mathbf{G}_1 & \dots & \mathbf{Spin}\,(\mathbf{x}_1^n)\,\mathbf{G}_N \\
-\mathbf{G}_1 & \dots & -\mathbf{G}_N \\
\vdots & \ddots & \vdots \\
\mathbf{Spin}\,(\mathbf{x}_N^n)\,\mathbf{G}_1 & \dots & \mathbf{Spin}\,(\mathbf{x}_N^n)\,\mathbf{G}_N \\
-\mathbf{G}_1 & \dots & -\mathbf{G}_N
\end{bmatrix}
\right)
\begin{bmatrix}
\delta\mathbf{u}_1 \\
\delta\boldsymbol{\theta}_1 \\
\vdots \\
\delta\mathbf{u}_N \\
\delta\boldsymbol{\theta}_N
\end{bmatrix}
\tag{3.66}
$$

Where $\mathbf{P}_{ab}$ is defined in equation (3.44) to be:

$$
\mathbf{P}_{ab} = \left(\delta_{ab} - \frac{1}{N}\right)\mathbf{I} =
\begin{cases}
\mathbf{I} - \frac{1}{N}\mathbf{I} & \text{for} \quad a = b \\
-\frac{1}{N}\mathbf{I} & \text{for} \quad a \neq b
\end{cases}
\tag{3.67}
$$

With further simplification, $(\delta\mathbf{v}_d)_R$ may be written as

$$
(\delta\mathbf{v}_d)_R \quad = \quad
\begin{bmatrix}
\mathbf{H}_{11} & \dots & \mathbf{0} \\
\vdots & \ddots & \vdots \\
\mathbf{0} & \dots & \mathbf{H}_{NN}
\end{bmatrix}
\cdot
\left(
\begin{bmatrix}
\mathbf{I} & \dots & \mathbf{0} \\
\vdots & \ddots & \vdots \\
\mathbf{0} & \dots & \mathbf{I}
\end{bmatrix}
\right.
$$

$$
-
\begin{bmatrix}
\mathbf{P}_{T11} & \dots & \mathbf{P}_{T1N} \\
\vdots & \ddots & \vdots \\
\mathbf{P}_{TN1} & \dots & \mathbf{P}_{TNN}
\end{bmatrix}
-
\begin{bmatrix}
\mathbf{S}_1 \\
\mathbf{I} \\
\vdots \\
\mathbf{S}_N \\
\mathbf{I}
\end{bmatrix}
\begin{bmatrix}
\mathbf{G}_1^T \\
\vdots \\
\mathbf{G}_N^T
\end{bmatrix}^T
\left.
\vphantom{\begin{bmatrix}\mathbf{S}_1\\\mathbf{I}\\\vdots\\\mathbf{S}_N\\\mathbf{I}\end{bmatrix}}
\right)
\delta\mathbf{v}
\tag{3.68}
$$

$$
= \quad \mathbf{H}\,(\mathbf{I} - \mathbf{P}_T - \mathbf{P}_R)\,\delta\mathbf{v} = \mathbf{HP}\delta\mathbf{v}
$$

Where

$$
\mathbf{P}_{T_{ab}} =
\begin{bmatrix}
\frac{1}{N}\mathbf{I} & \mathbf{0} \\
\mathbf{0} & \mathbf{0}
\end{bmatrix}
\qquad \text{and} \qquad
\mathbf{H}_{aa} =
\begin{bmatrix}
\mathbf{I} & \mathbf{0} \\
\mathbf{0} & \mathbf{H}_a
\end{bmatrix}
\tag{3.69}
$$

while

$$
\mathbf{S}_a =
\begin{bmatrix}
-\mathbf{Spin}\,(\mathbf{x}_a^n) \\
\mathbf{I}
\end{bmatrix}
\tag{3.70}
$$

Finally $\mathbf{I} - \mathbf{P}_T - \mathbf{P}_R$ is abbreviated into $\mathbf{P}$. Matrix $\mathbf{P}$ is a nonlinear projector operator, shown by Haugen[4] to satisfy $\mathbf{P}^2 = \mathbf{P}$, which is a necessary characteristic of a projector matrix.

In order to accommodate nodal eccentricities, the eccentrically located degrees of freedom $\acute{\mathbf{v}}_a$ are used instead of the element degrees of freedom $\mathbf{v}_a$. The relationship between the variation of eccentric degrees of freedom $\delta\acute{\mathbf{v}}_a$ and the variation of dummy degrees of fredom $\delta\mathbf{v}_a$ was previously found to be

$$\delta\mathbf{v}_a = \mathbf{E}_a \delta\acute{\mathbf{v}}_a \qquad \text{where} \qquad \mathbf{E}_a = \left[\begin{array}{cc} \mathbf{I} & -\mathbf{Spin}\left(\mathbf{e}_a^n\right) \\ \mathbf{0} & \mathbf{I} \end{array} \right] \qquad (3.71)$$

Observe that for all nodes with eccentricity vector $\mathbf{e}_a^n = \mathbf{0}$, $\mathbf{E}_a$ reduces to the identity matrix, thus leaving the dummy degrees of freedom unchanged for that node. For an element with N nodes, (3.71) expands to

$$\delta\mathbf{v} = \left[\begin{array}{cccc} \mathbf{E}_1 & \mathbf{0} & \ldots & \mathbf{0} \\ \mathbf{0} & \mathbf{E}_2 & \ldots & \mathbf{0} \\ \vdots & \vdots & \ddots & \vdots \\ \mathbf{0} & \mathbf{0} & \ldots & \mathbf{E}_N \end{array} \right] \delta\acute{\mathbf{v}} = \mathbf{E}\delta\acute{\mathbf{v}} \qquad (3.72)$$

Introduction of equation (3.72) into equation (3.68), finally yields the expression for the variation of co-rotated deformational displacement vector with respect to inertial, eccentric, degrees of freedom for an element with N nodes:

$$(\delta\mathbf{v}_d)_R = \mathbf{HPE}\delta\acute{\mathbf{v}} \qquad (3.73)$$

The variation of the co-rotated deformational displacement vector has now been found with respect to a set of inertial degrees of freedom. The choice of inertial system has, however, not been specified. To enable use of already existing linear elements in the rotating frame, the inertial system is chosen to be that of the shadow element configuration. Thus, equation (3.68) may be rewritten as

$$(\delta\tilde{\mathbf{v}}_d)_R = \tilde{\mathbf{H}}\tilde{\mathbf{P}}\delta\tilde{\mathbf{v}} \qquad (3.74)$$

Since the visible degrees of freedom are defined in the global coordinate system, the variation needed is $(\delta\mathbf{v}_d)_R$ with respect to $\delta\mathbf{v}$. Taking advantage of the transformation between local and global coordinate systems, and expressing the eccentricity matrix $\mathbf{E}$ in global coordinates, equation (3.73) may finally be written as

$$(\delta\tilde{\mathbf{v}}_d)_R = \tilde{\mathbf{H}}\tilde{\mathbf{P}}\mathbf{T}_n\delta\mathbf{v} = \tilde{\mathbf{H}}\tilde{\mathbf{P}}\mathbf{TE}\delta\acute{\mathbf{v}} \qquad (3.75)$$

3.3 Potential energy

In this section the potential energy of a displacement based co-rotated element is established. From the strain energy, the internal force vector of the element is derived by means of variation. Finally, the tangent stiffness is found through variation of the force vector.

3.3.1   Minimum potential energy

The potential energy, Π, of a system is defined as the systems *ability* to do work.

Consider a body subjected to a pointload P at point S and distributed loading $\boldsymbol{\tau}$ over the area A_τ (fig. *3.4*). The volume of the body is V. P and $\boldsymbol{\tau}$ are *conservative*, that is they are independent of the displacement history, and thus only functions of the final displacement state and not on the path to this state. The material of the body is hyperelastic, that is: The same stress-strain relationship applies both in loading and in unloading.
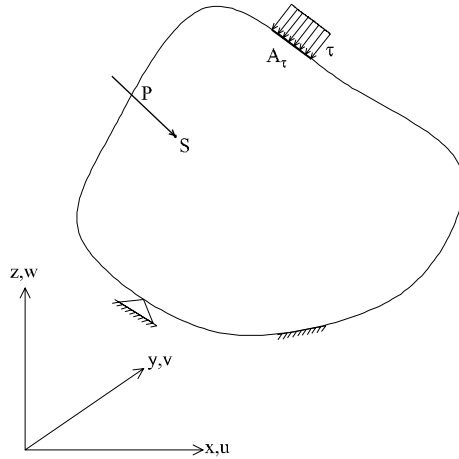
Figure 3.4: *Body subjected to point load and distributed load.*

The load potential of the forces acting on the body is:

$$H = \int_{A_\tau} \boldsymbol{\tau} \mathbf{u} \, dA + P\mathbf{u} \tag{3.76}$$

where $\mathbf{u} = \begin{bmatrix} u & v & w \end{bmatrix}^T$ is the displacement vector of the point at which the load acts.

The strain energy of the system is given by

$$U = \int_V \int_0^{\epsilon} \boldsymbol{\sigma}^T d\boldsymbol{\epsilon} \, dV \tag{3.77}$$

Thus, the total potential energy of the body is given by

$$\Pi = U - H \tag{3.78}$$

According to the principle of stationary energy, the prerequisite for static equilibrium of the body is

$$\delta\Pi = \delta U - \delta H = 0 \tag{3.79}$$

3.3.2 Consistent element formulation

An element formulation is said to be *consistent* if the force vector is found through variation of the strain energy of the element and the tangent stiffness matrix is found through variation of the force vector. A consistent formulation ensures that all the phenomena included when establishing the strain energy will also be accounted for in the force vector and the stiffness matrix.

Thus, for an element with strain energy U, the consistent force vector, $\mathbf{f}$, is found from

$$\delta U = \frac{\partial U}{\partial v_i}\delta v_i = \delta \mathbf{v}^T \mathbf{f} \tag{3.80}$$

whereas the consistent tangent stiffness matrix, $\mathbf{k}_T$, is found from the relationship

$$\delta^2 U = \frac{\partial}{\partial v_j}\left(\frac{\partial U}{\partial v_i}\delta v_i\right)\delta v_j = \frac{\partial^2 U}{\partial v_i \partial v_j}\delta v_i \delta v_j = \delta \mathbf{v}^T \mathbf{k}_T \delta \mathbf{v} \tag{3.81}$$

When Newton's method is used for the correctional steps in an iterative nonlinear analysis procedure (see section 3.4.1), the best rate of convergence towards the correct solution is in general obtained by using a tangent stiffness matrix that is consistent with the internal force vector used.

3.3.3 Strain energy of a displacement based co-rotated element

For the local coordinate system, the relationship between strain $\tilde{\boldsymbol{\epsilon}}$ and deformational displacement $\tilde{\mathbf{v}}_d$ is expressed as

$$\tilde{\boldsymbol{\epsilon}} = \tilde{\mathbf{B}}\tilde{\mathbf{v}}_d \tag{3.82}$$

The strain displacement matrix $\tilde{\mathbf{B}}$ is by choice expressed with respect to the shadow element configuration C_{0n} in order to use engineering strains. This approach is consistent with that employed by Nour-Omid and Rankin [15].

The stress vector is in general $\tilde{\boldsymbol{\sigma}}(\tilde{\boldsymbol{\epsilon}})$. As defined above, the strain energy of the

element is now written as

$$U = \int_V \int_0^\epsilon \tilde{\boldsymbol{\sigma}}^T d\tilde{\boldsymbol{\epsilon}} dV \tag{3.83}$$

3.3.4   Consistent internal force vector

The force vector of the element in local coordinates is by definition given by the first variation of U:

$$\delta U = \int_V \tilde{\boldsymbol{\sigma}} \delta \tilde{\boldsymbol{\epsilon}} dV = \int_V \tilde{\boldsymbol{\sigma}} \tilde{\mathbf{B}} (\delta \tilde{\mathbf{v}}_d)_R = (\delta \tilde{\mathbf{v}}_d^T)_R \int_V \tilde{\mathbf{B}}^T \tilde{\boldsymbol{\sigma}} = (\delta \tilde{\mathbf{v}}_d^T)_R \tilde{\mathbf{f}}_e \tag{3.84}$$

where

$$\tilde{\mathbf{f}}_e = \int_V \tilde{\mathbf{B}}^T \tilde{\boldsymbol{\sigma}} \tag{3.85}$$

$\tilde{\mathbf{f}}_e$ is the internal force vector of the element, expressed in local coordinates. However, since the system equations are assembled in the global coordinate system, it is necessary to also find the internal force vector in global coordinates. By substituting the transposed of equation (3.75) from page 33 for $(\delta \tilde{\mathbf{v}}_d^T)_R$ into equation (3.84), the internal force vector expressed in global coordinates is obtained:

$$\delta U = (\delta \tilde{\mathbf{v}}_d^T)_R \tilde{\mathbf{f}}_e = \left(\tilde{\mathbf{H}} \tilde{\mathbf{P}} \mathbf{T} \mathbf{E} \delta \acute{\mathbf{v}} \right)^T \tilde{\mathbf{f}}_e = \delta \acute{\mathbf{v}}^T \mathbf{E}^T \mathbf{T}^T \tilde{\mathbf{P}}^T \tilde{\mathbf{H}}^T \tilde{\mathbf{f}}_e = \delta \acute{\mathbf{v}}^T \mathbf{f} \tag{3.86}$$

Where $\mathbf{f}$ is the internal force vector expressed in the global coordinate system.

$$\mathbf{f} = \mathbf{E}^T \mathbf{T}^T \tilde{\mathbf{P}}^T \tilde{\mathbf{H}}^T \tilde{\mathbf{f}}_e \tag{3.87}$$

3.3.5   Consistent tangent stiffness

In addition to ensuring a good rate of convergence for the correctional steps in an iterative nonlinear analysis procedure, the use of a consistent tangent stiffness in a linearized buckling type analysis guarantees that all the effects accounted for in the internal force vector are also considered in the buckling analysis.

Consistent tangent stiffness is defined by the variation of the internal force vector $\mathbf{f}$ with respect to the visible degrees of freedom, $\acute{\mathbf{v}}$:

$$\delta \mathbf{f} = \frac{\partial \mathbf{f}}{\partial \acute{\mathbf{v}}} \delta \acute{\mathbf{v}} = \mathbf{K}_T \delta \acute{\mathbf{v}} \tag{3.88}$$

Applying (3.88) to (3.87) yields:

$$
\begin{aligned}
\delta \mathbf{f} &= \delta \mathbf{E}^T \mathbf{T}^T \tilde{\mathbf{P}}^T \tilde{\mathbf{H}}^T \tilde{\mathbf{f}}_e + \mathbf{E}^T \delta \mathbf{T}^T \tilde{\mathbf{P}}^T \tilde{\mathbf{H}}^T \tilde{\mathbf{f}}_e + \mathbf{E}^T \mathbf{T}^T \delta \tilde{\mathbf{P}}^T \tilde{\mathbf{H}}^T \tilde{\mathbf{f}}_e \\
&+ \mathbf{E}^T \mathbf{T}^T \tilde{\mathbf{P}}^T \delta \tilde{\mathbf{H}}^T \tilde{\mathbf{f}}_e + \mathbf{E}^T \mathbf{T}^T \tilde{\mathbf{P}}^T \tilde{\mathbf{H}}^T \delta \tilde{\mathbf{f}}_e \quad\quad\quad (3.89) \\
&= \left(\mathbf{K}_{GE} + \mathbf{K}_{GR} + \mathbf{K}_{GP} + \mathbf{K}_{GM} + \mathbf{K}_{MG} \right) \delta \acute{\mathbf{v}} = \mathbf{K}_T \delta \acute{\mathbf{v}}
\end{aligned}
$$

The different terms of the tangent stiffness[5] are as follows

$\mathbf{K}_{GE}$ - eccentricity geometric stiffness
$\mathbf{K}_{GR}$ - rotational geometric stiffness
$\mathbf{K}_{GP}$ - projection geometric stiffness
$\mathbf{K}_{GM}$ - moment correction geometric stiffness
$\mathbf{K}_{MG}$ - material and internal geometric stiffness

In the following, each of the contributions to the tangent stiffness will be explained in detail.

Eccentricity geometric stiffness

The eccentricity geometric stiffness arises from variation of the eccentricity matrix $\mathbf{E}$, and relates the changes in the internal force vector due to changes in the eccentrically located degrees of freedom. In linearized buckling analysis, this stiffness term enables the model to account for the effect of nodal eccentricity on the buckling load.

Example: If the eccentricity geometric stiffness is omitted in linearized buckling analyses of the two cantilever beams shown in figure 3.5, the two analyses will be yielding the exact same buckling load, as long as the eccentricity is modelled by use of the mathematical approach presented in this chapter.
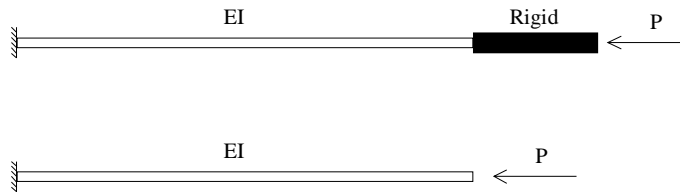

Figure 3.5: *Cantilevers subjected to axial loading at the free end.*

---

[5]The tangent stiffness is divided into *material stiffness* and *geometric stiffness*. Material stiffness is independent of the state of stress in the element. Geometric stiffness on the other hand, depends on the state of stress in the element, and more specifically, it is zero for a zero stress state.

If the eccentricity geometric stiffness is included, the linearized buckling analysis will yield a buckling load for the cantilever subjected to the eccentrically positioned load that is less than that for the cantilever without the rigid eccentricity.

For an N-noded element, the transposed of the eccentricity matrix $\mathbf{E}$ is defined in equation (3.72) on page 33. Variation of $\mathbf{E}^T$ is given by:

$$\delta\mathbf{E}^T = \begin{bmatrix} \delta\mathbf{E}_1^T & \mathbf{0} & \cdots & \mathbf{0} \\ \mathbf{0} & \delta\mathbf{E}_2^T & \cdots & \mathbf{0} \\ \vdots & \vdots & \ddots & \delta\mathbf{E}_N^T \end{bmatrix} \tag{3.90}$$

Variation of the nodal eccentricity matrix $\mathbf{E}_a$ is given by

$$\delta\mathbf{E}_a^T = \begin{bmatrix} \delta\mathbf{I} & \mathbf{0} \\ -\delta\mathbf{Spin}\left(\mathbf{e}_a^n\right) & \delta\mathbf{I} \end{bmatrix} = \begin{bmatrix} \mathbf{0} & \mathbf{0} \\ -\mathbf{Spin}\left(\delta\mathbf{e}_a^n\right) & \mathbf{0} \end{bmatrix} \tag{3.91}$$

Contracted with a nodal force vector

$$\mathbf{f}_a = \mathbf{T}_a^T\tilde{\mathbf{P}}_a^T\tilde{\mathbf{H}}_a^T\tilde{\mathbf{f}}_{ea} = \begin{bmatrix} \mathbf{n}_a^T & \mathbf{m}_a^T \end{bmatrix}^T \tag{3.92}$$

where $\mathbf{n}_a$ is a vector containing the internal forces corresponding to the translational degrees of freedom and $\mathbf{m}_a$ is a vector containing internal moments corresponding to the rotational degrees of freedom, the variation of the transposed of the nodal eccentricity matrix may be rewritten as:

$$\begin{aligned}
\delta\mathbf{E}_a^T\mathbf{f}_a &= \begin{bmatrix} \mathbf{0} & \mathbf{0} \\ -\mathbf{Spin}\left(\delta\mathbf{e}_a^n\right) & \mathbf{0} \end{bmatrix}\begin{bmatrix} \mathbf{n}_a \\ \mathbf{m}_a \end{bmatrix} = \begin{bmatrix} \mathbf{0} \\ -\mathbf{Spin}\left(\delta\mathbf{e}_a^n\right)\mathbf{n}_a \end{bmatrix} \\[2ex]
&= \begin{bmatrix} \mathbf{0} \\ \mathbf{Spin}\left(\mathbf{n}_a\right)\delta\mathbf{e}_a^n \end{bmatrix} = \begin{bmatrix} \mathbf{0} \\ -\mathbf{Spin}\left(\mathbf{n}_a\right)\mathbf{Spin}\left(\delta\boldsymbol{\omega}_a\right)\mathbf{e}_a^n \end{bmatrix} \\[2ex]
&= \begin{bmatrix} \mathbf{0} \\ \mathbf{Spin}\left(\mathbf{n}_a\right)\mathbf{Spin}\left(\mathbf{e}_a^n\right)\delta\boldsymbol{\omega}_a \end{bmatrix} \\[2ex]
&= \begin{bmatrix} \mathbf{0} & \mathbf{0} \\ \mathbf{0} & \mathbf{Spin}\left(\mathbf{n}_a\right)\mathbf{Spin}\left(\mathbf{e}_a^n\right) \end{bmatrix}\begin{bmatrix} \delta\mathbf{u}_a \\ \delta\boldsymbol{\omega}_a \end{bmatrix} = \mathbf{N}_a\delta\acute{\mathbf{v}}_a
\end{aligned} \tag{3.93}$$

The eccentricity geometric stiffness for the element is therefore:

$$\delta\mathbf{E}^T\mathbf{T}^T\tilde{\mathbf{P}}^T\tilde{\mathbf{H}}^T\tilde{\mathbf{f}}_e = \delta\mathbf{E}^T\mathbf{f} = \sum_{a=1}^{N}\delta\mathbf{E}_a^T\mathbf{f}_a = \sum_{a=1}^{N}\mathbf{N}_a\delta\acute{\mathbf{v}}_a = \mathbf{K}_{GE}\delta\acute{\mathbf{v}} \tag{3.94}$$

Where

$$\mathbf{K}_{GE} = \mathbf{N} = \begin{bmatrix} \mathbf{N}_1 & \mathbf{0} & \dots & \mathbf{0} \\ \mathbf{0} & \mathbf{N}_2 & \dots & \mathbf{0} \\ \vdots & \vdots & \ddots & \vdots \\ \mathbf{0} & \mathbf{0} & \dots & \mathbf{N}_N \end{bmatrix} \tag{3.95}$$

and

$$\mathbf{N}_a = \begin{bmatrix} \mathbf{0} & \mathbf{0} \\ \mathbf{0} & \mathbf{Spin}\,(\mathbf{n}_a)\,\mathbf{Spin}\,(\mathbf{e}_a^n) \end{bmatrix} \tag{3.96}$$

Rotational geometric stiffness

The rotational geometric stiffness arises from the variation of the transformation matrix between initial configuration C_0 and shadow configuration C_{0n}, and reflects the variation in the force vector with respect to the rigid body rotation of the element. A rigid rotation of a stressed element obviously rotates the stresses, which in turn causes the internal forces to change direction in order to preserve equilibrium.

Again, contracted with the local projected internal force vector $\tilde{\mathbf{f}} = \tilde{\mathbf{P}}^T \tilde{\mathbf{H}}^T \tilde{\mathbf{f}}_e$, where $\tilde{\mathbf{f}}$ contains pairs of internal forces and moments for each node, the rota-

tional geometric stiffness can be found from:

$$\mathbf{E}^T \delta \mathbf{T}^T \tilde{\mathbf{P}}^T \tilde{\mathbf{H}}^T \tilde{\mathbf{f}}_e \;\; = \;\; \mathbf{E}^T \delta \mathbf{T}^T \tilde{\mathbf{f}}$$

$$= \;\; \mathbf{E}^T \begin{bmatrix} \delta \mathbf{T}_n^T & \mathbf{0} & \dots & \mathbf{0} & \mathbf{0} \\ \mathbf{0} & \delta \mathbf{T}_n^T & \dots & \mathbf{0} & \mathbf{0} \\ \vdots & \vdots & \ddots & \vdots & \vdots \\ \mathbf{0} & \mathbf{0} & \dots & \delta \mathbf{T}_n^T & \mathbf{0} \\ \mathbf{0} & \mathbf{0} & \dots & \mathbf{0} & \delta \mathbf{T}_n^T \end{bmatrix} \begin{bmatrix} \tilde{\mathbf{n}}_1 \\ \tilde{\mathbf{m}}_1 \\ \vdots \\ \tilde{\mathbf{n}}_N \\ \tilde{\mathbf{m}}_N \end{bmatrix}$$

$$= \;\; \mathbf{E}^T \begin{bmatrix} \delta \mathbf{T}_n^T \tilde{\mathbf{n}}_1 \\ \delta \mathbf{T}_n^T \tilde{\mathbf{m}}_1 \\ \vdots \\ \delta \mathbf{T}_n^T \tilde{\mathbf{n}}_N \\ \delta \mathbf{T}_n^T \tilde{\mathbf{m}}_N \end{bmatrix} = \mathbf{E}^T \begin{bmatrix} \mathbf{T}_n^T \mathbf{Spin}\,(\delta \tilde{\boldsymbol{\omega}}_r)\, \tilde{\mathbf{n}}_1 \\ \mathbf{T}_n^T \mathbf{Spin}\,(\delta \tilde{\boldsymbol{\omega}}_r)\, \tilde{\mathbf{m}}_1 \\ \vdots \\ \mathbf{T}_n^T \mathbf{Spin}\,(\delta \tilde{\boldsymbol{\omega}}_r)\, \tilde{\mathbf{n}}_N \\ \mathbf{T}_n^T \mathbf{Spin}\,(\delta \tilde{\boldsymbol{\omega}}_r)\, \tilde{\mathbf{m}}_N \end{bmatrix}$$

$$\text{(3.97)}$$

$$= \;\; \mathbf{E}^T \begin{bmatrix} -\mathbf{T}_n^T \mathbf{Spin}\,(\tilde{\mathbf{n}}_1)\, \delta \tilde{\boldsymbol{\omega}}_r \\ -\mathbf{T}_n^T \mathbf{Spin}\,(\tilde{\mathbf{m}}_1)\, \delta \tilde{\boldsymbol{\omega}}_r \\ \vdots \\ -\mathbf{T}_n^T \mathbf{Spin}\,(\tilde{\mathbf{n}}_N)\, \delta \tilde{\boldsymbol{\omega}}_r \\ -\mathbf{T}_n^T \mathbf{Spin}\,(\tilde{\mathbf{m}}_N)\, \delta \tilde{\boldsymbol{\omega}}_r \end{bmatrix}$$

$$= \;\; -\mathbf{E}^T \mathbf{T}^T \begin{bmatrix} \mathbf{Spin}\,(\tilde{\mathbf{n}}_1) \\ \mathbf{Spin}\,(\tilde{\mathbf{m}}_1) \\ \vdots \\ \mathbf{Spin}\,(\tilde{\mathbf{n}}_N) \\ \mathbf{Spin}\,(\tilde{\mathbf{m}}_N) \end{bmatrix} \delta \tilde{\boldsymbol{\omega}}_r$$

$$= \;\; -\mathbf{E}^T \mathbf{T}^T \tilde{\mathbf{F}}_{nm} \delta \tilde{\boldsymbol{\omega}}_r = -\mathbf{E}^T \mathbf{T}^T \tilde{\mathbf{F}}_{nm} \tilde{\mathbf{G}} \mathbf{T} \mathbf{E} \delta \acute{\mathbf{v}}$$

$$= \;\; \mathbf{K}_{GR} \delta \acute{\mathbf{v}}$$

This derivation makes use of the following relationships:

$$\delta \mathbf{T}_n^T \;\; = \;\; \mathbf{T}_n^T \mathbf{Spin}\,(\delta \tilde{\boldsymbol{\omega}}_r) \qquad \mathbf{Spin}\,(\delta \tilde{\boldsymbol{\omega}}_r)\, \tilde{\mathbf{n}}_a = -\mathbf{Spin}\,(\tilde{\mathbf{n}}_a)\, \delta \tilde{\boldsymbol{\omega}}_r$$

$$\delta \tilde{\boldsymbol{\omega}}_r \;\; = \;\; \tilde{\mathbf{G}} \delta \tilde{\mathbf{v}}$$

$$\text{(3.98)}$$

Thus, the rotational geometric stiffness for an element with N nodes is given by:

$$\mathbf{K}_{GR} = -\mathbf{E}^T \mathbf{T}_n^T \tilde{\mathbf{F}}_{nm} \tilde{\mathbf{G}} \mathbf{T} \mathbf{E} \qquad\qquad \text{(3.99)}$$

where

$$
\tilde{\mathbf{F}}_{nm} = \begin{bmatrix} \mathbf{Spin}\,(\tilde{\mathbf{n}}_1) \\ \mathbf{Spin}\,(\tilde{\mathbf{m}}_1) \\ \vdots \\ \mathbf{Spin}\,(\tilde{\mathbf{n}}_N) \\ \mathbf{Spin}\,(\tilde{\mathbf{m}}_N) \end{bmatrix} \quad \text{and} \quad \tilde{\mathbf{f}} = \begin{bmatrix} \tilde{\mathbf{n}}_1 \\ \tilde{\mathbf{m}}_1 \\ \vdots \\ \tilde{\mathbf{n}}_N \\ \tilde{\mathbf{m}}_N \end{bmatrix} = \tilde{\mathbf{P}}^T \tilde{\mathbf{H}}^T \tilde{\mathbf{f}}_e \qquad (3.100)
$$

Equilibrium projection geometric stiffness

The equilibrium projection geometric stiffness arises from the variation of the projector matrix $\tilde{\mathbf{P}}^T$, and reflects the variation of the force vector due to variations in the element geometry.

By decomposing the force vector $\tilde{\mathbf{H}}^T \tilde{\mathbf{f}}_e$ into unbalanced element forces $\tilde{\mathbf{f}}_u = (\mathbf{I} - \tilde{\mathbf{P}}^T)\tilde{\mathbf{H}}^T \tilde{\mathbf{f}}_e$ and balanced element forces $\tilde{\mathbf{f}}_b = \tilde{\mathbf{P}}^T \tilde{\mathbf{H}}^T \tilde{\mathbf{f}}_e$ (that is $\tilde{\mathbf{H}}^T \tilde{\mathbf{f}}_e = \tilde{\mathbf{f}}_u + \tilde{\mathbf{f}}_b$), the equilibrium projection geometric term in equation (3.89) may be rewritten as follows:

$$
\begin{aligned}
\mathbf{E}^T \mathbf{T}^T \delta \tilde{\mathbf{P}}^T \tilde{\mathbf{H}}^T \tilde{\mathbf{f}}_e &= \mathbf{E}^T \mathbf{T}^T \left(\delta \mathbf{I} - \delta \tilde{\mathbf{P}}_T^T - \delta \tilde{\mathbf{P}}_R^T \right) \tilde{\mathbf{H}}^T \tilde{\mathbf{f}}_e \\
&= \mathbf{E}^T \mathbf{T}^T (-\delta \tilde{\mathbf{P}}_R^T) \tilde{\mathbf{H}}^T \tilde{\mathbf{f}}_e \\
&= -\mathbf{E}^T \mathbf{T}^T (\delta \tilde{\mathbf{G}}^T \tilde{\mathbf{S}}^T + \tilde{\mathbf{G}}^T \delta \tilde{\mathbf{S}}^T) \tilde{\mathbf{H}}^T \tilde{\mathbf{f}}_e \\
&= -\mathbf{E}^T \mathbf{T}^T (\delta \tilde{\mathbf{G}}^T \tilde{\mathbf{S}}^T + \tilde{\mathbf{G}}^T \delta \tilde{\mathbf{S}}^T)(\tilde{\mathbf{f}}_b + \tilde{\mathbf{f}}_u) \qquad (3.101) \\
&= -\mathbf{E}^T \mathbf{T}^T ((\delta \tilde{\mathbf{G}}^T \tilde{\mathbf{S}}^T + \tilde{\mathbf{G}}^T \delta \tilde{\mathbf{S}}^T)\tilde{\mathbf{f}}_b \\
&\quad + (\delta \tilde{\mathbf{G}}^T \tilde{\mathbf{S}}^T + \tilde{\mathbf{G}}^T \delta \tilde{\mathbf{S}}^T)\tilde{\mathbf{f}}_u) \\
&= -\mathbf{E}^T \mathbf{T}^T (\tilde{\mathbf{G}}^T \delta \tilde{\mathbf{S}}^T \tilde{\mathbf{f}}_b + \delta \tilde{\mathbf{P}}^T \tilde{\mathbf{f}}_u)
\end{aligned}
$$

$\tilde{\mathbf{S}}^T$ represents the rigid body rotation vectors for the element. Hence, $\tilde{\mathbf{S}}^T \tilde{\mathbf{f}}_b = \mathbf{0}$, since the balanced forces do not produce any work on a structure during rigid body displacement or rotation. Furthermore, $\delta \tilde{\mathbf{P}}^T \tilde{\mathbf{f}}_u$ can be neglected because it will be very small when C_{0n} and C_n are close. It can also be shown that the term is identically zero if $\tilde{\mathbf{G}}$ so simple that it can be written as $\tilde{\mathbf{G}} = \tilde{\mathbf{X}}\mathbf{A}$, where $\mathbf{X}$ is an invertible 3x3 matrix and $\mathbf{A}$ is a constant matrix (see [17]). Equation

(3.101) therefore reduces to

$$
\begin{aligned}
\mathbf{E}^T\mathbf{T}^T\delta\tilde{\mathbf{P}}^T\tilde{\mathbf{H}}^T\tilde{\mathbf{f}}_e &= -\mathbf{E}^T\mathbf{T}^T\tilde{\mathbf{G}}^T\delta\tilde{\mathbf{S}}^T\tilde{\mathbf{f}}_b \\
&= -\mathbf{E}^T\mathbf{T}^T\tilde{\mathbf{G}}^T\sum_{a=1}^{N}\left[\ \mathbf{Spin}((\delta\tilde{\mathbf{x}}_a^n)_R)\quad \mathbf{0}\ \right]\left[\begin{array}{c}\tilde{\mathbf{n}}_a \\[6pt] \tilde{\mathbf{m}}_a\end{array}\right] \\
&= -\mathbf{E}^T\mathbf{T}^T\tilde{\mathbf{G}}^T\sum_{a=1}^{N}\mathbf{Spin}\left((\delta\tilde{\mathbf{x}}_a^n)_R\right)\tilde{\mathbf{n}}_a \\
&= \mathbf{E}^T\mathbf{T}^T\tilde{\mathbf{G}}^T\sum_{a=1}^{N}\mathbf{Spin}\left(\tilde{\mathbf{n}}_a\right)(\delta\tilde{\mathbf{x}}_a^n)_R \\
&= \mathbf{E}^T\mathbf{T}^T\tilde{\mathbf{G}}^T\sum_{a=1}^{N}\left[\ \mathbf{Spin}(\tilde{\mathbf{n}}_a)\quad \mathbf{0}\ \right]\left[\begin{array}{c}(\delta\tilde{\mathbf{u}}_{da})_R \\[6pt] (\delta\tilde{\boldsymbol{\omega}}_{da})_R\end{array}\right] \\
&= -\mathbf{E}^T\mathbf{T}^T\tilde{\mathbf{G}}^T\tilde{\mathbf{F}}_n^T(\delta\tilde{\mathbf{v}}_d)_R \\
&= -\mathbf{E}^T\mathbf{T}^T\tilde{\mathbf{G}}^T\tilde{\mathbf{F}}_n^T\tilde{\mathbf{H}}\tilde{\mathbf{P}}\mathbf{T}\mathbf{E}\delta\acute{\mathbf{v}} \\
&= -\mathbf{E}^T\mathbf{T}^T\tilde{\mathbf{G}}^T\tilde{\mathbf{F}}_n^T\tilde{\mathbf{P}}\mathbf{T}\mathbf{E}\delta\acute{\mathbf{v}} \\
&= \mathbf{K}_{GP}\delta\acute{\mathbf{v}}
\end{aligned}
\tag{3.102}
$$

where the relationship $\tilde{\mathbf{F}}_n^T\cdot\tilde{\mathbf{H}}=\tilde{\mathbf{F}}_n^T$ has been used. Hence

$$
\mathbf{K}_{GP}=-\mathbf{E}^T\mathbf{T}^T\tilde{\mathbf{G}}^T\tilde{\mathbf{F}}_n^T\tilde{\mathbf{P}}\mathbf{T}\mathbf{E}
\tag{3.103}
$$

where

$$
\tilde{\mathbf{F}}_n=\left[\begin{array}{c}\mathbf{Spin}\left(\tilde{\mathbf{n}}_1\right) \\ \mathbf{0} \\ \vdots \\ \mathbf{Spin}\left(\tilde{\mathbf{n}}_N\right) \\ \mathbf{0}\end{array}\right]\qquad\text{and}\qquad \tilde{\mathbf{f}}_b=\left[\begin{array}{c}\tilde{\mathbf{n}}_1 \\ \tilde{\mathbf{m}}_1 \\ \vdots \\ \tilde{\mathbf{n}}_N \\ \tilde{\mathbf{m}}_N\end{array}\right]=\tilde{\mathbf{P}}^T\tilde{\mathbf{H}}^T\tilde{\mathbf{f}}_e
\tag{3.104}
$$

Moment correction geometric stiffness

The moment correction geometric stiffness stems from variation of the deformational rotation pseudo-vector Jacobian $\tilde{\mathbf{H}}$. Splitting the internal force vector into translational internal forces $\tilde{\mathbf{n}}$ and rotational internal moments $\tilde{\mathbf{m}}$, the mo-

ment correction term in (3.89) from page 37 may be written as:

$$\mathbf{E}^T\mathbf{T}^T\tilde{\mathbf{P}}^T(\delta\tilde{\mathbf{H}}^T)_R\tilde{\mathbf{f}}_e = \mathbf{E}^T\mathbf{T}^T\tilde{\mathbf{P}}^T \begin{bmatrix} \mathbf{0} & \mathbf{0} & \dots & \mathbf{0} & \mathbf{0} \\ \mathbf{0} & (\delta\tilde{\mathbf{H}}_1^T)_R & \dots & \mathbf{0} & \mathbf{0} \\ \vdots & \vdots & \ddots & \vdots & \vdots \\ \mathbf{0} & \mathbf{0} & \dots & \mathbf{0} & \mathbf{0} \\ \mathbf{0} & \mathbf{0} & \dots & \mathbf{0} & (\delta\tilde{\mathbf{H}}_N^T)_R \end{bmatrix} \begin{bmatrix} \tilde{\mathbf{n}}_1 \\ \tilde{\mathbf{m}}_1 \\ \vdots \\ \tilde{\mathbf{n}}_N \\ \tilde{\mathbf{m}}_N \end{bmatrix}$$

$$= \mathbf{E}^T\mathbf{T}^T\tilde{\mathbf{P}}^T \begin{bmatrix} \mathbf{0} \\ (\delta\tilde{\mathbf{H}}_1^T)_R\tilde{\mathbf{m}}_1 \\ \vdots \\ \mathbf{0} \\ (\delta\tilde{\mathbf{H}}_N^T)_R\tilde{\mathbf{m}}_N \end{bmatrix}$$

$$= \mathbf{E}^T\mathbf{T}^T\tilde{\mathbf{P}}^T \begin{bmatrix} \mathbf{0} \\ \tilde{\mathbf{M}}_1(\delta\tilde{\boldsymbol{\omega}}_{d1})_R \\ \vdots \\ \mathbf{0} \\ \tilde{\mathbf{M}}_N(\delta\tilde{\boldsymbol{\omega}}_{dN})_R \end{bmatrix}$$

$$= \mathbf{E}^T\mathbf{T}^T\tilde{\mathbf{P}}^T\tilde{\mathbf{M}}\tilde{\mathbf{P}}\mathbf{T}\mathbf{E}\delta\acute{\mathbf{v}} = \mathbf{K}_{GM}\delta\acute{\mathbf{v}}$$

(3.105)

where

$$\tilde{\mathbf{M}} = \begin{bmatrix} \mathbf{0} & \mathbf{0} & \dots & \mathbf{0} & \mathbf{0} \\ \mathbf{0} & \tilde{\mathbf{M}}_1 & \dots & \mathbf{0} & \mathbf{0} \\ \vdots & \vdots & \ddots & \vdots & \vdots \\ \mathbf{0} & \mathbf{0} & \dots & \mathbf{0} & \mathbf{0} \\ \mathbf{0} & \mathbf{0} & \dots & \mathbf{0} & \tilde{\mathbf{M}}_N \end{bmatrix}$$

(3.106)

In [4], $\tilde{\mathbf{M}}_a$ is defined from the relationship

$$\delta\tilde{\mathbf{H}}_a^T\tilde{\mathbf{m}}_a = \frac{\partial\tilde{\mathbf{H}}_a^T}{\partial\tilde{\boldsymbol{\omega}}_a}\tilde{\mathbf{m}}_a\delta\tilde{\boldsymbol{\omega}}_a = \tilde{\mathbf{M}}_a\delta\tilde{\boldsymbol{\omega}}_a.$$

(3.107)

According to Haugen[4], Nour-Omid and Rankin[15] established this relationship on the form

$$\begin{aligned} \tilde{\mathbf{M}}_a &= \left(-\tfrac{1}{2}\mathbf{Spin}\left(\tilde{\mathbf{m}}_a\right) + \eta\left((\tilde{\mathbf{m}}_a^T\tilde{\boldsymbol{\theta}}_a)\mathbf{I} + \tilde{\boldsymbol{\theta}}_a\tilde{\mathbf{m}}_a^T - 2\tilde{\mathbf{m}}\tilde{\boldsymbol{\theta}}^T\right)\right. \\ &\quad + \left.\nu\mathbf{Spin}\left(\tilde{\boldsymbol{\theta}}_a\right)^2\tilde{\mathbf{m}}_a\tilde{\boldsymbol{\theta}}_a^T\right)\tilde{\mathbf{H}} \end{aligned}$$

(3.108)

η is defined in equation (3.55) on page 30, whereas ν is found from the following expression:

$$\eta = \frac{\tilde{\theta}_a(\tilde{\theta}_a + \sin\theta_a) - 8\sin^2(\frac{1}{2}\tilde{\theta}_a)}{4\tilde{\theta}_a^4 \sin^2(\frac{1}{2}\tilde{\theta}_a)} \qquad (3.109)$$

Since $\nu \to 0/0$ as $\tilde{\theta}_a \to 0$, ν should be computed from the truncated power series

$$\nu \approx \frac{1}{360} + \frac{1}{7560}\tilde{\theta}_a^2 + \frac{1}{201600}\tilde{\theta}_a \qquad \text{for} \qquad \tilde{\theta}_a < 0.05 \quad \text{radians} \qquad (3.110)$$

in order to avoid numerical problems for small angles.

Material stiffness and internal geometric stiffness

Variation of the local internal force vector $\tilde{\mathbf{f}}_e$ yields material stiffness and, in some cases, internal geometric stiffness:

$$\delta\tilde{\mathbf{f}}_e = \frac{\partial\mathbf{f}}{(\partial\tilde{\mathbf{v}})_R}(\delta\tilde{\mathbf{v}})_R = \tilde{\mathbf{K}}_e(\delta\tilde{\mathbf{v}})_R \qquad (3.111)$$

Thus, the material and internal geometric stiffness is

$$\mathbf{K}_{MG} = \mathbf{E}^T\mathbf{T}^T\tilde{\mathbf{P}}^T\tilde{\mathbf{H}}^T\tilde{\mathbf{K}}_e\tilde{\mathbf{H}}\tilde{\mathbf{P}}\mathbf{TE} \qquad (3.112)$$

Complete form of the consistent tangent matrix

Introducing equations (3.94), (3.99), (3.103), (3.105) and (3.112) into equation (3.89) from page 37, the following expression for the consistent tangent stiffness is found:

$$\begin{aligned}
\mathbf{K}_T &= \mathbf{K}_{GE} + \mathbf{E}^T\mathbf{T}^T\left(\tilde{\mathbf{K}}_{MG} + \tilde{\mathbf{K}}_{GR} + \tilde{\mathbf{K}}_{GM} + \tilde{\mathbf{K}}_{GP}\right)\mathbf{TE} \\
&= \mathbf{N} + \mathbf{E}^T\mathbf{T}^T\left(\tilde{\mathbf{P}}^T\tilde{\mathbf{H}}^T\tilde{\mathbf{K}}_e\tilde{\mathbf{H}}\tilde{\mathbf{P}} + \tilde{\mathbf{P}}^T\tilde{\mathbf{M}}\tilde{\mathbf{P}} - \tilde{\mathbf{F}}_{nm}\tilde{\mathbf{G}}\right. \qquad (3.113) \\
&\quad - \left.\tilde{\mathbf{G}}^T\tilde{\mathbf{F}}_n^T\tilde{\mathbf{P}}\right)\mathbf{TE}
\end{aligned}$$

where

$$\tilde{\mathbf{F}}_{nm} = \begin{bmatrix} \mathbf{Spin}\,(\tilde{\mathbf{n}}_1) \\ \mathbf{Spin}\,(\tilde{\mathbf{m}}_1) \\ \vdots \\ \mathbf{Spin}\,(\tilde{\mathbf{n}}_N) \\ \mathbf{Spin}\,(\tilde{\mathbf{m}}_N) \end{bmatrix} \qquad \tilde{\mathbf{F}}_n = \begin{bmatrix} \mathbf{Spin}\,(\tilde{\mathbf{n}}_1) \\ \mathbf{0} \\ \vdots \\ \mathbf{Spin}\,(\tilde{\mathbf{n}}_N) \\ \mathbf{0} \end{bmatrix}$$

$$\tilde{\mathbf{f}} = \begin{bmatrix} \tilde{\mathbf{n}}_1 \\ \tilde{\mathbf{m}}_1 \\ \vdots \\ \tilde{\mathbf{n}}_N \\ \tilde{\mathbf{m}}_N \end{bmatrix} = \tilde{\mathbf{P}}^T \tilde{\mathbf{H}}^T \tilde{\mathbf{f}}_e$$

$$\mathbf{N} = \begin{bmatrix} \mathbf{N}_1 & \mathbf{0} & \dots & \mathbf{0} \\ \mathbf{0} & \mathbf{N}_1 & \dots & \mathbf{0} \\ \vdots & \vdots & \ddots & \vdots \\ \mathbf{0} & \mathbf{0} & \dots & \mathbf{N}_N \end{bmatrix} \qquad \mathbf{N}_a = \begin{bmatrix} \mathbf{0} & \mathbf{0} \\ \mathbf{0} & \mathbf{Spin}\,(\mathbf{n}_a)\,\mathbf{Spin}\,(\mathbf{e}_a^n) \end{bmatrix}$$

$$\mathbf{f} = \begin{bmatrix} \mathbf{n}_1 \\ \mathbf{m}_1 \\ \vdots \\ \mathbf{n}_N \\ \mathbf{m}_N \end{bmatrix} = \mathbf{T}^T \tilde{\mathbf{P}}^T \tilde{\mathbf{H}}^T \tilde{\mathbf{f}}_e$$

$$\tag{3.114}$$

$\tilde{\mathbf{K}}_e$ is found from the relationship

$$\delta \tilde{\mathbf{f}}_e = \tilde{\mathbf{K}}_e (\delta \tilde{\mathbf{v}}_d)_R \tag{3.115}$$

3.4 Governing equations for non-linear analysis

In this section the governing equations for non-linear finite element analysis is presented.

3.4.1 Residual equation

Consider a structure with internal forces $\mathbf{f}$ and external forces $\mathbf{p}$. The residual $\mathbf{r}$ of the structure is defined as the difference between internal and external forces:

$$\mathbf{r} = \mathbf{f} - \mathbf{p} \tag{3.116}$$

If the structure is in equlibrium, the residual is $\mathbf{0}$.

$\mathbf{f}$, $\mathbf{p}$ and $\mathbf{r}$ are functions of the displacement state $\mathbf{v}$ and the load level represented by λ. The magnitude of all external loads are thus assumed to be uniquely

defined by the load parameter λ. In linear analysis, the internal force vector is given as $\mathbf{f} = \mathbf{K}_l \mathbf{v}$ where $\mathbf{K}_l$ is a constant matrix, and the external force vector is also constant. Thus, equation (3.116) may be solved directly, to find the unknown displacement state as $\mathbf{v} = \mathbf{K}_l^{-1} \mathbf{p}$. However, in non-linear analysis, where the internal force vector is non-linearly dependent on the displacement state, the solution procedure is not quite as simple. The internal force vector is now written as $\mathbf{f} = \mathbf{f}(\mathbf{v})$ and equation (3.116) can genereally not be solved directly. We may however solve the residual equation in increments, starting at a known equilibrium position and solving for small increments of external load. Depending on the size of the increments and the nonlinearity of the system, this will in general cause an inaccuracy or a so-called "drift" from the equilibrium path. This may however be remedied by introducing iterative correctional steps.

The incremental form of the equilibrium equation (3.116) is found by variation:

$$
\begin{aligned}
\delta \mathbf{r}(\mathbf{v}, \lambda) \quad &= \quad \delta \mathbf{f}(\mathbf{v}) - \delta \mathbf{p}(\lambda) = \frac{\partial \mathbf{f}}{\partial \mathbf{v}} \delta \mathbf{v} - \frac{\partial \mathbf{p}}{\partial \lambda} \\
&= \quad \frac{\partial \mathbf{f}}{\partial \mathbf{v}} \delta \mathbf{v} - \frac{\partial \mathbf{p}}{\partial \lambda} \delta \lambda = \mathbf{0} \qquad\qquad (3.117)
\end{aligned}
$$

Introducing $\mathbf{K} = \frac{\partial \mathbf{f}}{\partial \mathbf{v}}$ and $\mathbf{q} = \frac{\partial \mathbf{p}}{\partial \lambda}$, the incremental residual equation reduces to:

$$
\begin{aligned}
\delta \mathbf{r} \quad &= \quad \mathbf{K} \delta \mathbf{v} - \mathbf{q} \delta \lambda = \mathbf{0} \\
\mathbf{0} \quad &= \quad \mathbf{K} \frac{\delta \mathbf{v}}{\delta \lambda} - \mathbf{q} \\
\mathbf{0} \quad &= \quad \mathbf{K} \mathbf{v}' - \mathbf{q} \\
\mathbf{v}' \quad &= \quad \mathbf{K}^{-1} \mathbf{q} \qquad \text{where} \qquad \mathbf{v}' = \frac{\delta \mathbf{v}}{\delta \lambda} \qquad\qquad (3.118)
\end{aligned}
$$

Equation (3.118) is a first order differential equation, and it can be solved using the (forward) Euler method (see for instance [53]).

Over each increment, $\mathbf{v}$ and λ experience finite changes $\Delta \mathbf{v}$ and $\Delta \lambda$:

$$
\begin{aligned}
\mathbf{v}_{i+1} \quad &= \quad \mathbf{v}_i + \Delta \mathbf{v}_i \\
\frac{\Delta \mathbf{v}}{\Delta \lambda} \quad &\approx \quad \frac{\delta \mathbf{v}}{\delta \lambda} = \mathbf{K}^{-1} \mathbf{q} \\
\Delta \mathbf{v}_i \quad &\approx \quad \mathbf{K}_i^{-1} \mathbf{q}_i \Delta \lambda_i \\
\mathbf{v}_{i+1} \quad &= \quad \mathbf{v}_i + \mathbf{K}_i^{-1} \mathbf{q}_i \Delta \lambda_i = \mathbf{v}_i + \mathbf{w}_i \Delta \lambda_i \qquad\qquad (3.119)
\end{aligned}
$$

where $\mathbf{w}_i = \mathbf{K}_i^{-1} \mathbf{q}_i$ is called the incremental velocity vector at increment i. Thus, the displacment at step $i + 1$ is found by adding the displacement increment, $\Delta \mathbf{v}$, to the displacement vector at step i, $\mathbf{v}_i$. $\Delta \mathbf{v}$ is found by extrapolating along the tangent of the equlibrium path with load increment $\Delta \lambda$, and solving with respect to $\Delta \mathbf{v}$.
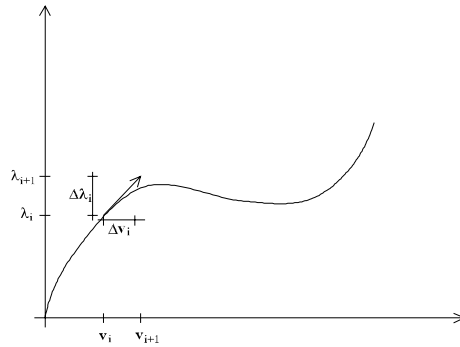
Figure 3.6: *Incremental displacement and load magnitude at step i.*

The size of the load factor increment may be determined by several different methods. In a "**load-control**" algorithm the total load λ_{tot} is divided into a number of increments that are applied to the structure until $\lambda = \lambda_{tot}$. This algorithm has one obvious flaw: Since λ always increases, the algorithm is not able to follow parts of the equilibrium path where the load is decreasing. In "**arc-length**" type algorithms, first proposed by Riks [54] and Wempner [55], the load increment is determined by use of a restraining criterion limiting the length of the *combination* of $\Delta \mathbf{v}_i$ and $\Delta \lambda_i$. These types of algorithms are able to traverse all kinds of single (as opposed to multiple) limit points. The basics of the different methods are shown in figures *3.7* and *3.8*.
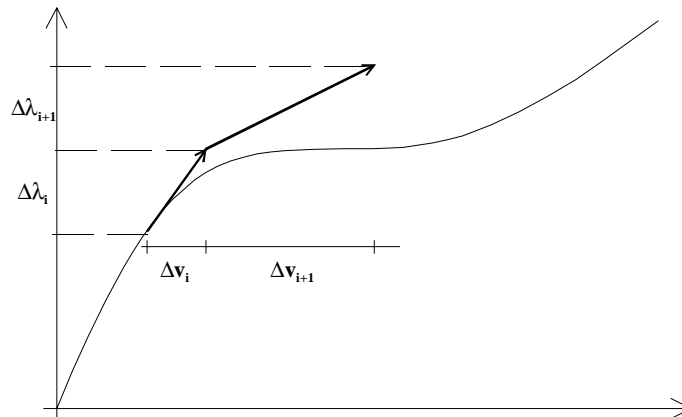
Figure 3.7: *Load control algorithm.*

As already pointed out, the use of a pure incremental solution of the differential equation (3.118) causes an inaccuracy or *drift* that tends to increase as the analysis proceeds. However, since the equilibrium path of the structure is defined by the residual equation, it is possible to perform iterative correctional steps to obtain accurate results. Furthermore, as long as the correctional iter-
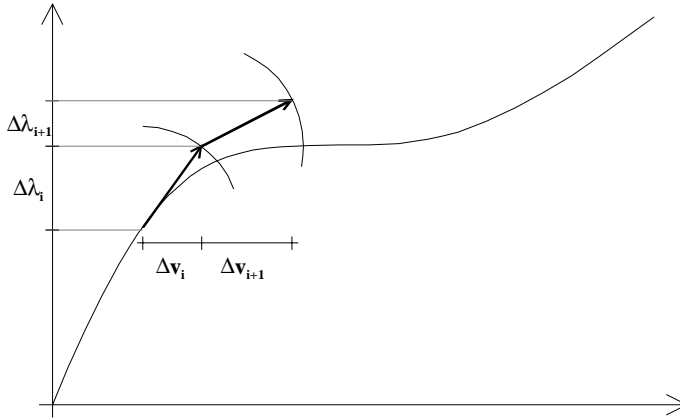
Figure 3.8: *Arc-length control algorithm.*

ations converge towards the correct solution at each step, drift is eliminated, forcing the solution to be correct after each increment. The correctional strategy used when obtaining the results from nonlinear analyses in this work, is the orthogonal-trajectory corrector proposed by Fried [56] combined with Newton's method for sets of equations (see for instance [24]).

Newton's method converges quadratically as it approaches the correct solution if the tangent stiffness $\mathbf{K} = \frac{\partial \mathbf{f}}{\partial \mathbf{v}}$ is used. If the correct tangent stiffness is not used, the method may still converge quadratically, but most likely it will converge considerably slower, if at all.

3.4.2   Linearized buckling analysis

The basic concept of the linearized buckling analysis is that the tangent stiffness varies linearly with respect to the loading parameter λ. This gives rise to an eigenvalue problem, which can be expressed as:

$$(\mathbf{K}_0 + \lambda \mathbf{K}_G)\, \mathbf{v}_\lambda = \mathbf{0} \qquad\qquad (3.120)$$

where $\mathbf{K}_0$ is the initial stiffness of the structure and $\mathbf{K}_G$ is the rate of change of the stiffness about the initial configuration with respect to the load parameter λ.

Usually the linearized buckling analysis is performed with reference to the unloaded initial state, for which $\mathbf{K}_0$ is the material stiffness and $\mathbf{K}_G$ is the geometric stiffness for a load of unity. However, for some problems it may be of interest to split the load into a constant part (independent of λ and a variable part. For such problems, the initial state of the structure is an already loaded

state. Hence, $\mathbf{K}_0$ is a mix of material stiffness and geometric stiffness corresponding to the constant load, whereas $\mathbf{K}_G$ is the geometric stiffness for the variable load with a load parameter of unity. The algorithm for analysing such a problem is given below.

1. Establish material stiffness for the system, $\mathbf{K}_M$

2. If any external loads are to be held constant, build external load vector $\mathbf{q}_0$ based on these loads. If not, set $\mathbf{K}_0 = \mathbf{K}_M$ and proceed to step 5.

3. Solve $\mathbf{r}_0 = \mathbf{K}_M^{-1}\mathbf{q}_0$.

4. Build $\mathbf{K}_0$ as the tangent stiffness corresponding to the initial geometry, and internal forces corresponding to displacements $\mathbf{r}_0$.

5. Set $\lambda = 1.0$ and build external load vector $\mathbf{q}_1$. Obtain displacements as $\mathbf{r}_1 = \mathbf{K}_0^{-1}\mathbf{q}_1$.

6. Build $\mathbf{K}_1$ as the tangent stiffness corresponding to the initial geometry, and internal forces corresponding to displacements $\mathbf{r}_1$. Set $\mathbf{K}_G = \mathbf{K}_1 - \mathbf{K}_0$.

7. Solve the generalized eigenvalue problem, $(\mathbf{K}_0 + \lambda\mathbf{K}_G)\mathbf{r} = \mathbf{0}$ to obtain critical buckling loads and buckling modes for the system.

The linearized buckling analysis most often yield the same critical buckling load as a solution of the system's differential equation with respect to stability.

Chapter 4

A consistent 3D beam element with internal geometric stiffness

In the previous chapter, the co-rotated finite element formulation was presented, following the approach of Haugen[4, 17] and Rankin et al.[14, 15]. It was based on the assumption that deformation of each element is small, while permitting large displacements. Furthermore, the degrees of freedom used in the formulation were displacements (including rotations) and the material of the element was assumed to be elastic, although not necessarily linearly elastic.

As mentioned in section 1.2, the beam elements usually implemented in co-rotated formulations, are simple linear beam elements. These elements, which are based on a linear relationship between strain and displacement, are well tested for linear problems, and they are easily implemented into the co-rotated formulation. However, they often require quite refined element meshes in order to produce the desired degree of accuracy.

For some structural models, refined element meshes may be necessary also for other purposes, such as modelling geometric imperfections with sufficient accuracy, or in codes using lumped loading. In general, however, it is desirable to keep the number of elements at a minimum in order to reduce the computational cost.

If fewer elements of a complex kind is needed to obtain a certain degree of accuracy than what is the case for a less complex element, the complex element

will always be more efficient for large models.

In this chapter a consistent beam element is developed based on a nonlinear strain/displacement relationship, resulting in a beam element with internal geometric stiffness. Geometric stiffness from axial stress is included, enabling the element to account for flexural buckling in linearized buckling analysis, and increasing its accuracy when used in nonlinear analysis of structures with axial forces. In order to enable the element to account for lateral torsional buckling, geometric stiffness from bending stress is also included. This also enhances the accuracy of the element when used in nonlinear analysis of structures subjected to transverse loading. Although assuming a nonlinear strain/displacement relationship, the assumption of small displacements is maintained.

The two parts of the internal geometric stiffness can be implemented independently, and when using the formulation in a linearized buckling analysis, the geometric stiffness can be separated from the material stiffness. When implementing the element in the co-rotated formulation presented in chapter 3, the verification (chapter 5) shows that the resulting beam element has superior accuracy compared with the standard Euler-Bernoulli element implemented in the same co-rotated formulation.

4.1   Basics and assumptions
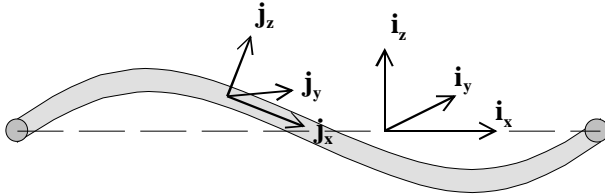
4.1.1   Coordinate systems

Figure 4.1: *Beam element coordinate systems in 3D space.*

Two different coordinate systems are used in the development of the new beam element.

The *element coordinate system* is defined by the three orthogonal axes x, y and z, with corresponding orthonormal vectors $\mathbf{i}_x$, $\mathbf{i}_y$ and $\mathbf{i}_z$. The axes are oriented such that the x-axis coincides with the initial shape of the beam axis. Thus, for elements that are not initially straight, the element coordinate system may vary depending on the position along the beam axis. The y and z axes are the principal axes of the cross section of the undeformed element.

For an initially straight, two-noded beam element, the element coordinate system will correspond to the local coordinate system when implementing the element in the co-rotated formulation described in chapter 3.

Each cross section of the beam element has its own coordinate system, called the *cross-section coordinate system*, identified by the triad $\begin{bmatrix} \mathbf{j}_x & \mathbf{j}_y & \mathbf{j}_z \end{bmatrix}$. An entity given in cross-section coordinate system is identified by a bar ($^-$). For the undeformed element, the cross-section coordinate system and the element coordinate system coincide.

4.1.2 Discretization

In finite element methods, a continuum is *discretized* into a number of finite elements. Within each element, the displacement and rotation components are assumed to be unique functions of a finite number of degrees of freedom. For beam elements, the obvious discretization is to express the element displacements in terms of the translations and rotations at the element ends.

Consider a beam element in 3D space with a coordinate system identified by the orthogonal axes x, y and z. An arbitrary displacement at a point on the element axis is described by the three independent displacement components u, v and w in the x, y and z direction, respectively. The degrees of freedom (dofs) of the element are listed in the column matrix $\mathbf{v}$, while the shape functions for the displacements in the three directions are listed in the row-matrices $\mathbf{N}_u$, $\mathbf{N}_v$ and $\mathbf{N}_w$, respectively.

$$u = \mathbf{N}_u\mathbf{v} \qquad v = \mathbf{N}_v\mathbf{v} \qquad w = \mathbf{N}_w\mathbf{v} \qquad (4.1)$$

For simplicity, $\mathbf{N}_v$ and $\mathbf{N}_w$ are combined into $\mathbf{N}_{vw}$:

$$\begin{bmatrix} v \\ w \end{bmatrix} = \begin{bmatrix} \mathbf{N}_v \\ \mathbf{N}_w \end{bmatrix} \mathbf{v} = \mathbf{N}_{vw}\mathbf{v} \qquad (4.2)$$

$\mathbf{N}_u$, $\mathbf{N}_v$ and $\mathbf{N}_w$ are functions of the position along the beam axis, whereas $\mathbf{v}$ is independent of the coordinates. Thus, differentiation of the displacement components with respect to x gives

$$u_{,x} = \mathbf{N}_{u,x}\mathbf{v} \qquad v_{,x} = \mathbf{N}_{v,x}\mathbf{v} \qquad w_{,x} = \mathbf{N}_{w,x}\mathbf{v} \qquad (4.3)$$

and the second derivatives of the displacement components are:

$$u_{,xx} = \mathbf{N}_{u,xx}\mathbf{v} \qquad v_{,xx} = \mathbf{N}_{v,xx}\mathbf{v} \qquad w_{,xx} = \mathbf{N}_{w,xx}\mathbf{v} \qquad (4.4)$$

The rotation of a point on the beam element axis is defined by the rotation vector $\boldsymbol{\omega}$:

$$\boldsymbol{\omega} = \begin{bmatrix} \omega_x \\ \omega_y \\ \omega_z \end{bmatrix} = \begin{bmatrix} \mathbf{N}_{\omega x} \\ \mathbf{N}_{\omega y} \\ \mathbf{N}_{\omega z} \end{bmatrix} \mathbf{v} = \mathbf{N}_\omega \mathbf{v} \qquad (4.5)$$

ω_x, ω_y and ω_z are the rotation components about the x-, y- and z-axis, respectively.

Similarly, the curvature at a point on the beam element axis is given by:

$$\boldsymbol{\kappa} = \begin{bmatrix} \kappa_x \\ \kappa_y \\ \kappa_z \end{bmatrix} = \begin{bmatrix} \mathbf{N}_{\kappa x} \\ \mathbf{N}_{\kappa y} \\ \mathbf{N}_{\kappa z} \end{bmatrix} \mathbf{v} = \mathbf{N}_\kappa \mathbf{v} \qquad (4.6)$$

κ_x, κ_y and κ_z are the curvature components about the x-, y- and z-axis, respectively.

As for the displacements, the shape functions listed in $\mathbf{N}_\omega$ and $\mathbf{N}_\kappa$ are dependent only on the position along the beam element axis. Hence, differentiation of the rotation vector and the vector of curvature with respect to the position along the beam axis can be expressed as

$$\boldsymbol{\omega}_{,x} = \mathbf{N}_{\omega,x} \mathbf{v} \qquad \text{and} \qquad \boldsymbol{\kappa}_{,x} = \mathbf{N}_{\kappa,x} \mathbf{v} \qquad (4.7)$$

respectively.

4.1.3   Separation of axial strain

Axial strain in a beam is induced either by axial loading or bending. Depending on the material properties and the boundary conditions of the element, bending introduces axial strain that is not necessarily zero at the center of the cross-section, but the total axial strain can always be separated into *center line strain* and *bending strain*. As the name indicates, center line strain is the magnitude of the axial strain at the center line of the beam, and it is constant throughout the cross-section. The bending strain varies linearly over the cross section, as long as Naviers' hypothesis[1] is valid.

Hence, the total axial strain, ϵ, may be expressed as

$$\epsilon = \epsilon_c + \bar{\epsilon}_{yy} + \bar{\epsilon}_{zz} \qquad (4.8)$$

where ϵ_c is the center line axial strain, and $\bar{\epsilon}_{yy}$ and $\bar{\epsilon}_{zz}$ are axial strain from bending about the y- and z-axis, respectively. As the bar indicates, $\bar{\epsilon}_{yy}$ and $\bar{\epsilon}_{zz}$ are measured in the cross-section coordinate system.

[1]Navier's hypothesis: *Plane sections through a beam taken normal to its axis remain plane and normal to the axis after the beam is subjected to bending* [57]. This assumption is widely used as long as shear deformations are small.
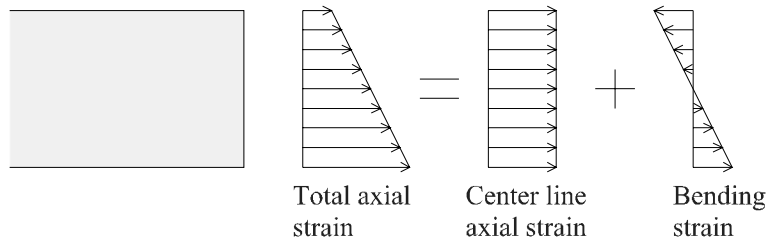
Total axial strain   Center line axial strain   Bending strain

Figure 4.2: *Separation of axial strain into center line axial strain and bending strain.*

4.1.4 Hyperelastic material

The material is assumed to be *hyperelastic*, that is a material for which stress is uniquely defined by the strain. Thus, axial stress σ is given by:

$$\sigma = \sigma\left(\epsilon\right) \qquad \text{with variation} \qquad \delta\sigma = \frac{\partial\sigma}{\partial\epsilon}\delta\epsilon = E\left(\epsilon\right)\delta\epsilon \qquad (4.9)$$

Similarly, shear stress is given by

$$\tau = \tau\left(\gamma\right) \qquad \text{with variation} \qquad \delta\tau = \frac{\partial\tau}{\partial\gamma}\delta\gamma = G\left(\gamma\right)\delta\gamma \qquad (4.10)$$

where γ is the shear strain.

4.2 Geometric relationships

In order to establish the non-linear relationship between strain and displacement, the geometry of an element in a deformed state need to be studied.

4.2.1 Axial strain due to transverse displacement

Consider a beam element that after an axial elongation u is fixed axially at both ends and subjected to transverse displacements. Since the ends are constrained, this obviously causes the element to alter its length, thereby introducing axial strain.

Figure *4.3* shows an infinitesimal segment of the beam element. The original length of this segment is dx, and it is given a net transverse displacement causing the segment to rotate through an angle ϕ. As a minor simplification, the element segment is considered to be straight. The elongation of the segment along its
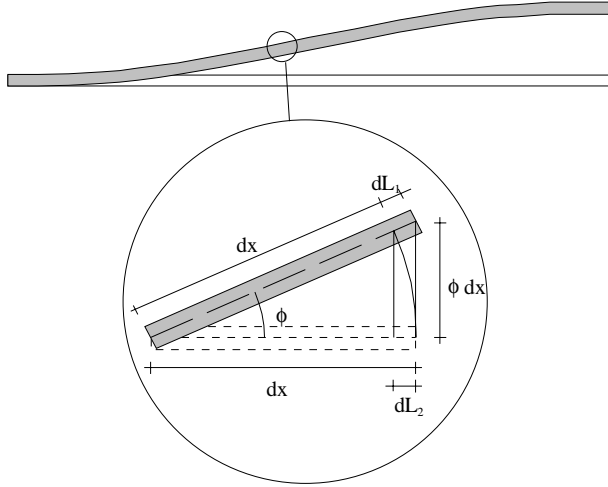
Figure 4.3: *Elongation of an infinitesimal part of an element due to transversal displacement.*

axis is dL_1, whereas dL_2 is the projection of the elongation onto its initial (undeformed) position. Due to the fact that the difference between dL_1 and dL_2 is very small, and dL_2 is easier to adapt for use in the element formulation, dL_2 is used for the elongation of the beam. dL_2 can be written as

$$dL_2 = (1 - \cos(\phi))dx \tag{4.11}$$

Exploiting the assumption that ϕ is small, the cosine term in equation (4.11) may be replaced by its power series representation about $\phi = 0$:

$$\cos(\phi) \quad \approx \quad 1 - \frac{1}{2}\phi^2 \tag{4.12}$$

$$dL_2 \quad \approx \quad (1 - (1 - \frac{1}{2}\phi^2))dx = \frac{1}{2}\phi^2 dx \tag{4.13}$$

The total elongation of the element is now found as the sum of the axial displacement, du, and the elongation due to transverse displacement, dL_2. The corresponding strain is

$$\epsilon_c = \frac{dL_2 + du}{dx} = \frac{\frac{1}{2}\phi^2 dx + du}{dx} = \frac{1}{2}\phi^2 + u_{,x} \tag{4.14}$$

For small ϕ superposition may be used, such that

$$\phi^2 = v_{,x}^2 + w_{,x}^2 \tag{4.15}$$

Equation (4.14) becomes

$$\epsilon_c = u_{,x} + \frac{1}{2}v_{,x}^2 + \frac{1}{2}w_{,x}^2 = \mathbf{N}_{u,x}\mathbf{v} + \frac{1}{2}\mathbf{v}^T\mathbf{N}_{vw,x}^T\mathbf{N}_{vw,x}\mathbf{v} \tag{4.16}$$

where $\mathbf{N}_{vw}$ is defined in equation (4.2) from page 53. The variation of ϵ_c with respect to deformational displacement $\mathbf{v}$ can then be written as

$$
\begin{aligned}
\delta\epsilon_c &= \mathbf{N}_{u,x}\delta\mathbf{v} + \tfrac{1}{2}\delta\mathbf{v}^T\mathbf{N}_{vw,x}^T\mathbf{N}_{vw,x}\mathbf{v} + \tfrac{1}{2}\mathbf{v}^T\mathbf{N}_{vw,x}^T\mathbf{N}_{vw,x}\delta\mathbf{v} \\
&= \mathbf{N}_{u,x}\delta\mathbf{v} + \mathbf{v}^T\mathbf{N}_{vw,x}^T\mathbf{N}_{vw,x}\delta\mathbf{v}
\end{aligned}
\tag{4.17}
$$

4.2.2 Rotation of internal bending moment

When a cross section of a beam element is subjected to rotation, the orientation of the internal bending moments acting on the section changes. This gives rise to geometric terms in the internal force vector and thus geometric stiffness.

In order to obtain the correct expressions for the stiffness terms due to the translational and the rotational dofs, the beam element in a deflected state is studied. Assuming that all deformations are small, the rotation of the element
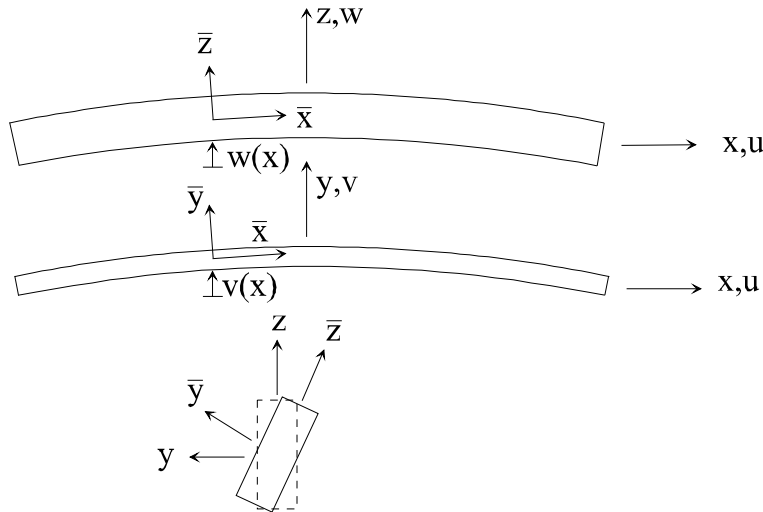
Figure 4.4: *Deformed beam element. Shown from three perspectives.*

coordinate axes into their cross-sectional counterparts is found by considering a coordinate system with axes of unit length, and using the Pytagorean rule in the cross-section plane.
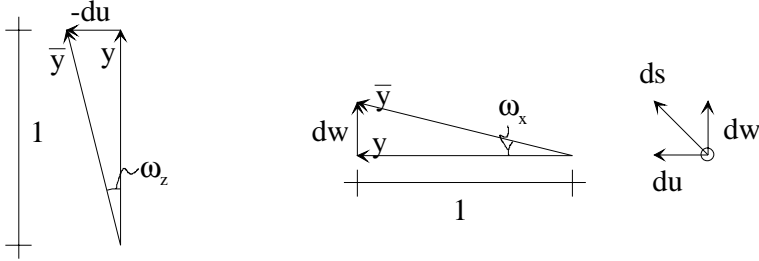
Rotation of $x-$axis into $\bar{x}-$axis
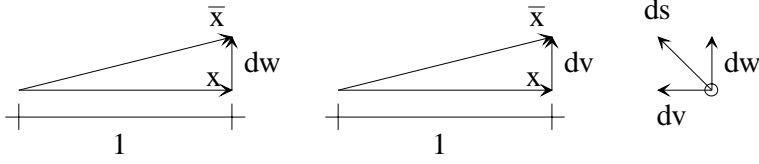
$$dw = -\omega_y \qquad\qquad dv = \omega_z \qquad\qquad (4.18)$$

$$ds = \sqrt{dv^2 + dw^2} \quad \Rightarrow \quad \text{Rot. of x-axis:} \quad \alpha = \frac{ds}{1} = \sqrt{\omega_z^2 + \omega_y^2} \qquad (4.19)$$

The local x-axis, $\bar{x}$, is given by $\bar{x} = \begin{bmatrix} 1 & dv & dw \end{bmatrix}^T$. Provided that the deformations are small, the assumption that $|\bar{x}| = |x| = 1$ is sufficiently accurate, and the unit vector along the local x-axis is given as

$$\mathbf{j}_x = \bar{\mathbf{x}} = \begin{bmatrix} 1 & \omega_z & -\omega_y \end{bmatrix}^T \qquad\qquad (4.20)$$

Rotation of $y-$axis into $\bar{y}-$axis

$$du = -\omega_z \qquad\qquad dw = \omega_x \qquad\qquad ds = \sqrt{du^2 + dw^2} \qquad (4.21)$$

The rotation of the y-axis is thus given by:

$$\beta = \frac{ds}{1} = \sqrt{\omega_y^2 + \omega_z^2} \qquad\qquad (4.22)$$

Analogous with the unit vector along the $\bar{x}$-axis, the unit vector along the local y-axis, $\bar{y}$ is given by

$$\mathbf{j}_y = \bar{\mathbf{y}} = \begin{bmatrix} du & 1 & dw \end{bmatrix}^T = \begin{bmatrix} -\omega_z & 1 & \omega_x \end{bmatrix}^T \qquad (4.23)$$

Rotation of $z-$axis into $\bar{z}-$axis
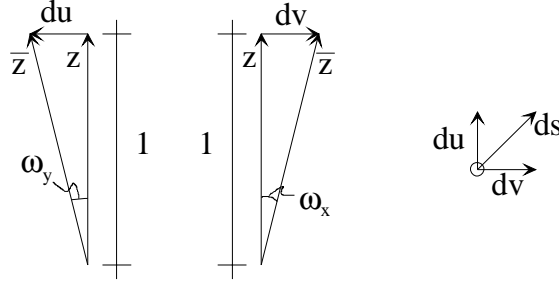
$$du = \omega_y \qquad dv = \omega_x \qquad ds = \sqrt{du^2 + dv^2} \qquad (4.24)$$

Thus, the rotation of the z-axis is given by:

$$\varrho = \frac{ds}{1} = \sqrt{\omega_y^2 + \omega_x^2} \qquad (4.25)$$

Along the local $\bar{z}$-axis, the unit vector is found in the same manner as for the local $\bar{x}$- and $\bar{y}$-axes.

$$\mathbf{j}_z = \bar{\mathbf{z}} = \begin{bmatrix} du & -dv & 1 \end{bmatrix}^T = \begin{bmatrix} \omega_y & -\omega_x & 1 \end{bmatrix}^T \qquad (4.26)$$

Transformation matrix from element coordinate system to cross-section coordinate system

By gathering the unit vectors from equations (4.20) through (4.26), the transformation matrix from element coordinate system to cross-sectional coordinate system is obtained.

$$\mathbf{T} = \begin{bmatrix} \mathbf{j}_x^T \\ \mathbf{j}_y^T \\ \mathbf{j}_z^T \end{bmatrix} = \begin{bmatrix} 1 & \omega_z & -\omega_y \\ -\omega_z & 1 & \omega_x \\ \omega_y & -\omega_x & 1 \end{bmatrix} \qquad (4.27)$$

Observe that when introducing the vector of rotation $\boldsymbol{\omega}$ from equation (4.5) on page 54, the transformation matrix (4.27) can be written as $\mathbf{T} = \mathbf{I} - \mathbf{Spin}(\boldsymbol{\omega})$, where $\mathbf{I}$ is the 3x3 unit matrix. Hence, the variation of $\mathbf{T}$ is

$$\delta\mathbf{T} = \delta\mathbf{I} - \delta\mathbf{Spin}(\boldsymbol{\omega}) = -\mathbf{Spin}(\delta\boldsymbol{\omega}) \qquad (4.28)$$

4.2.3 Transformation of the vector of curvature

Equation (4.6) from page 54 defines the vector of curvature.

Premultiplication of $\boldsymbol{\kappa}$ with the transformation matrix $\mathbf{T}$ of equation (4.27), gives the vector of curvature in the cross-section coordinate system:

$$\bar{\boldsymbol{\kappa}} \quad = \quad \mathbf{T}\boldsymbol{\kappa} = \mathbf{T}\mathbf{N}_{\kappa}\mathbf{v}$$

$$= \quad \begin{bmatrix} \bar{\kappa}_x \\ \bar{\kappa}_y \\ \bar{\kappa}_z \end{bmatrix} = \begin{bmatrix} 1 & \omega_z & -\omega_y \\ -\omega_z & 1 & \omega_x \\ \omega_y & -\omega_x & 1 \end{bmatrix} \begin{bmatrix} \kappa_x \\ \kappa_y \\ \kappa_z \end{bmatrix} \qquad (4.29)$$

$$= \quad \begin{bmatrix} \kappa_x + \omega_z\kappa_y - \omega_y\kappa_z \\ -\omega_z\kappa_x + \kappa_y + \omega_x\kappa_z \\ \omega_y\kappa_x - \omega_x\kappa_y + \kappa_z \end{bmatrix}$$

From equation (4.29), the variation of the cross-section vector of curvature can be expressed as

$$\begin{aligned} \delta\bar{\boldsymbol{\kappa}} \quad &= \quad \delta\mathbf{T}\mathbf{N}_{\kappa}\mathbf{v} + \mathbf{T}\mathbf{N}_{\kappa}\delta\mathbf{v} = -\mathbf{Spin}\left(\delta\boldsymbol{\omega}\right)\mathbf{N}_{\kappa}\mathbf{v} + \mathbf{T}\mathbf{N}_{\kappa}\delta\mathbf{v} \\ &= \quad \mathbf{T}\mathbf{N}_{\kappa}\delta\mathbf{v} + \mathbf{Spin}\left(\mathbf{N}_{\kappa}\mathbf{v}\right)\mathbf{N}_{\omega}\delta\mathbf{v} \end{aligned} \qquad (4.30)$$

where the relationship $\delta\boldsymbol{\omega} = \mathbf{N}_{\omega}\mathbf{v}$ has been used.

4.2.4   Strain

The cross-section coordinate system is defined such that y and z are the cross section axes, see figure *4.1* on page 52. Making use of Navier's hypothesis, the axial strain may therefore be written as

$$\epsilon = \epsilon_c + z\bar{\kappa}_y + y\bar{\kappa}_z \qquad (4.31)$$

with variation

$$\delta\epsilon = \delta\epsilon_c + z\delta\bar{\kappa}_y + y\delta\bar{\kappa}_z \qquad (4.32)$$

Similarly, the torsional shear strain is given by

$$\gamma = \sqrt{y^2 + z^2}\,\bar{\kappa}_x \qquad (4.33)$$

with variation

$$\delta\gamma = \sqrt{y^2 + z^2}\,\delta\bar{\kappa}_x \qquad (4.34)$$

Strictly speaking, the latter two equations are only valid for circular cross-sections. However, as will be seen in section 4.5.3, the element formulation can be changed in order to accommodate other types of cross-sections by introducing the St.Venant torsional constant I_t.

4.3 Variation of the strain energy - Force vector

The strain energy of the beam element is given by

$$U = \int_V \int_0^\gamma \tau \, d\gamma \, dV + \int_V \int_0^\epsilon \sigma \, d\epsilon \, dV \tag{4.35}$$

Where

τ and γ	are shear stress and strain, respectively,
σ and ϵ	are axial stress and strain, respectively, and
V	is the volume of the element.

Since one of the basic assumptions is that Navier's hypothesis is valid, deformation due to shear is not included in this element formulation, and thus τ and γ are due to torsion only.

The internal force vector of the element is found from variation of equation (4.35):

$$\delta U = \frac{\partial U}{\partial \mathbf{v}} \delta \mathbf{v} = \delta \mathbf{v}^T \mathbf{f} \tag{4.36}$$

Introducing equations (4.35), (4.32) and (4.34) into equation (4.36), the following expression for the variation of the strain energy is found:

$$
\begin{aligned}
\delta U &= \int_V \tau \, \delta\gamma \, dV + \int_V \sigma \, \delta\epsilon \, dV \\
&= \int_V \tau \sqrt{y^2 + z^2} \, \delta\bar{\kappa} + \int_V \sigma \left(z\delta\bar{\kappa}_y + y\delta\bar{\kappa}_z + \delta\epsilon_c \right) dV \\
&= \int_V \left[\ \tau\sqrt{y^2 + z^2} \quad z\sigma \quad y\sigma \ \right] \delta\bar{\boldsymbol{\kappa}} \, dV + \int_V \sigma \, \delta\epsilon_c dV
\end{aligned} \tag{4.37}
$$

Introducing

$$\mathbf{D}^T = \left[\ \sqrt{y^2 + z^2}\,\tau \quad z\,\sigma \quad y\,\sigma \ \right] \tag{4.38}$$

and making use of (4.30) and (4.17) from page 60 and 57, respectively, δU can

be expressed as

$$
\begin{aligned}
\delta U \;=\;& \int_V \mathbf{D}^T \delta\bar{\boldsymbol{\kappa}}\, dV + \int_V \sigma\, \delta\epsilon_c\, dV \\[2ex]
\;=\;& \int_V \mathbf{D}^T \left(\mathbf{T}\mathbf{N}_\kappa \delta\mathbf{v} + \mathbf{Spin}\left(\mathbf{N}_\kappa \mathbf{v}\right) \mathbf{N}_\omega \delta\mathbf{v} \right) dV \\
+\;& \int_V \sigma \left(\mathbf{N}_{u,x}\delta\mathbf{v} + \mathbf{v}^T \mathbf{N}_{vw,x}^T \mathbf{N}_{vw,x}\delta\mathbf{v} \right) dV \\[2ex]
\;=\;& \int_V \left(\mathbf{D}^T \mathbf{T}\mathbf{N}_\kappa \delta\mathbf{v} + \mathbf{D}^T \mathbf{Spin}\left(\mathbf{N}_\kappa \mathbf{v}\right) \mathbf{N}_\omega \delta\mathbf{v} \right) dV \\
+\;& \int_V \left(\sigma\, \mathbf{N}_{u,x}\delta\mathbf{v} + \sigma\, \mathbf{v}^T \mathbf{N}_{vw,x}^T \mathbf{N}_{vw,x}\delta\mathbf{v} \right) dV \\[2ex]
\;=\;& \delta\mathbf{v}^T \int_V \left(\mathbf{N}_\kappa^T \mathbf{T}^T \mathbf{D} - \mathbf{N}_\omega^T \mathbf{Spin}\left(\mathbf{N}_\kappa \mathbf{v}\right) \mathbf{D} \right) dV \\
+\;& \delta\mathbf{v}^T \int_V \left(\sigma\, \mathbf{N}_{u,x}^T + \sigma\, \mathbf{N}_{vw,x}^T \mathbf{N}_{vw,x}\mathbf{v} \right) dV
\end{aligned}
\tag{4.39}
$$

Thus, the internal force vector of the element is

$$
\begin{aligned}
\mathbf{f} \;=\;& \int_V \left(\mathbf{N}_\kappa^T \mathbf{T}^T \mathbf{D} - \mathbf{N}_\omega^T \mathbf{Spin}\left(\mathbf{N}_\kappa \mathbf{v}\right) \mathbf{D} \right) dV \\
+\;& \int_V \left(\mathbf{N}_{u,x}^T \sigma + \sigma\, \mathbf{N}_{vw,x}^T \mathbf{N}_{vw,x}\mathbf{v} \right) dV
\end{aligned}
\tag{4.40}
$$

4.4 Variation of the force vector - tangent stiffness

In order to establish the variation of the force vector, and thereby the tangent stiffness of the element, the variation of the vector $\mathbf{D}$ and the variation of the axial stress σ need to be established.

Variation of D

The following material assumptions apply:

$$
\begin{aligned}
\delta\tau &= G(\gamma)\delta\gamma = G(\gamma)\sqrt{y^2+z^2}\delta\bar{\kappa}_x \\
\delta\sigma &= E(\epsilon)\delta\epsilon = E(\epsilon)\left(z\delta\bar{\kappa}_y + y\delta\bar{\kappa}_z + \delta\epsilon_c\right) \\
G(\gamma) &= \frac{\partial\tau}{\partial\gamma} \qquad E(\epsilon) = \frac{\partial\sigma}{\partial\epsilon}
\end{aligned}
\tag{4.41}
$$

$$
\begin{aligned}
\delta\mathbf{D} &=
\begin{bmatrix}
\sqrt{y^2+z^2}\,\delta\tau \\
z\,\delta\sigma \\
y\,\delta\sigma
\end{bmatrix}
=
\begin{bmatrix}
\sqrt{y^2+z^2}\,G(\gamma)\sqrt{y^2+z^2}\,\delta\bar{\kappa}_x \\
z\,E(\epsilon)\left(z\delta\bar{\kappa}_y + y\delta\bar{\kappa}_z + \delta\epsilon_c\right) \\
y\,E(\epsilon)\left(z\delta\bar{\kappa}_y + y\delta\bar{\kappa}_z + \delta\epsilon_c\right)
\end{bmatrix} \\[2ex]
&=
\begin{bmatrix}
\left(y^2+z^2\right)G(\gamma)\,\delta\bar{\kappa}_x \\
z^2 E(\epsilon)\delta\bar{\kappa}_y + zyE(\epsilon)\delta\bar{\kappa}_z \\
zyE(\epsilon)\delta\bar{\kappa}_y + y^2 E(\epsilon)\delta\bar{\kappa}_z
\end{bmatrix}
+
\begin{bmatrix}
0 \\
zE(\epsilon)\delta\epsilon_c \\
yE(\epsilon)\delta\epsilon_c
\end{bmatrix} \\[2ex]
&=
\begin{bmatrix}
\left(y^2+z^2\right)G(\gamma) & 0 & 0 \\
0 & z^2 E(\epsilon) & zyE(\epsilon) \\
0 & zyE(\epsilon) & y^2 E(\epsilon)
\end{bmatrix}
\begin{bmatrix}
\delta\bar{\kappa}_x \\
\delta\bar{\kappa}_y \\
\delta\bar{\kappa}_z
\end{bmatrix} \\[2ex]
&\quad +
\begin{bmatrix}
0 \\
zE(\epsilon) \\
yE(\epsilon)
\end{bmatrix}\delta\epsilon_c
\end{aligned}
\tag{4.42}
$$

Making use of (4.30) and (4.17) from page 60 and 57, respectively, this becomes

$$
\begin{aligned}
\delta\mathbf{D} &= \mathbf{C}_1\delta\bar{\boldsymbol{\kappa}} + \mathbf{C}_2\delta\epsilon_c \\
&= \mathbf{C}_1\left(\mathbf{T}\mathbf{N}_\kappa\delta\mathbf{v} + \mathbf{Spin}\left(\mathbf{N}_\kappa\mathbf{v}\right)\mathbf{N}_\omega\delta\mathbf{v}\right) \\
&\quad + \mathbf{C}_2\left(\mathbf{N}_{u,x}\delta\mathbf{v} + \mathbf{v}^T\mathbf{N}_{vw,x}^T\mathbf{N}_{vw,x}\delta\mathbf{v}\right) \\
&= \mathbf{C}_1\mathbf{T}\mathbf{N}_\kappa\delta\mathbf{v} + \mathbf{C}_1\mathbf{Spin}\left(\mathbf{N}_\kappa\mathbf{v}\right)\mathbf{N}_\omega\delta\mathbf{v} \\
&\quad + \mathbf{C}_2\mathbf{N}_{u,x}\delta\mathbf{v} + \mathbf{C}_2\mathbf{v}^T\mathbf{N}_{vw,x}^T\mathbf{N}_{vw,x}\delta\mathbf{v}
\end{aligned}
\tag{4.43}
$$

Where

$$
\mathbf{C}_1 =
\begin{bmatrix}
\left(y^2+z^2\right)G(\gamma) & 0 & 0 \\
0 & z^2 E(\epsilon) & zyE(\epsilon) \\
0 & zyE(\epsilon) & y^2 E(\epsilon)
\end{bmatrix}
\quad\text{and}\quad
\mathbf{C}_2 =
\begin{bmatrix}
0 \\
zE(\epsilon) \\
yE(\epsilon)
\end{bmatrix}
\tag{4.44}
$$

Variation of axial stress σ

From (4.41), (4.44), (4.30) and (4.17) it follows that

$$
\begin{aligned}
\delta\sigma &= \frac{\partial\sigma}{\partial\epsilon}\delta\epsilon = E(\epsilon)\left(z\delta\bar{\kappa}_y + y\delta\bar{\kappa}_z + \delta\epsilon_c\right) \\
&= \begin{bmatrix} 0 & zE(\epsilon) & yE(\epsilon) \end{bmatrix}\delta\bar{\boldsymbol{\kappa}} + E(\epsilon)\delta\epsilon_c \\
&= \mathbf{C}_2^T\left(\mathbf{T}\mathbf{N}_\kappa\delta\mathbf{v} + \mathbf{Spin}\left(\mathbf{N}_\kappa\mathbf{v}\right)\mathbf{N}_\omega\delta\mathbf{v}\right) \\
&\quad + E(\epsilon)(\mathbf{N}_{u,x}\delta\mathbf{v} + \mathbf{v}^T\mathbf{N}_{vw,x}^T\mathbf{N}_{vw,x}\delta\mathbf{v}) \\
&= \mathbf{C}_2^T\mathbf{T}\mathbf{N}_\kappa\delta\mathbf{v} + \mathbf{C}_2^T\mathbf{Spin}\left(\mathbf{N}_\kappa\mathbf{v}\right)\mathbf{N}_\omega\delta\mathbf{v} + E(\epsilon)\mathbf{N}_{u,x}\delta\mathbf{v} \\
&\quad + E(\epsilon)\mathbf{v}^T\mathbf{N}_{vw,x}^T\mathbf{N}_{vw,x}\delta\mathbf{v}
\end{aligned}
\tag{4.45}
$$

Variation of internal force vector f

From equation (4.40):

$$
\begin{aligned}
\delta\mathbf{f} &= \int_V\left[\overbrace{\mathbf{N}_\kappa^T\delta\mathbf{T}^T\mathbf{D}}^{I} + \overbrace{\mathbf{N}_\kappa^T\mathbf{T}^T\delta\mathbf{D}}^{II} - \overbrace{\mathbf{N}_\omega^T\mathbf{Spin}\left(\mathbf{N}_\kappa\delta\mathbf{v}\right)\mathbf{D}}^{III}\right. \\
&\quad \left. - \overbrace{\mathbf{N}_\omega^T\mathbf{Spin}\left(\mathbf{N}_\kappa\mathbf{v}\right)\delta\mathbf{D}}^{IV}\right]dV \\
&\quad + \int_V\left[\overbrace{\mathbf{N}_{u,x}^T\delta\sigma}^{V} + \overbrace{\delta\sigma\,\mathbf{N}_{vw,x}^T\mathbf{N}_{vw,x}\mathbf{v}}^{VI} + \overbrace{\sigma\,\mathbf{N}_{vw,x}^T\mathbf{N}_{vw,x}\delta\mathbf{v}}^{VII}\right]dV
\end{aligned}
\tag{4.46}
$$

The different terms in this equation are evaluated separately.

Term I

Using equation (4.28) from page 59, this term may be expressed as

$$
\mathbf{N}_\kappa^T\delta\mathbf{T}^T\mathbf{D} = \mathbf{N}_\kappa^T\left(-\mathbf{Spin}\left(\mathbf{N}_\omega\delta\mathbf{v}\right)\right)^T\mathbf{D} = -\mathbf{N}_\kappa^T\mathbf{Spin}\left(\mathbf{D}\right)\mathbf{N}_\omega\delta\mathbf{v}
\tag{4.47}
$$

Term *II*

$$
\begin{aligned}
\mathbf{N}_\kappa^T \mathbf{T}^T \delta \mathbf{D} &= \mathbf{N}_\kappa^T \mathbf{T}^T (\mathbf{C}_1 \mathbf{T} \mathbf{N}_\kappa \delta \mathbf{v} + \mathbf{C}_1 \mathbf{Spin}\,(\mathbf{N}_\kappa \mathbf{v})\, \mathbf{N}_\omega \delta \mathbf{v} \\
&+ \mathbf{C}_2 \mathbf{N}_{u,x} \delta \mathbf{v} + \mathbf{C}_2 \mathbf{v}^T \mathbf{N}_{vw,x}^T \mathbf{N}_{vw,x} \delta \mathbf{v}) \\
&= \mathbf{N}_\kappa^T \mathbf{T}^T \mathbf{C}_1 \mathbf{T} \mathbf{N}_\kappa \delta \mathbf{v} + \mathbf{N}_\kappa^T \mathbf{T}^T \mathbf{C}_1 \mathbf{Spin}\,(\mathbf{N}_\kappa \mathbf{v})\, \mathbf{N}_\omega \delta \mathbf{v} \\
&+ \mathbf{N}_\kappa^T \mathbf{T}^T \mathbf{C}_2 \mathbf{N}_{u,x} \delta \mathbf{v} + \mathbf{N}_\kappa^T \mathbf{T}^T \mathbf{C}_2 \mathbf{v}^T \mathbf{N}_{vw,x}^T \mathbf{N}_{vw,x} \delta \mathbf{v}
\end{aligned}
\tag{4.48}
$$

In the evaluation of this term, equation (4.43) was used.

Term *III*

$$
\mathbf{N}_\omega^T \mathbf{Spin}\,(\mathbf{N}_\kappa \delta \mathbf{v})\, \mathbf{D} = -\mathbf{N}_\omega^T \mathbf{Spin}\,(\mathbf{D})\, \mathbf{N}_\kappa \delta \mathbf{v}
\tag{4.49}
$$

Term *IV*

Making use of (4.43), this term evaluates to

$$
\begin{aligned}
\mathbf{N}_\omega^T \mathbf{Spin}\,(\mathbf{N}_\kappa \mathbf{v})\, \delta \mathbf{D} &= \mathbf{N}_\omega^T \mathbf{Spin}\,(\mathbf{N}_\kappa \mathbf{v})\, (\mathbf{C}_1 \mathbf{T} \mathbf{N}_\kappa \delta \mathbf{v} \\
&+ \mathbf{C}_1 \mathbf{Spin}\,(\mathbf{N}_\kappa \mathbf{v})\, \mathbf{N}_\omega \delta \mathbf{v} \\
&+ \mathbf{C}_2 \mathbf{N}_{u,x} \delta \mathbf{v} + \mathbf{C}_2 \mathbf{v}^T \mathbf{N}_{vw,x}^T \mathbf{N}_{vw,x} \delta \mathbf{v}) \\
&= \mathbf{N}_\omega^T \mathbf{Spin}\,(\mathbf{N}_\kappa \mathbf{v})\, \mathbf{C}_1 \mathbf{T} \mathbf{N}_\kappa \delta \mathbf{v} \\
&+ \mathbf{N}_\omega^T \mathbf{Spin}\,(\mathbf{N}_\kappa \mathbf{v})\, \mathbf{C}_1 \mathbf{Spin}\,(\mathbf{N}_\kappa \mathbf{v})\, \mathbf{N}_\omega \delta \mathbf{v} \\
&+ \mathbf{N}_\omega^T \mathbf{Spin}\,(\mathbf{N}_\kappa \mathbf{v})\, \mathbf{C}_2 \mathbf{N}_{u,x} \delta \mathbf{v} \\
&+ \mathbf{N}_\omega^T \mathbf{Spin}\,(\mathbf{N}_\kappa \mathbf{v})\, \mathbf{C}_2 \mathbf{v}^T \mathbf{N}_{vw,x}^T \mathbf{N}_{vw,x} \delta \mathbf{v}
\end{aligned}
\tag{4.50}
$$

Term *V*

By utilizing equation (4.45) for $\delta \sigma$, the fifth term can be expressed as

$$
\begin{aligned}
\mathbf{N}_{u,x} \delta \sigma &= \mathbf{N}_{u,x}^T \mathbf{C}_2^T \mathbf{T} \mathbf{N}_\kappa \delta \mathbf{v} + \mathbf{N}_{u,x}^T \mathbf{C}_2^T \mathbf{Spin}\,(\mathbf{N}_\kappa \mathbf{v})\, \mathbf{N}_\omega \delta \mathbf{v} \\
&+ \mathbf{N}_{u,x}^T E(\epsilon) \mathbf{N}_{u,x} \delta \mathbf{v} + \mathbf{N}_{u,x}^T E(\epsilon) \mathbf{v}^T \mathbf{N}_{vw,x}^T \mathbf{N}_{vw,x} \delta \mathbf{v}
\end{aligned}
\tag{4.51}
$$

Term VI

$$
\begin{aligned}
\delta\sigma\mathbf{N}_{vw,x}^{T}\mathbf{N}_{vw,x}\mathbf{v} \;=\; & \mathbf{N}_{vw,x}^{T}\mathbf{N}_{vw,x}\mathbf{v}\mathbf{C}_{2}^{T}\mathbf{T}\mathbf{N}_{\kappa}\delta\mathbf{v} \\
+\; & \mathbf{N}_{vw,x}^{T}\mathbf{N}_{vw,x}\mathbf{v}\mathbf{C}_{2}^{T}\mathbf{Spin}\left(\mathbf{N}_{\kappa}\mathbf{v}\right)\mathbf{N}_{\omega}\delta\mathbf{v} \\
+\; & \mathbf{N}_{vw,x}^{T}\mathbf{N}_{vw,x}\mathbf{v}E(\epsilon)\mathbf{N}_{u,x}\delta\mathbf{v} \\
+\; & \mathbf{N}_{vw,x}^{T}\mathbf{N}_{vw,x}\mathbf{v}E(\epsilon)\mathbf{v}^{T}\mathbf{N}_{vw,x}^{T}\mathbf{N}_{vw,x}\delta\mathbf{v}
\end{aligned}
\tag{4.52}
$$

This term was evaluated by using (4.45) for $\delta\sigma$.

Term VII

$$
\sigma\mathbf{N}_{vw,x}^{T}\mathbf{N}_{vw,x}\delta\mathbf{v} \;=\; \sigma\mathbf{N}_{vw,x}^{T}\mathbf{N}_{vw,x}\delta\mathbf{v}
\tag{4.53}
$$

Tangent stiffness $\mathbf{k}_{T}$

The tangent stiffness matrix, $\mathbf{k}_{T}$, of the element is defined from the variation of the force vector:

$$
\delta\mathbf{f} = \mathbf{k}_{T}\delta\mathbf{v}
\tag{4.54}
$$

Hence, the tangent stiffness of this element is found by reassembly of terms I through VII above:

$$
\begin{aligned}
\mathbf{k}_{T} \;=\; \int_{V} \Big[& \mathbf{N}_{\kappa}^{T}\mathbf{T}^{T}\mathbf{C}_{1}\mathbf{T}\mathbf{N}_{\kappa} + E(\epsilon)\mathbf{N}_{u,x}^{T}\mathbf{N}_{u,x} + \sigma\mathbf{N}_{vw,x}^{T}\mathbf{N}_{vw,x} \\
+\; & E(\epsilon)\mathbf{N}_{vw,x}^{T}\mathbf{N}_{vw,x}\mathbf{v}\mathbf{v}^{T}\mathbf{N}_{vw,x}^{T}\mathbf{N}_{vw,x} \\
-\; & \mathbf{N}_{\omega}^{T}\mathbf{Spin}\left(\mathbf{N}_{\kappa}\mathbf{v}\right)\mathbf{C}_{1}\mathbf{Spin}\left(\mathbf{N}_{\kappa}\mathbf{v}\right)\mathbf{N}_{\omega} \\
+\; & \mathbf{N}_{\kappa}^{T}\mathbf{T}^{T}\mathbf{C}_{1}\mathbf{Spin}\left(\mathbf{N}_{\kappa}\mathbf{v}\right)\mathbf{N}_{\omega} - \mathbf{N}_{\omega}^{T}\mathbf{Spin}\left(\mathbf{N}_{\kappa}\mathbf{v}\right)\mathbf{C}_{1}\mathbf{T}\mathbf{N}_{\kappa} \\
+\; & \mathbf{N}_{\kappa}\mathbf{T}^{T}\mathbf{C}_{2}\mathbf{N}_{u,x} + \mathbf{N}_{u,x}^{T}\mathbf{C}_{2}^{T}\mathbf{T}\mathbf{N}_{\kappa} \\
+\; & \mathbf{N}_{\kappa}^{T}\mathbf{T}^{T}\mathbf{C}_{2}\mathbf{v}^{T}\mathbf{N}_{vw,x}^{T}\mathbf{N}_{vw,x} + \mathbf{N}_{vw,x}^{T}\mathbf{N}_{vw,x}\mathbf{v}\mathbf{C}_{2}^{T}\mathbf{T}\mathbf{N}_{\kappa} \\
+\; & \mathbf{N}_{u,x}^{T}\mathbf{C}_{2}^{T}\mathbf{Spin}\left(\mathbf{N}_{\kappa}\mathbf{v}\right)\mathbf{N}_{\omega} - \mathbf{N}_{\omega}^{T}\mathbf{Spin}\left(\mathbf{N}_{\kappa}\mathbf{v}\right)\mathbf{C}_{2}\mathbf{N}_{u,x} \\
+\; & \mathbf{N}_{vw,x}^{T}\mathbf{N}_{vw,x}\mathbf{v}\mathbf{C}_{2}^{T}\mathbf{Spin}\left(\mathbf{N}_{\kappa}\mathbf{v}\right)\mathbf{N}_{\omega} \\
-\; & \mathbf{N}_{\omega}^{T}\mathbf{Spin}\left(\mathbf{N}_{\kappa}\mathbf{v}\right)\mathbf{C}_{2}\mathbf{v}^{T}\mathbf{N}_{vw,x}^{T}\mathbf{N}_{vw,x} \\
+\; & E(\epsilon)\mathbf{N}_{u,x}^{T}\mathbf{v}^{T}\mathbf{N}_{vw,x}^{T}\mathbf{N}_{vw,x} + E(\epsilon)\mathbf{N}_{vw,x}^{T}\mathbf{N}_{vw,x}\mathbf{v}\mathbf{N}_{u,x} \\
+\; & \mathbf{N}_{\omega}^{T}\mathbf{Spin}\left(\mathbf{D}\right)\mathbf{N}_{\kappa} - \mathbf{N}_{\kappa}^{T}\mathbf{Spin}\left(\mathbf{D}\right)\mathbf{N}_{\omega} \Big] dV
\end{aligned}
\tag{4.55}
$$

In (4.55) the terms are ordered in such a fashion that each line forms a symmetric contribution to the tangent stiffness matrix. The only exception is the terms in line eight and nine, which *together* form a symmetric contribution to $\mathbf{k}_{T}$.

4.5 Beam element with internal geometric stiffness - implementation

To assess the element formulation presented above, it has been implemented in the co-rotated finite element method program *Cfem*, developed by Haugen[4].

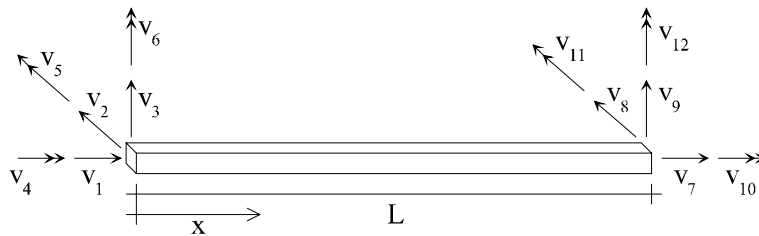Only linear elastic material is considered in the implementation.

4.5.1 Element basics

Figure 4.5: *Beam element with two nodes and twelve degrees of freedom.*

The linear element chosen as basis for this implementation is a two-noded beam element with six degrees of freedom at each node, see figure *4.5*.

For the axial displacement and the angle of twist, linear interpolation is used, whereas the standard cubic beam functions are used in the bending degrees of freedom. Hence, the following shape functions are used for interpolation of the displacements:
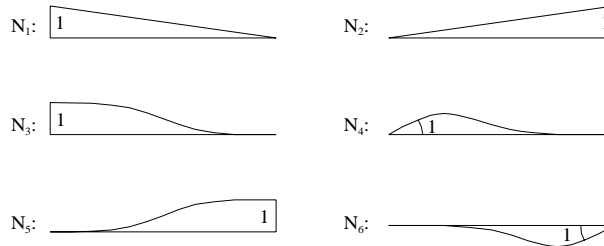
The mathematical representation of the shape functions is:

$$
\begin{array}{llll}
N_1 & = & 1 - \frac{x}{L} & \qquad N_2 & = & \frac{x}{L} \\
N_3 & = & 1 - \frac{3x^2}{L^2} + \frac{2x^3}{L^3} & \qquad N_4 & = & x - \frac{2x^2}{L} + \frac{x^3}{L^2} \\
N_5 & = & \frac{3x^2}{L^2} - \frac{2x^3}{L^3} & \qquad N_6 & = & -\frac{x^2}{L} + \frac{x^3}{L^2}
\end{array} \tag{4.56}
$$

The displacement components can now be expressed as

$$u = \begin{bmatrix} N_1 & 0 & 0 & 0 & 0 & 0 & N_2 & 0 & 0 & 0 & 0 & 0 \end{bmatrix} \mathbf{v} = \mathbf{N}_u \mathbf{v}$$

$$v = \begin{bmatrix} 0 & N_3 & 0 & 0 & 0 & N_4 & 0 & N_5 & 0 & 0 & 0 & N_6 \end{bmatrix} \mathbf{v} = \mathbf{N}_v \mathbf{v}$$

(4.57)

$$\begin{aligned} w &= \begin{bmatrix} 0 & 0 & N_3 & 0 & -N_4 & 0 & 0 & 0 & N_5 & 0 & -N_6 & 0 \end{bmatrix} \mathbf{v} \\ &= \mathbf{N}_w \mathbf{v} \end{aligned}$$

where $\mathbf{v} = \begin{bmatrix} v_1 & v_2 & v_3 & v_4 & v_5 & v_6 & v_7 & v_8 & v_9 & v_{10} & v_{11} & v_{12} \end{bmatrix}^T$.

Interpolation of the angle of twist of the element is the same as for the axial displacement:

$$\theta = \begin{bmatrix} 0 & 0 & 0 & N_1 & 0 & 0 & 0 & 0 & 0 & N_2 & 0 & 0 \end{bmatrix} \mathbf{v} = \mathbf{N}_\theta \mathbf{v} \qquad (4.58)$$

θ is the rotation of a point about the element x-axis, whereas the rotation about the cross-section y- and z-axes can be found from differentiation of the transverse displacements. Thus, the rotation vector for the element is

$$\boldsymbol{\omega} = \begin{bmatrix} \omega_x \\ \omega_y \\ \omega_z \end{bmatrix} = \begin{bmatrix} \theta \\ -w_{,x} \\ v_{,x} \end{bmatrix} = \begin{bmatrix} \mathbf{N}_\theta \\ -\mathbf{N}_{w,x} \\ \mathbf{N}_{v,x} \end{bmatrix} \mathbf{v} = \mathbf{N}_\omega \mathbf{v} \qquad (4.59)$$

Similarly, the curvature of the element axis can be found from differentiation of the rotation vector:

$$\boldsymbol{\kappa} = \begin{bmatrix} \kappa_x \\ \kappa_y \\ \kappa_z \end{bmatrix} = \frac{\partial}{\partial x} \begin{bmatrix} \omega_x \\ \omega_y \\ \omega_z \end{bmatrix} = \begin{bmatrix} \mathbf{N}_{\theta,x} \\ -\mathbf{N}_{w,xx} \\ \mathbf{N}_{v,xx} \end{bmatrix} \mathbf{v} = \mathbf{N}_\kappa \mathbf{v} \qquad (4.60)$$

4.5.2   Axial locking

Since the shape functions of the axial displacement and the transverse displacements are of different order (or rather that the first derivative of the axial displacement is of different order than the square of the first derivative of the transverse displacements), the formulation results in an element much too stiff when experiencing transverse deformation. The reason for this can be found by studying equation (4.16) in page 56. $u_{,x}$ is always constant along the element axis, whereas $\frac{1}{2}v_{,x}^2 + \frac{1}{2}w_{,x}^2$ is not. Therefore all transverse displacements will be associated with centerline axial strain in parts of the element, in turn giving rise to "unphysical" strain energy. This phenomenon may be called *axial*

locking, and is analogous with the more commonly known term *shear locking*. To remedy this problem, the terms involving transversal displacement in the axial strain expression are replaced by the mean of these terms. Thus, the axial strain given by equation (4.16) reduces to

$$\epsilon_c = u_{,x} + \frac{1}{2}\overline{v_{,x}^2} + \frac{1}{2}\overline{w_{,x}^2} \tag{4.61}$$

where

$$\overline{v_{,x}^2} = \frac{1}{L}\int_0^L \mathbf{v}^T \mathbf{N}_{v,x}^T \mathbf{N}_{v,x} \mathbf{v} dx \quad \text{and} \quad \overline{w_{,x}^2} = \frac{1}{L}\int_0^L \mathbf{v}^T \mathbf{N}_{w,x}^T \mathbf{N}_{w,x} \mathbf{v} dx \tag{4.62}$$

Observe that

$$\mathbf{N}_{v,x}^T \mathbf{N}_{v,x} + \mathbf{N}_{w,x}^T \mathbf{N}_{w,x} = \mathbf{N}_{vw,x}^T \mathbf{N}_{vw,x} \tag{4.63}$$

causing the centerline axial strain in equation (4.61) to become

$$\begin{aligned}
\epsilon_c &= u_{,x} + \tfrac{1}{2}\overline{v_{,x}^2} + \tfrac{1}{2}\overline{w_{,x}^2} = \mathbf{N}_{u,x}\mathbf{v} + \mathbf{v}^T \tfrac{1}{2L}\int_0^L \mathbf{N}_{vw,x}^T \mathbf{N}_{vw,x} dx\, \mathbf{v} \\
&= \mathbf{N}_{u,x}\mathbf{v} + \tfrac{1}{2L}\mathbf{v}^T \mathbf{k}_g \mathbf{v}
\end{aligned} \tag{4.64}$$

where

$$\mathbf{k}_g = \int_0^L \mathbf{N}_{vw,x}^T \mathbf{N}_{vw,x} dx \tag{4.65}$$

The effect of the substitution introduced in equation (4.61) is that all instances of $\mathbf{N}_{vw,x}^T \mathbf{N}_{vw,x}$ in the force vector and the tangent stiffness are replaced by $\frac{1}{L}\mathbf{k}_g$.

4.5.3   f and $\mathbf{k}_T$ for a linear elastic material

The one-dimensional linear elastic material model is characterized by the relationships

$$\begin{aligned}
\sigma &= E\epsilon & \delta\sigma &= E\delta\epsilon \\
\tau &= G\gamma & \delta\tau &= G\delta\gamma
\end{aligned} \tag{4.66}$$

where the constants E and G are the modulus of elasticity and the shear modulus for torsion, respectively.

Since all terms in (4.55) from page 66 need to be integrated over the cross-section area of the element, (A), it is of interest to study this integral for some

of the matrices in the case of linear elastic material model.

$$\int_A \mathbf{C}_1 dA = \int_A \begin{bmatrix} (y^2 + z^2)G & 0 & 0 \\ 0 & z^2E & zyE \\ 0 & zyE & y^2E \end{bmatrix} dA$$

$$= \begin{bmatrix} GI_t & 0 & 0 \\ 0 & EI_{yy} & 0 \\ 0 & 0 & EI_{zz} \end{bmatrix} = \mathbf{E} \qquad (4.67)$$

$$\int_A \mathbf{C}_2 dA = \int_A \begin{bmatrix} 0 \\ zE \\ yE \end{bmatrix} dA = \mathbf{0} \qquad (4.68)$$

Here, it has been taken advantage of the fact that the y and z-axes are the principal axes of the cross-section. In equation (4.67), the polar moment of inertia, $\int_A \left(y^2 + z^2 \right) dA$, which is applicable only for circular sections, is replaced by St. Venant torsion I_t.

The vector $\mathbf{D}$ and the stress σ also need to be established. By introducing (4.31) from page 60, (4.64) and (4.66) into (4.38) from page 61, vector $\mathbf{D}$ can be expressed as

$$\mathbf{D} = \begin{bmatrix} \sqrt{y^2 + z^2}\,\tau \\ z\sigma \\ y\sigma \end{bmatrix} = \begin{bmatrix} \sqrt{y^2 + z^2}\,G\sqrt{y^2 + z^2}\,\bar{\kappa}_x \\ zE(z\bar{\kappa}_y + y\bar{\kappa}_z + \epsilon_c) \\ yE(z\bar{\kappa}_y + y\bar{\kappa}_z + \epsilon_c) \end{bmatrix}$$

$$= \begin{bmatrix} (y^2 + z^2)G & 0 & 0 \\ 0 & z^2E & zyE \\ 0 & zyE & y^2E \end{bmatrix} \begin{bmatrix} \bar{\kappa}_x \\ \bar{\kappa}_y \\ \bar{\kappa}_z \end{bmatrix} + \begin{bmatrix} 0 \\ zE \\ yE \end{bmatrix} \epsilon_c \qquad (4.69)$$

$$= \mathbf{C}_1 \mathbf{T} \mathbf{N}_\kappa \mathbf{v} + \mathbf{C}_2 \left(\mathbf{N}_{u,x} \mathbf{v} + \tfrac{1}{L} \mathbf{v}^T \mathbf{k}_g \mathbf{v} \right)$$

whereas σ is found from (4.66) and (4.31):

$$\sigma = E\epsilon = E(z\bar{\kappa}_y + y\bar{\kappa}_z + \epsilon_c)$$

$$= \mathbf{C}_2 \mathbf{T} \mathbf{N}_\kappa \mathbf{v} + E \left(\mathbf{N}_{u,x} \mathbf{v} + \tfrac{1}{2L} \mathbf{v}^T \mathbf{k}_g \mathbf{v} \right) \qquad (4.70)$$

Force vector

For a linear elastic material, the force vector of the element is now found from equation (4.40) on page 62.

$$
\begin{aligned}
\mathbf{f} \;=\; & \int_0^L \int_A \left[\mathbf{N}_\kappa^T \mathbf{T}^T \mathbf{D} - \mathbf{N}_\omega^T \mathbf{Spin}\,(\mathbf{N}_\kappa \mathbf{v})\,\mathbf{D} \right] dA \, dx \\
& + \int_0^L \int_A \left[\mathbf{N}_{u,x}^T \sigma + \sigma \tfrac{1}{L} \mathbf{k}_g \mathbf{v} \right] dA \, dx \\
\;=\; & \int_0^L \int_A \left[\mathbf{N}_\kappa^T \mathbf{T}^T \left(\mathbf{C}_1 \mathbf{T} \mathbf{N}_\kappa \mathbf{v} + \mathbf{C}_2 \left(\mathbf{N}_{u,x}\mathbf{v} + \tfrac{1}{L}\mathbf{v}^T \mathbf{k}_g \mathbf{v} \right) \right) \right. \\
& \quad - \; \mathbf{N}_\omega^T \mathbf{Spin}\,(\mathbf{N}_\kappa \mathbf{v}) \left(\mathbf{C}_1 \mathbf{T} \mathbf{N}_\kappa \mathbf{v} + \mathbf{C}_2 \left(\mathbf{N}_{u,x}\mathbf{v} + \tfrac{1}{L}\mathbf{v}^T \mathbf{k}_g \mathbf{v} \right) \right) \\
& \quad + \; \mathbf{N}_{u,x}^T \left(\mathbf{C}_2 \mathbf{T} \mathbf{N}_\kappa \mathbf{v} + E \left(\mathbf{N}_{u,x}\mathbf{v} + \tfrac{1}{2L}\mathbf{v}^T \mathbf{k}_g \mathbf{v} \right) \right) \\
& \quad + \; \left. \left(\mathbf{C}_2 \mathbf{T} \mathbf{N}_\kappa \mathbf{v} + E \left(\mathbf{N}_{u,x}\mathbf{v} + \tfrac{1}{2L}\mathbf{v}^T \mathbf{k}_g \mathbf{v} \right) \right) \tfrac{1}{L}\mathbf{k}_g \mathbf{v} \right] dA \, dx
\end{aligned}
\tag{4.71}
$$

Hence

$$
\begin{aligned}
\mathbf{f} \;=\; & \int_0^L \left[\mathbf{N}_\kappa^T \mathbf{T}^T \mathbf{E} \mathbf{T} \mathbf{N}_\kappa \mathbf{v} - \mathbf{N}_\omega^T \mathbf{Spin}\,(\mathbf{N}_\kappa \mathbf{v})\,\mathbf{E}\mathbf{T}\mathbf{N}_\kappa \mathbf{v} \right] dx \\
& + \; \tfrac{1}{2L} E A \mathbf{k}_g \mathbf{v}\mathbf{v}^T \mathbf{k}_g \mathbf{v} + E A L \mathbf{N}_{u,x}^T \mathbf{N}_{u,x} \mathbf{v} + \tfrac{1}{2} E A \mathbf{N}_{u,x}^T \mathbf{v}^T \mathbf{k}_g \mathbf{v} \\
& + \; E A \mathbf{N}_{u,x} \mathbf{v} \mathbf{k}_g \mathbf{v}
\end{aligned}
\tag{4.72}
$$

Tangent stiffness matrix

The tangent stiffness matrix of the element evaluates to

$$
\begin{aligned}
\mathbf{k}_T \;=\; & \int_0^L \left[\mathbf{N}_\kappa^T \mathbf{T}^T \mathbf{E} \mathbf{T} \mathbf{N}_\kappa - \mathbf{N}_\omega^T \mathbf{Spin}\,(\mathbf{N}_\kappa \mathbf{v})\,\mathbf{E}\,\mathbf{Spin}\,(\mathbf{N}_\kappa \mathbf{v})\,\mathbf{N}_\omega \right. \\
& \quad + \; \mathbf{N}_\kappa^T \mathbf{T}^T \mathbf{E}\,\mathbf{Spin}\,(\mathbf{N}_\kappa \mathbf{v})\,\mathbf{N}_\omega - \mathbf{N}_\omega^T \mathbf{Spin}\,(\mathbf{N}_\kappa \mathbf{v})\,\mathbf{E}\mathbf{T}\mathbf{N}_\kappa \\
& \quad + \; \left. \mathbf{N}_\omega^T \mathbf{Spin}\,(\mathbf{E}\mathbf{T}\mathbf{N}_\kappa \mathbf{v})\,\mathbf{N}_\kappa - \mathbf{N}_\kappa^T \mathbf{Spin}\,(\mathbf{E}\mathbf{T}\mathbf{N}_\kappa \mathbf{v})\,\mathbf{N}_\omega \right] dx \\
& \quad + \; \tfrac{1}{L} E A \mathbf{k}_g \mathbf{v}\mathbf{v}^T \mathbf{k}_g + \tfrac{1}{2L} E A \mathbf{v}^T \mathbf{k}_g \mathbf{v}\mathbf{k}_g + E A L \mathbf{N}_{u,x}^T \mathbf{N}_{u,x} \\
& \quad + \; E A \mathbf{N}_{u,x} \mathbf{v}\mathbf{k}_g + E A \mathbf{N}_{u,x}^T \mathbf{v}^T \mathbf{k}_g + E A \mathbf{k}_g \mathbf{v}\mathbf{N}_{u,x}
\end{aligned}
\tag{4.73}
$$

4.5.4   Beam element with internal torsional dof

With only two degrees of freedom available for the angle of twist, it is limited
to a linear variation along the element. A single beam element is therefore
unable to describe lateral torsional buckling, since the element clearly can not
describe a torsional rotation of the mid-section of the element if the end points
are constrained against torsional rotation. Even two elements will give a very
crude representation of the angle of twist along the beam. The more elements
used to model the beam, the more accurate the results will be.

An attempt was made to improve the element's torsional behaviour through
incorporation of an additional internal torsional rotation degree of freedom in
the formulation. The additional dof was made *hierarcical*, meaning that the
displacement field associated with the internal dof was superimposed on the ex-
isting linear field. This modification, however, did not improve the performance
of the element considerably, and the idea was therefore not pursued, and the
modification is omitted in this dissertation.

4.5.5   The element formulation used in linearized buckling analyses

In linearized buckling analyses, an initial state of stress is found using the initial
stiffness of the model. This state of stress is superimposed on the model in its
initial state. Thus, all terms in the expressions of the force vector and the
stiffness matrix that indicate that the element is in a deformed state (or rather
only exist in a deformed state) should be omitted in linearized buckling analysis.
For this type of analysis, the following expressions should therefore be used for
the force vector:

$$\mathbf{f}_{lin} = \int_0^L \mathbf{N}_\kappa^T \mathbf{T}^T \mathbf{E} \mathbf{T} \mathbf{N}_\kappa \mathbf{v} dx + EAL \mathbf{N}_{u,x}^T \mathbf{N}_{u,x} \mathbf{v} + EA \mathbf{N}_{u,x} \mathbf{v} \mathbf{k}_g \mathbf{v} \qquad (4.74)$$

and the stiffness matrix:

$$\begin{aligned}
\mathbf{k}_{lin} \quad = \quad & \int_0^L \Big[\mathbf{N}_\kappa^T \mathbf{T}^T \mathbf{E} \mathbf{T} \mathbf{N}_\kappa \\
& + \; \mathbf{N}_\kappa^T \mathbf{T}^T \mathbf{E} \mathbf{Spin} \left(\mathbf{N}_\kappa \mathbf{v} \right) \mathbf{N}_\omega - \mathbf{N}_\omega^T \mathbf{Spin} \left(\mathbf{N}_\kappa \mathbf{v} \right) \mathbf{E} \mathbf{T} \mathbf{N}_\kappa \\
& + \; \mathbf{N}_\omega^T \mathbf{Spin} \left(\mathbf{E} \mathbf{T} \mathbf{N}_\kappa \mathbf{v} \right) \mathbf{N}_\kappa - \mathbf{N}_\kappa^T \mathbf{Spin} \left(\mathbf{E} \mathbf{T} \mathbf{N}_\kappa \mathbf{v} \right) \mathbf{N}_\omega \Big] dx \\
& + \; EAL \mathbf{N}_{u,x}^T \mathbf{N}_{u,x} + EA \mathbf{N}_{u,x} \mathbf{v} \mathbf{k}_g
\end{aligned} \qquad (4.75)$$

4.5.6 Loss of energy

A finite element formulation derived from the strain energy for use in static structural analyses, usually produces results that converge towards the correct solution from the "stiff side" when refining the element mesh.

The element described in this chapter, however, gives results that sometimes converge towards the correct solution from the flexible side. This seems to indicate that there is a loss of energy somewhere in the element formulation.
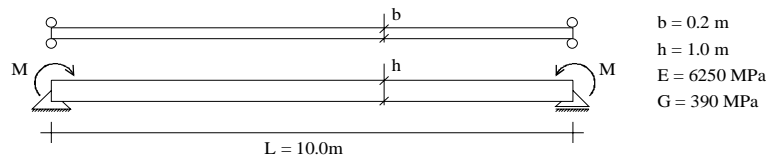
Figure 4.6: *A simply supported beam subjected to constant bending moment about the strong axis.*

In order to illustrate the problem, a simply supported beam with a high depth to width ratio is analyzed through lateral torsional buckling and beyond. The beam is subjected to a constant bending moment about the strong axis, see figure *4.6.*
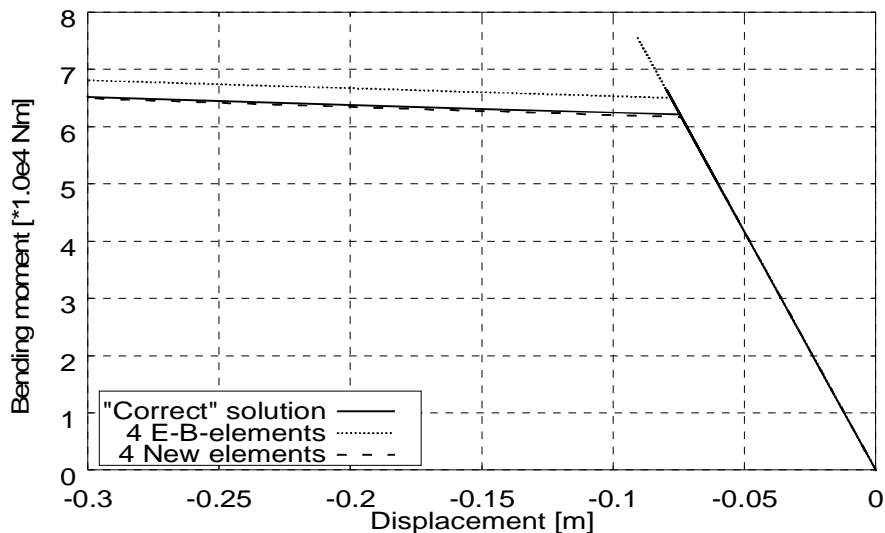
Figure 4.7: *Simply supported beam subjected to constant moment about the strong axis. Bending moment as function of vertical displacement of mid-point.*

Results from the analyses are shown in figure *4.7.* The graph shows the bending moment about the initially horisontal strong axis as a function of the ver-

tial displacement of the beam mid-point. Three different element meshes have been studied. First, the results presented as the "correct" solution have been found by using 200 Euler-Bernoulli beam elements to model the beam. For reference, results from an analysis where the beam has been modelled using 4 Euler-Bernoulli elements have been included. The final curve shows bending moment/displacement curve for an element mesh consisting of 4 elements of the type developed in this chapter, presented simply as the "new element".

It is seen that the curve for the new element lies slightly under the "correct" solution. This indicates that the new element is slightly too flexible. Observe, however, that the accuracy obtained with the new element is far better than that obtained with the standard Euler-Bernoulli elements.

A definitive explanation for why the element looses energy has not been found. However, the most likely explanation probably lies in the simplification introduced in equation (4.61) on page 69 in order to prevent axial locking. This simplification is comparable to an under-integration of the affected parts of the force vector and stiffness matrix, which could explain the loss of energy.

It will be shown in the next chapter, that convergence from the "soft" side is also found in linearized buckling analysis.

4.6   Shear stiffness

Since one of the basic assumptions for the new element was that Navier's hypothesis was valid, shear deformation is not included in the formulation. The effect of shear deformation may, however, be added a posteriori based on the mean shear strain angle in the element. The method for doing this can be found in, for instance, [58].

The following dimensionless constants are conveniently introduced:

$$\alpha_y = \frac{12EI_{zz}}{G_y A_{sy} L^2} \qquad \text{and} \qquad \alpha_z = \frac{12EI_{yy}}{G_z A_{sz} L^2} \qquad (4.76)$$

G_y and G_z are the shear moduli for shear in the y and z-direction, respectively. Correspondingly A_{sy} and A_{sz} are the shear areas for shear in the y- and z-direction, respectively.

The shear stiffness is incorporated into the stiffness matrix and the force vector in two steps:

- All terms involving displacement in the y-direction are divided by $(1+\alpha_y)$,

and all the terms involving displacement in the z-direction are divided by $(1 + \alpha_z)$. The easiest way to incorporate this is to build the force vector and stiffness matrix using the following adjusted values for the 2nd area moments:

$$I^*_{yy} = \frac{I_{yy}}{1 + \alpha_z} \qquad \text{and} \qquad I^*_{zz} = \frac{I_{zz}}{1 + \alpha_y} \qquad (4.77)$$

- Add the matrix $\mathbf{k}_s$ to the tangent stiffness matrix and $\mathbf{k}_s\mathbf{v}$ to the force vector. $\mathbf{k}_s$ are

$$\mathbf{k}_s = \mathbf{T}_s^T \mathbf{k}_s^* \mathbf{T}_s \qquad (4.78)$$

where $\mathbf{T}_s$ and $\mathbf{k}_s^*$ are given as

$$\mathbf{T}_s = \begin{bmatrix} 0 & -\frac{1}{L} & 0 & 0 & 0 & 1 & 0 & \frac{1}{L} & 0 & 0 & 0 & 0 \\ 0 & 0 & -\frac{1}{L} & 0 & 1 & 0 & 0 & 0 & \frac{1}{L} & 0 & 0 & 0 \\ 0 & -\frac{1}{L} & 0 & 0 & 0 & 0 & 0 & \frac{1}{L} & 0 & 0 & 0 & 1 \\ 0 & 0 & -\frac{1}{L} & 0 & 0 & 0 & 0 & 0 & \frac{1}{L} & 0 & 1 & 0 \end{bmatrix} \qquad (4.79)$$

and

$$\mathbf{k}_s^* = \begin{bmatrix} \alpha_y & 0 & -\alpha_y & 0 \\ 0 & \alpha_z & 0 & -\alpha_z \\ -\alpha_y & 0 & \alpha_y & 0 \\ 0 & \alpha_z & 0 & -\alpha_z \end{bmatrix} \qquad (4.80)$$

respectively.

Chapter 5

Numerical verification

In order to assess the element formulation described in the previous two chapters, a series of test analyses have been performed. The results are compared with analytical solutions when available. In some cases, where no theoretical solutions are found, the results are compared to numerical results, obtained by use of other analysis tools.

The element presented as "standard elem." in the following is a standard (linear) Euler-Bernoulli type element implemented in the co-rotated formulation described in chapter 3, whereas the "new elem." is the element described in section 4.5. Unless otherwise stated, eccentricities are, if present, modelled using rigid eccentricities.

In most of the cases studied in this chapter, the results are given in tabular form. However, in some cases the results are presented as graphs, since this is the form used by referenced studies.

5.1 Linearized buckling analyses

The linearized buckling type analysis is based on the same assumptions usually adopted by the classical (differential equation) treatment of the problem. The results from a linearized buckling analysis of a system should therefore approximate the corresponding solution of the differential equation for the problem (where available).

The formulation presented in the previous chapters includes a consistent tangent

stiffness. Thus, all the phenomena reflected in the force vector are also contained in the tangent stiffness, and hence in the geometric stiffness of the element. This formulation should therefore be able to predict all kinds of global structural instability for beam elements.

5.1.1   Flexural buckling of column
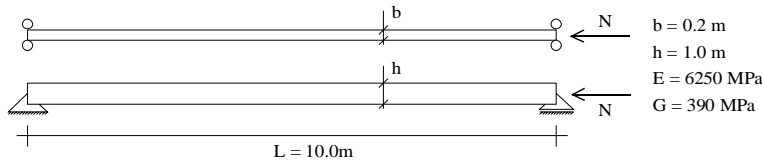
Figure 5.1: *Simply supported beam subjected to axial compression force.*

In the infancy of structural stability, Euler studied lateral buckling of a simply supported column subjected to an axial compression force at one end, as shown in figure *5.1.* By solving the differential equation, Euler found that the critical axial load for this beam was

$$N_{cr} = \frac{\pi^2 EI}{L^2} = 411233.5 \text{ N} \qquad (5.1)$$

where I is the second moment of area about the weak axis of the cross section. Linearized buckling analyses by Cfem, for different element meshes, gave the following estimates of the buckling load

No. of elem.	Standard elem.	Error	New elem.	Error
1	—	—	500000.0 N	21.6 %
2	500000.0 N	21.6 %	414327.0 N	0.75 %
3	449955.3 N	9.4 %	411882.5 N	0.16 %
4	432776.8 N	5.2 %	411444.1 N	0.05 %
8	416545.0 N	1.3 %	411247.0 N	0.003 %

The error is measured with respect to the buckling load predicted by Euler, equation (5.1).

5.1.2 Lateral torsional buckling of simply supported beam
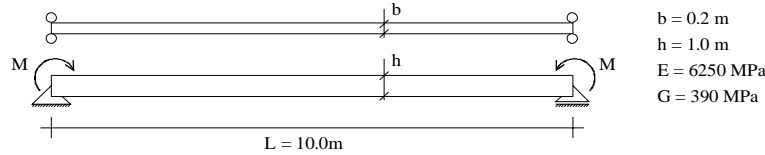
Figure 5.2: *Simply supported beam subjected to constant moment.*

The classic case of lateral torsional buckling is the simply supported beam subjected to constant moment, as shown in figure *5.2*. The moment acts about the strong axis of the cross-section. Simply supported in this context also means that the cross section of the beam is prevented from rotation about the longitudinal axis at the supports.

Solution of the differential equation, see for instance [30], gives the following buckling load for this problem

$$M_{cr} = \frac{\pi}{L}\sqrt{EI_{yy}GI_t} = 611387.6 \, \text{Nm} \tag{5.2}$$

Linearized buckling analyses by Cfem:

No. of elements	Standard elem.	Error	New elem.	Error
2	747903.7 Nm	22.3 %	595197.4 Nm	2.65 %
3	664970.1 Nm	8.8 %	606119.6 Nm	0.86 %
4	640321.9 Nm	4.7 %	608389.1 Nm	0.42 %
8	618349.1 Nm	1.1 %	610840.9 Nm	0.09 %

The error is measured with respect to the buckling load defined by the analytical solution in equation (5.2).

5.1.3 Flexural buckling of eccentrically loaded cantilever

No references have been found in which problems involving loads applied through rigid eccentricities are studied by use of differential equations. One exception is lateral torsional buckling of simple beams subjected to eccentricly applied concentrated forces, studied, for instance, by Timoshenko and Gere [30]. However, in these cases the differential equations are based on severe simplifications, and the results obtained are therefore not particularly well suited for verificational purposes. However, the simplified procedure adopted in this test, and described below, is believed to give a strong indication of the usefulness of the formulation with respect to rigid eccentricities.
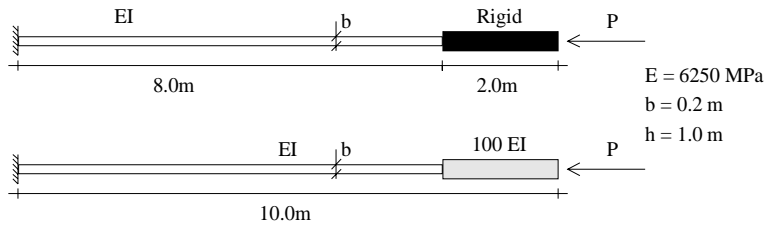
Figure 5.3: *Cantilever beam subjected to axial compression, applied through* **a**) *rigid eccentricity,* **b**) *very stiff end section*

The geometry of first problem is shown in figure *5.3*. The buckling loads obtained for the two systems are not expected to coincide completely, but they should be quite close if the rigid eccentricity is handled correctly. The buckling load of the system with the rigid eccentricity is expected to be the higher, since this system is slightly stiffer. Using 16 elements to model the flexible part of the cantilever and, where needed, 4 elements to model the stiff part, analyses from Cfem and ABAQUS[59] yield:

	New elem. (Cfem)		ABAQUS	
	Stiff	Rigid	Stiff	Rigid
Buckling load	104.10 kN	104.11 kN	104.15 kN	160.73 kN
Deviation	0.0 %	0.01 %	0.05 %	54.4 %

The new element seems to handle the eccentricity correctly, whereas this version of ABAQUS seems to have a problem with the geometric stiffness in case of rigid eccentricities.

5.1.4   Simply supported beam with eccentric loading
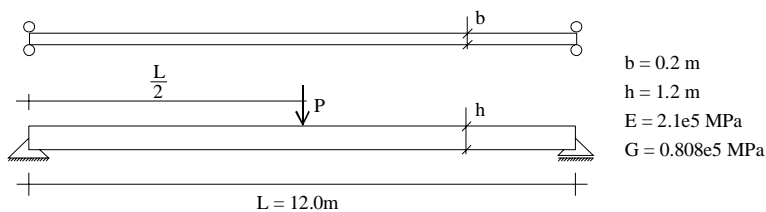
Figure 5.4: *Simply supported beam subjected to point load at upper edge.*

In [30], Timoshenko and Gere solve the differential equation for the system shown in figure *5.4* with respect to stability, but simplifications made restrict their solution to small eccentricties. It is therefore not particularly suited for comparison. Instead, the results from a beam model of the system in figure *5.4*

are compared with the same type of results from a shell model of the beam. In the beam model, a rigid eccentricity is used to model the position of the load, whereas in the shell model the load is applied directly in a node at the edge of the model.

The shell analyses are performed by ABAQUS, with 1200 shell elements of type S4R. For the beam element analyses, 24 beam elements were used.

	ABAQUS		Cfem	Analytical
Load position	Shell	Beam	New elem.	Timoshenko
Upper edge	21498 kN	23098 kN	21361 kN	21459 kN
Centroid	23424 kN	23098 kN	23189 kN	23177 kN
Lower edge	25176 kN	23098 kN	25093 kN	24895 kN

These results show good agreement between the analysis of the shell element model in ABAQUS and the beam element model in Cfem. Observe that for loading with no eccentricity, the beam model in ABAQUS also yields good results. Load eccentricity seems to be disregarded in the ABAQUS beam analysis.

5.2 Nonlinear analysis

5.2.1 Cantilever subjected to point load at end point

$P = 600$ kN

$A = 4.8e\text{-}3 \text{ m}^2$
$I = 4.45e\text{-}5 \text{ m}^4$
$E = 2.1e5$ MPa
$G = 8.0775e4$ MPa

$L = 5.0$ m
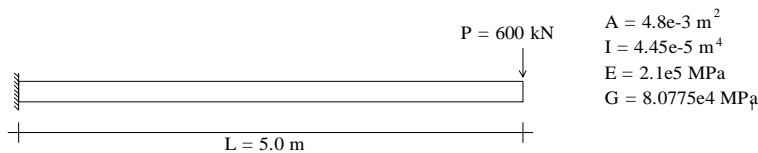
Figure 5.5: *Cantilever beam subjected to transverse point load at free end.*

The beam in figure 5.5 was studied by both Cardona [60] and by Crivelli [21] for different element meshes. In both studies, the effect of shear was included. Therefore the approach to shear stiffness discussed in section 4.6 was used in these Cfem analyses. The cross section area of the beam was taken as shear area. The vertical tip deflection and tip rotation of the cantilever compare wih Cardona's results as follows:

Number of	Tip deflection		Tip rotation	
elements	Cardona	New elem.	Cardona	New elem.
1	1.833	2.142	0.747	0.669
2	2.078	2.156	0.688	0.672
4	2.139	2.158	0.676	0.672
8	2.154	2.158	0.676	0.672
16	2.157	2.158	0.672	0.672

5.2.2   Cantilever subjected to two point loads
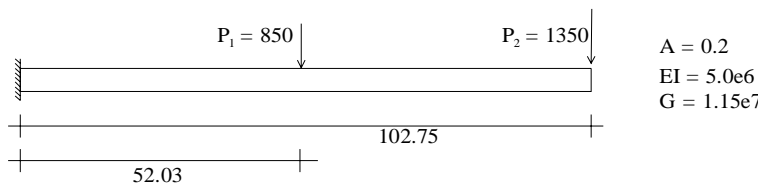
Figure 5.6: *Cantilever beam subjected to two transverse point loads. One at the free end and the other at about the midpoint.*

According to [21], an analytical solution to this problem has been found by Ebner and Ucciferro[61]. In addition, both Cardona [60] and Crivelli [21] have studied it using the finite element method. In the following table results from analyses using the new element are compared with corresponding results from Crivelli as well as with the analytical solution, for three different element meshes. Longitudal and transverse displacement as well as rotation of the free end are tabulated.

Number of elements		2	4	8
	Longitudal disp.	28.99	30.26	30.62
Crivelli	Transverse disp.	65.86	66.63	66.87
	Rotation	1.1	1.06	1.05
	Longitudal disp.	30.65	30.75	30.76
New elem.	Transverse disp.	66.80	66.98	67.00
	Rotation	1.04	1.04	1.04
	Longitudal disp.	30.75	30.75	30.75
Analytic solution	Transverse disp.	66.96	66.96	66.96
	Rotation	-	-	-

For these analyses also, the cross section area was taken as shear area.

5.2.3 Curved cantilever subjected to transverse point load
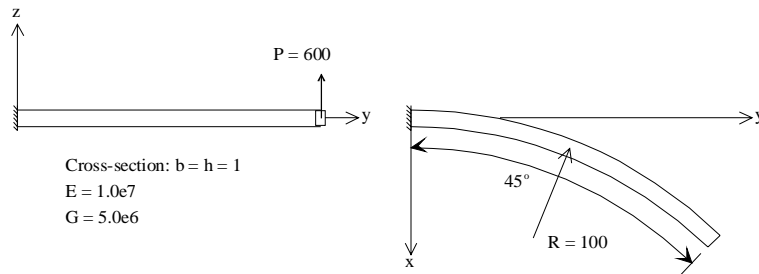
Figure 5.7: *Curved cantilever with rectangular cross-section subjected to transverse point load at the free end.*

Figure 5.7 shows a problem that has been studied by Bathe and Bolourchi [62]. It was also used by Crivelli [21] for verification of his beam element. Eight straight elements are used for modelling the cantilever.

The final position of the cantilever tip as found in the different studies, is:

Load	Measured	Bathe et. al.	Crivelli	New elem.
	x-position	22.33	22.31	22.27
300	y-position	58.84	58.85	58.78
	z-position	40.08	40.08	40.16
	x-position	18.62	18.59	18.55
450	y-position	53.32	53.34	52.24
	z-position	48.39	48.39	48.47
	x-position	15.79	15.75	15.73
600	y-position	47.23	47.25	47.15
	z-position	53.37	53.37	53.44

For the quadratic cross section of this cantilever beam, the shear area was set to $(b \times h)/1.2 = 0.833$.

As shown in the table, the results found in this study agree quite well with those found by both Bathe and Bolourchi and Crivelli.

5.2.4   William's toggle beam
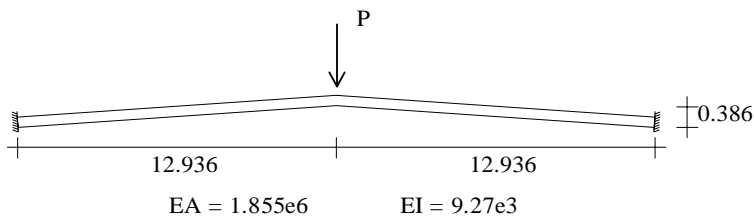
Figure 5.8: *William's toggle beam; two beams rigidly jointed together and clamped at both ends, and subjected to load P at the apex.*

An analytical solution for this problem was found by Williams [63], who also did experiments to verify his analytical approach.

The analyses in Cfem were performed using the new beam element. Two different element meshes were employed, the first using one element to model each half of the beam, and the second using four elements per half. The results are
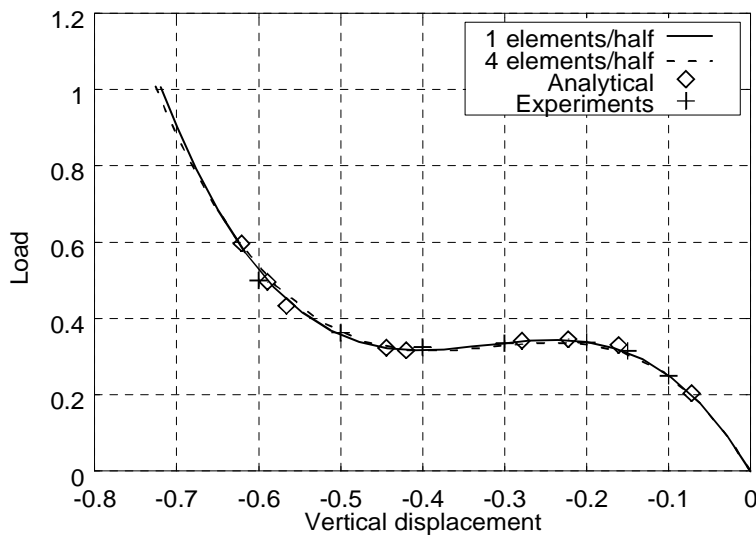
Figure 5.9: *Williams toggle beam; comparison between analyses using 1 and 4 elements per half beam, and experimental and analytical results.*

presented as solid and slashed lines in figure 5.9, and they show good agreement with the results obtained by Williams.

5.2.5   M.I.T. Dome

Cross-section

A = 0.049
I_t = 0.02961
I_y = 0.0208
I_z = 0.0208
E = 439.8e3
G = 159.0e3
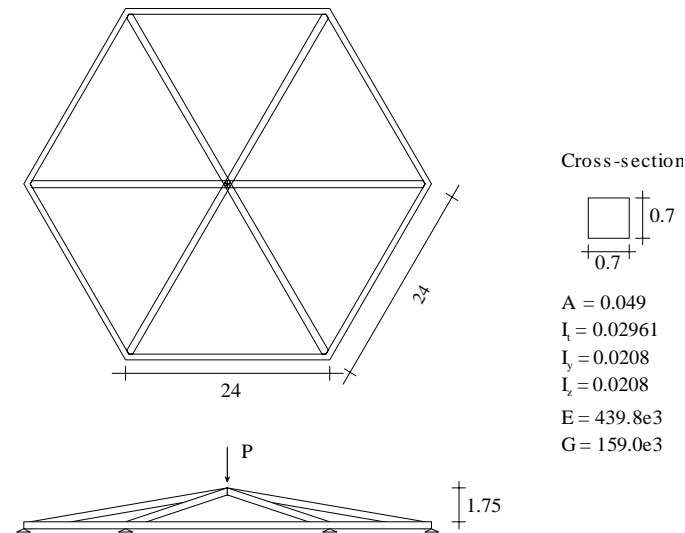
Figure 5.10: *M.I.T. Dome; dome structure in plexi-glass.*

This problem consists of twelve members forming a three dimensional dome structure with rigid joints, and with a hexagonal base. The dome is simply supported at each of the six vertices of the hexagonal base, and these supports are allowed to move in the plane perpendicular to the load. A point load is applied vertically at the apex of the dome. In order to make it stable, the apex node is restricted to movement in the loading direction, and it is prevented from rotation about the vertical axis. As the results in figure *5.11* show, the analyses using the new element places themselves neatly among the results obtained by Nee [64], Crivelli [21] and Meek [65].

5.3   Conclusion

The new element developed in chapter 4 has been tested for a number of problems both in two and three dimensions, and it has been found to yield satisfactory results for both linearized buckling analysis and nonlinear analysis.
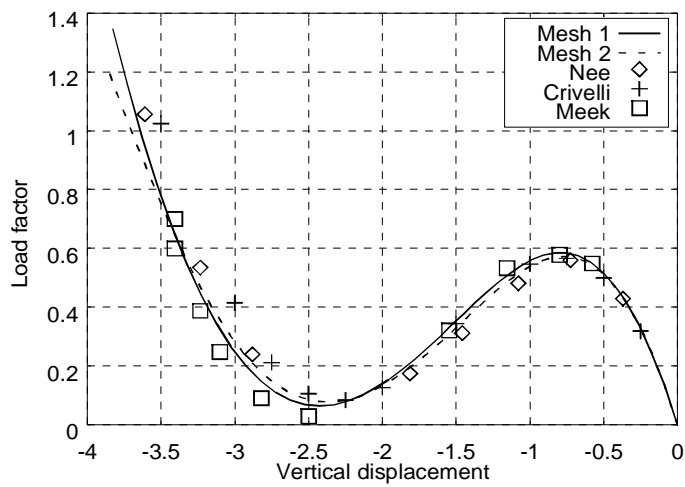
Figure 5.11: *Results from analyses of MIT Dome; Mesh 1 uses 2 elements for each diagonal member and 1 element per horizontal member. Corresponding numbers for mesh 2 are 4 and 2 elements, respectively.*

Part II

Numerical studies

Chapter 6

Linearized buckling

Most design codes account for stability problems in a simplified manner. Stresses computed by ordinary linear analysis are adjusted by correction factors which depend on the slenderness ratio of the members.

Strictly speaking, correct use of this procedure requires a total system analysis with respect to buckling to be made. However, most structures can, with adequate accuracy, be simplified into a series of simple beams and columns, requiring only that the buckling loads for *these* individual members are known. By providing tabulated data for the buckling loads of a relatively limited number of beam and column configurations, design codes can therefore enable the engineer to account for stability problems even in quite complex structures.

Although buckling loads for a large number of simple beams and columns have been found analytically by solving differential equations, this approach is not always possible. Therefore numerical methods, such as the linearized buckling analysis, often has to be applied. Although such methods only yield numerical values for the buckling loads, curve fitting can be used to obtain approximate, parameterized formulas.

In this chapter a number of simple beam configurations are studied using the linearized buckling analysis feature of Cfem. The emphasis is on problems involving lateral torsional buckling, as this seems to be the area most in need of more and better information.

6.1   Test beams

6.1.1   Geometry

For the most part, two sets of beams with constant rectangular cross-sections are used in this chapter. Each set consists of three different beams. Given the same load and boundary conditions, the beams have different *slenderness ratios*, for both flexural and lateral torsional buckling.
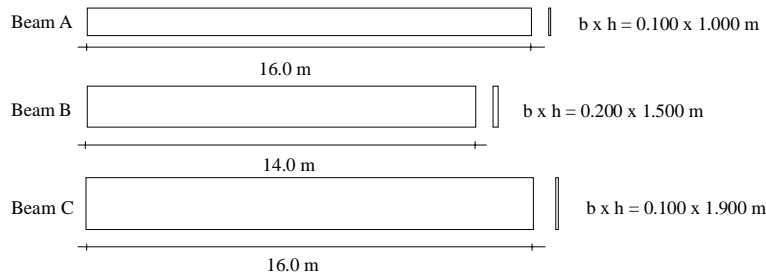
The first set of test beams, labeled A, B and C, is used for deriving formulas, based on curve fitting.
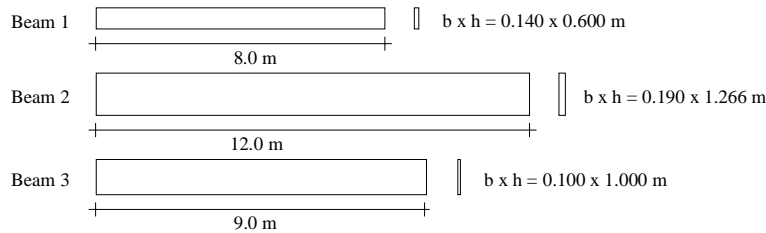
Consisting of the beams labeled 1,2 and 3, the second set of test beams is used for testing and verification of the derived formulas.

In addition to the two sets of beams with constant rectangular cross-sections, a number of tapered beams with rectangular cross-sections, the geometry of which will be commented on in due course, are used.

6.1.2   Material

All beams have the same material properties, corresponding to glulam with all lamellas of strength class T30 according to NS3470 [2]. Only characteristic values, including the lamination factor, are referred and used in the analyses. No notice is taken to service class or load duration classes.

Parameter	Symbol	Value
Char. bending strength	f_{mk}	39.0 MPa
Char. tensile strength	f_{t0k}	23.4 MPa
Char. compression strength	f_{c0k}	35.1 MPa
For stability calculations		
Modulus of elasticity	E_{0k}	10062.5 MPa
Shear modulus	G_k	632.5 MPa
For deformation calculations		
Modulus of elasticity	E_0	14145.0 MPa
Shear modulus	G	885.5 MPa

Consistent with the discussion in section 2.3, the 5-percentile values of the stiffness parameters, E_{0k} and G_k, are used for all analyses referred in this chapter.

6.1.3 Boundary conditions and loading

A beam prone to lateral torsional buckling, must, at least, be partially restrained against torsional rotation at one point along the beam axis, in order to prevent it from tipping over. In the following, when a beam point is said to be *simply supported*, it means that it is prevented from all three translations and also prevented from torsional rotation. On the other hand, if a beam point is said to be *built-in*, all translations and rotations are suppressed at that point.

6.1.4 Discretization

The analyses have been performed using the new beam element described in section 4.5(page 67) and implemented in the corotated formulation described in chapter 3. The number of elements used in each analysis vary from case to case, but is held constant within each test series.

In the modelling of eccentricities, the *rigid* eccentricities described in chapter 3 were used in order to avoid possible numerical problems associated with the use of very short and stiff beam elements.

All distributed loading is lumped to the element nodes.

6.2   Effect of eccentric loading

Timoshenko and Gere [30] study lateral torsional buckling of simple beams for
a number of different of boundary conditions and load configurations. For the
most part, however, the loading is applied at the centroid of the beam cross
section.

The topic of this section is beams subjected to eccentric loading. A couple of dif-
ferent load and boundary condition configurations are studied, and approximate
expressions for the lateral torsional buckling loads of the beams are established.

6.2.1   Simply supported beam with distributed loading
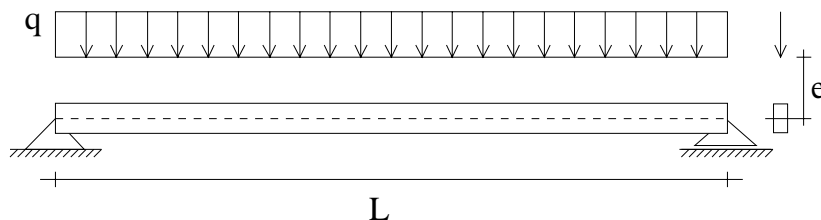
Figure 6.1: *Simply supported beam with eccentrically applied uniformly dis-
tributed load q*

Figure *6.1* shows a simply supported beam of length L with uniformly distrib-
uted loading q applied at a distance e from the centroid. The eccentricity e
is positive above the centroid, and both positive and negative values of e are
considered.

For the case of no eccentricity, that is $e = 0$, Timoshenko and Gere [30] find the
lateral torsional buckling load to be:

$$q_0 = \frac{28.3\sqrt{EI_{zz}GI_t}}{L^3} \tag{6.1}$$

Timoshenko and Gere do not, however, provide a formula for lateral torsional
buckling of simply supported beams with eccentrically applied uniformly dis-
tributed loading. Strømmen [66] did, however, find an approximate formula for
this problem, but his formula was based on an energy approach with an assumed
sinusoidal displacement field between the supports. This approach yielded a for-
mula that gives relatively inaccurate results for zero eccentricity, and will not
be commented on further in this work.

As an approximation to the buckling load for the system in figure *6.1*, the

following expression is proposed:

$$q_{cr} = \frac{28.3\sqrt{EI_{zz}GI_t}}{L^3} - k_1\left(\frac{e}{L}\right)\frac{EI_{zz}}{L^3} + k_2\left(\frac{e}{L}\right)^2\frac{EI_{zz}}{L^3}\sqrt{\frac{E}{G}} = q_0 - q_1(e) \quad (6.2)$$

Since equation (6.2) is to be fitted to computed results, a method of calibration must be chosen. A natural choice would be a nonlinear least square method. These methods do ensure the total deviation of (6.2) from the computed results to be minimized. This is, however, not necessarily the best fitting criterion. For timber beams, and indeed for all other kinds of beams, the most likely eccentric loading is applied some place within the cross section, or in the vicinity of the cross section boundaries. Thus, it is more important for equation (6.2) to be accurate for small values of the eccentricity than for larger values. Therefore a simple curve fitting method is used for calibration of (6.2), using only two points to determine the two arbitrary constants k_1 and k_2. (Actually, a third point has, in some respect, already been used, as the constant part of equation (6.2) is determined from the differential equation solution for zero eccentricity.)

The eccentricities used in the calibration are $e = \pm 0.5\,h$, which yielded $k_1 = 40.2$ and $k_2 = 14.0$ as reasonable values for the coefficients. This suggests the following approximate formula for the lateral torsional buckling load of a simply supported beam with eccentrictally applied uniformly distributed loading:

$$q_{cr} = \frac{28.3\sqrt{EI_{zz}GI_t}}{L^3} - 40.2\left(\frac{e}{L}\right)\frac{EI_{zz}}{L^3} + 14.0\left(\frac{e}{L}\right)^2\frac{EI_{zz}}{L^3}\sqrt{\frac{E}{G}} \quad (6.3)$$

Since formula (6.3) was established for beams A, B and C, it also has to be verified for other beam geometries. Therefore, some analyses have been carried out using test beams 1, 2 and 3. 40 elements were used to model each beam, for both the calibration and the verification analyses.

Dependency on eccentricity

Computations have been performed with eccentricity ranging from $-1.0\,h$ to $1.0\,h$.

The results are presented in figures *6.2* through *6.4*. In each of these figures, a curve has been included relating the deviation of equation (6.3) from the computed results. These curves relate to the right ordinate axis of the figures. Ideally, the deviation should be zero for zero eccentricity. The reason why this is not the case (about 0.1% off), is probably that the first term in equation (6.3), denoted by q_0 and taken from [30], is exact within 3 digits only.
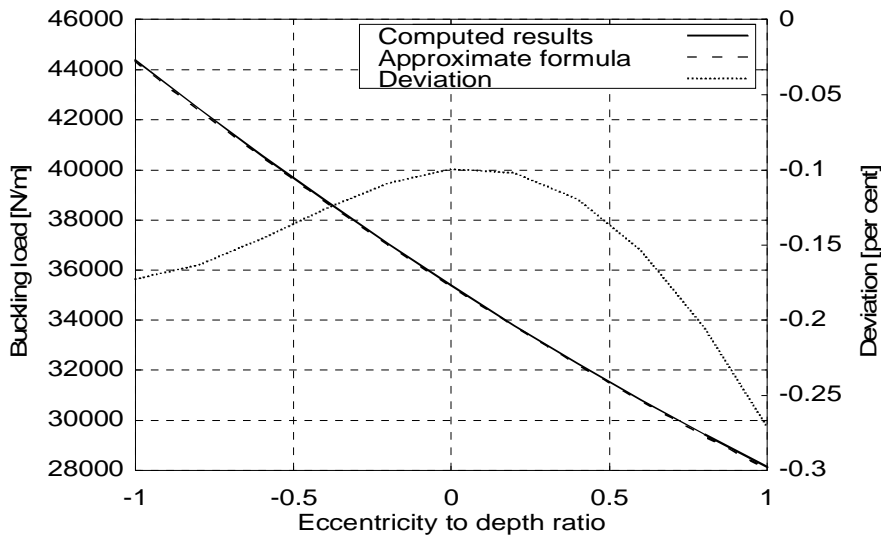
Figure 6.2: *Effect of eccentricity for beam 1. b x h = 0.14m x 0.6m. L = 8.0m. Uniformly distributed loading.*
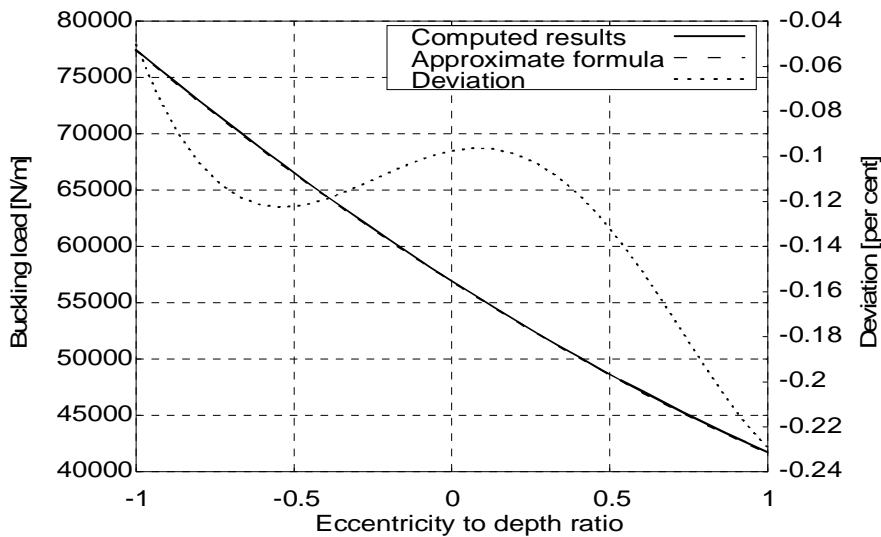
Figure 6.3: *Effect of eccentricity for beam 2. b x h = 0.19m x 1.266m. L = 12.0m. Uniformly distributed loading.*
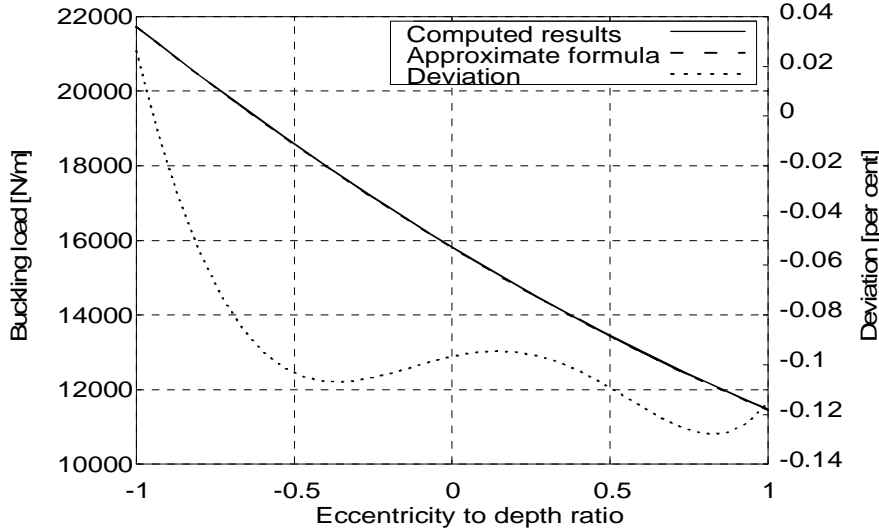
Figure 6.4: *Effect of eccentricity for beam 3. b x h = 0.1m x 1.0m. L = 9.0m. Uniformly distributed loading.*

Figures *6.2*, *6.3* and *6.4* clearly indicate that formula (6.3) predicts the lateral torsional buckling load with good accuracy, at least for eccentricities ranging from $-h$ to h. The deviation from the computed results does not exceed 0.3% for any of the analyzed test beams.

Dependency on strength class and $\frac{E}{G}$

So far, all the beams used for both calibration and verification of the proposed approximate formula had the same material properties, corresponding to glued laminated timber with all T30 lamellas. In order to check the validity of the approximate formula for beams with other material properties, two series of analyses were performed. Beams 1-3 were used for both series, and the eccentricity was set to $e = 0.5\,h$.

In the first series of analyses, the beams were given material properties corresponding to the strength classes T18 through T40 described in NS3470[2].

In the second series, the beams were assigned a wide variety of stiffness parameters and E/G-ratios.

The results from these computations are given in appendix C, section C.1, and they indicate that the approximate formula shows good agreement with the analyses for all sets of stiffness moduli.

6.2.2   Simply supported beam with point load
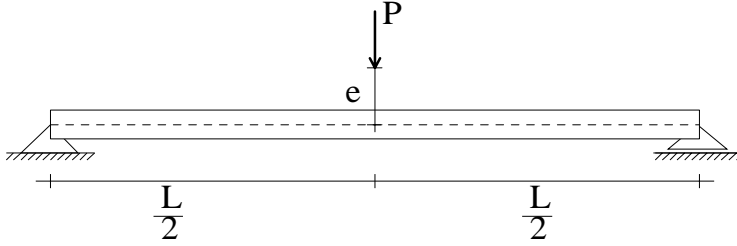
Figure 6.5: *Simply supported beam with eccentrically applied point load at mid-span.*

Figure 6.5 shows a simply supported beam with a vertical point load applied eccentrically at mid-span. Timoshenko and Gere [29] study this problem analytically, and find the following approximate lateral torsional buckling load, under the condition that the eccentricity is small:

$$P_{cr} = \frac{16.93\sqrt{EI_{zz}GI_t}}{L^2} - 29.46\frac{e}{L}\frac{EI_{zz}}{L^2} \tag{6.4}$$

How good is this formula, particularly for the size of eccentricities found in timber structures? In order to answer this question computations were carried out with the aim of determining the factors k_1 and k_2 in the somewhat more elaborate formula:

$$P_{cr} = \frac{16.93\sqrt{EI_{zz}GI_t}}{L^2} - k_1\frac{e}{L}\frac{EI_{zz}}{L^2} + k_2\left(\frac{e}{L}\right)^2\frac{EI_{zz}}{L^2}\frac{E}{G} \tag{6.5}$$

For calibration, beams A, B and C were used, and, as was the case for the simply supported beam with uniformly distributed loading, the calibration was carried out for $e = \pm 0.5\,h$. Suitable values for the coefficients of (6.5) were found to be:

$$k_1 = 31.5 \qquad\qquad k_2 = 1.9 \tag{6.6}$$

The actual computed buckling loads are included in appendix C, section C.1.2. This suggests the following formula

$$P_{cr} = \frac{16.93\sqrt{EI_{zz}GI_t}}{L^2} - 31.5\frac{e}{L}\frac{EI_{zz}}{L^2} + 1.9\left(\frac{e}{L}\right)^2\frac{EI_{zz}}{L^2}\frac{E}{G} \tag{6.7}$$

For verification, a number of computations were carried out using test beams 1, 2 and 3. In all computations, 40 elements were used to model the beam.

Dependency on eccentricity

Computations were performed with eccentricities ranging from $-1.0\,h$ to $1.0\,h$. Figures 6.6 through 6.8 contain the results from the verification analyses.
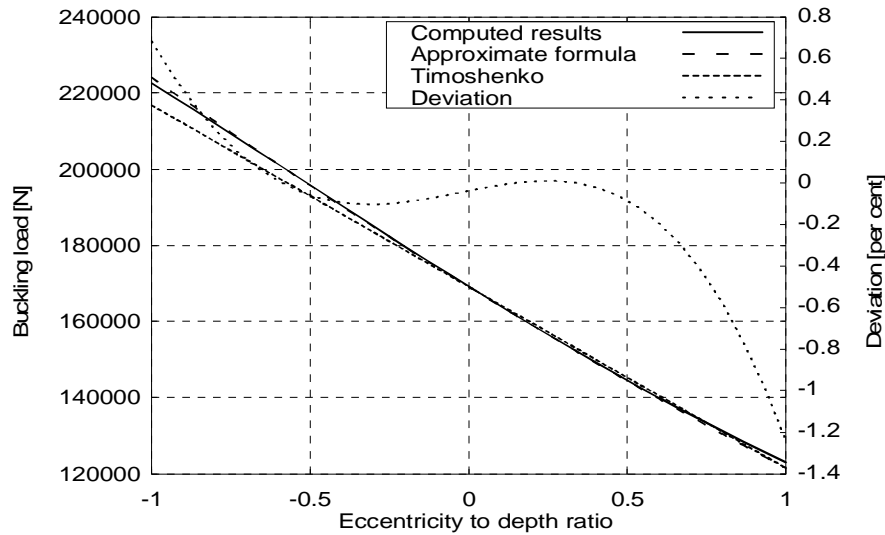
Figure 6.6: *Effect of eccentricity for beam 1. b x h = 0.14m x 0.6m. L = 8.0m. Point load at mid-span.*
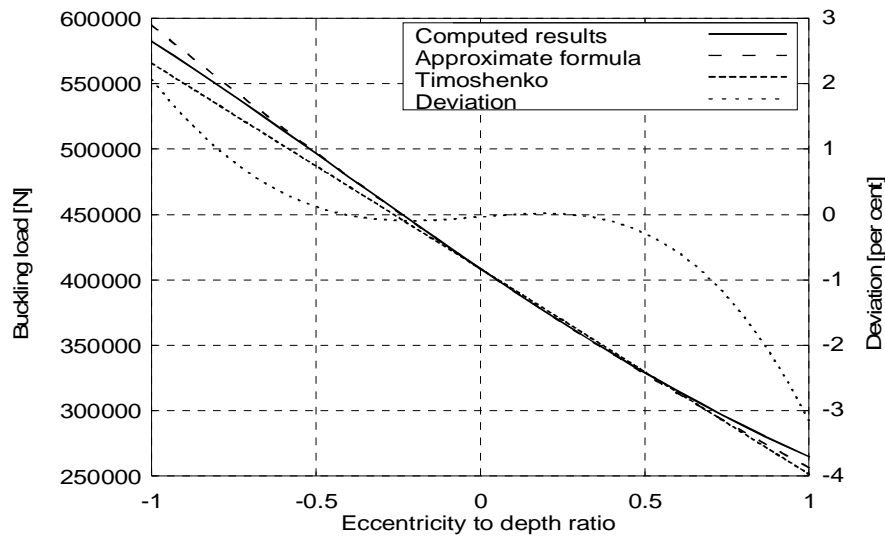
Figure 6.7: *Effect of eccentricity for beam 2. b x h = 0.19m x 1.266m. L = 12.0m. Point load at mid-span.*
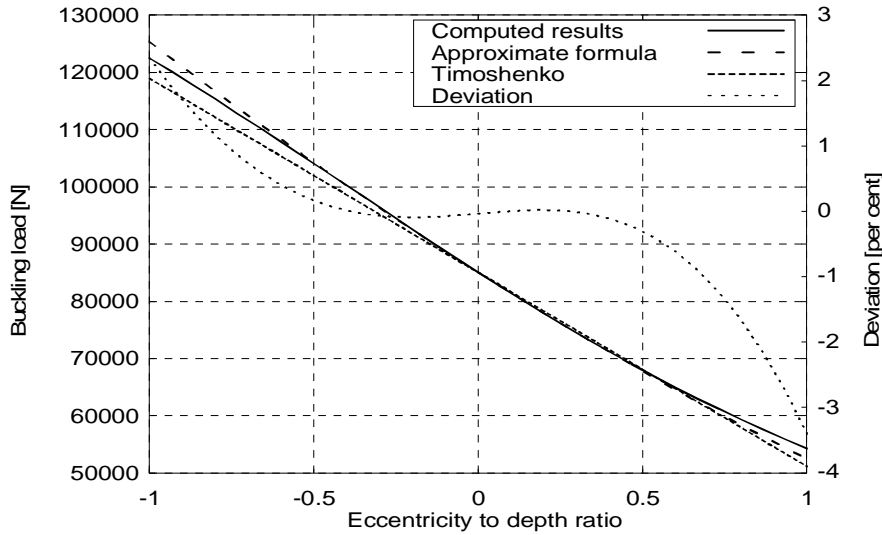
Figure 6.8: *Effect of eccentricity for beam 3. b x h = 0.1m x 1.0m. L = 9.0m. Point load at mid-span.*

Although the approximate formula yields results that are somewhat inaccurate for large eccentricities, figures *6.6*, *6.7* and *6.8* seem to indicate that it predicts the buckling load within 1% for ratios of eccentricity to beam depth of about ±0.7. However, for ratios in this range, Timoshenko's formula also yields quite accurate results, at least for positive values of e/h. For negative values of e/h, on the other hand, Timoshenko's approximation gives less accurate results than equation (6.7).

Dependency on strength class and $\frac{E}{G}$

As for the uniformly loaded beam, analyses aimed at testing the sensitivity with respect to the material parameters were carried out also for the point loading. Beams 1, 2 and 3 were used for the testing, and the eccentricity was set to $e = 0.5h$. The results, shown in appendix C, section C.1.2, show that the approximate formula is quite insensitive to the stiffness parameters.

6.3   Combined flexural and lateral torsional buckling

As a simplification, lateral torsional buckling of a beam is often considered as flexural buckling of the compression side of the beam. This is a somewhat crude simplification, it clearly indicates that there is a connection between the lateral torsional buckling load and any axial compression (or indeed tension).
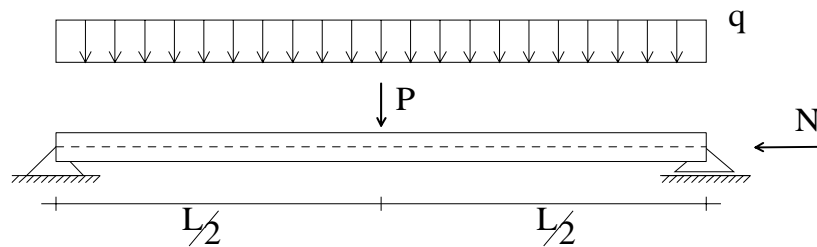
Figure 6.9: *System used to establish interaction curves. Only one of the point load P and the distributed loading q is present at a given time*

In order to establish the degree of interaction, analyses have been performed using test beams 1, 2 and 3 (see section 6.1, page 90). The system being analysed is shown in figure *6.9*. It consists of a beam which is either simply supported or built-in at both ends, and which is subjected to either a uniformly distributed load (q) or a point load (P) at mid-span. In addition, it is subjected to an axial compression load (N).

Linearized buckling analyses were performed with one type of loading (transverse or axial) held constant throughout each analysis. The other load, which was allowed to vary, represents the buckling load for that level of constant loading. By performing such analyses for different levels of constant loading, and recording the corresponding buckling loads, interaction curves were established.

Beam 1
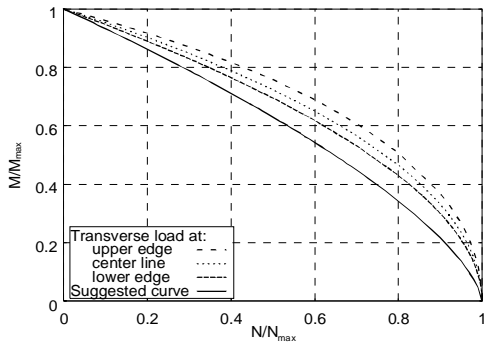
Figure 6.10: *Simply supported beam subjected to point load at mid-span*
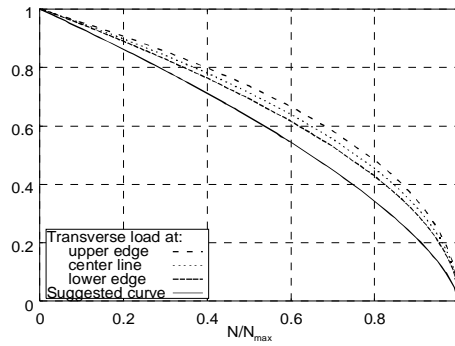
Figure 6.11: *Simply supported beam subjected to distributed load*
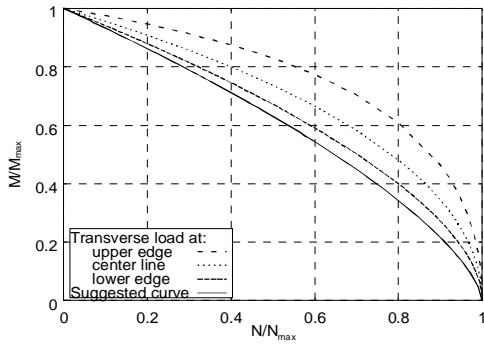
Figure 6.12: *Built-in beam subjected to point load at mid-span*
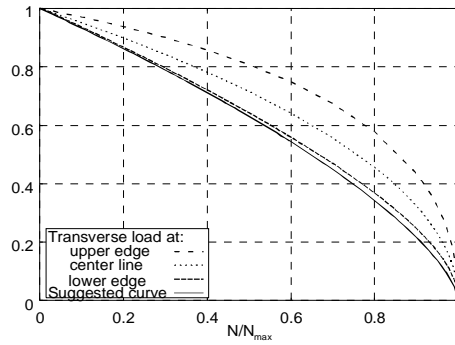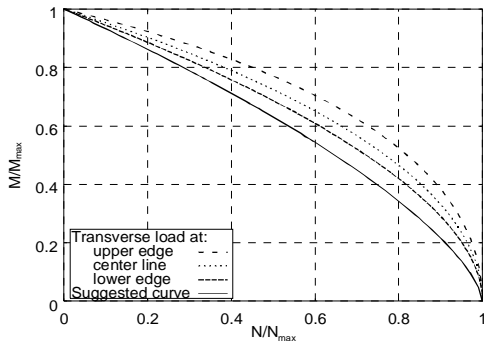

Figure 6.13: *Built-in beam subjected to distributed load*

Beam 2

Figure 6.14: *Simply supported beam subjected to point load at mid-span*
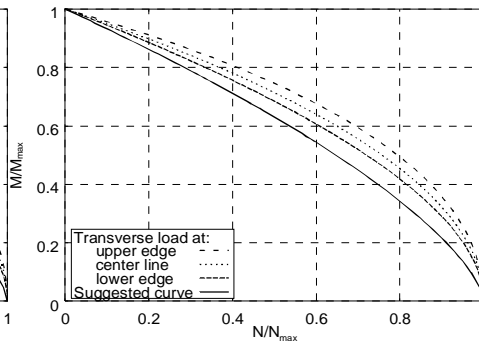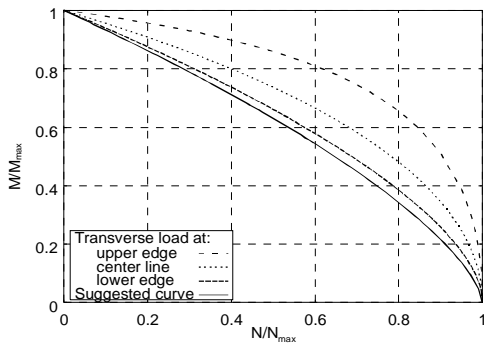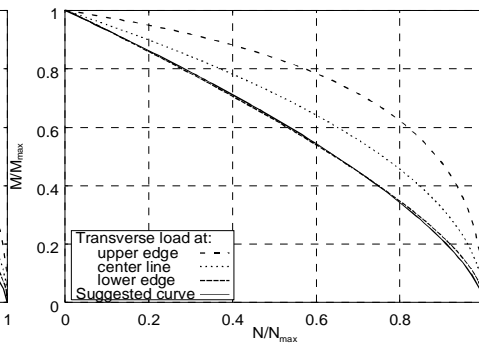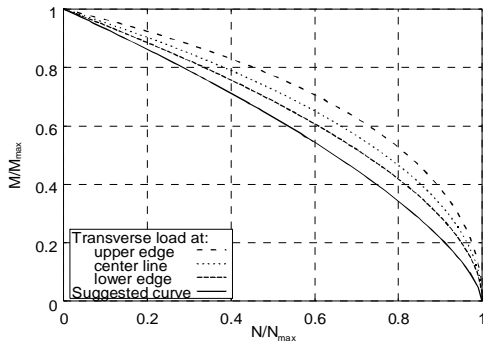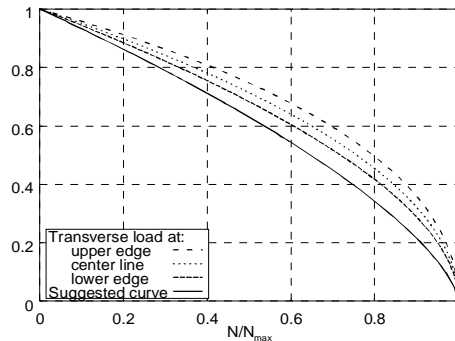

Figure 6.15: *Simply supported beam subjected to distributed load*

Figure 6.16: *Built-in beam subjected to point load at mid-span*

Figure 6.17: *Built-in beam subjected to distributed load*

Beam 3

Figure 6.18: *Simply supported beam subjected to point load at mid-span*

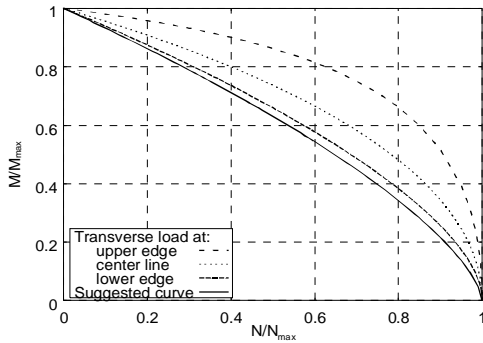**Figure 6.19:** *Simply supported beam subjected to distributed load*

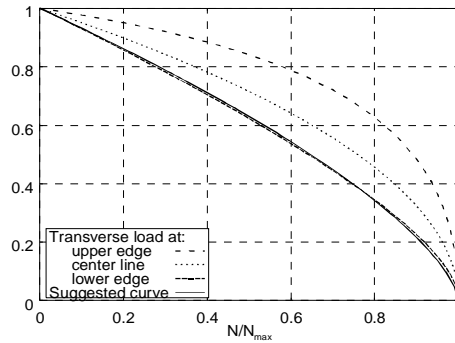**Figure 6.20:** *Built-in beam subjected to point load at mid-span*

Figure 6.21: *Built-in beam subjected to distributed load*

Figures *6.10* through *6.21* clearly indicates an interaction between flexural buckling and lateral torsional buckling. It should be noted that the axes are scaled with respect to the buckling load, N_{max}, and the critical bending moment, M_{max}. N_{max} is the critical load for the beam with no transverse loading, and M_{max} is the critical moment dut to q or P, with $N = 0$. It follows from this that even though a smaller value of M/M_{max} is permitted for one beam than for another, for a particular value of N/N_{max}, the actual magnitude of the permissible bending moment can be larger, since M_{max} can be different for the two beams.

The results suggest an interaction curve defined by

$$\left(\frac{N}{N_{max}}\right) + \left(\frac{M}{M_{max}}\right)^{\frac{3}{2}} = 1.0 \tag{6.8}$$

This curve is also included in the figures. It clearly represents a conservative approximation, particularly for transverse loading applied at the upper edge of the beam.

6.4 Effective (buckling) lengths

The lateral torsional buckling moment of a simply supported beam of length L subjected to uniform bending moment is:

$$M_{cr} = \frac{\pi}{L}\sqrt{EI_{zz}GI_t} \tag{6.9}$$

Equation (6.9) can be used to tabulate buckling loads for beams with other loading and/or boundary conditions. A particular beam that buckles for a maximum bending moment of M has the same buckling moment as a beam of length L and with uniform bending moment $M_{cr} = m \cdot M$. Thus, the buckling load of the given beam is given by either:

$$M_{cr} = m \cdot M = \frac{\pi}{L}\sqrt{EI_{zz}GI_t} \tag{6.10}$$

or

$$M = \frac{\pi}{m \cdot L}\sqrt{EI_{zz}GI_t} \tag{6.11}$$

where m can be called *equivalent uniform bending moment factor* in the first case and *buckling length factor* in the second. $L_k = m \cdot L$ is the *effective length* or *buckling length* of the beam. For easy access to buckling loads of different configurations of the beams, m can be tabulated for a number of load- and boundary configurations. Such tables may, for instance, be found in [2] and [45].

The table in [2] has some inconsistencies which were corrected by the author in [67]. The corrected table, which was found by numerical computations with the element formulation presented in the theoretical part of this thesis, is included here as table 6.1 for reference.

In addition to the cases presented in [67] and table 6.1, a few other cases have also been studied. The computations are reported more thoroughly in appendix C, section C.2; here the essence is shown in table 6.2, which is an extension of table 6.1.

Load, bending moment and boundary conditions about horizontal axis	Boundary conditions about vertical axis	Factor m
M ... μM		$0.60+0.40\mu\geq0.40$
M ... μM		$0.30+0.20\mu\geq0.20$
q		0.90
		0.55
q		0.80
		0.70
q		0.80
		0.75
F ... F, $\frac{L}{4}$ $\frac{L}{2}$ $\frac{L}{4}$		1.00
		0.55
F, cL		$0.56+0.74c(1-c)$
		$0.28+0.80c(1-c)$
		$0.49+0.60c-0.85c^2\geq0.35$
F, cL		$0.47+0.50c(1-c)$
		$0.39+0.58c(1-c)$
		$0.47+0.41c-0.49c^2$
$\frac{L}{2}$ F $\frac{L}{2}$		0.70
		0.65
M		2.00
q		0.50
F		0.80

Table 6.1: *Table of buckling lengths/equivalent moment factors for a number of beam configurations.*
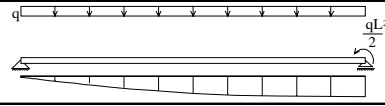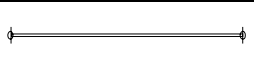
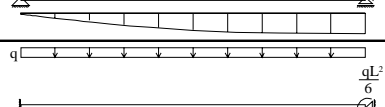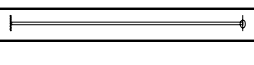| Load, bending moment and boundary conditions about horizontal axis	Boundary conditions about vertical axis	Factor m
(uniformly distributed load q, bending moment $\frac{qL^2}{2}$, cantilever)	(beam pinned both ends)	0.80
	(beam fixed both ends)	0.65
(uniformly distributed load q, bending moment $\frac{qL^2}{6}$, propped cantilever)	(beam pinned both ends)	0.60

Table 6.2: *Table of buckling lengths/equivalent moment factors for a number of beam configurations. Note that the factor m in the last case is not based on the largest bending moment in the beam, but rather the bending moment at the hinged end.*

6.5 Tapered beams

Tapered glulam beams are frequently used to support roofs of medium sized buildings. Typical span lengths are 15-25 meters. According to reference [68], the current Norwegian practice is a roof angle below 4 degrees.

A large number of analyses have been carried out in order to establish guidelines for a simplified treatment of lateral torsional buckling of tapered beams.

Only simply supported beams subjected to uniformly distributed loading is studied, but loading applied at both the centroid and the upper edge is considered. In addition, analyses have been performed on double tapered beams braced at mid-span, but then only for loading applied at the centroid.

Due to an almost infinite number of possible variations of beam geometry, a dimension selector provided by Moelven Limtre AS is used as basis for the analyses. However, the dimension selector is based on a roof angle of 2 degrees, which does not comply with a desired angle span from 0 to 4 degrees. Therefore, only the width, the depth at the lowest end and the beam length is taken from the dimension selector. The apex depth of the double tapered beams and the depth at the deepest end of the single tapered beam are varied between the depth at the shallowest end to a depth resulting in a roof angle of 4 degrees.

Each beam is modelled using 40 elements, and the material properties described in section 6.1.2 (page 90) are used. The boundary constraints at both ends are applied at the center of the cross-section.

By comparing the lateral torsional buckling load from each computation with the lateral torsional buckling load of a beam of constant depth, h_{eqv}, but otherwise having the same geometrical specifications, load configuration, material and boundary conditions, and solving for h_{eqv}, an equivalent depth is found.

The expression used for the lateral torsional buckling load of a simply supported beam subjected to uniformly distributed loading applied at the centroid is equation (6.1), that is

$$q_{cr} = \frac{28.3\sqrt{EI_{zz}GI_t}}{L^3} \tag{6.12}$$

and for the load applied at the upper edge, equation (6.2) with $e = h/2$ is used.

$$q_{cr} = \frac{28.3\sqrt{EI_{zz}GI_t}}{L^3} - 40.2\left(\frac{h}{2L}\right)\frac{EI_{zz}}{L^3} + 14.0\left(\frac{h^2}{4L^2}\right)\frac{EI_{zz}}{L^3}\sqrt{\frac{E}{G}} \tag{6.13}$$

The buckling load of a beam braced at mid-span can be found as

$$q_{cr} = \frac{\pi\sqrt{EI_{zz}GI_t}}{0.763\left(\frac{L}{2}\right)^3} = \frac{8\pi\sqrt{EI_{zz}GI_t}}{0.763L^3} \tag{6.14}$$

corresponding to the first case of table 6.2[1] with beam length $L/2$. Each geometry set will form one curve in a diagram depicting equivalent depth as a function of roof angle. Due to the vast number of analyses carried out (each of the four analysis series consists of 1298 individual analyses), only the enveloping curves of the curve cascades resulting from the analyses are shown in the figures. The other curves position themselves in the grey area between the enveloping curves.

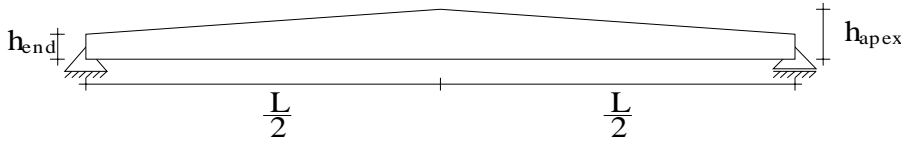## 6.5.1   Symmetric double tapered beams

Figure 6.22: *Double tapered beam.*

L, b and $h_{end} = h_1$ are taken from diagram *C.4* of appendix C (page 180), where each cell provides the geometry for one set of double tapered beams. The parameters are held constant for each geometry set, whereas h_{apex} is varied from $h_{apex} = h_1$ to $h_{apex} = h_2$, causing the roof angle to vary between 0 and 4 degrees.

---

[1]Note that the more accurate m-factor, $m = 0763$, from appendix C is used rather than $m = 0.8$ as suggested by table 6.2 on page 105
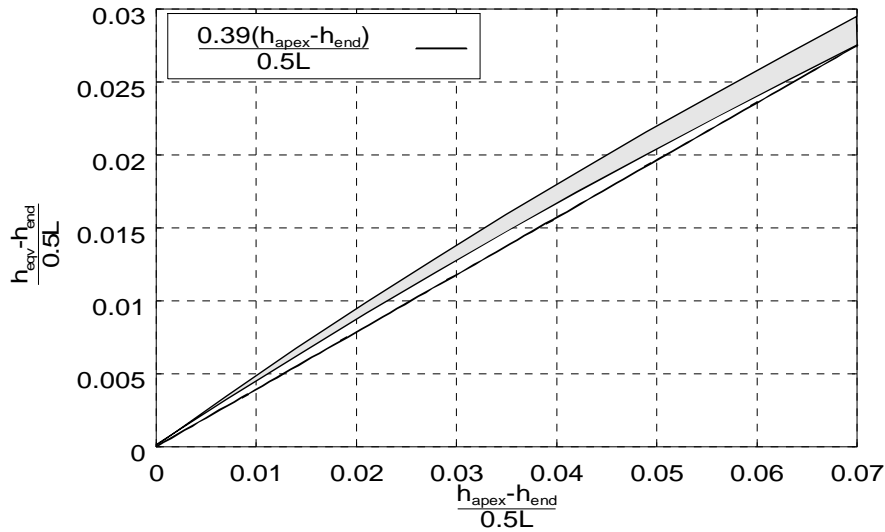
Loading applied at centroid

Figure 6.23: *Equivalent beam depths for symmetric double tapered beams with uniformly distributed loading at the centroid.*

Figure *6.23* shows the equivalent beam depths for simply supported symmetric double tapered beams with uniformly distributed loading applied at the centroid. Included is also a curve representing the approximate expression:

$$\frac{h_{eqv} - h_{end}}{\frac{1}{2}L} = 0.4 \cdot \frac{h_{eqv} - h_{end}}{\frac{1}{2}L} \tag{6.15}$$

which may be rewritten as

$$h_{eqv} = 0.6 \cdot h_{end} + 0.4 \cdot h_{apex} \tag{6.16}$$

A conservative approximation to the buckling load of a simply supported symmetric double tapered beam with distributed loading, and with depth varying from h_{end} at the ends to h_{apex} at the apex, can be found as the buckling load of an equivalent beam of uniform depth h_{eqv} determined by equation (6.16). For this load configuration, the approximate approach underestimates the buckling load by at most 3% for the geometry sets studied.

Loading applied at the upper edge

Figure *6.24* shows the equivalent beam depths for simply supported symmetric double tapered beams subjected to distributed loading applied at the upper edge.
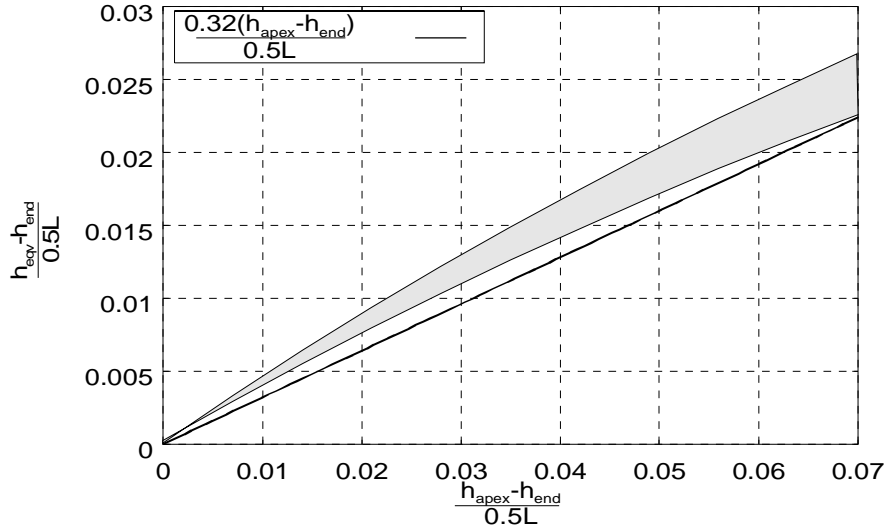
Figure 6.24: *Equivalent beam depths for double tapered beams with evenly distributed loading at the upper edge. Axis scaled as in figure 6.23.*

A curve representing the approximate formula

$$h_{eqv} = 0.68 \cdot h_{end} + 0.32 \cdot h_{apex} \tag{6.17}$$

is also shown in the figure. Application of this approximate formula yields lateral torsional buckling loads that are up to 6% lower than the one found from an analysis of a double tapered beam, for the tested geometry sets.

Figure *6.25* shows the same data as figure *6.24*, but the axes are scaled in order to reduce the spread of the data. The new approximate expression for the equivalent beam depth, which is also included in figure *6.25*, is:

$$h_{eqv} = h_{apex} \cdot 0.19 \cdot \left(\frac{h_{end}}{L}\right)^{-0.2} + h_{end} \cdot \left(1 - 0.19 \cdot \left(\frac{h_{end}}{L}\right)^{-0.2}\right) \tag{6.18}$$

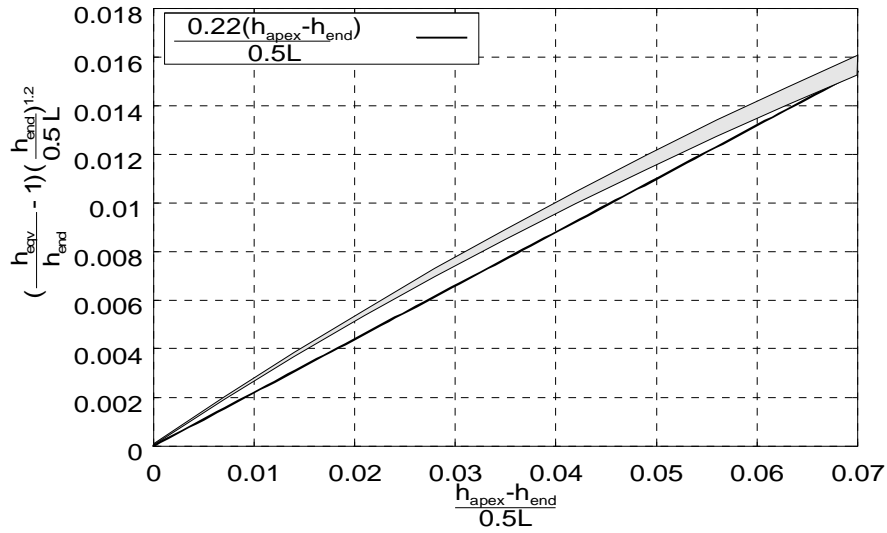With this formula, the maximum error will be lower than 2.5% for the geometry sets used in the analyses.

Figure 6.25: *Equivalent beam depths for double tapered beams with evenly distributed loading at the upper edge.*
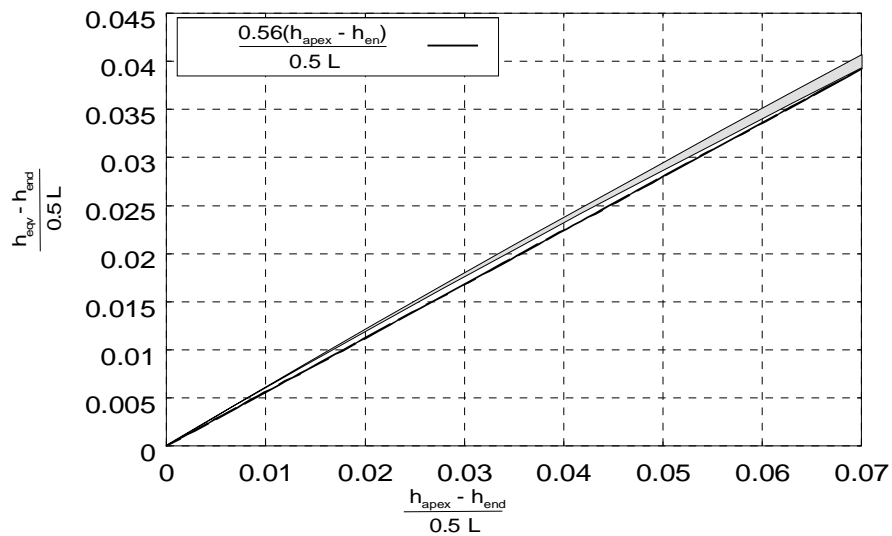
Braced at mid-span

Figure 6.26: *Equivalent beam depths for double tapered beams with uniformly distributed loading at the centroid and braced at mid-span. Axes scaled as in figure 6.23.*

Figure *6.26* shows equivalent beam depths for the simply supported symmetric double tapered beams that are subjected to uniformly distributed loading applied at the centroid, and that are braced at mid-span. The bracing was performed by restraining against both transverse displacement and torsional rotation. Included is also the approximate expression:

$$h_{eqv} = 0.44 h_{end} + 0.56 h_{apex} \qquad (6.19)$$

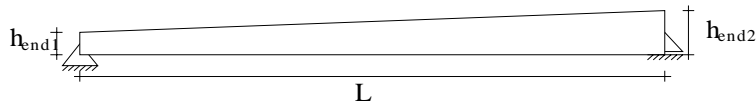## 6.5.2   Single tapered beams

Figure 6.27: *Single tapered beam*

Each cell in diagram *C.4*(page 180)(appendix C, section C.3) provides geometry data for one set of single tapered beams. The width b and the length L is taken directly from the diagram, as is $h_{end1} = h_1$. h_{end2} is varied between $h_{end2} = h_1$ and $h_{end2} = h_1 + L \tan 4°$.
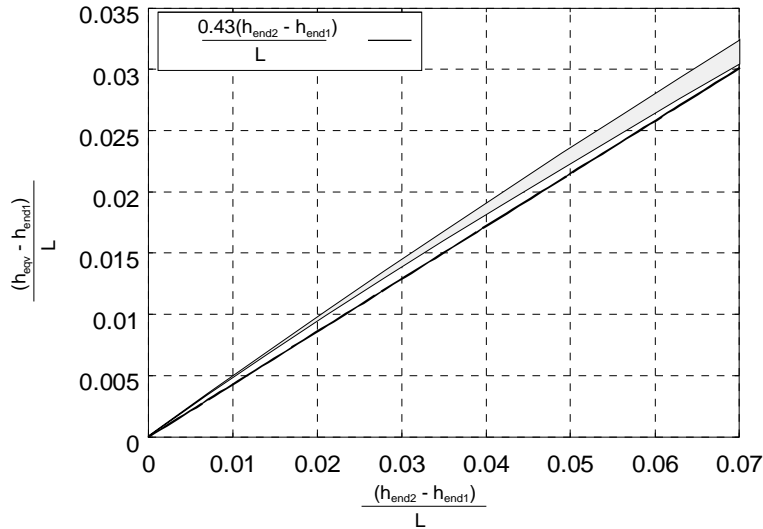
Loading applied at the centroid

Figure 6.28: *Equivalent beam depths for single tapered beams with uniformly distributed loading at the centroid.*

Figure *6.28* relates equivalent beam depth to the end depths of single tapered beams subjected to uniformly distributed loading applied at the centroid. A conservative approximation to the equaivalent beam depth is:

$$
\begin{aligned}
\frac{h_{eqv} - h_{end1}}{L} &= 0.43 \frac{h_{end2} - h_{end1}}{L} \\
&\Updownarrow \\
h_{eqv} &= 0.43 h_{end2} + 0.57 h_{end1}
\end{aligned}
\tag{6.20}
$$

This is depicted by the lower straight line in figure *6.28*. Use of this approximation gives a critical load which is at most 3.5% lower than the one found by the finite element computations.
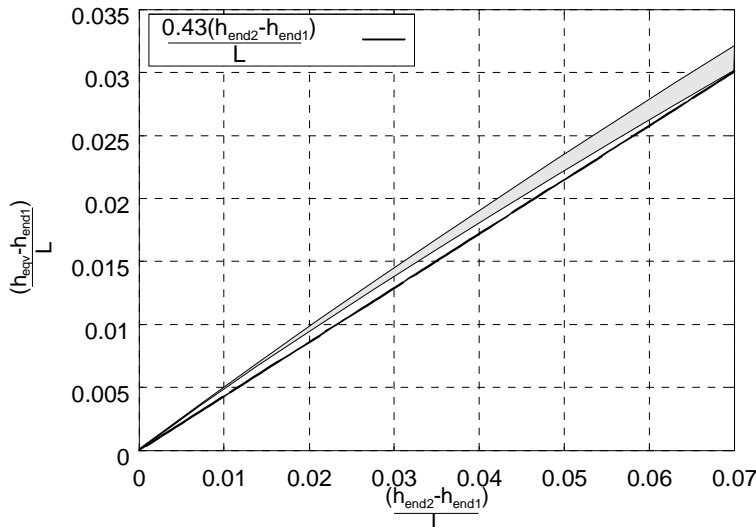
Loading applied at the upper edge

Figure 6.29: *Equivalent beam depths for single tapered beams with uniformly distributed loading at the upper edge.*

Figure *6.29* shows the equivalent beam depths for single tapered beams with uniformly distributed loading applied at the upper edge. As figure *6.29* shows practically the same picture as figure *6.28*, it may be concluded that equation (6.20) also applies to this case, with about the same accuracy.

6.6   Braced beams

The load bearing capacity of a beam prone to lateral torsional buckling may be considerably increased by bracing the beam against lateral displacements, or indeed against both lateral displacement and torsional rotation. The bracing can be placed at one or several discrete points, or along a portion of the length of the beam.

For simply supported beams, it will be shown that by linearized buckling analysis, there is only one single point in the cross-sectional plane where a lateral brace does not increase the lateral torsional buckling load of the beam. The position of this point is established for a few simple cases.

The effect of bracing on the lateral torsional buckling load of beams is also, to some extent, studied, as is the bracing stiffness necessary to prevent lateral displacement of the braced point.

This study only considers lateral bracing that is applied at the mid-span of the beams.

6.6.1 Simply supported beam with constant moment

Center of rotation

In [30], Timoshenko and Gere establish a differential equation for a simply supported beam subjected to constant bending moment, for use in stability calculations. The derivation was based on the assumption that the lateral and vertical displacement of the cross section were uniquely defined by the torsional rotation of the cross section. See figure *6.30*.
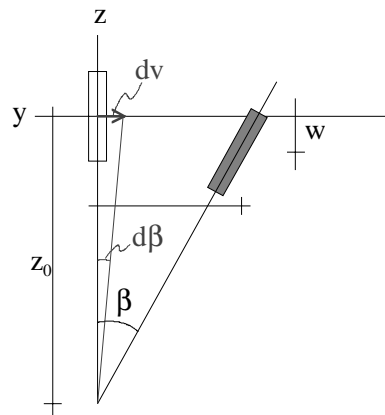

Figure 6.30: *Lateral and vertical displacement of a cross section in a buckling beam. Basis for establishment of differential equation.*

Timoshenko and Gere arrived at three differential equations, one being:

$$
\begin{aligned}
GI_t \frac{d\beta}{dx} &= -\frac{dv}{dx}M \\
&\Updownarrow \\
\frac{dv}{d\beta} &= -\frac{GI_t}{M}
\end{aligned}
\tag{6.21}
$$

Studying figure *6.30*, $\frac{dv}{d\beta}$ is recognized as the distance z_0 from the centroid of the cross section to the center of rotation. In [30], the buckling moment was found to be

$$M_{cr} = \frac{\pi}{L}\sqrt{GI_t EI_{zz}} \qquad (6.22)$$

Subsituting M_{cr} for M in equation (6.21), an expression for z_0 is found:

$$z_0 = \frac{dv}{d\beta} = -\frac{L}{\pi}\sqrt{\frac{GI_t}{EI_{zz}}} \qquad (6.23)$$

Assuming that the theory is correct, that is, the cross section has a fixed center of rotation, equation (6.21) implies that a bracing at any point but the center of rotation represents a restriction on the beam rotation, and therefore increases the buckling load. However, nothing can be concluded as to the magnitude of this increase.

Position of bracing
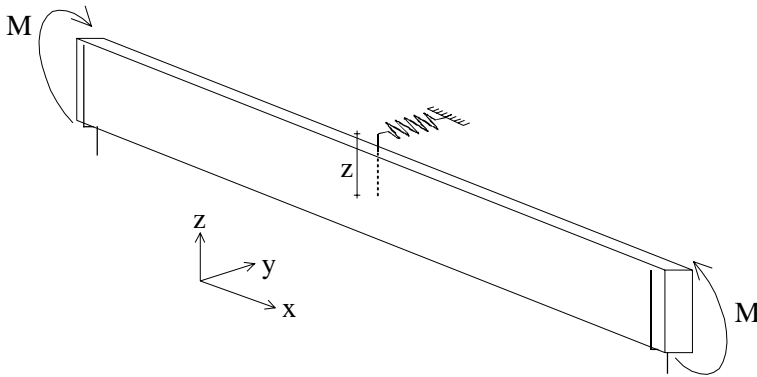
Figure 6.31: *Simply supported beam subjected to constant bending moment. Bracing at mid-span, eccentrically applied at a distance z from the centroid.*

In order to investigate how the buckling load varies as the brace is placed at different locations in the cross sectional plane, the beam in figure *6.31* is studied. Using 20 of the beam elements described in section 4.5(page 67) to model the beam, and assuming the bracing to be infinitely stiff, the position of the bracing is varied and the lateral torsional buckling load of the beam, as determined from a linearized buckling analysis, is recorded. This type of study is carried out for test beams 1, 2 and 3 described in section 6.1, and for a range of bracing positions of $-1.5z_0$ to $0.5z_0$.

Figure *6.32* shows the results of this study. The buckling loads are scaled with respect to the second buckling load of the beams, determined with no bracing
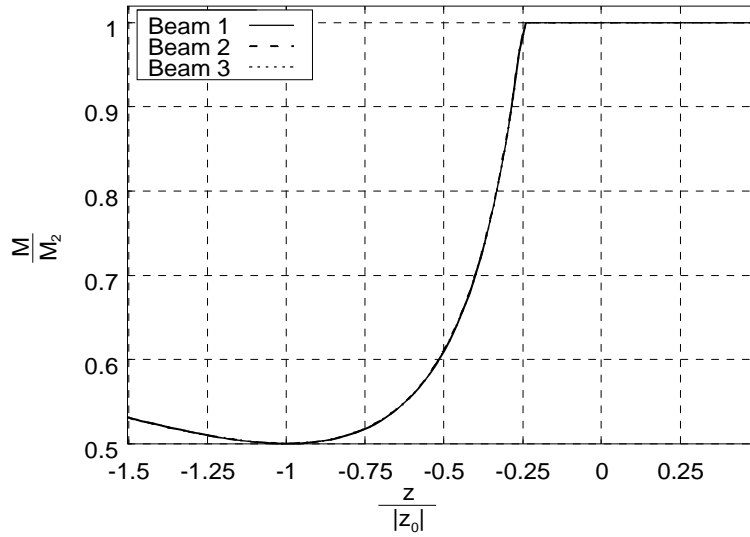
Figure 6.32: *Buckling loads for simply supported beams 1-3 subjected to constant bending moment, and with a rigid bracing at mid-span at a distance z from the centroid.*

present, whereas the position is scaled with respect to the distance from the centroid to the center of rotation, given by equation (6.23). This format causes the curves for the three different beams to coincide.

These results confirm that if the bracing is positioned in the center of rotation, where $z/|z_0| = -1$, it has no effect on the buckling load. For all other positions it increases the buckling load.

If the brace is positioned above the point for which $z/|z_0| \approx -0.250$, the beam is forced to buckle in two half-waves, and the buckling load of the beam is doubled. The point at which this occurs can be found from:

$$z_\infty \approx 0.250 z_0 = -0.250 \frac{L}{\pi} \sqrt{\frac{GI_t}{EI_{zz}}} = -0.080 \, L \sqrt{\frac{GI_t}{EI_{zz}}} \qquad (6.24)$$

The following points are worth noting:

- The limit bracing position z_∞ is valid only for an infinitely stiff bracing.

- No additional capacity is gained if the brace is positioned above z_∞.

- If the brace is positioned below z_∞, it cannot force the beam to buckle in two half waves no matter how stiff the brace is.
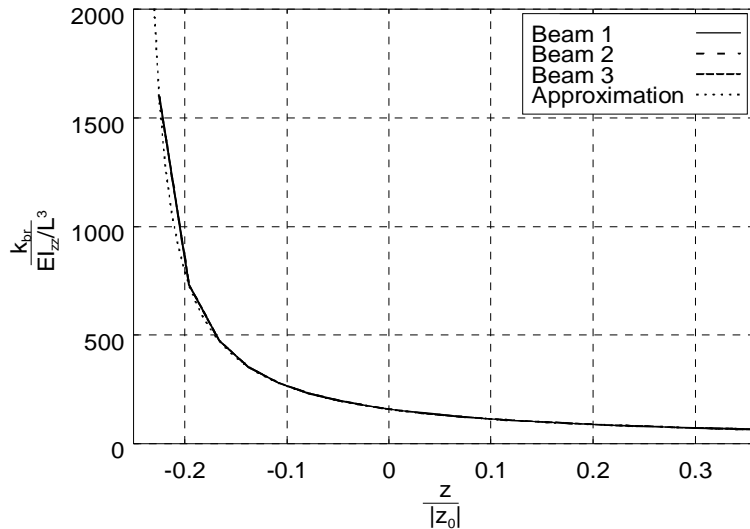
Stiffness of bracing at mid-span

Figure 6.33: *Simply supported beam subjected to constant moment. Necessary stiffness of bracing for varying bracing eccentricities.*

The assumption of the bracing being infinitely stiff, is of course not a realistic one. However, analyses show that for more realistic values of the bracing stiffness the buckling load/bracing position diagram maintains its shape, but that the limit position, shown by the sharp knee in figure *6.32* is moved in the positive direction along the bracing position axis. Therefore, analyses were performed to establish the bracing stiffness necessary to force the beam to buckle in two half waves (as opposed to one) for varying bracing eccentricity. A large number of analyses underly these results, since the bracing stiffness had to be found iteratively (each iteration involved one analysis). Thus, about 2000 analyses had to be performed in order to arrive at the results shown in figure *6.33*.

By scaling the bracing eccentricity by $|z_0|$ and the bracing stiffness by a factor, $\frac{EI_{zz}}{L^3}$, representing the bending stiffness about the weak axis, the results from the three different beams are made to coincide.

Since bracing applied lower than z_∞ is not able to force a beam to buckle in two halves, only bracing application points above the point identified by z_∞ is examined.

Figure *6.33* also includes the curve for an approximate analytical expression for the required stiffness. This expression has been found by assuming that the necessary bracing stiffness for bracing eccentricity z_∞ is infinity (assymptote at $z/|z_0| = -0.25$), and fitting the results to a suitable and simple expression. The

result is:

$$k_{br} = \frac{1}{0.0253\dfrac{z}{|z_0|} + 0.00633} \frac{EI_{zz}}{L^3} > 0 \qquad (6.25)$$

6.6.2 Simply supported beam with point load applied at mid-span
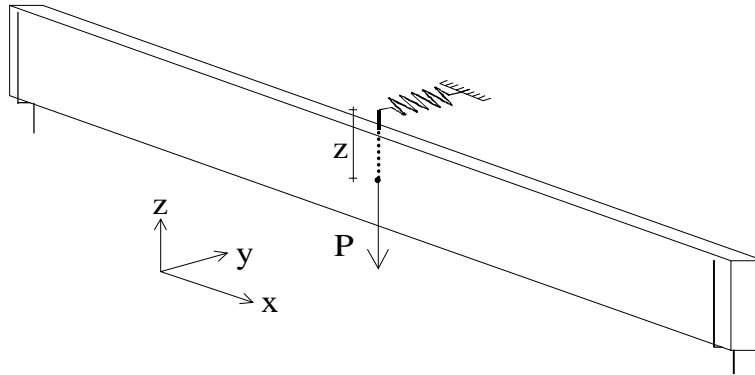
Figure 6.34: *Simply supported beam subjected to point load at mid-span. Bracing at mid-span, at eccentrically applied at a distance z from the centroid.*

Center of rotation

Assuming that a center of rotation, like the one found for the beam subjected to constant bending moment, can also be found for the beam in figure *6.34*, an effort was made to compute the distance z_0 from the centroid of the mid-span cross section to the center of rotation. The expression for z_0 was assumed to have the form

$$z_0 = -\frac{L}{a}\sqrt{\frac{GI_t}{EI_{zz}}} \qquad (6.26)$$

and an iterative algorithm was applied to determine the unknown a. Similar analyses were performed for the three test beams 1, 2 and 3 of section 6.1, with the following results:

Beam	z_0	a
1	-1.10613 m	3.349
2	-1.70945 m	3.349
3	-1.30422 m	3.349

In addition, one set of analyses was performed using the geometry of beam 3, but with the material properties of steel. For this beam the value of a was also found to be 3.349.

Thus, the center of rotation for the mid-span cross-section of a simply supported beam with a point load applied at mid-span can be expressed as:

$$z_0 = -\frac{L}{3.35}\sqrt{\frac{GI_t}{EI_{zz}}} \tag{6.27}$$

Position of bracing
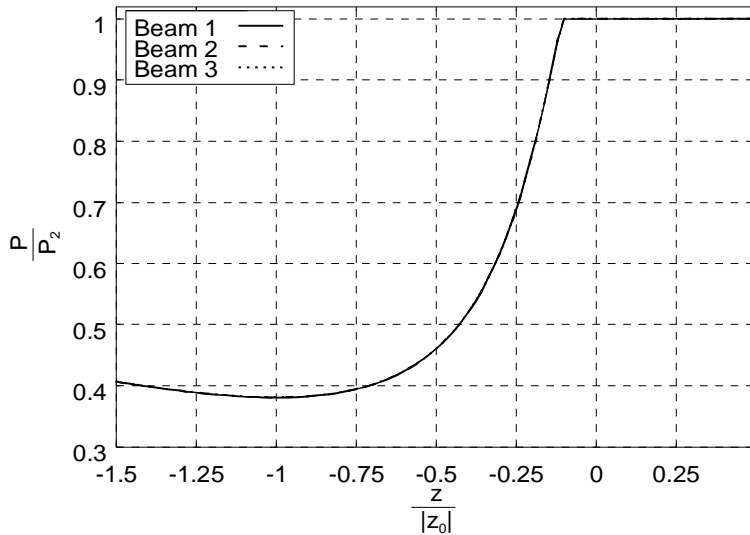
Figure 6.35: *Buckling loads for simply supported beams 1-3 subjected to a point load at mid-point, and with a rigid bracing at mid-point at a distance z from the centroid.*

Inspired by the simple formula obtained for the effective bracing position for the simply supported beam with constant bending moment, it was decided to perform similar analyses for the simply supported beam with a point load at mid-span. The results, which are scaled similarly to those in figure *6.32*, are presented in figure *6.35*. Note that this figure is correct only when the stiffness of the bracing is infinitely large.

According to figure *6.35*, the lowest point at which the beam is forced to buckle in two half-waves is given by $z/|z_0| \approx -0.107$ (this has actually been found using a separate iterative algorithm). Hence, the bracing can be positioned at a distance z_∞ below the centroid, and still effectively force the beam to buckle in two half-waves. z_∞ is given by:

$$z_\infty \approx -0.107 \frac{L}{3.349} \sqrt{\frac{GI_t}{EI}} = -0.032 \, L \sqrt{\frac{GI_t}{EI_{zz}}} \qquad (6.28)$$

Stiffness of bracing at mid-span
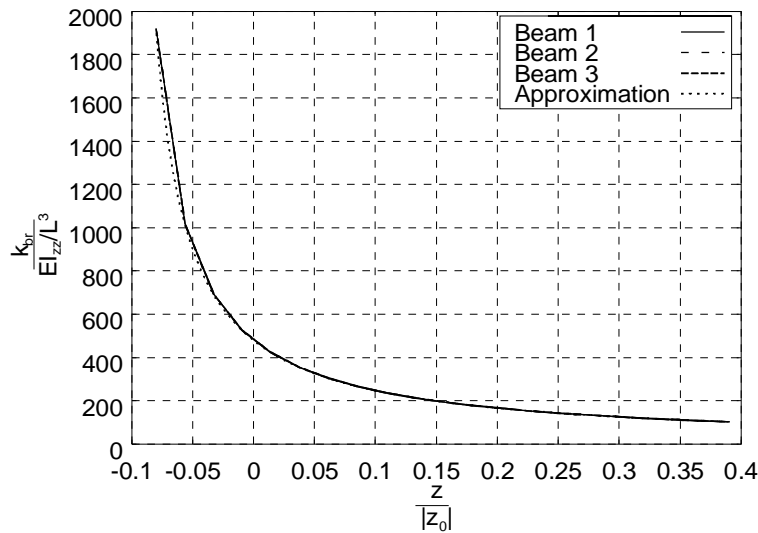
Figure 6.36: *Necessary bracing stiffness as a function of bracing position for simply supported beams with a point load in the centroid position at mid-span.*

Figure *6.36* relates the bracing stiffness necessary to force the beam to buckle in two half-waves, as a function of the bracing position. The following approximate expression is also included in the figure:

$$k_{br} = \frac{1}{0.0195 \dfrac{z}{|z_0|} + 0.00209} \frac{EI_{zz}}{L^3} > 0 \qquad (6.29)$$

6.6.3   Simply supported beam with distributed loading
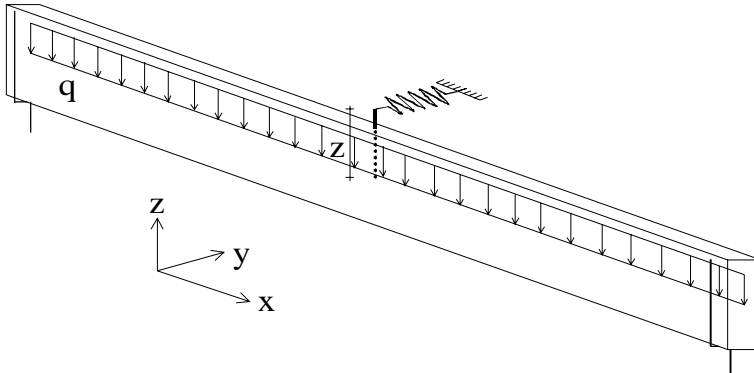
Figure 6.37: *Simply supported beam subjected to uniformly distributed load-ing applied at the centroid. Bracing at mid-span, eccentrically applied at a distance z from the centroid.*

Center of rotation

The point load on the simply supported beam is now replaced by a uniformly distributed load applied at the centroid. Again, the center of rotation is determined numerically through an iterative procedure. As before, the distance from the centroid to the center of rotation is assumed to be of the form:

$$z_0 = -\frac{L}{a}\sqrt{\frac{GI_t}{EI_{zz}}} \qquad (6.30)$$

A large number of computations gave the following values of a for the different beams:

Beam	z_0	a
1	-1.14519 m	3.235
2	-1.76971 m	3.235
3	-1.35010 m	3.235

Hence,

$$z_0 = \frac{L}{3.235}\sqrt{\frac{GI_t}{EI_{zz}}} \qquad (6.31)$$

Position of bracing
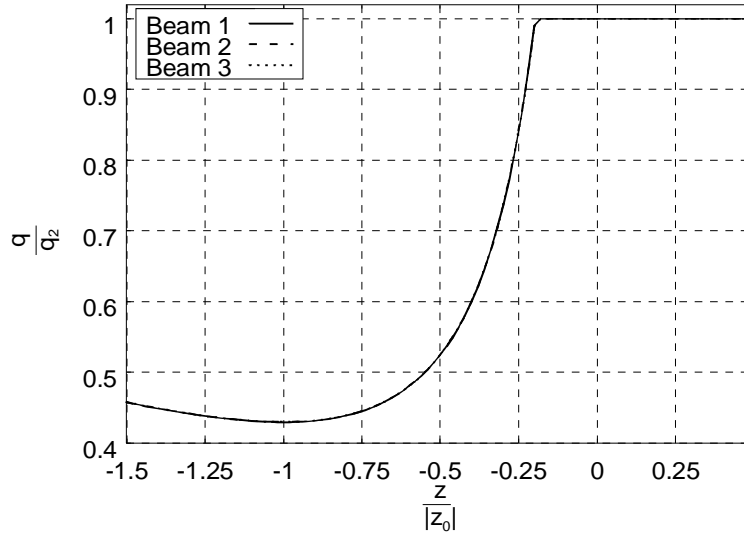
Figure 6.38: Buckling loads for simply supported beams 1, 2 and 3 subjected to uniformly distributed loading at the centroid , and with a rigid bracing at mid-span at a distance z from the centroid.

Figure *6.38* shows the buckling load of the beams as functions of the bracing position. The position is scaled by $|z_0|$ and the buckling load is scaled by the buckling load corresponding to the second buckling mode of the unconstrained beam.

The lowest point at which the bracing forces the beam to buckle in two half-waves is given by the sharp bend in the curves. From iterative analyses, it was found that this bend is located at $z/|z_0| \approx -0.197$. Thus, the maximum distance z from the centroid at which the bracing can be placed and still force the beam to buckle in two half-waves is determined by:

$$z_\infty \approx 0.197 z_0 = -0.197 \frac{L}{3.235} \sqrt{\frac{GI_t}{EI_{zz}}} = -0.061\, L \sqrt{\frac{GI_t}{EI_{zz}}} \qquad (6.32)$$

Stiffness of bracing at mid-span

Figure *6.39* shows the stiffness necessary to force the beam to buckle in two half-waves for varying bracing eccentricities. The same scaling is applied as for the previous beams. Included is also a hyperbolic approximate formula, with
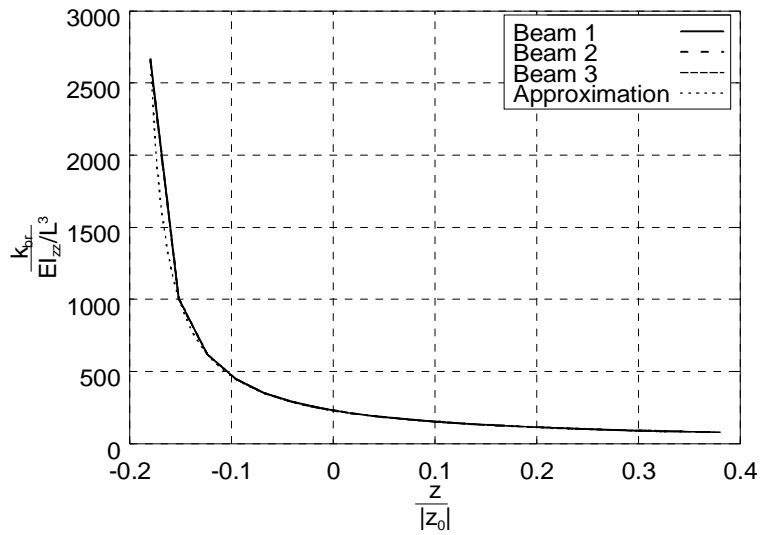
Figure 6.39: *Stiffness necessary to force the beam to buckle in two half-waves for varying bracing eccentricities.*

the mathematical representation:

$$k_{br} = \frac{1}{0.221\dfrac{z}{z_0} + 0.0435}\frac{EI_{zz}}{L^3} > 0 \tag{6.33}$$

Chapter 7

Nonlinear analysis results

Linearized buckling analysis is a useful tool for deriving simplified methods for buckling problems. Such methods should by their very nature provide conservative results.

A more versatile method of analysis is a complete, finite element based nonlinear analysis. Such an analysis is capable of quite accurate representation of both loading, including eccentric application, and boundary conditions, including bracing and its exact point of application. Geometric imperfections can also be accounted for, providing their size and shape are known, and it is, in principle, possible to also handle quite complex material properties.

In this chapter, some topics related to nonlinear analysis of timber structures are adressed.

7.1   Test beams

Test beams 1, 2 and 3, defined in section 6.1 (page 90) are used also in this chapter.

A simple *stress utilization factor*, given by the linear interpolation

$$s = \frac{\sigma_b}{f_{md}} + \frac{\sigma_a}{f_{c0d}} \tag{7.1}$$

where σ_b and σ_a are the design bending stress and axial stress, respectively, is defined. f_{md} and f_{c0d} are the design bending and axial strength, respectively. If

no material factors or factors accounting for moisture content or load duration
is included, the design strength equals the characteristic strengths.

The following simple failure criterion

$$s > 1.0 \tag{7.2}$$

is adopted in this study. This is consistent with NS3470 [2].

7.2   Torsional geometric imperfection

In most FEM-analysis tools, beam elements are only visualized by the beam axis.
This is usually sufficient for a 2D analysis, but in the 3D case, the orientation of
the cross section may vary along the beam axis, a variation that can not easily
be presented in a model where the beam elements are shown as mere lines.
Consequently, the geometric imperfection imposed on beam elements usually
consists of mere translations of the beam axis, and not rotations about the axis.

In this section some simple analyses have been performed in order to investigate
the importance of torsional imperfections relative to transverse imperfections.
By transverse imperfection is meant the deviation of the beam axis from the
intended shape, whereas torsional imperfection represents a twist of the cross-
sections.

7.2.1   Geometric imperfection

Section 5.4 in Eurocode 5 [3] provides some guidelines to nonlinear analysis of
plane frames. It is required that "*the imperfect shape of the structure should
be assumed to correspond to an initial deformation which is in approximate
affinity to the relevant deformation figure, and found by applying an angle ϕ of
inclination to the structure or relevant parts, together with an initial sinusoidal
curvature between the nodes of the structure corresponding to a minimum ec-
centricity e.*"   "*The value of e should as a minimum be taken as* $0.003 \cdot L$."
However, no guidelines are provided for 3D structures.

NS3470 provides no guidelines whatsoever for nonlinear analysis of timber struc-
tures. In section 7.2.3 it does, however, state that the maximum deviation from
straightness for columns and beams prone to buckling should not exceed $1/300$
of the length for structural timber and $1/450$ for glued laminated timber. These
fractions may be used as basis for modelling of geometric imperfection.

In this study, the shape of the geometric imperfection is assumed to coincide with the shape of the first buckling mode of the beam, as obtained from a linearized buckling analysis. Only transverse loading is active in the buckling. Three types of geometrical imperfection are studied. First, the imperfection consists only of the transverse part of the buckling shape. Second, the imperfection consists only of the torsional part of the buckling shape. Finally, an imperfection consisting of the total buckling shape is studied. In all three cases the maximum deviation from the intended geometry is set to 1/450 of the length of the beam.

The results from the nonlinear analyses are presented as curves relating the loading to the vertical displacement at mid-span, for each of the three different assumptions for the imperfection. In addition, a similar load-displacement curve is included for a bifurcation type analysis (see section 2.1.4, page 9).

For each load-displacement curve presented, a point is included indicating the load bearing capacity of the beam, defined by the failure criterion (7.2).

The beam geometry is that of beam 2 in section 6.1(page 90), and the material is as presented in section 6.1.2(page 90). Consistent with the discussion in section 2.3 (page 11), the characteristic values of the stiffness moduli are used. Since the purpose of the analyses is the relative behaviour, no material factors or other factors accounting for environment or load duration are used.

20 elements of the new element presented in section 4.5 (page 67) are used to model each beam.

7.2.2 Simply supported beam subjected to distributed loading

Figures *7.1*, *7.2* and *7.3* show results from analyses of a simply supported beam subjected to a uniformly distributed load at the upper edge, the centroid and at the lower edge, respectively. Of the three kinds of geometric imperfection, the purely torsional one is clearly the most critical. However, since this form (and size) of imperfection is extremely unlikely to occur in a real beam, it is not very interesting.

More interesting is it that all analyses predict that the combined transverse and torsional imperfection results in lower load capacity than the purely transverse imperfection.
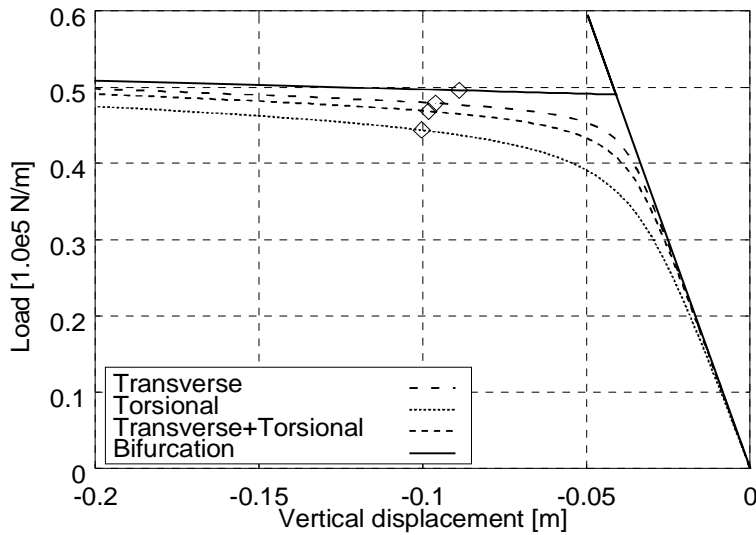
Figure 7.1: *Load-displacement curves for a simply supported beam subjected to distributed loading at the upper edge. Various types of geometrical imperfections.*
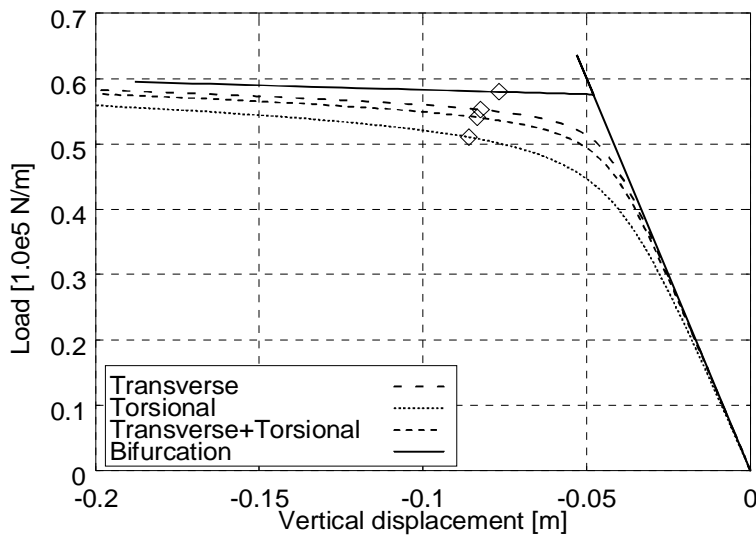
Figure 7.2: *Load-displacement curves for a simply supported beam subjected to distributed loading at the centroid. Various types of geometrical imperfections.*
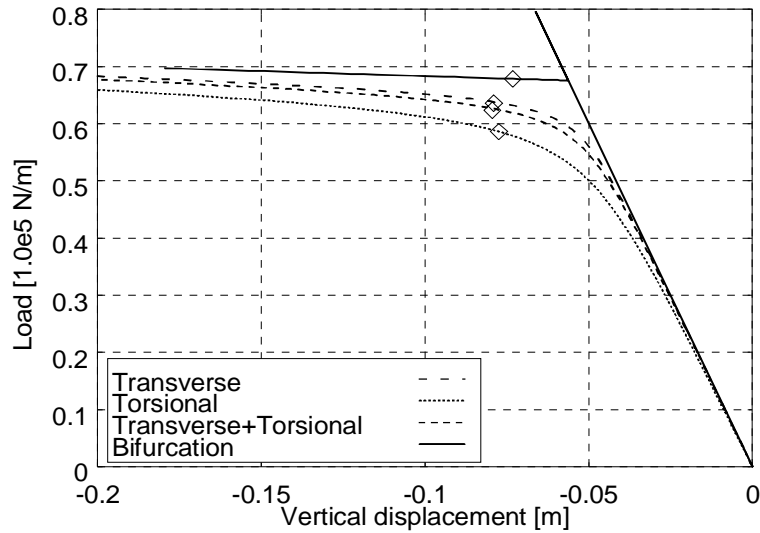
Figure 7.3: *Load-displacement curves for a simply supported beam subjected to distributed loading at the lower edge. Various types of geometrical imperfections.*

| Load position | Load capacity | | Decrease |
	Transverse imperfection	Combined imperfection	
Upper edge	47.90 kN/m	46.84 kN/m	2.2 %
Centroid	55.24 kN/m	54.07 kN/m	2.1 %
Lower edge	63.56 kN/m	62.34 kN/m	1.9 %

This table shows that there is a small, yet consistent, decrease in the load bearing capacity of the beam when subjecting it to a combined imperfection as compared to a pure transverse imperfection.

A couple of beams with other sets of loading and boundary conditions have been studied. The results showed the same tendencies as those presented above, and they are therefore not discussed further.

7.3 Combined flexural and lateral torsional buckling

In section 6.3(page 99), interaction curves were found by means of linearized buckling analysis for the test beams 1, 2 and 3 of section 6.1(page 90).

In this section, some of the configurations that were analyzed in 6.3 are reanalyzed, but this time by a complete nonlinear analysis. Comparison of these results with the results from the linearized buckling analyses, will give an indication of the applicability of the linearized buckling results.

This study is limited to six of the beam configurations studied in section 6.3. The geometric imperfection imposed in each case is a scaled version of the shape of the first buckling mode, found from a linearized buckling analysis of the beam subjected to the bending inducing loading only. Both the transverse and the torsional part of the imperfection is included, and maximum amplitude of the imperfection is set to $L/450$. The material properties are those presented in section 6.1.2 (page 90, and the 5-percentile stiffness moduli are used. No material factors or other correction factors accounting for moisture content or load durability are applied.

The loading is divided into two categories, one designated by M or M-type loading which is the type of loading that causes bending (e.g. transverse loading and applied moments). The other type is designated by N or N-type loading which is loading that causes axial forces only (in the linear case).

The resulting interaction curves are presented twice, with different scaling:

- **Scaling 1**: The vertical and horizontal axes are scaled by the maximum design M-type loading acting alone and the maximum design N-type loading acting alone, respectively, *as found from nonlinear analyses.*

- **Scaling 2**: The vertical and horizontal axes are scaled by the buckling load for M-type loading acting alone, and buckling load for N-type loading acting alone, respectively, *as found from linearized buckling analyses.*

The reason for this, will become apparent in the discussion of the results.

For reasons of comparison, the interaction curves found by the linearized buckling analyses are also included.

Each beam is modelled by 20 elements.

7.3.1 Analysis procedure

The analyses were carried out using the nonlinear analysis facilities of Cfem.

In this program, a common *virtual time* variable λ is used for defining the load history. The two types of loading, M and N are each assigned a function

dependent on λ so that for a given λ, the load combination is:

$$q_{comb} = f_1(\lambda) \cdot N + f_2(\lambda) \cdot M \qquad (7.3)$$

By defining $f_1(\lambda)$ and $f_2(\lambda)$ such that only one of them varies at a given "time" λ, the load bearing capacity for one of the loads, at a given level of the other load, can be found. Thus, $f_1(\lambda)$ and $f_2(\lambda)$ were defined as:
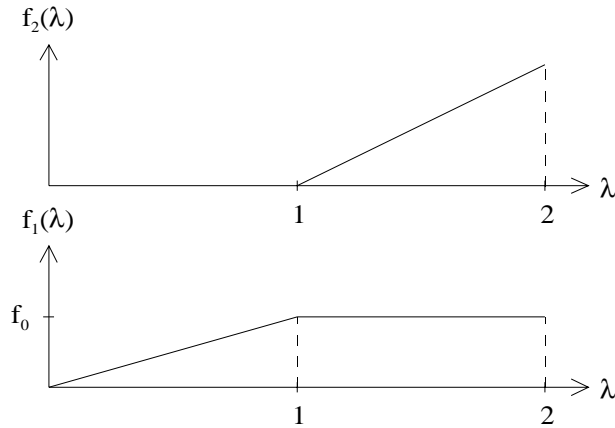
For a particular axial load level f_0, the utilization factor s exceeds 1 for a virtual time λ_u. The corresponding M-type load level is then found as:

$$M_u = f_2(\lambda_u - 1.0) \cdot M \qquad (7.4)$$

It may be argued that equation (7.3) isincorrect, since superposition is invalid in nonlinear analysis. However, analyses using the reverse definition for q_{comb}, namely $q_{comb} = f_2(\lambda) \cdot N + f_1(\lambda) \cdot M$ resulted in the same interaction curves as those using equation (7.3).

Through a series of analyses, where, for each series, the load types and boundary conditions are held constant, while f_0 is varied, interaction curves between N- and M-type loading are found.

7.3.2　Interaction curves

Beam 1

Figure 7.4: *Simply supported beam with constant bending moment.*

Figure 7.5: *Simply supported beam with uniformly distributed loading at the upper edge.*

Beam 2

Figure 7.6: *Simply supported beam with point load at mid-span, at the lower edge.*
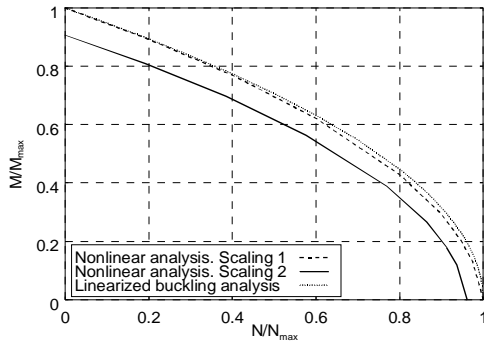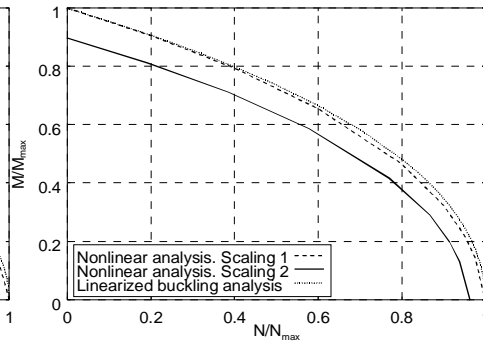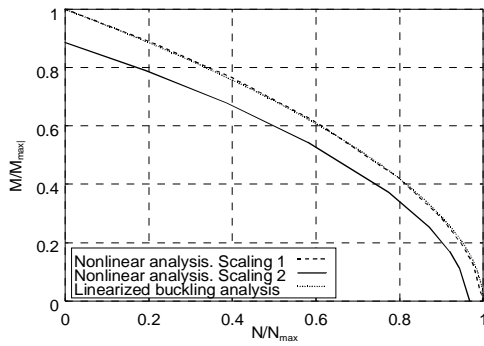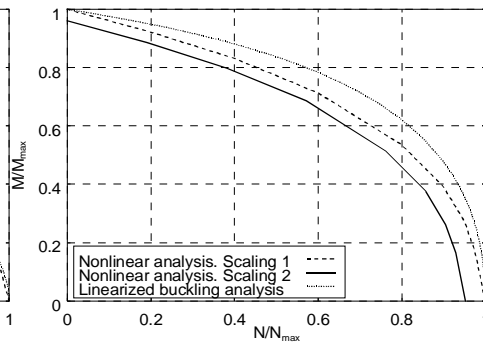

Figure 7.7: *Beam built in at both ends and subjected to uniformly distributed loading at the upper edge.*

Beam 3
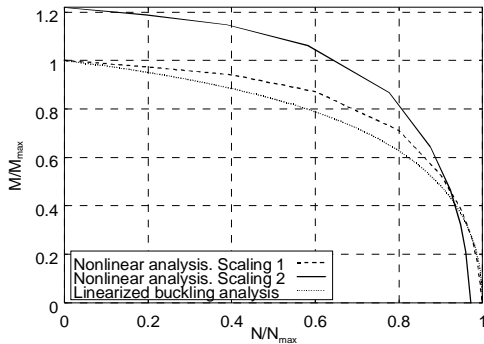
Figure 7.8: *Beam built in at both ends and subjected to uniformly distributed loading at the upper edge.*
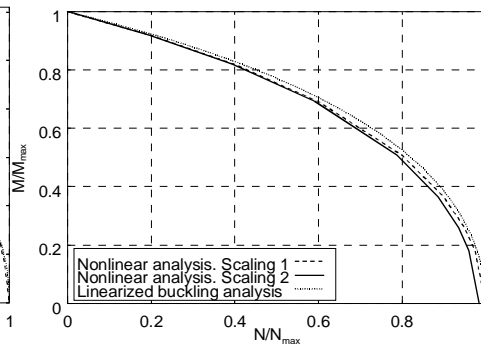
Figure 7.9: *Simply supported beam subjected to a point load at midspan, at the upper edge.*

In figure *7.4* through *7.9* all interaction curves using scaling 1 lie fairly close to their linearized buckling counterpart, indicating that the linearized buckling analyses can be used to obtain a good estimate of the interaction curves. Observe, however, that for the cases, save one, the interaction curves obtained by nonlinear analysis lie below those found by linearized buckling analysis. Thus, care should be taken before using the interaction curves obtained from the linearized buckling analysis, as they tend to be slightly non-conservative. This can be accounted for in the suggested interaction formula, (6.8) from section 6.3, by changing the factor $3/2$ in the M-type term to a smaller value.

The curves obtained by scaling 2 are scaled with respect to the buckling and lateral torsional buckling load *of the linearized buckling analysis*. An interaction curve obtained by nonlinear analysis that is positioned below the corresponding interaction curve from a linearized buckling analysis, indicates that the nonlinear analysis predicts less M-type loading than the corresponding linearized buckling analysis. This is consistent with the expectation that a beam with an imposed geometric imperfection can take less loading than that predicted by the differential equation for the same, but mathematically straigh beam. Indeed, for zero M-type loading, all the beams show that the nonlinear analysis predicts a critical load that is lower than the linearized buckling load. However, figure *7.8* shows that for this configuration the critical bending moment predicted by a nonlinear analysis actually exceeds the corresponding moment predicted by the linearized buckling analysis, by as much as 20%. This phenomenon can be explained by studying the load-displacement curves for the different configurations.

Consider the simply supported version of beam 1, subjected to a uniformly distributed loading q at the upper edge. The interaction curve for this beam is given in figure *7.5*. In figure *7.10*, the loading q is plotted as a function of the vertical displacement at mid-span. The square boxes indicate the ultimate load
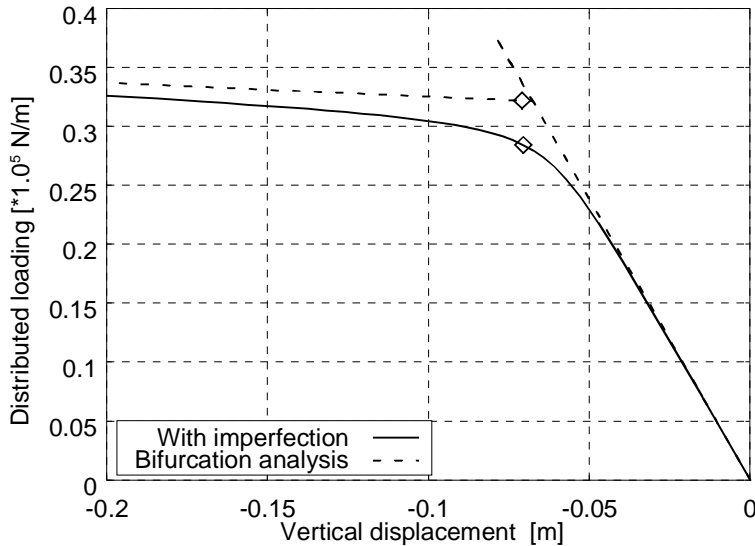
Figure 7.10: *Load-displacement diagram for a simply supported beam 1 subjected to uniformly distributed loading q at the upper edge.*

for the beam defined by the failure criterion of equation (7.2). The load level at the branching point on the load-displacement curve from the bifurcation analysis, is approximately the same as a linearized buckling analysis would yield. The bifurcation curve shows a very low stiffness after the bifurcation point is reached (the curve is practically horizontal beyond this point). The curve obtained by nonlinear analysis with geometrical imperfection can be viewed as an "imperfect version" of the load-displacement curve from the bifurcation analysis, and the same behaviour is reflected in this curve (although the bifurction point is never actually reached). Thus, since the ultimate load is reached at a fairly moderate displacement, the "nonlinear ultimate load" is in this case lower than the one predicted by the linearized buckling analysis.

Figure *7.11* shows the same load displacement diagram for beam 3 with built in ends and subjected to a uniformly distributed loading at the upper edge.

Again, the bifurcation point is a good representation of the result obtained by a linearized buckling analysis. In this case both curves show that the beam retains stiffness beyond the bifurcation point, and the ultimate load is significally higher than the bifurcation load and thus the linearized buckling load.
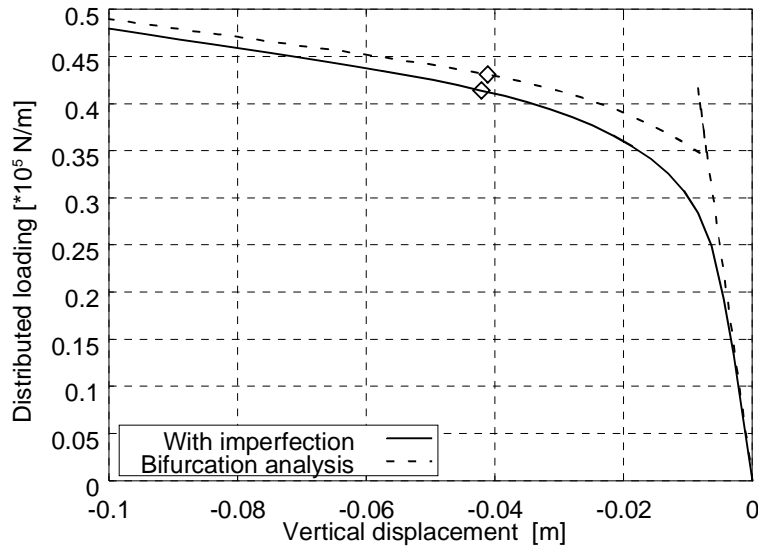
Figure 7.11: *Load-displacement diagram for beam 3, with built in ends, subjected to uniformly distributed loading at the upper edge.*

7.4 Double tapered beam
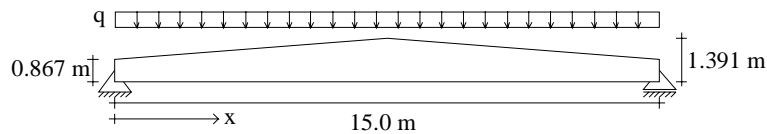
Figure 7.12: *Simply supported beam subjected to uniformly distributed loading at the upper edge.*

In order to assess the validity of the simplified handling of lateral torsional buckling of double tapered beams arrived at in section 6.5.1, an analysis have been carried out for the system shown in figure *7.12*. First, the system is analyzed according to the rules of NS3470 [2] with the use of the expressions found in section 6.5.1 for the lateral torsional buckling factor. The second approach is to make use of the nonlinear facility of Cfem.

The beam is made of glued laminated timber with properties as described in section 6.1.2. No material factor or other factors accounting for environment and load duration are used. Consistent with the discussion in section 2.3(page 11), the 5-percentile values of the stiffness parameters are used in the nonlinear analysis.

7.4.1   Simplified analysis

Equation (6.18) on page 108 is used to find the equivalent beam depth of the double tapered beam:

$$
h_{eqv} = 1.391 \cdot 0.19 \cdot \left(\frac{0.867}{15}\right)^{-0.2} + 0.867 \cdot \left(1 - 0.19 \cdot \left(\frac{0.867}{15}\right)^{-0.2}\right) = 1.043m
$$

$$(7.5)$$

According to equation (6.13) (page 106), the critical flexural buckling load found from a linearized buckling analysis for this beam is approximately

$$
q_{cr} = 14.1 kN/m \tag{7.6}
$$

Now that q_{cr} has been found, the equivalent beam is abandoned. In order to find the slenderness ratio for lateral torsional buckling, the critical bending stress σ_{cr}, which is the maximum bending stress in the beam when subjected to the critical load, needs to be found. The location of the cross section at which σ_{cr} occurs, is in a tapered beam found by seeking the maximum bending stress. Aune [46] finds that the maximum bending stress occurs at

$$
x = \frac{L h_{end}}{2 h_{apex}} = 4.67m \tag{7.7}
$$

The corresponding beam depth is

$$
h_{cr} = h_{end} + \frac{h_{apex} - h_{end}}{L/2} x = 1.193m \tag{7.8}
$$

The bending moment at the distance x from the left end is $M_{cr} = \frac{1}{2}q_{cr}Lx - \frac{1}{2}q_{cr}x^2 = 340.1 kNm$, and thus, the critical bending stress is

$$
\sigma_{cr} = \frac{M_{cr}}{\frac{1}{6}bh_{cr}^2} = 8.7 MPa \tag{7.9}
$$

According to section 12.1.7 in NS3470, the slenderness ratio and the lateral torsional buckling factor can be found from

$$
\lambda_m = \sqrt{\frac{f_{mk}}{\sigma_{cr}}} = 2.11 \qquad k_{vipp} = \frac{1}{\lambda_m^2} = 0.223 \tag{7.10}
$$

For the code checking expressions, reference is made to section 12.1.12 in NS3470. Note that in the code checking, the computed bending stress must be multiplied by the amplification factor $1/k_{vipp}$. The factor k_{fa} is found to be $k_{fa} = 0.871$ for $\alpha = 4°$.

The code checks should be applied at the critical section and also at the apex. For the unknown load q, the bending moment at the critical section is $M_\gamma = 24.1q$, whereas it is $M_{\gamma,apex} = 28.1q$ at the apex. Thus, the load capacity of the double tapered beam is the lowest value of q obtained from

$$M_\gamma = 24.1q = min \begin{cases} \frac{k_{vipp} \cdot f_{md} \cdot \frac{1}{6} bh_c^2}{1 + 3.7 \tan^2 \alpha} \\ \frac{k_{vipp} \cdot k_{fa} \cdot f_{md} \cdot \frac{1}{6} bh_c^2}{1 - 4.4 \tan^2 \alpha} \end{cases} \tag{7.11}$$

and

$$M_{\gamma,apex} = 28.1q = min \begin{cases} \frac{k_{vipp} \cdot f_{md} \cdot \frac{1}{6} bh_{apex}^2}{1 + 1.4 \tan^\alpha + 5.4 \tan^2 \alpha} \\ \frac{f_{t90d} \cdot \frac{1}{6} bh_{apex}^2}{0.2 \tan \alpha} \end{cases} \tag{7.12}$$

This simplified analysis gives a load bearing capacity of the double tapered beam of $q = 12.6 kN/m$ (from (7.11)).

7.4.2 Nonlinear analysis

A scaled version of the first buckling shape of the double tapered beam is taken to be its geometrical imperfection. The buckling shape is found from a linearized buckling analysis, and is scaled such that the maximum deviation from the intended shape is $L/450 = 0.033m$. Both translation and rotation is included in the imperfection.

30 elements are used in the modelling of the beam. The formulation used is described in section 4.5 (see page 67). A code check according to section 12.1.12 in NS3470 is performed for the ends of each element at each load step. A linear interpolation is performed with respect to the utilization about the strong axis and utilization about the weak axis. Figure *7.13* shows the load as a function of the vertical displacement at mid-span for both nonlinear and bifurcation analysis. In both cases the ultimate load is marked by a box. The ultimate load predicted by nonlinear analysis was found to be 14.7 kN/m, which is about 17% higher than that predicted by the simplified analysis, and about 4% higher than q_{cr}. The explanation for the latter finding is found in the behavious described above in section 7.3.2 (page 130). The simplified method should always yield a load capacity less than or equal to the critical load found from a linearized buckling analysis. On this background, the load found from the simplified analysis in this case seems to be a reasonable approximation.

Studying the load-displacement curve in figure *7.13*, it is seen that the ultimate load is reached for a relatively large vertical displacement, about 0.39 m. The horizontal displacement at the apex was actually about 1.2 m. This seems to indicate that for this particular beam a displacement based failure criteron is appropriate.
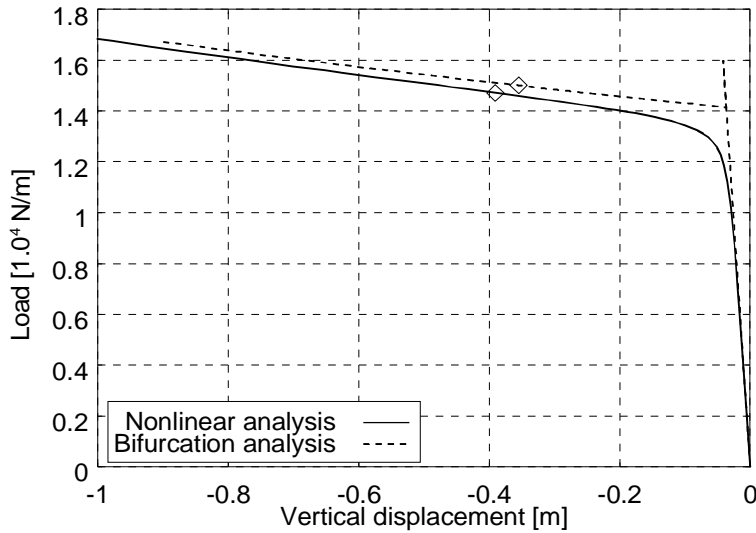
Figure 7.13: *Load as a function of vertical displacement for a simply supported beam subjected to uniformly distributed loading at the upper edge.*

7.5   A case study

In this section, a roof and wall "shelter" structure is designed, first by use of a simplified design based on the existing Norwegian design code NS3470, and then by a design based on nonlinear analysis in combination with the rules of NS3470.

7.5.1   Problem identification

An extension to an existing factory building, intended for storage purposes, is to be built with glulam in the supporting structure. The indoor height of the new storage room should be at least 10 meters, and the length of the structure is set to 32 meters. A large gate is positioned in one of the gables may stay open in all kinds of weather. The other gable is closed. The existing building is considered strong enough as support for the extension. The structural system of the storage extension is shown in figure *7.14*. The cross-sectional properties of the different members of the structure are as follows:

- Rafters: Rectangular with $b \times h = 0.17$ m $\times$ 1.12 m

- Column: Rectangular with $b \times h = 0.17$ m $\times$ 0.84 m
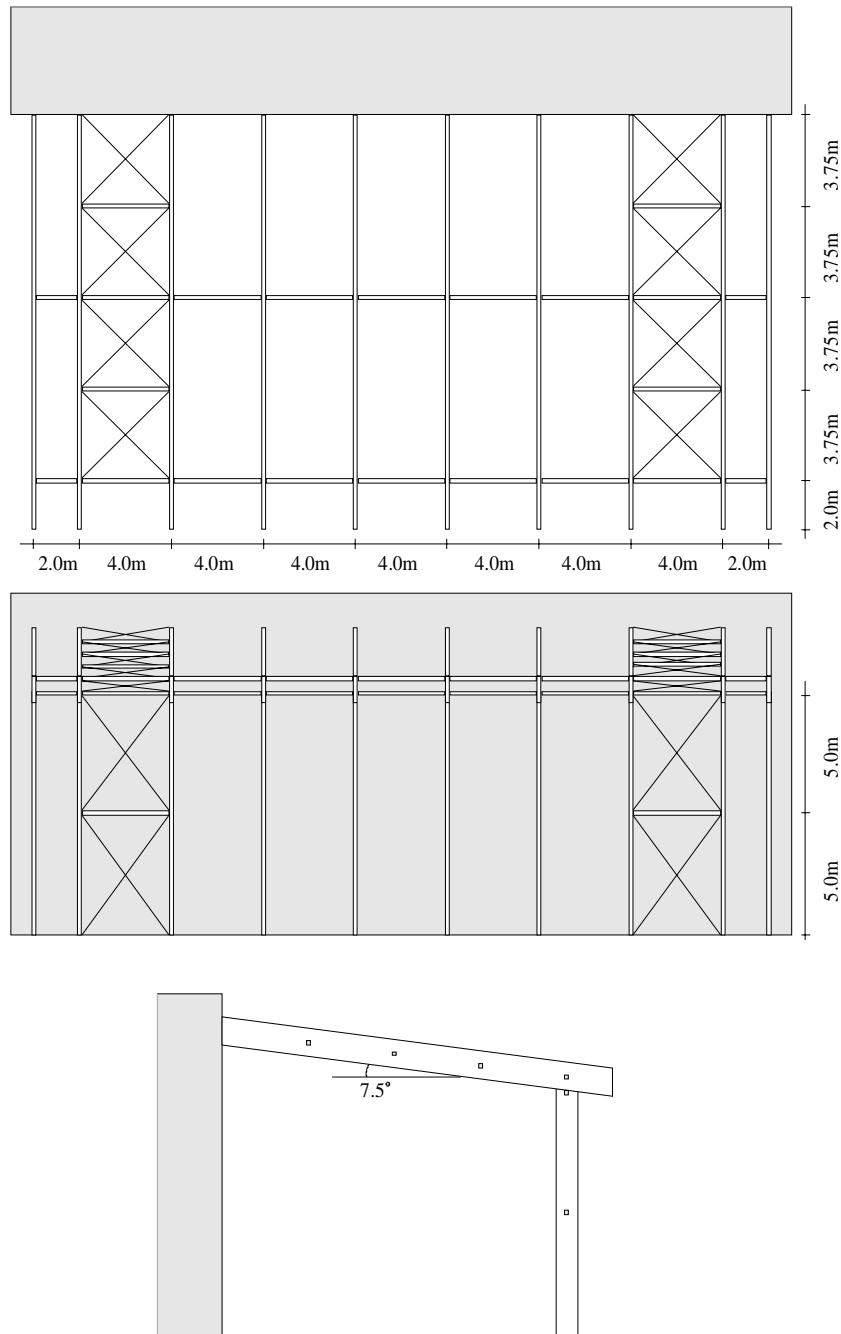
Figure 7.14: *Sketch of a lean-to shelter structure in three different perpendicular planes.*

- Bracing: Quadratic with sides $b = h = 0.16$ m

- Wind crosses: Circular. Diameter $d = 32$ mm.

The uniformly distributed design load on the roof is $q_1 = 6.3$ kN/m^2, whereas the net design wind pressure on the external wall is $q_2 = 1.3$ kN/m^2. Both loads are assumed to act on the edges of their respective members. Hence, q_1 is acting on the top of the roof beams, while q_2 is acting as pressure on the outer wall surface[1]. For the roof, only loading positioned in the free span between the walls is included in the calculations (that is, no load on the overhang).

All bracing is applied at the center lines of the main structure components.

The glulam members of the structure are considered to be made from lamellas satisfying the T30 strength class in NS3470[2]. Multiplied with the *lamination factor*, the characteristic material properties are as given in the table below. In addition, the design properties adjusted for moisture and load duration effects, are given in the same table. The material factor is set to $\gamma_m = 1.21$, whereas the factor accounting for load duration and moisture effect is $k_r = 0.9$.

Property		Characteristic		Design
Bending strength	f_{mk}	39.0 MPa	f_{md}	29.0 MPa
Compression strength	f_{c0k}	35.1 MPa	f_{c0d}	26.1 MPa
Tension strength	f_{t0k}	23.4 MPa	f_{t0d}	17.4 MPa
Modulus of elasticity				
Mean value	E_0	14145.0 MPa		
5-percentile value	E_{0k}	10062.5 MPa	E_{0d}	7484.5 MPa
Shear modulus				
Mean value	G	885.5 MPa		
5-percentile value	G_k	632.5 MPa	G_d	470.5 MPa

The purpose of this study is the structural behaviour of the glulam members. No attention is paid to problems related to connections. Furthermore, only loading in two planes are considered, namely loading perpendicular to the roof plane and perpendicular to the longitudinal wall plane (no loading on the gable planes), and only ultimate limit state is considered.

---

[1] Since the wind pressure consists of both pressure on the outer side of the wall and suction on the inner side, this may be a somewhat questionable assumption. However, it is conservative as well as convenient.

7.5.2 Simplified design according to NS3470

The loading is lumped, so that each rafter and column experience the loading from half their adjacent spans. Thus, the loading on the most critical rafter is:

$$q_{\text{rafter}} = 4.0 \text{ m} \cdot 6.3 \text{ kN/m}^2 = 25.2 \text{ kN/m} \tag{7.13}$$

whereas the transverse (wind) design load and the axial design load on the most critical column becomes

$$q_{\text{column}} = 5.2 \text{ kN/m} \quad \text{and} \quad N_{\text{column}} = 189.0 \text{ kN} \tag{7.14}$$

respectively. Axial force in the roof beams is disregarded in these calculations.

Rafter

Strict interpretation of NS3470, recognizes lateral torsional bracing only when applied on the compression side of the rafters. For the present structure the bracing is located at the centroid of the rafter. Nevertheless, in this design the bracing is considered to have full effect.

Under the influence of bending, each rafter is assumed to buckle in two half waves due to the bracing. NS3470 provides a table of buckling lengths (similar to table 6.1 on page 104), but required configuration, which is
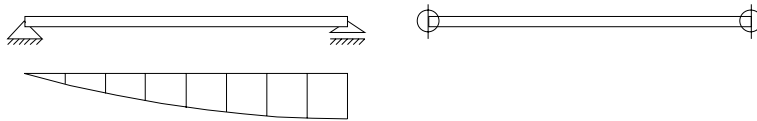
is not included. However, a combination of two cases in the table is used to find an estimate of the buckling length. Both are subcases of the first entry in table 6.1. $\mu = 0.0$ is unconservative, yielding a buckling length on the low side, while on the other hand, $\mu = 1.0$ yields too large a buckling length. The mean value, that is $\mu = 0.5$ is used in these calculations, resulting in a buckling length of 0.8 times half the rafter length. This is in good agreement with the result presented in table 6.2 (page 105). Also, due consideration must be taken to the application of the loading. Since the load is applied at the upper side of the beam, NS3470 suggests that the buckling length is increased by adding two times the beam depth. Given that the span of the beam is $L = 15.0 \text{ m}/\cos 7.5° = 15.1$ m, the buckling length is then found to be:

$$L_{\text{effective}} = 0.8 \cdot \frac{15.1m}{2} + 2 \cdot 1.12m = 8.28m \tag{7.15}$$

According to section 12.1.7 in NS3470, the slenderness ratio for lateral torsional buckling can be found from the formula

$$\lambda_m = \frac{0.065}{b} \sqrt{L_{\text{effective}} \cdot h} = \frac{0.065}{0.17 \text{ m}} \sqrt{8.28 \text{ m} \cdot 1.12 \text{ m}} = 1.16 \qquad (7.16)$$

resulting in a *design factor* accounting for lateral torsional buckling:

$$k_{\text{vipp}} = 1.56 - 0.75 \cdot 1.16 = 0.69 \qquad (7.17)$$

The maximum bending stress in the rafter is

$$\sigma_{m\gamma} = \frac{\frac{1}{8} \cdot q_{\text{rafter}} \cdot L_0^2}{\frac{1}{6} \cdot b \cdot h^2} = \frac{\frac{1}{8} \cdot 25.2 \text{ kN/m} \cdot (15.0 \text{ m})^2}{\frac{1}{6} \cdot 0.17 \text{ m} \cdot (1.12 \text{ m})^2} = 19.9 \text{ MPa} \qquad (7.18)$$

This gives a utilization of the rafter of

$$\frac{\sigma_{m\gamma}}{k_{vipp} \cdot f_{md}} = \frac{19.9 \text{ MPa}}{0.69 \cdot 29.0 \text{ MPa}} = 0.99 \qquad (7.19)$$

Column

Any one of the columns not connected to the wind bracing system may be considered a simply supported beam with an axial loading of N_{column} and a uniformly distributed loading of q_{column} acting at the upper side of the beam. Thus, the buckling length for flexural buckling is $L_{\text{k}} = L = 10.0$ m, whereas the buckling length for lateral torsional buckling is $L_{\text{effective}} = 0.9 \cdot 10.0$ m $+ 2 \cdot 0.88$ m $= 11.76$ m.

The slenderness ratio and the design factor for lateral torsional buckling for this member is:

$$\lambda_m = \frac{0.065}{b} \sqrt{L_{\text{effective}} \cdot h} = \frac{0.065}{0.17 m} \sqrt{11.76 \text{ m} \cdot 0.84 \text{ m}} = 1.20 \qquad (7.20)$$

and

$$k_{\text{effective}} = 1.56 - 0.75 \cdot \lambda_m = 1.56 - 0.75 \cdot 1.20 = 0.66 \qquad (7.21)$$

respectively.

Using the formula provided in appendix B in NS3470, the design factor due to flexural buckling is found to be $k_\lambda = 0.065$ (slenderness ratio $\lambda = 203.8$).

The design bending stress and axial compression stress are:

$$\sigma_{c0\gamma} = \frac{N_{\text{column}}}{A} = 1.32 \text{ MPa} \qquad \text{and} \qquad \sigma_{m\gamma} = \frac{M_{\text{max}}}{W} = 3.25 \text{ MPa} \qquad (7.22)$$

In addition, Appendix B in NS3470 defines a factor based on the Euler load of the column being considered, $k_{eu} = 0.068$. The utilization of the column is, according to section 12.1.11 in NS3470, found to be

$$\frac{\sigma_{c0\gamma}}{k_\lambda \cdot f_{c0d}} + \frac{\sigma_{m\gamma}}{k_{mboxeffective} \cdot f_{md}} \cdot \frac{1}{1 - \frac{k_\lambda}{k_{eu}} \cdot \frac{\sigma_{c0\gamma}}{f_{c0d}}} = 0.96 \qquad (7.23)$$

7.5.3 Nonlinear analysis

For simplicity, only half the structure is modeled for use in the nonlinear analyses.

In order to properly account for buckling, some kind of geometric imperfection need to be imposed on the structure. The rafters are assigned imperfections that roughly reflect a lateral torsional buckling mode with two half-waves, whereas the imperfection of the columns reflected lateral torsional buckling in one half wave. The shape of the geometric imperfections were found using the linearized buckling facility of Cfem. Figure *7.15* shows a greatly exaggerated version of the geometric imperfection. This shape is scaled such that the amplitude of the deviation from the intended member plane is $\frac{1}{450}$ of the half-wave length.
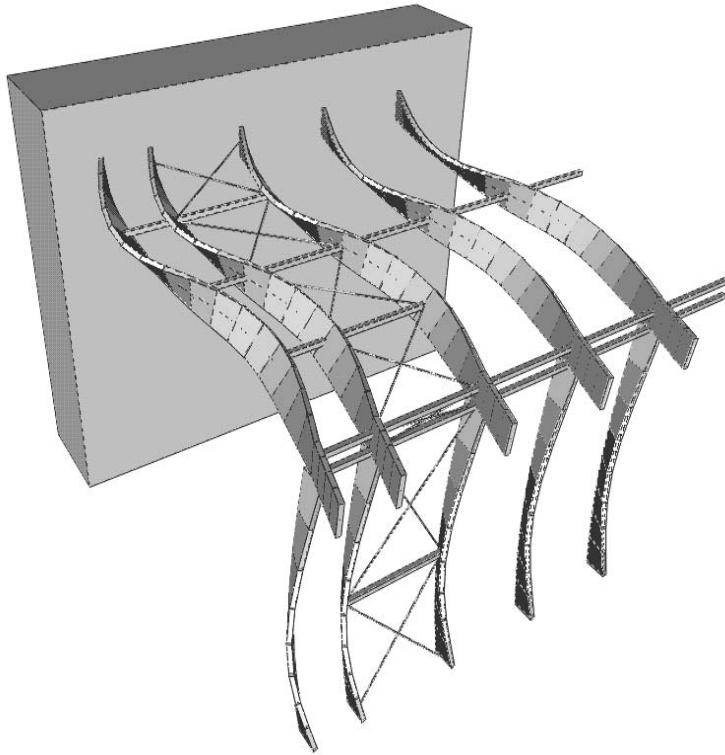
Figure 7.15: *Shape of imperfection used in nonlinear analyses.*

It should be emphasized that while this kind of imperfection is believed to be well suited for finding the load bearing capacity of the rafters and columns, it does not provide much information/imperfection for the bracing system.

In the model, the rafters are assumed to be simply supported at the end connected to the existing structure and at the top0 of the columns, which also implies that the rafters are restrained from rotating about their axes at these points. The connection between rafters and columns is modelled by a linear coupling between the lower edge of the rafter and the top of the column. All translations are synchronized, as are the rotational dofs about the column axis (the vertical axis). The free ends of the bracing system indicating the symmetry plane, were simply supported but were allowed to move in the longitudinal direction of the structure.

Four nonlinear analyses were performed, each with a different version of the material properties. The simple failure criterion from section 7.1 (page 123) was used for to determine the ultimate design load of the structure. q_1 and q_2 were lumped and used as reference loading, and they were imposed on the

structure simultaneously and proportionally with a factor λ. $\lambda = 1.0$ at the time of failure would indicate that the combination of q_1 and q_2 represents the ultimate design load from the analysis.

Stiffness parameters	Strength parameters	λ
Mean characteristic values	Design values	1.30
5-percentile characteristic values	Design values	1.18
5-percentile design values	Design values	0.99
5-percentile design values	Characterstic values	1.05

In the table above, the results from the analyses are presented in terms of the value of λ at the time of failure.
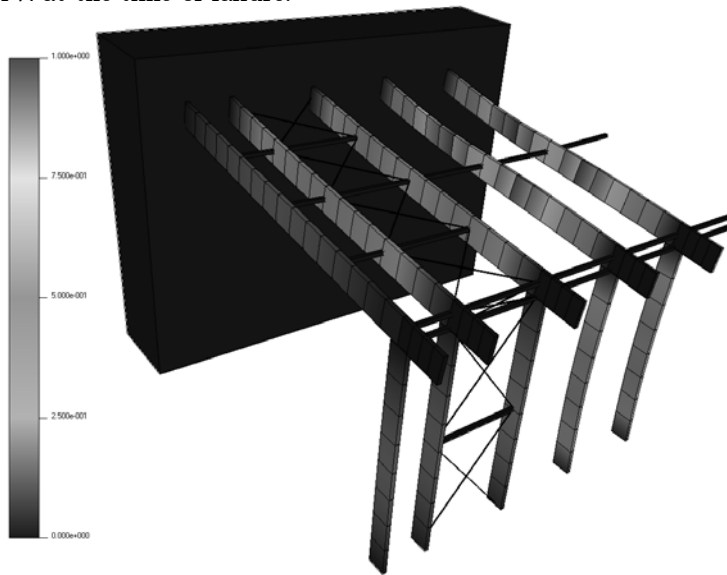
Figure 7.16: *Utilization plot for an analysis at failure.*

Figure *7.16* shows a utilization plot of the structure at the time of failure for the last of the analyses presented in the table. The plots in figure *7.15* and *7.16* were obtained using the visualization program GLview [69].

All, save one, of the nonlinear analysis predict an ultimate load that was 5-30% higher than the load imposed on the structure. In one case the ultimate load is predicted to be 1% lower than the applied loading (suggests failure). In contrast, the simplified design predicted an ultimate load which is 1% higher than the combination of q_1 and q_2.

Since the results from the last three nonlinear analyses all lie close to the result

obtained by the simplified analysis, nothing can be concluded as to what set of material properties should be used in the nonliear analyses. However, since there is no reason to believe that the simplified analysis (in this case) should yield non-conservative results, it seems unecessary harsh having to use material properties that result in a lower ultimate load predicted by the nonlinear analysis, which, after all, is a more accurate method of analysis. This emphasizes the importance of establishing good, realistic values of the stiffness parameters for practical design by use of nonlinear computations.

Chapter 8

Simplified design rules

Both timber design codes considered in this study, the Norwegian NS3470 [2] and the European EC5 [3], rely heavily on simplified methods for the handling of structural stability, allthough EC5 also offers a procedure for numerical analysis of plane systems.

In this section some aspects of the simplified methods described in the two timber codes mentioned, will be commented upon, with basis in the results found in chapter 6 and 7. In spite of a limited number of results, suggested changes are put forward.

8.1 Combined flexural and lateral torsional buckling

According to Eurocode 5, members subjected to loading causing both bending and axial compression, should satisfy the following conditions:

$$
\begin{aligned}
\left(\frac{\sigma_{c0d}}{f_{c0d}}\right)^2 + \frac{\sigma_{mzd}}{f_{mzd}} + k_m \frac{\sigma_{myd}}{f_{myd}} &\leq 1 \\
\left(\frac{\sigma_{c0d}}{f_{c0d}}\right)^2 + k_m \frac{\sigma_{mzd}}{f_{mzd}} + \frac{\sigma_{myd}}{f_{myd}} &\leq 1 \\
\frac{\sigma_{c0d}}{k_{cz} f_{c0d}} + \frac{\sigma_{mzd}}{f_{mzd}} + k_m \frac{\sigma_{myd}}{f_{myd}} &\leq 1 \\
\frac{\sigma_{c0d}}{k_{cy} f_{c0d}} + k_m \frac{\sigma_{mzd}}{f_{mzd}} + \frac{\sigma_{myd}}{f_{myd}} &\leq 1
\end{aligned}
\tag{8.1}
$$

where

σ_{c0d}, f_{c0d}	-	design compression stress and strength, respectively
$\sigma_{myd}, \sigma_{mzd}$	-	design bending stress about local y- and z-axis, respectively
f_{myd}, f_{mzd}	-	design bending strength about local y- and z-axis, respectively
k_{cy}, k_{cz}	-	buckling factor for flexural buckling about local y- and z-axis, respectively
k_m	-	cross-section factor; 0.7 for rectangular cross-sections

In addition, the bending stress about the strong beam axis should satisfy:

$$\sigma_{md} \leq k_{\mathrm{crit}} f_{md} \tag{8.2}$$

where k_{crit} is the lateral torsional buckling factor.

In NS3470, members subjected to both bending and axial compression is required to satisfy an interaction formula in which both flexural and lateral torsional buckling is accounted for.

In section 6.3 (page 99), a simplified view of lateral torsional buckling was outlined, the essence of which is that lateral torsional buckling may be viewed as flexural buckling of the compression zone of the beam. Crude as this may be, it clearly indicates that any axial compression (or indeed tension) must affect the lateral torsional buckling load. The requirements of EC5 (equations (8.1) and (8.2)) do not seem to recognize this connection, whereas NS3470 does. The study presented in section 6.3 indicated that axial compression had indeed a considerable effect on the lateral torsional buckling load.
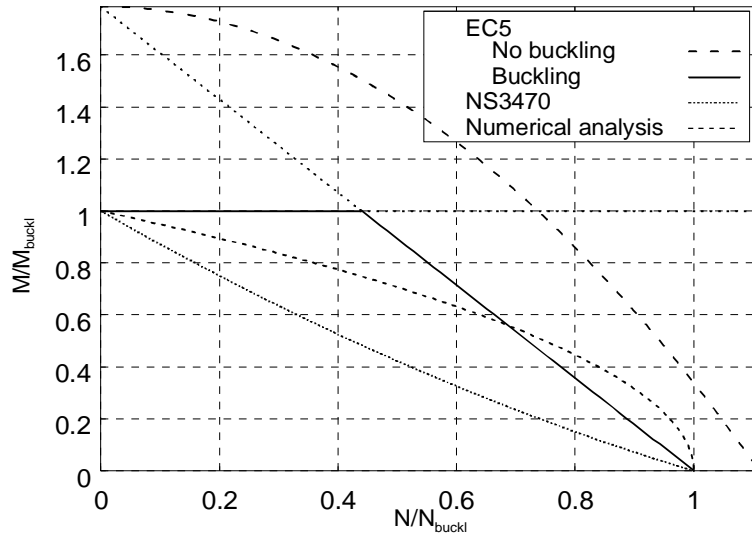
Figure 8.1: *Interaction curves for simply supported beam subjected to constant bending and axial compression.*

Figure *8.1* shows the interaction curves implied by the two design codes for a simply supported beam subjected to constant bending moment M about the strong axis and axial compression N. The geometry of the beam has been chosen to be those of beam 2 in section 6.1, and the material properties are described in section 6.1.2. The interaction curve obtained by numerical computations presented in section 6.3 is also included.

The curves in figure *8.1* clearly indicates that the interaction assumptions, or rather lack of such, in EC5 are non-conservative for axial compression up to approximately 2/3 of the ideal buckling load of the beam(-column). NS3470, on the other hand, seems to be unduly conservative.

A fairly obvious suggestion for EC5, which would ensure stability to be treated conservatively, is to introduce a linear interaction between flexural buckling and lateral torsional buckling. This can be achieved by replacing the two last lines in equation (8.1) by

$$
\begin{aligned}
\frac{\sigma_{c0d}}{k_{cz}f_{c0d}} + \frac{\sigma_{mzd}}{f_{mzd}} + k_m \frac{\sigma_{myd}}{k_{\text{crit}y}f_{myd}} &\leq 1 \\
\frac{\sigma_{c0d}}{k_{cy}f_{c0d}} + k_m \frac{\sigma_{mzd}}{f_{mzd}} + \frac{\sigma_{myd}}{k_{\text{crit}y}f_{myd}} &\leq 1
\end{aligned}
\tag{8.3}
$$

where k_{crity} is the factors accounting for lateral torsional buckling, assuming y to be the strong axis.

The Norwegian code (NS3470) should also be modified to account for linear interaction. This is not only an improvement, but also a simplification.

A less conservative approach is to use a nonlinear ineraction form, for instance in the form

$$\left(\frac{M}{M_{\text{buckl}}}\right)^n + \frac{N}{N_{\text{buckl}}} \leq 1.0 \tag{8.4}$$

where M and N are the bending moment and axial load acting on a particular cross-section, respectively. M_{buckl} is the lateral torsional buckling moment for zero N, and N_{buckl} is the flexural buckling load for zero M. The value of n should be $\sim 1.0 - 1.5$, but more computations are required before this parameter can be fixed.

8.2   Tapered beams

With regards to tapered beams, NS3470 [2] states that *due care should be taken with respect to lateral torsional buckling*[1]. However, the code offers no guidelines as to how this should be done.

In section 6.5, lateral torsional buckling of single and double tapered beams was adressed. The results from this study were used to derive equivalent uniform depths for such beams, enabling the designer to find the lateral torsional buckling factor for a tapered beam by applying the rules for a beam of equivalent, constant depth. However, this equivalent beam depth is dependent on both boundary and loading conditions. Only a few of the simplest sets of boundary and loading conditions were considered, and they do not form a base for general guidelines to the problem of torsional buckling of tapered beams.

However, for simply supported tapered beams with uniformly distributed loading, either at the centroid or at the upper edge, formulas (6.16), (6.17), (6.19) and (6.20) provide useful information. More work is obviously needed, and perhaps the best way to go is to derive similar formulas for a certain number of boundary and loading conditions for single beams. the formulas already derived seem to indicate that it may not be possible to find one or a few formulas covering a wide range of beam configurations.

---

[1] Author's translation

8.3 Bracing

Both NS3470 [2] and EC5 [3] seem to acknowledge bracing to prevent lateral torsional buckling only if it is applied to the compression flanges. Paragraf 5.4.5.2(4) in Eurocode 5 states that *The design stabilising force F_d for the compression flange of a rectangular beam should be..*, whereas paragraf 12.4.5.1 in NS3470 states that *..Discrete bracing should restrict lateral displacement of cross section or part of cross section that is under compression..*[2]

The analyses presented in section 6.6 show that, for all combinations of boundary and loading conditions considered, bracing located at other parts of the cross sections is also be effective, provided the bracing is stiff enough. Specifically, all cases studied showed that bracing located at the centroid can be just as effective as bracing positioned at the compression flange, as long as it has adequate stiffness.

The results from section 6.6 do not provide sufficient information for deriving general design rules, but they clearly indicate that current codes take a conservative view on this problem. By studying some more beam configurations it should be possible to formulate improved guidelines for bracing individual beams. However, the analyses also demonstrate that this problem can be very adequately handled by numerical, finite element methods.

---

[2]Author's translation

Chapter 9

Conclusions and further work

The main objective of this work is to study instability of timber structures through numerical, finite element based methods. Both linearized buckling analyses and nonlinear static analyses need to be performed, and a formulation must be chosen. When subdividing each member of the structure into elements, it becomes apparant, that for practical purposes, each element only has to be able to represent small deformation, allthough the rigid body displacements may be large. The co-rotated formulation meets these demands quite well, and is therefore used in this work.

The first preliminary analyses carried out, revealed that while simple, linear beam elements can be used, high accuracy may require the use of many such elements. In an attempt to reduce the computational effort it was therefore decided to develop a consistent 3D beam element with internal geometric stiffness, based on 2nd order theory, for implementation in a co-rotated formulation.

9.1 Conclusions

In the first part of the work, the co-rotated formulation developed by Haugen [4, 17] and Rankin et al. [14, 15] is presented. One of the advantages of this type of finite element formulation, is the option to implement elements based on small displacements. These are usually well tested linear elements, but they can also be nonlinear elements based on 2nd order theory. Thus, the possibly large rigid

body displacements and rotations are handled by the co-rotated framework, whereas the relatively small deformation is accounted for by the elements put into the co-rotated frame. The beam elements usually implemented in co-rotated formulation are linear elements based on Euler-Bernoulli and Mindlin-Reissner theory.

A consistent 3D beam element, based on 2nd order theory, is developed for implementation in the co-rotated formulation. This element includes geometric terms accounting for the reorientation of the axial stresses during deformation. A version of the element, in which only linear elastic material is considered, is described and implemented in the co-rotated formulation. Tests (chapter 5) show that this element is considerably more accurate in its prediction of both flexural and lateral torsional buckling in linearized buckling analysis than the Euler-Bernoulli or Mindlin-Reissner based co-rotated elements. It also produces very accurate results for course element meshes when used in nonlinear analysis. The computations reported in chapter 5 indicate (at least for linearized buckling analyses) that as much as 3 to 4 times as many standard elements are required in order to obtain the same accuracy as the new element.

In some cases the implemented element converges towards the correct solution from the soft side, when the element mesh is refined. This is true both for linearized buckling analysis and nonlinear analysis. As a sign of energy loss, this is probably the effect of an underintegration performed in the implementation.

An attempt, in which an extra, hierarcical, torsional degree of freedom is included in the element, in order to enable single elements to account for lateral torsional buckling, is reported. However, this did not lead to any significant improvement of the element behaviour.

The second part of the work is concerned with computer simulations of structural timber members with respect to instability. Results from a vast number of individual analyses (of the order of 10 thousand), each representing a "numerical lab test", are presented. An attempt has been made to obtain insight and improve the understanding of most aspects of the problem, rather than concentrate on just a few. Thus, the work presented is in some cases not complete enough to form the basis for definite conclusions. For most of the analyses presented, the new beam element, implemented in the co-rotated formulation, has been used. For individual beam problems, quite fine element meshes have been used, so fine in fact that simpler elements would probably have given similar results. With the new element, the results would probably not have been much different for a coarser mesh, but since the computational effort for these problems are small in any case, a fine element has been used.

Simply supported beams subjected to eccentrically applied loading is studied by use of linearized buckling analysis, both for uniformly distributed loading and

for point loads applied at mid-span. By use of curve-fitting, formulas, in the form of second order polynomials are found for the buckling loads. For uniform loading, the approximate formula give very accurate predictions, at least for an eccentricity to depth ratio of ± 1. For point loads, the corresponding domain is ± 0.7.

Since EC5 [3] does not seem to recognize the effect of axial loading on the lateral torsional buckling load, analyses are performed in order to investigate this interaction. Both simply supported and built-in beams are studied, and both uniformly distributed loading and point loading applied at mid-span are considered. Transverse loading is positioned in turn at the upper edge, at the centroid and at the lower edge of the beam. Considerable interaction is found, and a conservative (at least for the cases studied) interaction formula is suggested. The interaction curves resulting from the analyses are for some cases verified by nonlinear analyses, which in most cases show good agreement with the results from the linearized buckling analyses.

A table relating lateral torsional buckling lengths for simple beams in NS3470 [2] is controlled using linearized buckling analysis, and a new and more accurate table is suggested. Two additional cases are also studied and reported.

An approach to approximate calculation of the lateral torsional buckling loads for tapered beams is presented. Only simly supported beams are tested, and only uniformly distributed loading is studied. However, both loading at the upper edge and the centroid is considered, for single and double tapered beams. Double tapered beams braced at mid-spand are also studied. The approach is assessed by a single nonlinear analysis.

Beams braced at mid-span are studied using linearized buckling analysis. For each of the cases studied, a point is found at which the bracing has no effect, as well as the limit point at which only rigid bracing is able to force the beam to buckle in two half-waves. For bracing posistioned above the limit point, the bracing stiffness neccessary to force the beam to buckle in two half-waves is computed, and approximate formulas for this stiffness is established. Only simply supported beams are considered, and the load cases are uniform bending, uniformly distributed loading and point load at mid-span. The loading is applied at the centroid. The results show that for all cases considered, a bracing positioned well beneath the centroid can still force the beam to buckle in two half-waves, and they clearly indicate that the bracing may still be effective even if it is not able to force the beam into a higher buckling mode.

For a few simple cases, the importance of including the torsional part of the geometrical imperfection, for beams prone to lateral torsional buckling, is studied. This is achieved by nonlinear analysis of beams with imperfections. It is found that the effect of using an imperfection consisting of both transverse

displacement and torsional rotation is small, and differs by no more than 2% compared to using only transverse imperfection.

A lean-to shelter structure is studied by both the simplified methods in NS3470 [2] and nonlinear analysis. The nonlinear analysis, which is performed using four different versions of the material properties, indicates the capabilities of this computational tool, and it is an example of the type of analysis future timber structures should be subjected to.

9.2 Suggestions for further work

The matrix expressions for the internal force vector and the tangent stiffness matrix that were derived for the new beam element (see sections 4.3 and 4.4) are rather complex, involving terms that have need to be integrated. Allthough somewhat simpler, this is also the case for the element presented for implementation. In the implementation, the matrix expressions are evaluated using matrix multiplication and numerical integration by Gauss' quadrature (see for instance [53]). However, since the computation time of the expressions is of importance for the overall performance of the element, some effort should be made to simplify the expressions in order to make the element more time-efficient. For large systems, it will always be more time-efficient to substitute a fine element mesh of simple elements with a coarser mesh of more complex and accurate elements, provided that the two meshes yield about the same degree of accuracy. A reduction of the computational cost of the new element means that the size of the system, at which the coarser mesh of complex elements becomes the more time-efficient, is reduced. It should, however, be kept in mind that for some problems a fine element mesh is needed for other purposes, and for such problems the new element is not needed.

The new beam element is only tested in the co-rotated formulation, but it is also believed to be well suited for use in ordinary linearized buckling analysis and 2nd order analysis. This should, however, be verified.

In appendix D and section 7.5 nonlinear analyses are presented, obtained by different material properties. NS3470 [2] does not specify the material properties for use in nonlinear analysis. EC5 [3] states that the 5-percentile values of the stiffness parameters should be used for 2nd order analysis of plane structures. The characteristic values should be reduced by factors accounting for moisture content and load duration effects and by a material factor. In addition, the design stresses should be used in the failure criterion. The material properties suggested by EC5 were amongst those tested, and the results showed that the nonlinear analyses yielded design loads that were consistently equal to or lower

than those predicted by simplified methods. Nonlinear analysis is undoubtedly a more accurate method of analysis than the simplified methods provided in the design codes, and having to use material properties that lead to results more conservative than those obtained by simplified means, seems to be a rather harsh punsihment for undertaking the extra work. It is therefore important to undertake an investigation of appropriate material properties for use in nonlinear analysis

A linear interaction formula for flexural and lateral torsional buckling loads may provide a sufficient estimate for use in design codes, and the results presented in this work suggest that this is conservative. A more accurate interaction curve will require some more studies. These apply mainly to beams with different sets of boundary conditions at the two ends, but also the effect of the application point of the transverse loading needs to be studied further.

Tables of lateral torsional buckling lengths represent useful information for the designer using simplified methods for beams. The table in NS3470 (revised through this work), is probably sufficient in most cases, but it is based on transverse loading being applied at the centroid. Even though NS3470 provides some vague guidelines as to how eccentric loading can be accounted for, these are crude and in some cases probably non-conservative. Some effort should therefore be put into obtaining better guidelines, for instance as to how the buckling lengths should be adjusted in order to account for loading at the upper and lower edge of the beams.

All the cases studied for braced beams involve simply supported beams. The natural extension of this work is to also study beams with other boundary conditions.

Finally, geometrical imperfections represent a problem that needs further investigation. In order to make nonlinear analyses a viable proporsition for practical design, it is neccessary to provide the engineer with guidelines for types and sizes of geometrical imperfections, preferably based on automatic and semi-automatic generation of the imperfections (in the shape of buckling modes).

References

[1] P. G. Bergan and T. G. Syvertsen. *Knekning av søyler og rammer.* Tapir. 2. opplag, In Norwegian only.

[2] Norges standardiseringsforbund. *NS3470 Prosjektering av trekonstruksjoner. Beregnings- og konstruksjonsregler, 4.utg. nov. 1989.* Norges standardiseringsforbund.

[3] European commmittee for standardization. *Eurocode 5 - Design of timber structures - Part 1-1: General rules and rules for buildings.* European commmittee for standardization, 1993.

[4] B. Haugen. *Buckling and stability problems for thin shell structures using high performance finite elements.* PhD thesis, University of Colorado, 1994.

[5] G. A. Wempner. Finite elements, finite rotations and small strains of flexible shells. *Int. J. Solids Structures*, (5):117–153, 1969.

[6] B. M. Fraeijs de Veubeke. The dynamics of flexible bodies. *Int. J. Engrg. Sci.*, pages 895–913, 1976.

[7] P. G. Bergan and G. Horrigmoe. Incremental variational principles and finite elment models for nonlinear problems. *Comput. Methods Appl. Mech. Engrg.*, (7):201–217, 1976.

[8] G. Horrigmoe and P. G. Bergan. Instability analysis of free-form shells by flat finite elements. *Comput. Methods Appl. Engrg.*, (16):11–35, 1978.

[9] P. G. Bergan and M. K. Nygård. Nonlinear shell analysis using free formulation finite elements. In *Finite Element Methods for Nonlinear Problems*, pages 317–338. Springer Verlag, Berlin, 1989.

[10] M. K. Nygård. *The free formulation for nonlinear finite elements with application to shells.* Dr. Ing. Thesis, Div. of Structural Mechanics, Norwegian Institute of Technology, Trondheim, Norway, 1986.

[11] J. H. Argyris, H. Balmer, J. St. Doltsinis, P. C. Dunne, M. Haase, M. Klieber, G. A. Malejannakis, J. P. Mlejenek, M. Muller, and D. W. Scharpf. Finite element method - the natural approach. *Comput. Methods Appl. Mech. Engrg.*, (17/18):1–106, 1979.

[12] J. H. Argyris. An excursion into large rotations. *Comput. Methods Appl. Mech. Engrg.*, (32):85–155, 1985.

[13] M. A. Crisfield. A consistent co-rotational formulation for nonlinear three-dimensional beam element. *Comput. Methods Appl. Mech. Engrg.*, (81):131–150, 1990.

[14] C. C. Rankin and F. A. Brogan. An element-independent corotational procedure for the treatment of large rotations. *ASME J. Pressure Vessel Technology*, (108):165–174, 1986.

[15] B. Nour-Omid and C. C. Rankin. Finite rotation analysis and consistent linearization using projectors. In *Computat. Methods Appl. Mech.*, volume 93, pages 353–384, 1991.

[16] J. G. Teigen. *Nonlinear analysis of concrete structures based on a 3D shear-beam element formulation*. Ph.d dissertation, Department of Mathematics, Mechanics Division, University of Oslo, Norway, 1994.

[17] B. Haugen and C. A. Felippa. A unified theory of co-rotational finite elements: I. Theory. So be pusblished.

[18] B. Haugen and C. A. Felippa. A unified theory of co-rotational finite elements: II. Applications. To be published.

[19] J.C Simo and L. Vu-Quoc. A three dimensional exact rod model incorporating shear and torsion-warping deformation. *Internat. J. Solids Structures*, (27(3)):371–393, 1991.

[20] G. Jelenić and M. Saje. A kinematically exact space finite strain beam model - finite element formulation by generalized virtual work principle. *Comput. Methods Appl. Mech. Engrg.*, (120):131–161, 1995.

[21] L. A. Crivelli. *A Total-Lagrangian Beam Element for Analysis of Nonlinear Space Structures*. PhD thesis, University of Colorado, 1991.

[22] T. J. R. Hughes. *The Finite Element Method. Linear Static and Dynamic Finite Element Analysis*. Prentice-Hall international, inc., 1987.

[23] C. A. Felippa. Lecture notes in nonlinear finite element methods. Volume I. College of Engineering. University of Colorado. Campus Box 429. Boulder, Colorado 80309, May 1992.

[24] C. A. Felippa. Lecture notes in nonlinear finite element methods. Volume II. College of Engineering. University of Colorado. Campus Box 429. Boulder, Colorado 80309, May 1992.

[25] M. Vašek. Non-linear small strain-separate effects solution of 3D beam systems. In S. Idelsohn, E. Oñate, and E. Dvorkin, editors, *Proceedings from Computational Mechanics: New trends and Applications*, Barcelona, Spain, 1998.

[26] S. P. Timoshenko. *History of strength of materials.* McGraw-Hill book company, inc., 1984.

[27] L. Prandtl. *KipperScheinungen.* Dissertation, Munich, 1899.

[28] A. G. M. Michell. *Phil. Mag.*, (48), 1899.

[29] S. P. Timoshenko and J. M. Gere. *Theory of elastic stability.* McGraw-Hill book company, inc., second edition, 1961.

[30] S. P. Timoshenko and J. M. Gere. *Theory of elastic stability.* McGraw-Hill book company, inc., first edition, 1936.

[31] A. R. Flint. The stability and strength of slender beams. *Engineering*, (170):545, 1950.

[32] A. R. Flint. The lateral stability of unrestrained beams. *Engineering*, (173):65, 1952.

[33] R. F. Hooley, M. ASCE, and B. Madsen. Lateral stability of glued laminated beams. In *Journal of the Structural Division, Proceedings of the American Society of Civil Engineering.*, June 1964.

[34] T. A. C. M. van der Put. Stability design and code rules for straight timber beams. In *Proceedings from CIB-W18. Meeting 23.*, September 1990.

[35] H. J. Burgess. Rectangular section deep beam-columns with continuous lateral restraint. In *Proceedings from CIB-W18. Meeting 21.*, September 1988.

[36] H. J. Burgess. Suggested changes in code bracing recommendations for beams and columns. In *Proceedings from CIB-W18. Meeting 22.*, September 1989.

[37] H. J. Burgess. Simple approaches for column bracing calculations. In *Proceedings from CIB-W18. Meeting 21.*, September 1988.

[38] H. Brüninghoff. Determination of bracing structures for compression members and beams. In *Proceedings from CIB-W18. Meeting 16.*, May/June 1983.

[39] H. J. Burgess. Lateral buckling theory for rectangular section deep beam-columns. In *Proceedings from CIB-W18. Meeting 20.*, September 1987.

[40] H. J. Burgess. Possible code approaches to lateral buckling in beams. In *Proceedings from CIB-W18. Meeting 19.*, September 1986.

[41] H. J. Blaß. Design of timber columns. In *Proceedings from CIB-W18. Meeting 20.*, September 1987.

[42] B. Johansson. Lateral-torsional buckling of eccentrically loaded timber columns. In *Proceedings from CIB-W18.*, February 1975.

[43] H. J. Larsen. The design of timber beams. In *Proceedings from CIB-W18. Meeting 5.*, October 1975.

[44] H. J. Larsen. Calculation of timber beams subjected to bending and normal force. In *Proceedings from CIB-W18.*, February 1975.

[45] H. J. Blass, P. Aune, et al. *Timber engineering STEP 1.* Centrum Hout, first edition edition, 1995.

[46] P. Aune. *Trekonstruksjoner - del 1.* Tapir, 1992.

[47] M. Heinisuo, A. Möttönen, T. Paloniemi, and P. Nevalainen. Automatic design of steel frames in cad-system. In *Proceedings of the 4th finnish mechanical days*, June 1991.

[48] A. Ibrahimbegović, H. Ahkourzadeh, J.-L. Batoz, M. Al Mikdad, and Ying qiao Guo. On the role of geometrically exact and second-order theories in buckling and post-buckling analysis of three-dimensional beam structures. In H. Liebowitz, editor, *An international journal, Computers & structures*, volume 61, December 1996.

[49] J. C. Simo. A finite strain beam formulation. the three dimensional dynamic problem. part i. In *Comput. Methods Appl. Mech. Engrg.*, volume 49, pages 55–70, 1985.

[50] S. Barnett and T. M. Cronin. *Mathematical Formulae for Engineering and Science Students.* Longman scientific & technical, fourth edition.

[51] K. M. Mathisen. *Large displacement analysis of flexible and rigid systems considering displacement-dependent loads and nonlinear constraints.* Dr. Ing. Thesis, Div. of Structural Mechanics, Norwegian Institute of Technology, Trondheim, Norway, 1990.

[52] M. L. Szwabowicz. Variational formulation in the geometrically non-linear thin elastic shell theory. In *Int. J. Solids Structures*, volume 22, pages 1161–1175, 1986.

[53] J. D. Faires and R. L. Burden. *Numerical Methods*. PWS Publishing Company, 1993.

[54] E. Riks. The application of newton's method to the problem of elastic stability. *J. Appl. Mech.*, (39):1060–1066, 1972.

[55] G. A. Wempner. Discrete approximations related to non-linear theories of solids. *Int. J. Solids Structures*, (7):1581–1599, 1971.

[56] I. Fried. Orthogonal trajectory accession on the non linear equilibrium curve. *Comput. Methods Appl. Mech. Engrg.*, (47):283–297, 1984.

[57] E. P. Popov. *Engineering mechanics of solids*. Prentice-Hall inc., 1990.

[58] K. Bell. *Matrisestatikk*. Tapir, 1987.

[59] Hibbit, Karlsson, and Sorensen. *ABAQUS 5.6 Theory Manual*. Hibbit, Karlsson and Sorensen, inc., 1997.

[60] A. Cardona. *An Integrated Approach to Mechanism Analysis*. PhD thesis, Universite de Liege, 1989.

[61] A. M. Ebner and J. J. Ucciferro. A theoretical and numerical comparison of elastic nonlinear finite element methods. *Computer & Structures*, (2):1043–1061, 1972.

[62] K. J. Bathe and S. Bolourchi. Large displacement analysis of three-dimensional beam structures. 1979.

[63] F. W. Williams. An approach to the nonlinear behaviour of the members of a rigid jointed plane framework with finite deflection. *Quart. J. Mech. Appl. Math.*, (17):451–469, 1964.

[64] K.M. Nee and A. Halder. Elastoplastic nonlinear post-buckling analysis of partially restrained space structures. *Comp. Meths. Appl. Mech. Engrg.*, (71):69–97, 1988.

[65] J.L. Meek and H.S. Tan. Geometrically nonlinear analysis of space frames by an increment iterative technique. *Comp. Meths. Appl. Mech. Engrg.*, (47):261–282, 1984.

[66] E. Strømmen. Lateral buckling of beams under transverse load. Technical report, Norwegian University of Science and Technology, Departement of structural engineering. Unpublished.

[67] T. E. Eggen, B. Haugen, and K. Bell. Vipping i NS3470. Technical Report R-2-97, Norges teknisk- naturvitenskapelige universitet, Institutt for konstruksjonsteknikk, 1997. In Norwegian only.

[68] Moelven Limtre A/S. *Limtreboka*. A.S. John Grieg, 1989.

[69] GLView™ - high performance scientific visualization program - user's manual. Viewtech report no.95-0001, rev 0. Trondheim, 1995.

Appendix A

The Rodrigues rotation matrix - a geometric approach

When dealing with finite rotations, one cannot simply add two rotation vectors, since the order in which the roations are added is of significance. A remedy for this problem, namely Rodrigues' representation of the rotation tensor, is presented below. A similiar geometric approach to the Rodrigues rotation matrix was shown by Argyris [12].

A.1   Rotation about an axis - the Rodrigues rotation matrix

Consider an arbitrary vector in space, $\mathbf{e}_0 = \begin{bmatrix} e_1 & e_2 & e_3 \end{bmatrix}$. $\mathbf{e}_0$ is to be rotated an angle θ about an axis represented by the unit vector $\mathbf{n} = \begin{bmatrix} n_1 & n_2 & n_3 \end{bmatrix}$. Introduce a local orthogonal coordinate system with one axis that coincides with $\mathbf{n}$, and in which the rotation of $\mathbf{e}_0$ may be represented by its projection into the plane orthogonal to the rotation axis. The axes of this local coordinate system are

$$
\begin{aligned}
\mathbf{j}_1 &= \mathbf{n} \times \mathbf{e}_0 = \mathbf{Spin}\,(\mathbf{n})\,\mathbf{e}_0 = \mathbf{N}\mathbf{e}_0 \\
\mathbf{j}_2 &= \mathbf{n} \times \mathbf{j}_1 = \mathbf{Spin}\,(\mathbf{n})\,\mathbf{j}_1 = \mathbf{N}^2\mathbf{e}_0 \qquad\qquad (A.1) \\
\mathbf{j}_3 &= \mathbf{n}
\end{aligned}
$$

where

$$\mathbf{N} = \mathbf{Spin}\,(\mathbf{n}) \tag{A.2}$$

The lengths of the axes are

$$
\begin{aligned}
|\mathbf{j}_1| &= |\mathbf{n}||\mathbf{e}_0|\sin(\mathbf{n}, \mathbf{e}_0) = |\mathbf{e}_0|\sin(\mathbf{n}, \mathbf{e}_0) = \mathbf{e}_{0,n} \\
|\mathbf{j}_2| &= |\mathbf{n}||\mathbf{j}_1|\sin(\mathbf{n}, \mathbf{j}_1) = |\mathbf{j}_1|\sin(90°) = \mathbf{e}_{0,n} \\
|\mathbf{j}_3| &= |\mathbf{n}| = 1
\end{aligned}
\tag{A.3}
$$
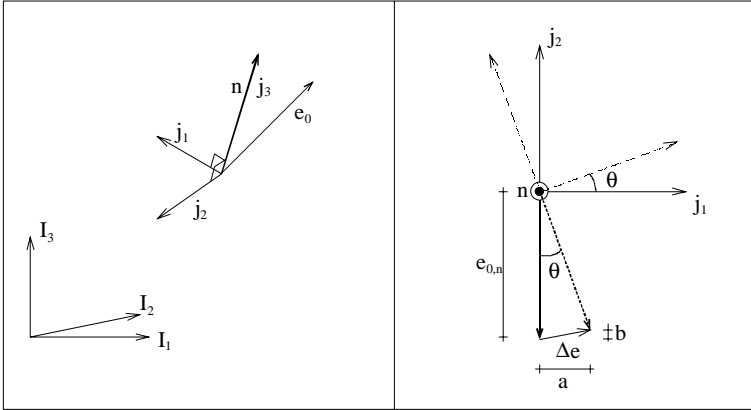
Figure A.1: *Local rotation coordinate system shown both in 3D and as projected into the plane defined by $\mathbf{j}_1$ and $\mathbf{j}_2$.*

Figure *A.1* shows the local coordinate system established for the rotation operation. The vector difference between the initial vector $\mathbf{e}_0$ and the rotated vector $\mathbf{e}_n$ is $\Delta\mathbf{e}$.

$$
\begin{aligned}
\Delta\mathbf{e} &= \mathbf{a} + \mathbf{b} \\
\mathbf{a} &= \mathbf{j}_1 \sin\theta \\
\mathbf{b} &= \mathbf{j}_2(1 - \cos\theta)
\end{aligned}
\tag{A.4}
$$

Hence, the rotated vector $\mathbf{e}_n$ is given by:

$$
\begin{aligned}
\mathbf{e}_n &= \mathbf{e}_0 + \Delta\mathbf{e} \\
&= \mathbf{e}_0 + \mathbf{j}_1 \sin\theta + \mathbf{j}_2(1 - \cos\theta) \\
&= \mathbf{e}_0 + \mathbf{N}\mathbf{e}_0 \sin\theta + \mathbf{N}^2\mathbf{e}_0(1 - \cos\theta) \\
&= \left(\mathbf{I} + \mathbf{N}\sin\theta + \mathbf{N}^2(1 - \cos\theta)\right)\mathbf{e}_0 \\
&= \mathbf{R}\mathbf{e}_0
\end{aligned}
\tag{A.5}
$$

Where

$$\mathbf{R} = \mathbf{I} + \mathbf{N}\sin\theta + \mathbf{N}^2(1 - \cos\theta) \tag{A.6}$$

is Rodrigues' representation of the rotation tensor.

A.2 The rotation matrix as an exponential function

The rotation matrix $\mathbf{R}$ may be written as the exponential of $\mathbf{Spin}(\boldsymbol{\theta})$, where $\boldsymbol{\theta} = \theta\mathbf{n}$ is the rotation pseudo-vector. This has obvious advantages concerning differentiation of $\mathbf{R}$. Cayley Hamilton's theorem, which states that *"every square matrix satisfies its own characteristic polynomial"*[50], is used as basis for this derivation.

A.2.1 Some useful relationships

If $\mathbf{A}$ is given by:

$$\mathbf{A} = \left[\begin{array}{ccc} a_{11} & a_{12} & a_{13} \\ a_{21} & a_{22} & a_{23} \\ a_{31} & a_{32} & a_{33} \end{array} \right] \tag{A.7}$$

then

$$
\begin{aligned}
tr\mathbf{A} &= a_{11} + a_{22} + a_{33} \\
tr\mathbf{A}^2 &= a_{11}^2 + a_{22}^2 + a_{33}^2 + 2\left(a_{12}a_{21} + a_{13}a_{31} + a_{23}a_{32}\right) \\
(tr\mathbf{A})^2 &= a_{11}^2 + a_{22}^2 + a_{33}^2 + 2\left(a_{11}a_{22} + a_{11}a_{33} + a_{22}a_{33}\right) \\
det\mathbf{A} &= a_{11}(a_{22}a_{33} - a_{32}a_{23}) - a_{21}(a_{12}a_{33} - a_{32}a_{13}) \\
&\quad + a_{31}(a_{12}a_{23} - a_{22}a_{13})
\end{aligned}
\tag{A.8}
$$

A.2.2 Characteristic equation

The characteristic equation of $\mathbf{A}$ is defined by:

$$det(\mathbf{A} - \mathbf{I}\lambda) = 0 \tag{A.9}$$

This may be expressed as

$$\begin{vmatrix} a_{11} - \lambda & a_{12} & a_{13} \\ a_{21} & a_{22} - \lambda & a_{23} \\ a_{31} & a_{32} & a_{33} - \lambda \end{vmatrix} = 0 \qquad (A.10)$$

or, in view of (A.8),

$$
\begin{aligned}
det(\mathbf{A} - \mathbf{I}\lambda) & = (a_{11} - \lambda \left[(a_{22} - \lambda)(a_{33} - \lambda) - a_{32}a_{23}\right] \\
& \quad - a_{21}(a_{12}(a_{33} - \lambda) - a_{32}a_{13}) + a_{31}(a_{12}a_{23} \\
& \quad - (a_{22} - \lambda)a_{13}) \\
& = a_{11}(a_{22}a_{33} - a_{32}a_{23}) - a_{21}(a_{12}a_{33} - a_{32}a_{12}) \\
& \quad + a_{31}(a_{12}a_{23} - a_{22}a_{13}) + (-a_{11}a_{22} - a_{11}a_{33} \\
& \quad - a_{22}a_{33} + a_{32}a_{23} + a_{12}a_{21} + a_{31}a_{13})\lambda \\
& \quad + (a_{11} + a_{22} + a_{33})\lambda^2 - \lambda^3 \\
& = det\mathbf{A} + \left(\tfrac{1}{2}tr\mathbf{A}^2 - \tfrac{1}{2}(tr\mathbf{A})^2\right)\lambda + tr\mathbf{A}\lambda^2 - \lambda^3
\end{aligned}
\qquad (A.11)
$$

Thus, the characteristic equation for a 3x3 matrix may generally be written as:

$$\lambda^3 - tr\mathbf{A}\lambda^2 + \frac{1}{2}\left((tr\mathbf{A})^2 - tr\mathbf{A}^2\right)\lambda - det\mathbf{A} = 0 \qquad (A.12)$$

Spin of the rotation pseudo-vector $\boldsymbol{\theta}$, $\mathbf{S} = \mathbf{Spin}\,(\boldsymbol{\theta})$, is now introduced in place of $\mathbf{A}$. In addition we recognize that $\mathbf{Spin}\,(\boldsymbol{\theta})$ may be written as $\theta\mathbf{N}$, where $\mathbf{N} = \mathbf{Spin}\,(\mathbf{n})$ and $\mathbf{n}$ is a unit vector representing the rotation axis.

$$\mathbf{S} = \mathbf{Spin}\,(\boldsymbol{\theta}) = \begin{bmatrix} 0 & -\theta_3 & \theta_2 \\ \theta_3 & 0 & -\theta_1 \\ -\theta_2 & \theta_1 & 0 \end{bmatrix} = \theta \begin{bmatrix} 0 & -n_3 & n_2 \\ n_3 & 0 & -n_1 \\ -n_2 & n_1 & 0 \end{bmatrix} = \theta\mathbf{N} \qquad (A.13)$$

Thus

$$
\begin{aligned}
tr\mathbf{S} & = 0 + 0 + 0 = 0 \\
(tr\mathbf{S})^2 & = (0 + 0 + 0)^2 = 0 \\
det\mathbf{S} & = 0(0 + \theta_1^2) - \theta_3(0 - \theta_1\theta_2) - \theta_2(\theta_3\theta_1 - 0) = 0 \\
tr\mathbf{S}^2 & = 0^2 + 0^2 + 0^2 + 2(-\theta_3^2 - \theta_2^2 - \theta_1^2) = -2\theta^2
\end{aligned}
\qquad (A.14)
$$

According to Cayley-Hamilton's theorem, a square matrix satisfies its own characteristic equation. Thus, by substituting $\mathbf{S}$ for λ in equation (A.12) the char-

acteristic equation may be written as:

$$
\begin{aligned}
\mathbf{S}^3 + \tfrac{1}{2}2\theta^2 \mathbf{S} &= 0 \\
\mathbf{S}^3 &= -\theta^2 \mathbf{S}
\end{aligned}
\tag{A.15}
$$

A.2.3 Exponential function of a matrix

Since we do not know how to deal with exponential functions of matrices directly, we use Taylor series to represent the exponential function:

$$
\exp \mathbf{A} = \sum_{n=1}^{\infty} \frac{\mathbf{A}^n}{n!} = \mathbf{I} + \mathbf{A} + \frac{\mathbf{A}^2}{2!} + \frac{\mathbf{A}^3}{3!} + \frac{\mathbf{A}^4}{4!} + \frac{\mathbf{A}^5}{5!} + \ldots
\tag{A.16}
$$

When substituting $\mathbf{S} = \mathbf{Spin}\,(\boldsymbol{\theta})$ for $\mathbf{A}$, equation (A.14) may be used in order to simplify the Taylor series:

$$
\exp \mathbf{S} = \mathbf{I} + \sum_{n=1}^{\infty} \frac{(-\theta^2)^{n-1}}{(2n-1)!}\mathbf{S} + \sum_{n=1}^{\infty} \frac{(-\theta^2)^{n-1}}{(2n)!}\mathbf{S}^2
\tag{A.17}
$$

Now, $\mathbf{S} = \theta \mathbf{N}$ is introduced:

$$
\begin{aligned}
\exp \mathbf{S} &= \mathbf{I} + \sum_{n=1}^{\infty} \frac{(-\theta^2)^{n-1}}{(2n-1)!}\theta \mathbf{N} + \sum_{n=1}^{\infty} \frac{(-\theta)^{n-1}}{(2n)!}\theta^2 \mathbf{N}^2 \\
&= \mathbf{I} + \underbrace{\left(\theta - \frac{\theta^3}{3!} + \frac{\theta^5}{5!} - \frac{\theta^7}{7!} + \ldots \right)}_{\sin\theta} \mathbf{N} \\
&\quad + \underbrace{\left(\frac{\theta^2}{2!} - \frac{\theta^4}{4!} + \frac{\theta^6}{6!} - \ldots \right)}_{(1-\cos\theta)} \mathbf{N}^2
\end{aligned}
\tag{A.18}
$$

Hence

$$
\exp\,(\mathbf{Spin}\,(\boldsymbol{\theta})) = \mathbf{I} + \mathbf{N}\sin\theta + \mathbf{N}^2(1 - \cos\theta) = \mathbf{R}(\boldsymbol{\theta})
\tag{A.19}
$$

Appendix B

Two-noded beam elements

Equation (3.47), in section 3.2.3, defines the variation of the rigid body rotations of an element with respect to the degrees of freedom as:

$$\delta\tilde{\boldsymbol{\omega}}_r = \tilde{\mathbf{G}}\delta\tilde{\mathbf{v}} \qquad (\text{B.1})$$

The matrix $\tilde{\mathbf{G}}$ is element type dependent. Hence, it will be the same for all displacement based beam elements with two nodes, each having 6 degrees of freedom, and it is the objective of this appendix to derive this matrix for such an element. This was also done by Haugen[4].

Initially, the orientation of the element is defined by the unit vector along the initial local z-axis of the element, $\mathbf{i}_3^0$.
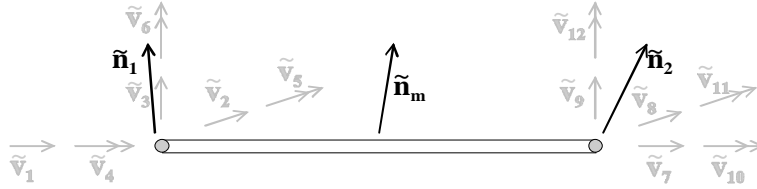
Figure B.1: *Beam element with twelve degrees of freedom.*

For the element shown in figure *B.1*, a particular configuration, C_n, is given by the rotation tensors $\mathbf{R}_1^n$ and $\mathbf{R}_2^n$, for node 1 and 2, respectively. The position of the nodes is defined by the vectors $\mathbf{x}_1$ and $\mathbf{x}_2$.

The local coordinate system of the element is $\begin{bmatrix} \mathbf{i}_1^n & \mathbf{i}_2^n & \mathbf{i}_3^n \end{bmatrix}$, with the local

x-axis defined by the straight line through node 1 and node 2:

$$\mathbf{i}_1^n = \frac{1}{|\mathbf{x}_2 - \mathbf{x}_1|}(\mathbf{x}_2 - \mathbf{x}_1) \tag{B.2}$$

Since the orientation of the nodes in configuration C_n is defined by $\mathbf{R}_1^n$ and $\mathbf{R}_2^n$, the unit orientation vectors $\mathbf{n}_1$ and $\mathbf{n}_2$ are:

$$\mathbf{n}_1 = \mathbf{R}_1^n \mathbf{i}_3^0 \qquad\qquad \mathbf{n}_2 = \mathbf{R}_2^n \mathbf{i}_3^0 \tag{B.3}$$

Defining the orientation of the beam in such a way that the local z-axis lies in the plane defined by $\mathbf{i}_1^n$ and $\mathbf{n}_m = \mathbf{n}_1 + \mathbf{n}_2$, the unit vector along the local y-axis, $\mathbf{i}_2^n$, is found from:

$$\mathbf{i}_2^n = -\frac{1}{|\mathbf{i}_1^n \times \mathbf{n}_m|}(\mathbf{i}_1^n \times \mathbf{n}_m) \tag{B.4}$$

Finally, the unit vector along the local z-axis is determined by:

$$\mathbf{i}_3^n = \mathbf{i}_1^n \times \mathbf{i}_2^n \tag{B.5}$$

The triad defined by $\begin{bmatrix} \mathbf{i}_1^n & \mathbf{i}_2^n & \mathbf{i}_3^n \end{bmatrix}$ also defines the transformation matrix between the global coordinate system and the local coordinate system for the element:

$$\mathbf{T}_n = \begin{bmatrix} \mathbf{i}_1^{nT} \\ \mathbf{i}_2^{nT} \\ \mathbf{i}_3^{nT} \end{bmatrix} \tag{B.6}$$

Thus, the orientation vectors in the local coordinate system are:

$$\tilde{\mathbf{n}}_1 = \mathbf{T}_n \mathbf{n}_1 \qquad\quad \tilde{\mathbf{n}}_2 = \mathbf{T}_n \mathbf{n}_2 \qquad\quad \tilde{\mathbf{n}}_m = \mathbf{T}_n \mathbf{n}_m \tag{B.7}$$

Observe that, in general, the orientation vector $\tilde{\mathbf{n}}_m$ has a length that differs from unity, it may have a component in the local x-direction, it always has a component in the local z-direction, but it never has a component in the local y-direction.

The $\tilde{\mathbf{G}}$-matrix is now found by studying the effect on the orientation of the element by a small pertrubation $\delta\tilde{v}_i$ of each degree of freedom $\tilde{v}_i$. Since, in principle, there is no difference between the two nodes, the variation is only shown for the degrees of freedom associated with node 1, that is $\tilde{v}_1$ through $\tilde{v}_6$.

Pertrubation $\delta\tilde{v}_2$:

Equivalent:
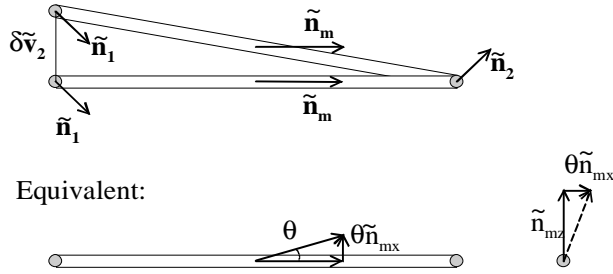
The application of the small pertubation $\delta\tilde{v}_2$ results in the following changes to the rigid body orientation:

$$
\begin{aligned}
\delta\tilde{\omega}_{1,2} &= -\frac{1}{L}\frac{n_{mx}}{n_{mz}}\delta\tilde{v}_2 \\
\delta\tilde{\omega}_{2,2} &= 0 \\
\delta\tilde{\omega}_{3,2} &= -\frac{1}{L}\delta\tilde{v}_2
\end{aligned}
\tag{B.8}
$$

Pertrubation $\delta\tilde{\mathbf{v}}_3$:
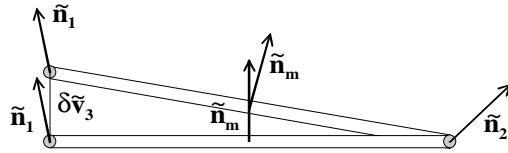
The rigid body rotation of $\tilde{\mathbf{n}}_m$ as a result of $\delta\tilde{v}_3$ being applied to the element is:

$$
\begin{aligned}
\delta\tilde{\omega}_{1,3} &= 0 \\
\delta\tilde{\omega}_{2,3} &= \frac{1}{L}\delta\tilde{v}_3 \\
\delta\tilde{\omega}_{3,3} &= 0
\end{aligned}
\tag{B.9}
$$

Pertrubation $\delta\tilde{v}_4$:
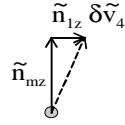
$$
\begin{aligned}
\delta\tilde{\omega}_{1,4} &= \frac{n_{1z}}{n_{mz}}\delta\tilde{v}_4 \\
\delta\tilde{\omega}_{2,4} &= 0 \\
\delta\tilde{\omega}_{3,4} &= 0
\end{aligned}
\tag{B.10}
$$

Pertrubation $\delta\tilde{v}_6$:
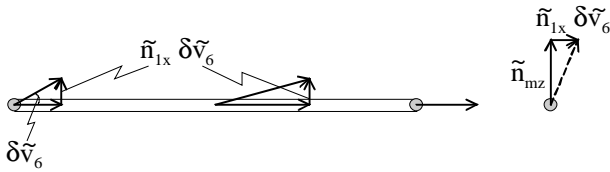
$$
\begin{aligned}
\delta\tilde{\omega}_{1,6} &= -\frac{\tilde{n}_{1x}}{\tilde{n}_{mz}} \\
\delta\tilde{\omega}_{2,6} &= 0 \\
\delta\tilde{\omega}_{3,6} &= 0
\end{aligned}
\tag{B.11}
$$

Small pertrubations $\delta\tilde{v}_1$ and $\delta\tilde{v}_5$ does not cause any change in the rigid body orientation of the element.

Applying the same kind of procedure to the degrees of freedom at the second

node, the following expression for $\tilde{\mathbf{G}}$ can be found:

$$\tilde{\mathbf{G}}^T = \begin{bmatrix} 0 & 0 & 0 \\ -\dfrac{1}{L}\dfrac{\tilde{n}_{mx}}{\tilde{n}_{mz}} & 0 & -\dfrac{1}{L} \\ 0 & \dfrac{1}{L} & 0 \\ \dfrac{\tilde{n}_{1z}}{\tilde{n}_{mz}} & 0 & 0 \\ 0 & 0 & 0 \\ -\dfrac{\tilde{n}_{1x}}{\tilde{n}_{mz}} & 0 & 0 \\ 0 & 0 & 0 \\ \dfrac{1}{L}\dfrac{\tilde{n}_{mx}}{\tilde{n}_{mz}} & 0 & \dfrac{1}{L} \\ 0 & -\dfrac{1}{L} & 0 \\ \dfrac{\tilde{n}_{2z}}{\tilde{n}_{mz}} & 0 & 0 \\ 0 & 0 & 0 \\ -\dfrac{\tilde{n}_{2x}}{\tilde{n}_{mz}} & 0 & 0 \end{bmatrix} \tag{B.12}$$

Appendix C

Results from linearized buckling analyses

C.1 Effect of eccentric loading

C.1.1 Simply supported beam with distributed loading

Calibration analyses (section 6.2.1)

e/h	Beam A		Beam B		Beam C	
	q_{cr} [N/m]	$q_0(e)$	q_{cr} [N/m]	$q_0(e)$	q_{cr} [N/m]	$q_0(eks)$
-1.00	3374.43	-559.62	67967.32	-18114.99	7581.52	-2148.91
-0.75	3226.40	-411.60	63033.17	-13180.83	6993.61	-1561.01
-0.50	3083.69	-268.89	58356.70	-8504.36	6437.69	-1005.09
-0.25	2946.45	-131.65	53958.10	-4105.76	5916.64	-484.04
0.00	2814.80	0.00	49852.33	0.00	5432.60	0.00
0.25	2688.82	125.98	46048.06	3804.26	4986.78	445.82
0.50	2568.55	246.25	42547.13	7305.19	4579.40	853.20
0.75	2453.97	360.83	39344.73	10507.60	4209.70	1222.90
1.00	2345.04	469.75	36430.15	13422.18	3876.08	1556.51

Dependency on eccentricity (section 6.2.1)

	Beam 1		Beam 2		Beam 3	
e/h	q_{cr}[N/m]	eqn.[N/m]	q_{cr} [N/m]	eqn. [N/m]	q_{cr}[N/m]	eqn. [N/m]
-1.00	44392.72	44316.04	77427.88	77388.76	21725.27	21730.95
-0.80	42454.46	42385.18	72946.70	72871.69	20429.04	20417.91
-0.60	40581.24	40522.08	68647.66	68564.13	19186.46	19168.30
-0.40	38775.56	38726.74	64542.93	64466.10	18001.36	17982.14
-0.20	37039.47	36999.15	60642.59	60577.58	16876.90	16859.41
0.00	35374.52	35339.32	56954.10	56898.58	15815.42	15800.13
0.20	33781.70	33747.25	53481.98	53429.10	14818.33	14804.28
0.40	32261.48	32222.94	50227.70	50169.13	13886.07	13871.87
0.60	30813.76	30766.38	47189.65	47118.68	13018.10	13002.89
0.80	29437.91	29377.58	44363.37	44277.76	12212.97	12197.36
1.00	28132.79	28056.53	41741.97	41646.34	11468.47	11455.27

Dependency on strength class (section 6.2.1)

The loading is positioned at the upper edge of the beam. That is: e = 0.3 m for beam 1, 0.633m for beam 2 and 0.5 m for beam 3.

	Beam 1		Beam 2		Beam 3	
Strength class	q_{cr}[N/m]	eqn.[N/m]	q_{cr} [N/m]	eqn. [N/m]	q_{cr}[N/m]	eqn. [N/m]
T18	19503.45	19477.16	30109.85	30070.08	8315.06	8305.98
T24	23459.85	23428.27	36221.02	36173.25	10002.82	9991.90
T30	27416.17	27379.30	42332.06	42276.28	11690.55	11677.79
T40	31093.80	31051.80	47996.90	47933.37	13254.45	13239.97

Dependency on E/G-ratio (section 6.2.1)

The same eccentricities are used as for the study of strength class sensitivity.

		Beam 1		Beam 2		Beam 3	
E[MPa]	G [MPa]	q_{cr}[N/m]	eqn.[N/m]	q_{cr} [N/m]	eqn. [N/m]	q_{cr}[N/m]	eqn. [N/m]
2.1e5	0.80e5	1734357.65	1732602.75	2745072.27	2742364.90	760556.98	759836.63
2.1e5	0.42e5	1234518.10	1233201.25	1941321.95	1939307.80	537408.44	536889.18
6250.0	632.5	25460.37	25430.17	39658.73	39612.80	10964.87	10953.69
7500.0	470.0	23459.85	23428.27	36221.02	36173.25	10002.82	9991.90
10062.5	632.5	31528.59	31486.19	48681.87	48617.72	13444.13	13429.45
10062.5	390.0	23993.48	23954.61	36635.06	36577.21	10102.51	10090.43

C.1.2   Simply supported beam with point load

Calibration (section 6.2.2)

	Beam A		Beam B		Beam C	
e/h	P_{cr}[N]	$P_0(e)$	P_{cr} [N]	$P_0(e)$	P_{cr}[N]	$P_0(e)$
-1.00	33691.25	-6765.43	596556.15	-179288.84	75923.86	-23956.76
-0.75	31989.08	-5063.26	553300.13	-136032.82	70209.44	-18242.35
-0.50	30281.44	-3355.61	508096.14	-90828.82	64176.26	-12209.16
-0.25	28587.38	-1661.55	462248.37	-44981.05	58017.63	-6050.53
0.00	26925.82	0.00	417267.31	0.00	51967.09	0.00
0.25	25314.33	1611.49	374599.31	42667.99	46251.16	5715.93
0.50	23768.01	3157.81	335361.89	81905.41	41041.45	10925.64
0.75	22298.74	4627.08	300197.19	117070.12	36429.33	15537.76
1.00	20914.82	6010.99	269280.80	147986.50	32430.14	19536.95

Dependency on eccentricity (section 6.2.2)

	Beam 1		Beam 2		Beam 3	
e/h	P_{cr}[N]	eqn.[N]	P_{cr} [N]	eqn. [N]	P_{cr}[N]	eqn. [N]
-1.00	222573.93	224093.72	582595.05	594633.86	122527.92	125407.07
-0.80	211966.29	212512.31	549150.73	554670.06	115371.82	116719.66
-0.60	201206.79	201225.17	514386.78	516071.13	107905.30	108342.20
-0.40	190410.26	190232.28	478896.84	478837.05	100261.41	100274.68
-0.20	179698.58	179533.65	443388.02	442967.83	92601.71	92517.10
0.00	169192.89	169129.28	408608.27	408463.47	85098.89	85069.46
0.20	159005.60	159019.17	375256.95	375323.97	77914.78	77931.76
0.40	149233.34	149203.32	343903.42	343549.33	71180.19	71104.01
0.60	139951.98	139681.72	314936.25	313139.55	64982.53	64586.20
0.80	131214.27	130454.39	288552.53	284094.63	59363.67	58378.33
1.00	123050.14	121521.31	264781.11	256414.56	54326.20	52480.40

Dependency on strength class (section 6.2.2)

The eccentricities used for these analyses are half of the beam depths, and are positioned above the centroid.

	Beam 1		Beam 2		Beam 3	
Strength class	P_{cr}[N]	eqn.[N]	P_{cr} [N]	eqn. [N]	P_{cr}[N]	eqn. [N]
T18	89389.08	89413.35	203504.45	203253.60	42053.67	41997.39
T24	107532.76	107561.18	244841.77	244538.20	50596.76	50528.63
T30	125676.05	125708.62	286178.15	285821.89	59139.65	59059.68
T40	142489.40	142529.67	324330.99	323934.84	67020.47	66931.66

Dependency on E/G-ratio (section 6.2.2)

The same eccentricities are used as for the strength class test.

		Beam 1		Beam 2		Beam 3	
E [MPa]	G [MPa]	P_{cr}[N]	eqn.[N]	P_{cr} [N]	eqn. [N]	P_{cr}[N]	eqn. [N]
2.1e5	0.80e5	8161211.45	8160782.65	19253757.51	19246914.04	3997486.14	3995880.24
2.1e5	0.42e5	5771068.61	5770305.33	13490865.43	13480032.84	2797586.43	2795078.55
6250.0	632.5	117835.76	117819.39	271742.18	271367.91	56249.74	56164.16
7500.0	470.0	107532.76	107561.18	244841.77	244538.20	50596.76	50528.63
10062.5	632.5	144527.46	144564.91	329104.88	328695.17	68010.60	67918.64
10062.5	390.0	108602.27	108812.74	243339.31	243617.80	50181.64	50249.60

C.2   Buckling lengths

In table 6.2 in section 6.4, buckling lengths was presented for two beam configurations not covered in [67]. Here, the numerical data from the analyses that formed the basis for these buckling lengths is presented.

C.2.1   The tested beams

The beams that are tested, have the geometry of beams A, B and C (section 6.1). However, to ensure compatibility with different types of material, they are given the following stiffness parameter in the analyses:

Parameter	Beam A	Beam B	Beam C
Depth (h)	1.0 m	1.5 m	1.9 m
width (b)	0.1 m	0.2 m	0.1 m
Length (L)	16.0 m	14.0 m	16.0 m
Youngs modulus (E)	10062.5 MPa	6250.0 MPa	10062.5 MPa
Shear modulus (G)	632.5 MPa	390.0 MPa	390.0 MPa

20 elements of the kind presented in section 4.5 were used to model each beam.
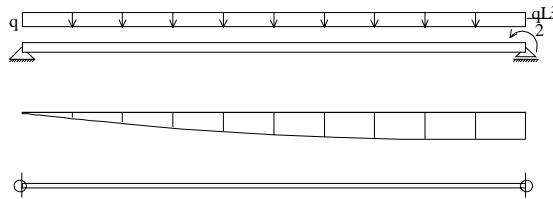
C.2.2   Case one

Figure C.1: *Simply supported beam subjected to uniformly distributed loading q and bending moment $M = \frac{qL^2}{2}$ about the strong axis. Both ends are simply supported about the weak axis.*

The results from the analyses are given in the table below, as is the computed factor m.

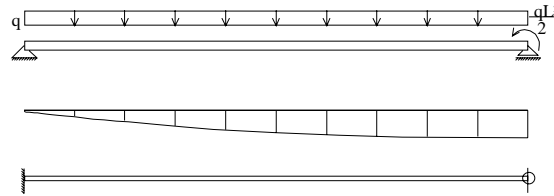|	Beam A	Beam B	Beam C
Load q_{cr}	818.7 N/m	8973.76 N/m	1240.77 N/m
Moment $M : cr$	104796.2 Nm	879422.6 Nm	158818.6 Nm
m	0.763	0.763	0.763

C.2.3 Case two

Figure C.2: *Simply supported beam subjected to uniformly distributed loading q and bending moment $M = \frac{qL^2}{2}$ about the strong axis. Left end is built in about the weak axis.*

Results:

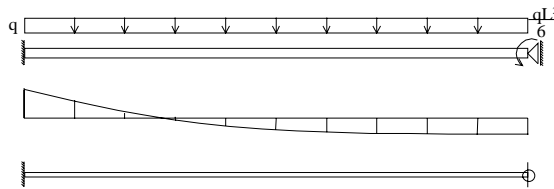|	Beam A	Beam B	Beam C
Load q_{cr}	993.6 N/m	10890.3 N/m	1505.7 N/m
Moment $M : cr$	127180.8 Nm	1067249.4 Nm	192729.6 Nm
m	0.628	0.628	0.628

C.2.4 Case three

Figure C.3: *Beam built in at the left end. The right end is left free to move vertically, while restrained against other translation and against rotation about the beam axis. The beam is subjected to a uniformly distributed load q and a bending moment $M = \frac{qL^2}{6}$ about the strong axis, at the right end.*

Results:

	Beam A	Beam B	Beam C
Load q_{cr}	3147.4 N/m	34499.2 N/m	4769.6 N/m
Moment $M : cr$	134289.1 Nm	1126973.9 Nm	203502.9 Nm
m	0.595	0.595	0.595

C.3   Tapered beams

The geometry used for the tapered beams in section 6.5 was based on a dimension selector provided by Moelven limtre A/S. The following figure shows a version of this dimension selector modified for use in this work.

L	10	11	12	13	14	15	16	17	18	20	22	24
b	115	115	115	115	115	115	115	115	115	165	165	190
$h_1\mid h_2$	400|750	433|818	467|887	500|955	533|1022	567|1128	600|1194	667|1366	700|1489	733|1572		
b	115	115	115	115	115	140	140	165	165	190	190	190
$h_1\mid h_2$	467|817	500|885	533|963	567|1022	600|1096	633|1157	667|1226	700|1329	767|1466	800|1569	867|1706	
b	115	115	115	140	140	140	165	165	165	190	190	190
$h_1\mid h_2$	533|883	567|952	600|1020	667|1156	700|1224	700|1224	700|1259	733|1327	767|1396	800|1499	900|1669	967|1806
b	115	115	140	140	140	165	165	165	190	190	190	215
$h_1\mid h_2$	567|917	600|985	600|1020	667|1122	700|1189	700|1224	767|1328	800|1394	800|1429	900|1599	967|1736	1000|1839
b	115	115	140	140	140	165	165	190	190	215	215	215
$h_1\mid h_2$	600|950	600|985	633|1018	700|1120	700|1155	733|1222	800|1324	867|1426	887|1461	967|1666	1000|1789	1100|1939
b	140	140	140	165	165	165	165	190	190	215	215	
$h_1\mid h_2$	633|983	667|1052	733|1153	733|1188	800|1289	867|1391	867|1428	933|1527	967|1598	1033|1732		
b	140	140	165	165	165	190	190	190	215	215		
$h_1\mid h_2$	667|1017	700|1085	733|1153	767|1222	833|1322	887|1391	900|1469	967|1561	967|1596	1000|1799		
b	140	165	165	165	190	190	190	215	215	215		
$h_1\mid h_2$	700|1050	733|1118	767|1187	800|1255	867|1356	900|1424	933|1492	1000|1594	1000|1629	1066|1695		
b	140	165	165	165	190	190	190	215	215			
$h_1\mid h_2$	733|1083	733|1118	800|1220	833|1288	867|1356	967|1457	967|1526	1000|1594	1066|1695			
b	140	165	165	165	190	190	190	215	215			
$h_1\mid h_2$	767|1117	787|1152	833|1253	867|1322	900|1389	967|1491	1000|1599	1033|1627	1100|1729			

Figure C.4: *Dimensions used for the analyses of the double tapered beams. L = length of beam in meters, b = width of beam in mm, h_1, h_2 are depths of beam in mm.*

Appendix D

Nonlinear analysis and buckling

In this appendix, one case of flexural and two cases of lateral torsional buckling are studied, first by use of the simplified methods provided by NS3470 [2] and EC5 [3], and then by nonlinear analysis. In the nonlinear analyses, the beams are studied for different material properties. Common for the different sets of material properties is that they all are based on material properties provided by NS3470 for T24. The results from this study is discussed briefly in section 2.3.

D.1   Material definition

The material of the beam is T24 as defined in NS3470. The properties are

Property	Symbol	Value
Bending strength	f_{mk}	24.0 MPa
Compression strength	f_{c0k}	21.5 MPa
Young's modulus (5-percentile)	E_{0k}	7500.0 MPa
Shear modulus (5-percentile)	G_k	470.0 MPa
Young's modulus (mean)	E_0	11000.0 MPa
Shear modulus (mean)	G	690.0 MPa

The beam is situated in an environment where the relative humidity is 70%. The axial load has a duration of 3 months. Thus, the modification factors and

design strength values according to the two different design codes are:

	NS3470		Eurocode 5	
Property	Symbol	Value	Symbol	Value
Service class		2		2
Load-duration class		B		med.-term
Modification factor	k_r	0.90	k_{mod}	0.80
Material factor	γ_m	1.1	γ_m	1.3
Height factor	k_h	1.0	k_h	1.0
Design bending strength	f_{md}	19.6 MPa	$f_{m,d}$	14.8 MPa
Design compr. strength	f_{c0d}	17.6 MPa	$f_{c,d}$	13.2 MPa
Design Young's modulus	E_{0d}	6136.4 MPa	$E_{0,d}$	4615.4 MPa
Design shear modulus	G_d	384.5 MPa	$G_{0,d}$	289.2 MPa

The parameters presented as E_{0d} and G_d, are found from E_{0k} and G_d in the same manner as the design strength properties are found from their characteristic counterparts.
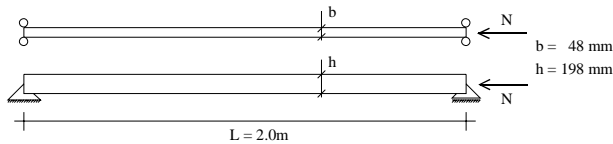
D.2   Flexural buckling

Figure D.1: *Euler-beam. Simply supported beam subjected to axial compression.*

The geometry of the beam is shown in figure *D.1*.

D.2.1   Simplified analysis

NS3470

The slenderness ratio of the beam is $\lambda = 144.3$, which according to "Tillegg B" causes the *slenderness correction factor* to become $k_\lambda = 0.144$. Section 12.1.10 then yields the maximum design load of the beam:

$$N_{NS3470} = \sigma_{c0\gamma} \cdot A = k_\lambda \cdot f_{c0d} \cdot A = 24.087 kN \qquad (D.1)$$

Eurocode 5

The slenderness ratio of the beam is $\lambda_y = 144.3$, which corresponds to a relative slenderness ratio of $\lambda_{rel,y} = 2.46$ (EC5, section 5.2.1). Based on the relative slenderness ratio, the slenderness correction factor becomes $k_{c,y} = 0.154$. Thus, the maximum design load of the beam according to Eurocode 5 is:

$$N_{EC5} = \sigma_{c,0,d} \cdot A = k_{c,y} \cdot f_{c,0,d} \cdot A = 19.320 kN \tag{D.2}$$

D.2.2 Nonlinear analysis

Now, the beam is analyzed using the full nonlinear analysis capability of Cfem. The geometric imperfection imposed on the beam has the shape of the first buckling mode as found from a linearized buckling analysis. The failure criterion used is

$$\frac{\sigma_c}{f_{c0d}} + \frac{\sigma_m}{f_{md}} \geq 1.0 \tag{D.3}$$

for the NS3470 analyses, and

$$\frac{\sigma_c}{f_{c,0,d}} + \frac{\sigma_m}{f_{m,d}} \geq 1.0 \tag{D.4}$$

for the Eurocode 5 analyses. σ_c and σ_m are the axial compression stress and bending stress, respectively.

Four analyses with three different sets of stiffness moduli are performed for each design code. First, the mean values are used, then the 5-percentile values, and finally the modified 5-percentile values. For the three first analyses, the design strengths are used in the failure criterion, but in the fourth analysis the characteristic strengths are used. 20 beam elements of the new kind described in section 4.5 is used in modelling each beam.

NS3470

The imperfection is scaled so that the amplitude is $\frac{L}{300} = 6.7$mm, which is the maximum allowable deviation from the straight line according to section 7.2.3 in NS3470.

Stiffness parameters	Strength parameters	Design load
Mean values	Design values	38.4 kN
5-percentile characteristic values	Design values	28.6 kN
5-percentile design values	Design values	24.1 kN
5-percentile design values	Characteristic values	24.8 kN

Eurocode 5

The imperfection is scaled so that the maximum imperfection is $0.003 \cdot L = 6\text{mm}$, which is consistent with section 5.4.4 in Eurocode 5.

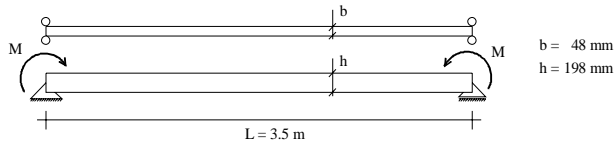| Stiffness parameters	Strength parameters	Design load
Mean values	Design values	36.3 kN
5-percentile characteristic values	Design values	27.5 kN
Mod. 5-percentile design values	Design values	18.4 kN
Mod. 5-percentile design values	Characteristic values	19.4 kN

D.3　Lateral torsional buckling

Figure D.2: *Simply supported beam subjected to constant bending moment about the strong axis.*

D.3.1　Simplified analysis

The effective buckling length of the beam is the same as the length of the beam, as this beam represents the reference case.

NS3470

According to section 12.1.7, the slenderness ratio with respect to lateral torsional buckling is

$$\lambda_m = \sqrt{\frac{f_{mk}}{\sigma_{cr}}} = \frac{0.065}{b}\sqrt{L \cdot h} = 1.127 \tag{D.5}$$

The lateral torsional buckling factor then becomes $k_{vipp} = 1.56 - 0.75 \cdot \lambda_m = 0.71$

Section 12.1.7 in NS3470 yields the maximum design load for the beam:

$$M_{NS3470} = k_{vipp} \cdot f_{md} \cdot \frac{1}{6}bh^2 = 4.36\text{kNm} \tag{D.6}$$

Eurocode 5

Eurocode 5 has the same rules for establishing the lateral torsional buckling factor (called k_{crit} in EC5) as NS3470. Thus, $k_{crit} = 0.71$. The maximum design load is given by section 5.2.2 in EC5:

$$M_{EC5} = k_{crit} \cdot f_{m,d} \cdot \frac{1}{6}bh^2 = 3.30\text{kNm} \tag{D.7}$$

D.3.2   Nonlinear analysis

The failure criterion used for the axially loaded beam is also used for these analyses. As geometrical imperfection, the shape of the first buckling mode is used, including both translation and rotation.

NS3470

The geometrical imperfection is scaled so that the maximum deviation from the intended shape is $L/300 = 0.012m$.

Stiffness parameters	Strength parameters	Design load
Mean values	Design values	5.14 kNm
5-percentile characteristic values	Design values	4.54 kNm
5-percentile design values	Design values	4.06 kNm
5-percentile design values	Characteristic values	4.30 kNm

Eurocode 5

For the analyses based on the Eurocode 5 design code, the geometrical imperfection is scaled so that the maximum imperfection is $0.003 \cdot L = 0.011m$

Stiffness parameters	Strength parameters	Design load
Mean values	Design values	4.10 kNm
5-percentile characteristic values	Design values	3.84 kNm
5-percentile design values	Design values	3.10 kNm
5-percentile design values	Characteristic values	3.45 kNm

D.4   Lateral torsional buckling 2

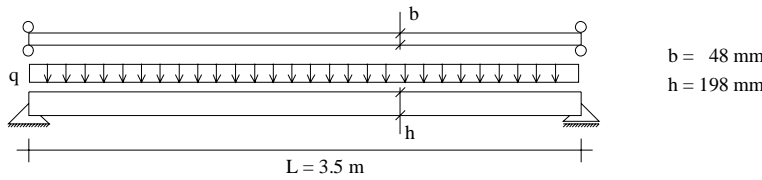b = 48 mm
h = 198 mm

L = 3.5 m

Figure D.3: *Simply supported beam subjected to uniformly distributed loading at the upper edge.*

D.4.1   Simplified analysis

The slenderness ratio of the beam is found by use of equation (6.3) from page 93, which gives the critical value of the uniformly distributed loading:

$$q_{cr} = 3.814 \text{kN/m} \tag{D.8}$$

The critical bending stress can then be found:

$$\sigma_{cr} = \frac{\frac{q_{cr}L^2}{8}}{\frac{1}{6}bh^2} = 18.623 \text{MPa} \tag{D.9}$$

According to both design codes, the slenderness ratio and lateral torsional buckling factor are then found as:

$$\lambda_m = \sqrt{\frac{f_m k}{\sigma_{cr}}} = 1.135 \qquad k_{vipp} = k_{crit} = 1.56 - 0.75\lambda_m = 0.71 \tag{D.10}$$

NS3470

According to section 12.1.7, the maximum design load for the beam can be found from

$$q_{NS3470} = \frac{8}{L^2} \cdot k_{vipp} f_{md} \frac{1}{6} bh^2 = 2.85\text{kN/m} \qquad (D.11)$$

Eurocode 5

Section 5.2.2 yields the following maximum design load:

$$q_{EC5} = \frac{8}{L^2} \cdot k_{crit} f_{m,d} \frac{1}{6} bh^2 = 2.15\text{kN/m} \qquad (D.12)$$

D.4.2 Nonlinear analysis

The shape of the first buckling mode is used as geometrical imperfection.

NS3470

The buckling shape is scaled so that the maximum deviation from the straight beam was $L/300 = 0.012m$.

Stiffness parameters	Strength parameters	Design load
Mean values	Design values	3.34 kN/m
5-percentile characteristic values	Design values	2.97 kN/m
5-percentile design values	Design values	2.68 kN/m
5-percentile design values	Characteristic values	2.86 kN/m

Eurocode 5

$0.003 \cdot L = 0.011m$ is the maximum geometric imperfection.

Stiffness parameters	Strength parameters	Design load
Mean values	Design values	2.65 kN/m
5-percentile characteristic values	Design values	2.50 kN/m
5-percentile design values	Design values	2.04 kN/m
5-percentile design values	Characteristic values	2.31 kN/m

D.5   Conclusion

The third set of material properties used in the nonlinear analyses, are those prescribed by Eurocode 5 for use in 2nd order analysis of plane structures. The analyses show, that use of this material property set consistently yields design loads that are lower than or equal to those predicted by the simplified methods.

All the sets of material properties studied, save the first one, yields design loads that are fairly close to those predicted by the simplified methods.